UNIVERSITEIT VAN PRETORIA
UNIVERSITY OF PRETORIA
YUNIBESITHI YA PRETORIA

Characterisation of expandable graphite and its flame retardant abilities in flame retardant systems for polyethylene

by

Hermanus Joachim Kruger

A thesis submitted in partial fulfilment
of the requirements for the degree

Doctor of Philosophy in Engineering

in the

Department of Chemical Engineering
Faculty of Engineering, the Built Environment and Information Technology

University of Pretoria
Pretoria

February 2017

Characterisation of expandable graphite and its flame retardant abilities in flame retardant systems for polyethylene

Student : *Hermanus Joachim Kruger*
Supervisor : *Professor Walter W. Focke*
Department : *Chemical Engineering*
University : *University of Pretoria*
Degree : *Doctor of Philosophy in Engineering*

Synopsis

In the pursuit of lower cost intumescent flame retardant (IFR) systems, the compound expandable graphite (EG) was identified. This compound delivers high flame retardant performance but provides non-uniform thermal shielding when exposed to open flame from below due to negative gravitational effects. It was theorised that this may be remedied either through ion exchange of the interstratified ions with low glass transition ions or through use in binary systems with other compounds. Two classes of commercial EG were identified, namely a low and a high expansion onset temperature EG compound. Extensive characterisation of each EG compound was undertaken to assess its composition, expansion mechanisms and onset temperatures in order to identify compatible compounds for binary use. The susceptibility of each compound to ion exchange was also assessed. An industrial IFR ethylenediamine phosphate (EDAP) and a novel flame retardant were synthesised for assessment in binary use with EG. Coupled with the above study, this project developed two novel fire testing techniques as low cost alternatives to well-established fire testing methods such as cone calorimetry.

The first technique involved an open flame fire testing method which allowed vertical or horizontal testing. Digital and infrared (IR) video recording during operation facilitated comparison of multiple performance indicators further strengthening this method. The second technique allowed assessment of the mass loss resistance of each compound during laser pyrolysis.

Characterisation of the EG compounds allowed development of structural models to describe each compound and explain the mechanisms of their expansion and gaseous release. Exhaustive ion exchange testing did not deliver favourable results, necessitating the pursuit of compounds for binary use with EG. A novel IFR was synthesised by neutralising 3,5-diaminobenzoic acid hydrochloride salt with ammonium dihydrogen phosphate. This compound, which melts at 257 °C, decomposes concurrently to release carbon dioxide gas which promotes intumescent charring. The flame retardant performance of this compound and EDAP as primary flame retardants and in combination with expandable graphite was evaluated. As a proof of concept, the novel compound was tested as a primary flame retardant using cone calorimetry after which its utility in binary systems with low temperature expandable graphite was tested. Substantial decreases in peak heat release rate (pHRR) and flame out time were achieved for all binary systems. This success led to testing of a number of combinations of low and high expansion onset EG and the other IFRs to identify the highest performing combination, which proved to be the 10-10 EDAP-EG system. Combinations of EG and the novel compound also showed excellent results. The novel fire testing techniques proved effective in identifying high performance combinations and showed comparable trends to those measured in cone calorimetry, at a greatly reduced cost and material requirement. IR analysis of open flame fire testing indicated increases in the temperatures required for ignition and burn through of the substrate. Observations, corroborated by optical video, showed that cohesive and uniform thermal shielding was achieved in all binary systems tested.

This study illustrates that systems of 10% EG combined with either 10% DABAP or 10% EDAP are both the most economical binary systems tested but are extremely high performance systems as well. Both of these systems delivered excellent results while being more economic than the widely used industrial system with a 25-30% EDAP loading. It is recommended that these compounds be considered for industrial use. Furthermore, the effective fire testing techniques developed in this study may be utilised in future fire testing to identify high performance compounds at a lower cost prior to further assessment through methods such as cone calorimetry.

KEYWORDS Expandable graphite; exfoliation; intumescent flame retardant; thermal analysis; cone calorimeter; characterisation; graphite oxide; graphite intercalation compound

Acknowledgements

Firstly, and most importantly I would like to thank my wife Danielle for her understanding and love and unwavering support during the many long hours and late nights. Many a late evening and weekend was spent checking that the machines were still running and grabbing the newest results and she always stayed by my side. I'd like to thank her for all her advice and input on my writing and thank her for always being willing to look over what I wrote. Without Danielle's mentorship as a highly skilled technical editor I would never have attained the writing and technical editing proficiency that I today possess.

As with all large projects a lot of hands go into the many facets of the project. Many people have supported me to achieve the goals I set out to achieve. I have had the privilege of working with a lot of great individuals during this project and had the privilege of supervising three sharp minds as well and feel honoured to have had this opportunity.

I would like to thank my supervisor for accepting me into the research group. Thanks for the many hours of technical advice and for all the off the cuff advice on McGuyvering my way through setting up some of the harder setups of the research. I would also like to thank Walter for his support on a personal level and for always making me feel like a valuable part of the team.

I'd also like to thank the following people:
Suzette, Isbe and Rainer who helped me organise things, learn how to use machines and helped keep everything running smoothly. All of the staff at the various University of Pretoria analytical departments for their time and help during the use of their equipment.

Hendrik and Hendrik, Washington, Stix and Hein for their friendship and for their advice on all the intricacies of how postgrad and the research group work. Dewan, Albert and Albertus for their great work. I had a great time supervising you and am glad to have seen you all go from student to graduate engineers.

All my other friends for being there for me. In particular Michael for his friendship at Tuksdorp postgraduate residence and my best friend Colin for being the man he is. For the years of fun together growing up and pushing each other to succeed and aim to become engineers. It has always, and continues to be, a privilege having you in my life. I am glad that we could encourage each other in our respective postgrad projects.

My parents for raising me into a passionate individual and instilling the strength I needed to get through school and undergrad to get to where I am now. I'd also like to thank them for supporting me in my studies at university.

Lastly I'd like to thank my bursars and financial supporters who made this project possible:

This work is based upon research supported by the South African Research Chairs Initiative of the Department of Science and Technology (DST) and the National Research Foundation (NRF). Any opinion, findings and conclusions or recommendations expressed in this material are those of the authors and therefore the NRF ad DST do not accept any liability with regard thereto.

Table of Contents

List of Tables

List of Figures

Nomenclature

Symbol	Name	Unit
A	area	m^2
A^-	negatively charged intercalant	-
C_n	intercalation medium	-
$C_n{}^+$	positively charged intercalation medium	-m
$C_n{}^+ \cdot A^-$	intercalated compound	-
D	diameter	m
d_{hkl}	distance between two diffracting lattice planes	m
F	force	N
h	height / distance	m
HA	intercalating agent	-
L	length	m
L	length	m
L/D	length/diameter	m/m
m	mass	kg
O_x	oxidising agent	-
pH	negative log hydrogen ion activity in an aqueous solution	-
r	radius	m
R_d	reducing agent	-
t	time	s / min
T	temperature	°C
T_O	expansion onset temperature	°C
t_{fo}	time to flame out	s
t_{ig}	time to ignition	
V	volume	m^3
X	guest molecules / atoms	-

Greek

Symbol	Name	Unit
α	alpha angle	°
β	beta angle	°
γ	Gamma angle	°
n	an integer value	-
ρ	roh / density	g/L
π	pi	-
θ	Thi / angle of the incident beam	°
λ	beam wavelength employed	m

List of acronyms

Acronym	Meaning
ASTM	American Society for Testing and Materials
ATR	Attenuated total reflectance
BET	Brunauer, Emmett Teller surface area measurement
C	Carbon
CB	Carbon black
CCD detector	Charge Coupled Device multichannel array detector
CHNS	Carbon, hydrogen, nitrogen, sulfur
D-band	Diamond (sp^3) band in Raman spectroscopy
DAP	Diammonium phosphate
DSC	Differential scanning calorimetry
DST	Department of Science and Technology
DTG	Derivative thermogravimetry
EDAP	Ethylene diamine phosphate
EDX	Energy dispersive x-ray
EG	Expandable graphite
ESA	Envelope surface area analyser
ESEM	environmental scanning electron microscopy
FE SEM	Field emission scanning electron microscopy
FIGRA	Fire growth rate
FR	Flame retardant
FTIR	Fourier transform infrared spectroscopy
G-band	Graphite (sp^2) band in Raman spectroscopy
GC	Gas chromatography
GIC	Graphite intercalation compound
GO	Graphite oxide
H	Hydrogen
HCl	Hydrochloric acid
HR	High resolution

Acronym	Meaning
HRR	Heat release rate
ICP	Inductively coupled plasma
ICP-MS	Inductively coupled plasma – mass spectrometry
IFR	Intumescent flame retardant
IR	Infrared
ISO	International Organisation for Standardisation
LDPE	Low density polyethylene
LLDPE	Linear low density polyethylene
LOI	Limiting oxygen index
MAHRE	Maximum average rate of heat release
MFI	Melt flow index
MLR	Mass loss rate
MS	Mass spectrometry
N	Nitrogen
PE	Polyethylene
pHRR	Peak heat release rate
PSD	Particle size distribution
PVC	Polyvinyl chloride
SEM	Scanning electron microscopy
S	Sulfur
SANAS	South African National Accreditation System
SDTA	Simultaneous differential thermal analysis
SEA	Specific extinction area
SPR	Smoke production rate
TEM	Transmission electron microscopy
TGA	Thermogravimetric analysis
tHR	Total heat release
TMA	Thermomechanical analysis
TSR	Total smoke release

Acronym	Meaning
wt.	Weight
wt.%	Weight percentage
XRD	X-ray diffraction
XRF	X-ray fluorescence

Introduction

Polyethylene has a high heat of combustion and a low propensity for char formation (Weil & Levchik, 2008). As a result, polyethylene-based products present a potential fire hazard in deep-level underground mining applications. It is therefore necessary to flame retard polyethylene products with suitable additives for critical applications. A wide range of effective flame retardants are available (Dasari *et al*, 2013b; Weil *et al*, 2008). EG is a partially oxidised, intercalated form of graphite. It contains intercalated guest species (e.g. sulfuric acid anions) in between the stacked graphene layers (Camino *et al*, 2001a; Furdin, 1998). A key property of EG is its tendency to exfoliate explosively, i.e. to expand rapidly in a worm-like manner when heated to high temperatures (Chung, 1987; Chung, 2002b; Wissler, 2006). When this occurs at the surface of a polymer that faces upwards, a loose cover of fluffy vermicular graphite is deposited. IFRs swell when exposed to fire or heat. This exfoliation forms a carbonaceous foam residue on the surface that acts as a heat insulator and a physical barrier to the transport of oxygen and pyrolysis products (Camino, Costa & Martinasso, 1989; Dasari *et al*, 2013b; Lewin, 1999a; Wang & Chow, 2005). Unlike the foam coating generated by conventional IFRs however, the cover from EG is weakly bonded to the polymer surface and there is no cohesion between adjacent EG "worms". This leads to poor performance when the fire is associated with strong convection currents, or when a sample is exposed to a flame from below.

Recent studies have highlighted the utility of EG, IFRs and their synergistic combinations in improving the fire behaviour of polyethylene (Han, Li & Zhao, 2007b; Pang & Song, 2012b; Qu & Xie, 2003a; Sun *et al*, 2013a; Weil *et al*, 2008; Xie & Qu, 2001a; Xie & Qu, 2001b). In spite of this, only a few such combinations have been explored to date. What sets this study apart is its aim to strengthen the weaknesses of EG while using lower amounts of the secondary compounds than they individually require to deliver effective flame retardant behaviour on their own. The success of such binary systems would allow production of cheaper flame retarded polymers for a wide range of applications where fire risk is prevalent.

The key objective of this study was to investigate whether addition of IFRs to EG flame retarded systems or modification of EG for flame retardant systems improves the cohesion between exfoliated EG strings and the polymer surface within which they are contained. Furthermore, there was a desire to achieve cohesiveness between the usually independent EG strings, thereby improving the barrier properties causing uniform and improved barrier properties. In addition to the aforementioned aims the development of novel and less expensive fire testing methods was desired.

In order to achieve a cohesive thermal layer of EG flame retarded material, two approaches were considered: ion exchange of low glass transition temperature ions with those intercalated into EG and binary use of EG with other IFRs in low density polyethylene (LDPE). It was theorised that both these approaches would promote bonding of the EG strings, provided that the thermal degradation and glass transition temperatures are appropriately low, so as to coincide with the exfoliation of EG. The fire performance of these additives, both on their own, and in selected combinations, was studied using cone calorimeter fire testing and developed open flame and laser pyrolysis tests.

Document overview

Four phases were identified to achieve the project goals:

- Ion exchange of industrially produced EG with low glass transition ions which could potentially bond the individual EG strings to one another creating a cohesive barrier. **Appendix A-1 and Chapter 2.**
- Characterisation of low and high expansion onset temperature industrial expandable graphite to quantify their flame retardant behaviour and abilities as primary flame retardants. **Chapter 1 & 2. Appendix A-2.**
- Development of a novel flame retardant which possesses charring or IFR behaviour for binary use with EG. If said flame retardant is found compatible, test whether said flame retardant will bond the expanded EG strings together creating a cohesive and uniform barrier. Utilise cone calorimetry to quantify fire performance of said compounds. Furthermore, the widely used industrial flame retardant EDAP may be used as a benchmark for the novel compound's performance and as an alternative binary compound. **Chapter 3, 4 & 5. Appendix A-3, A-4 & A-10.**
- Development of alternative low cost fire testing methods for fire testing of flame retarded polymers. **Chapter 6. Appendix A-5, A-6, A-7, A-8 & A-9.**

During the first year of this study, extensive testing was done for the first phase above. Unfortunately, no definitive success could be proved and this phase was abandoned in favour of the further phases.

NOTE: Any minor repetition between the chapters of the Thesis is attributed to the fact that each chapter reports the unique equipment, materials and testing configurations used individually. This was done to avoid confusion as to the exact methods and materials used for the results section of each chapter.

Chapter 1: Expandable graphite as flame retardant

Foreword

Preliminary research was conducted in order to understand the nature of GICs, EG and the methods required to characterise these materials. This chapter outlines the methods considered for characterisation of the commercial EG used in this study.

Executive summary

In recent years, the use of GICs has increased substantially (Kuilla *et al*, 2010). GIC research has consequently increased and there is a dire need to find new ways to engineer the properties of GICs for different applications (Dresselhaus & Dresselhaus, 1981). EG is one such GIC which can be used for a variety of applications with its use as an IFR being the most important. It was suggested that EG could be further modified in order to improve its flame retardant properties. Two possible methods of EG modification are co-intercalation and ion-exchange (Celzard, Marêché & Furdin, 2005; Lee, Cho & Drzal, 2005). Before modification of EG can be conducted, it is important to identify characterisation techniques which can characterise the raw and modified EG and allow one to quantify changes in the properties of EG.

The categories of characterisation techniques discussed include: particle analysis; visual characterisation using microscopy techniques; atomic and crystal structure characterisation; compositional analysis and thermal analysis.
Keywords: flame retardants; graphite intercalation compounds; expandable graphite; characterisation

1-1. Introduction

The GIC EG is a popular IFR because of its high availability and relatively low price. EG, when incorporated into a polymer medium, is an effective thermal shielding flame retardant. This property is due to its exfoliation behaviour which can result in volumetric increases of up to 300 times the original volume.

EG however, delivers non-uniform flame retardant behaviour in a polymer medium as its thermal shielding effect is less effective at the base of the medium due to negative gravitational effects. It was theorised that this behaviour could be remedied by chemically modifying EG using ion-exchange or co-intercalation mechanisms to create cohesive foaming behaviour, preventing gravitational effects. Two compounds identified for incorporation into EG to improve its flame retardant behaviour are phosphorus and boron as they possess inherent flame retardant properties (Dogan & Bayramli, 2010; Modesti & Lorenzetti, 2002). Many compounds, including phosphorus and boron, can significantly alter material properties, even when only present in trace amounts. In order to quantify the structural and compositional changes that occur when EG is modified, characterisation of neat and altered EG is necessary.

The objective of this review is to introduce the reader to EG and GICs and the diverse range of techniques which can be used to characterise the properties and structure of graphitic compounds.

1-2. Carbon

Carbon is a unique element, in that it has a wide range of allotropes (polymorphs) which gives rise to a multitude of possible molecular structure, some of which are displayed in Figure 1-1. These allotropes consist of different forms of hybridised and unhybridised carbon atoms, vastly changing the material properties. Allotropes of carbon include carbon nanotubes, charcoal, graphite, diamonds and fullerenes (Gao & Zhang, 1996).

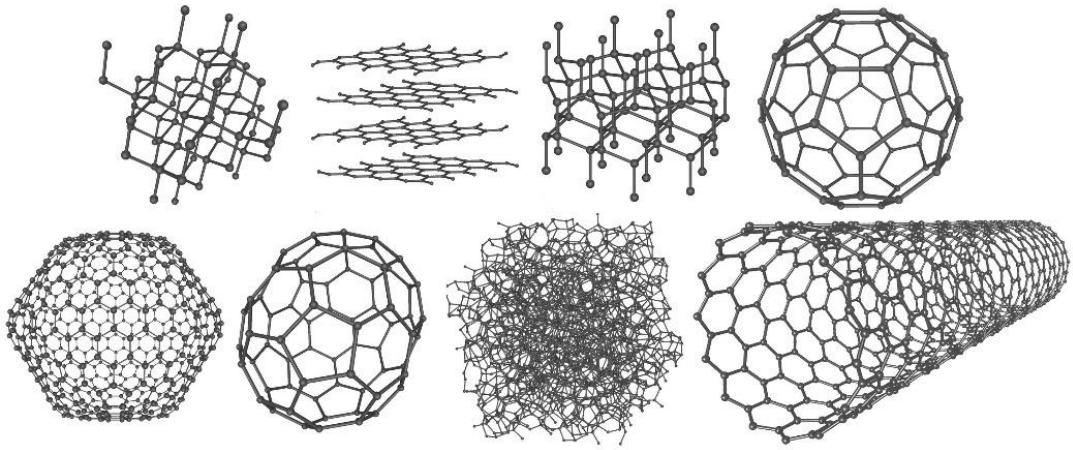

Figure 1-1: Some known carbon allotropes

When solid carbon is heated at pressures below 10 atmospheres, it does not melt but instead undergoes a sublimation transition straight into a gaseous form. Carbon has the highest melting/sublimation point of all the elements and, in the form of diamond, has the highest thermal conductivity of any element. The word graphene has always been used when discussing single layers within graphite but separation of such a mono-molecular layer of aromatic carbon was first achieved in 2004 by Kostya Novoselev and Andre Geim (Wehling *et al*, 2008). Graphene consists of a single atomic layer of sp_2 hybridised carbon atoms bonded covalently to form an extremely stable aromatic honeycomb structure (Kuilla *et al*, 2010; Smith, 2008: 606-633).

Due to its single molecular thickness, graphene is extremely thermally conductive across the carbon layer, which is why it is widely incorporated into smart phones, laptops and many electronic implements today in order to promote even heat conduction and prevent hotspots (Subrina, Kotchetkov & Balandin, 2009).

Carbon formation can occur in multiple ways, the most common of which is the pyrolysis of hydrocarbons. When a material is exposed to temperatures above 500˚C hydrogen contained in a hydrocarbon based material are released in the form of water vapour. This causes scattered domains of carbon to bond forming either graphitic sections of sp2 hybridised carbon or sp3 hybridised carbon chars. X-ray diffraction (XRD) allows one to observe peaks named the G and D-peaks which represent graphitic and amorphous structures. This is elaborated upon in section 1-7.4.1 (Russell, Gibbins & Williamson, 1999).

1-3. Graphite

1-3.1. Introduction to graphite

At atmospheric pressure and ambient temperature, the most stable allotrope of carbon is graphite (Callister, 2007: 431-432). Graphite is a carbon allotrope whose structure approximates multiple graphene layers stacked upon one another and bonded (between the layers) by weak van der Waals forces (Celzard *et al*, 2005). When considering graphene, one should note that each carbon atom contains a delocalised valence electron which can bond with a layer above or below it to form the ideal graphite structure shown in Figure 1-2 (Callister, 2007: 431-432). Figure 1-2 also illustrates the structure of fullerenes and nanotubes which are carbon allotropes with a different level of hybridisation to that of graphite (or graphene).

The structure of graphite displayed in Figure 1-2 is an idealisation, and is not a true representation of the structure of all graphite. Dependant on the origin of the graphite, the crystal structure of two samples can differ widely. Naturally occurring graphite is mined in many countries worldwide and, depending on the formation conditions, various structures can result.

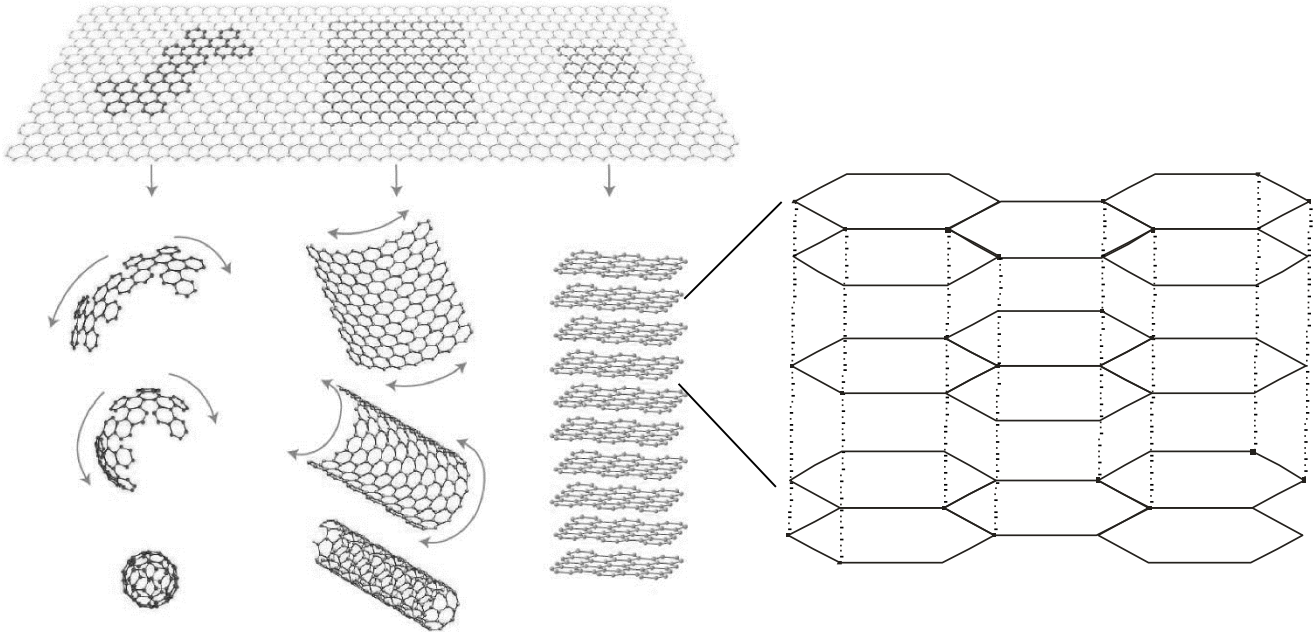

Figure 1-2: Simplified planar structure of graphite and other carbon allotropes (Geim & Novoselov, 2007)

Table 1-1 mentions some of the possible structures of graphite and the conditions which cause their formation.

Table 1-1: Graphite types and their properties

Overall graphite class	Subclass	Properties	Formation conditions
Micro-crystalline	Amorphous graphite [a]	Small crystal size	Coal under high pressure
Macro-crystalline	Vein graphite [b]	Highly crystalline	Fluid-deposition
Macro-crystalline	Flake graphite [b]	High impurities	Disseminated carbon in metamorphosed Silica
Synthetic	-	Can be as crystalline as desired	Variety of methods.

[a] (Wissler, 2006) [b] (Luque *et al*, 1998)

In all forms of graphite, the interplanar forces are orders of magnitude weaker than the planar forces. This parity allows one to introduce and exchange molecules into the inter-layer spaces (Celzard *et al*, 2005; Dittrich *et al*, 2013; Lee *et al*, 2005). This can occur through the process of intercalation which is discussed in detail in section 1-4.

Graphite is utilised in a diverse set of applications, including lubricants, electrodes, high temperature crucibles and even items as basic as pencils. A different material property of graphite is exploited for each of its many applications. Some of the key properties of graphite and the applications where they are utilised are mentioned in Table 1-2.

Table 1-2: Basic graphite properties and applications

Property	Application
Low in-plane resistance [a]	Pencil lead
Highly anisotropic [b]	Solid film lubricant
High thermal conductivity [c]	Polymer additive
High electrical conductivity [c]	Electronic applications

[a] (Ashcroft & Mermin, 1976) [b] (Aihara, Yamabe & Hosoya, 1994)
[c] (Dresselhaus *et al*, 1981)

In section 1-7, methods of characterising specific structural features of graphite are discussed. In order to understand these methods, the following information on graphite is established in the sections that follow:

- Flake graphite particle dimensions (section1-7.2)
- Crystal structure of graphite and GICs (section 1-7.4)

1-3.2 Flake graphite particle dimensions

Flake graphite is a popular graphite type for use in EG. Figure 1-3 displays the general shape of EG flake graphite.

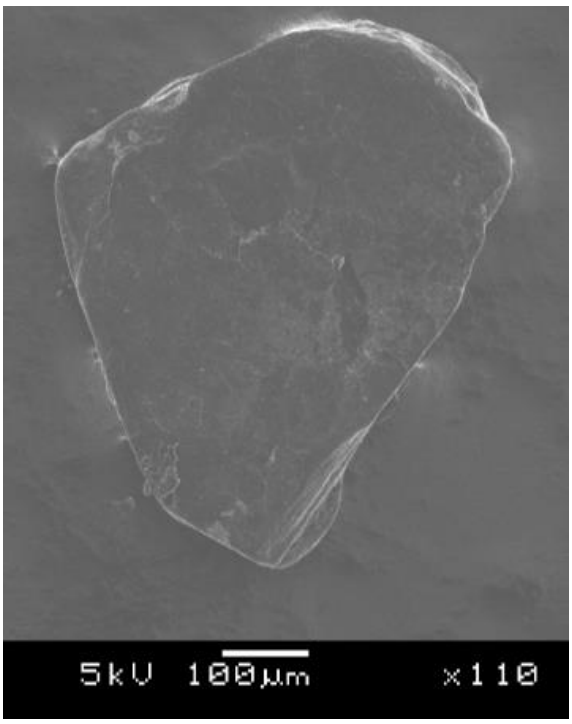

Figure 1-3: EG Scanning Electron Microscope Micrograph

An important characteristic of flake graphite is its shape. Flake EG is considered to have a circular profile from above and below and an ellipsoidal profile from the side, like a magnifying lens. For the purpose of particle sizing, graphite flakes may be approximated as a semi-ellipsoidal disk shape. Generally, graphite flakes are ±1 mm in diameter with a thickness which may reach 0.7 mm but which is generally narrower. Due to the small scale of flake graphite particles and the low density of graphites, characterisation techniques which measure physical properties are often negatively affected (Dresselhaus *et al*, 1981).

The extensive use of flake graphite to make GICs can be attributed to the fact that thin samples undergo intercalation much quicker and often yield more homogeneous, better staged results compared to thick samples. If a GIC has a more homogeneous distribution of intercalant molecules, the properties of the GIC are more consistent.

1-4 Intercalation and graphite intercalation compounds

1-4.1 Intercalation

One possible way in which a molecule or atom can enter a medium is through ion exchange. During ion exchange, a molecule or atom already contained within the medium is exchanged. The driving force for such a reaction is change in entropy. This process is different from the process of intercalation but may occur concurrently.

Intercalation is a reversible process whereby a guest molecule or atom, called the intercalant, moves into the space between two van der Waal's bonded layers and is included in the layered structure (Kikkawa *et al*, 2007: 86-89). A number of methods of intercalation exist, such as liquid intercalation, electrochemical intercalation, co-intercalation and two-zone vapour transport intercalation (Dresselhaus *et al*, 1981). The most commonly used mechanisms of intercalation are:

1. Charge transfer between the host structure and the intercalant species. The driving force for this mechanism can either be charge affinity or entropy change.
2. Neutralisation of a charge imbalance in the layers by inclusion of the intercalant. This process is conducted by sufficiently charging and separating the individual layers of the intercalation medium. Oxidation of the layers using a strong oxidising agent such as nitric acid allows the inclusion of negatively charged intercalant species into the medium, in order to neutralise the charge imbalance created. The driving force for this mechanism is charge affinity (Holleman, Wiber & Wiberg, 2001: 794).

In the section that follows, GICs will be introduced and the process of intercalation will be discussed using the GIC EG to exemplify the intercalation process.

1-4.2 Graphite intercalation compounds

GICs are simply graphitic compounds which have undergone intercalation of an appropriate intercalant species. Although the first synthesis of a GIC occurred in 1841, GICs were only studied for the first time in the early 1930s after the invention of XRD techniques. In recent years GIC research has intensified, leading to its increased popularity and growing range of applications. Today, more than 100 reagents have been intercalated into graphite, and a large portion of the resulting compounds have been characterised (Dresselhaus *et al*, 1981).

Some GICs have vastly differing chemical and physical properties to non-intercalated graphite. The magnitude of the change in each GIC property is affected both by the type of intercalant species and the degree of intercalation achieved. GICs can be engineered for certain applications by selecting the appropriate intercalating agent and intercalation conditions in order to give special properties to the GIC such as thermal and charge conduction and even exfoliation (Sorokina, Shornikova & Avdeev, 2007). Intercalation can be represented by a two-step process:

$$C_n + O_x \rightarrow C_n^+ + R_d \quad (1\text{-}1)$$

$$C_n^+ + A^- + HA \rightarrow C_n^+ \cdot A^- + HA \quad (1\text{-}2)$$

The Symbols in equations 1-1 and 1-2 represent the following compounds in the case of pure EG.

Symbol	Compound	Example
C_n	Intercalation medium	Graphite
O_x	Oxidising agent	HNO_3
C_n^+	Positively charged intercalation medium	$(C)^+$
R_d	Reducing agent	$(HNO_3)^-$
A^-	Negatively charged intercalant	$(SO_3)^-$ or $(HSO4)^-$
HA	Intercalating agent	H_2SO_4
$C_n^+ \cdot A^-$	Intercalated compound	$C_n(SO_3)_m$

Liquid intercalation can be conducted in a glass beaker by treating the intercalation medium (e.g. graphite or clays) with an oxidising and intercalating agent. Potassium permanganate and nitric acid are two of the most popular oxidising agents, but nitric acid is favoured due to its increased availability and reduced cost in comparison with other oxidising agents. Chromic acid may also be used as the oxidising agent (Celzard *et al*, 2005).

The intercalating agent provides the intercalant which will enter the intercalation medium. When sulfuric acid is used as the intercalating agent for instance, sulphate or hydrosulphate ions enter the medium. Figure 1-4 indicates the intercalation process represented by equations 1-1 and 1-2.

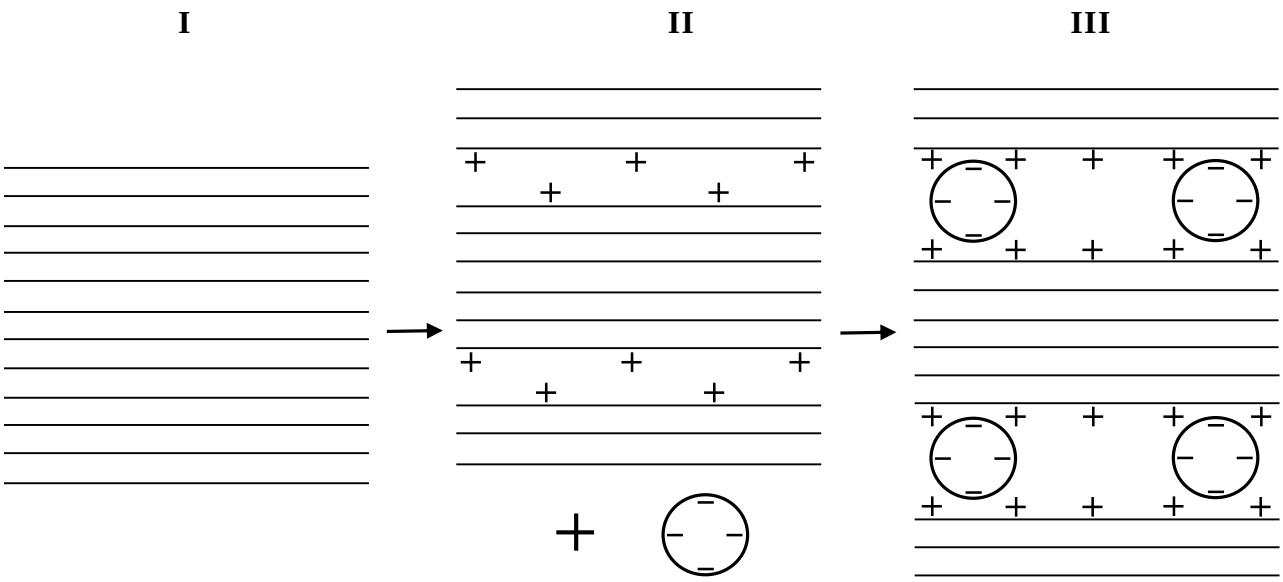

Figure 1-4: Simplified representation of intercalation

In Figure 1-4, the change in the medium between phase I and phase II represents the reaction that takes place according to equation 1-1. The transition from phase II to phase III represents the reaction in equation 2 (Ying *et al*, 2008). Figure 1-5 displays a 3D representation of phase III of the intercalation process displayed in Figure 1-4. The GIC in Figure 1-5 represents a system where H_2SO_4 is used as the intercalating agent and the primary compound of this study, EG results.

XRD is a valuable technique that is used to quantify the success of intercalation. When intercalation occurs, the "d-spacing" between layers increases and XRD can detect these changes, indicating whether the process was successful.

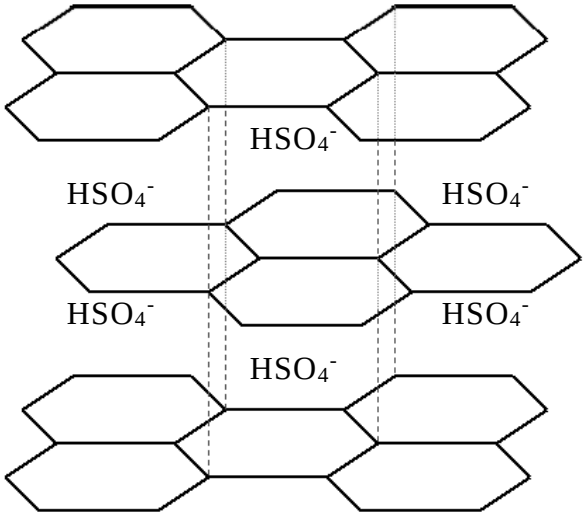

Figure 1-5: Structure of EG

The properties of GICs bring about a wide range of new applications for graphitic materials, some of which are displayed in Table 1-3.

Table 1-3: Important GIC properties

Property	**Application**
Increased thermal conductivity	Some GICs can attain thermal conductivities above that of copper giving rise to multiple applications
Exfoliation	Flame retardant applications such as those of EG
Decreased charge conductivity	Insulation application
Increased charge conductivity	Superconductors

(Dresselhaus *et al*, 1981; Foley *et al*, 1977; Hannay *et al*, 1965)

1-4.3 Crystal structure of graphite and GICs

In order to characterise graphitic compounds, a certain level of understanding of the possible crystal structures of carbon and specifically graphite is required. Different crystal lattice structures can be formed depending on the hybridisation state of carbon molecules in a carbon based material. The crystal structure of a material can be described by one or more unit cells, dependant on how many lattice systems exist in the material. A unit cell is defined as the smallest single entity which can describe a crystal lattice structure when repeated in all 3 directions. Figure 1-6 displays a basic unit cell (Giacovazzo *et al*, 2002: 370).

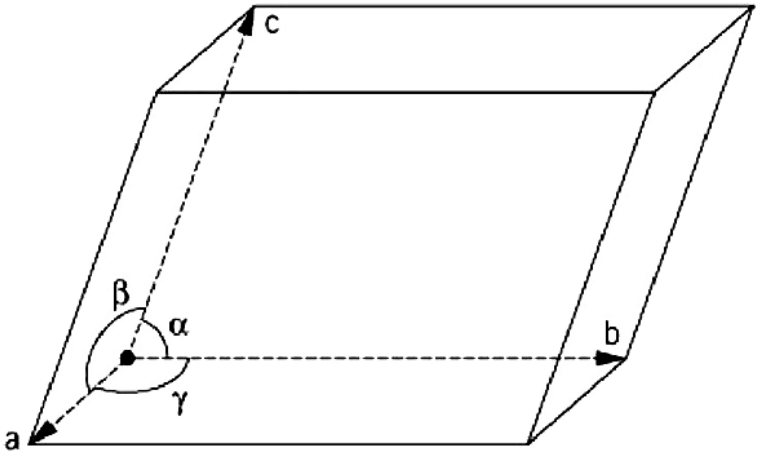

Figure 1-6: Basic crystallographic unit cell

One should note that a unit cell is described by the 3 lengths and 3 angles indicated in Figure 1-6. Graphites often contain multiple lattice structures due to impurities and non-ordered sections. Intercalation changes the dimensions of some of the unit cells in a structure as the unit cells expand to make space for the intercalant molecules. For this reason, GICs are described by additional unit cells to those of the graphites they are made from.

XRD is a technique used to directly quantify the success of intercalation or ion exchange reactions because it gives an indication of the unit cell dimensions in a structure. Seven crystal lattice systems exist and each is described by certain unit cell structures. This relationship is displayed in Table 1-4.

Table 1-4: Unit cell descriptions for each crystal lattice system

Crystal System		**Cell Parameters**
Triclinic		$a \neq b \neq c$; $\alpha \neq \beta \neq \gamma$
Monoclinic		$a \neq b \neq c$; $\alpha = \gamma = 90°, \beta \geq 90°$
Orthorhombic		$a \neq b \neq c$; $\alpha = \beta = \gamma = 90°$
Tetragonal		$a = b \neq c$; $\alpha = \beta = \gamma = 90°$
Trigonal	Hexagonal	$a = b \neq c$; $\alpha = \beta = 90°, \gamma = 120°$
	Rhombohedral	$a = b = c$; $\alpha = \beta = \gamma \neq 90°$
Hexagonal		$a = b \neq c$; $\alpha = \beta = 90°, \gamma = 120°$
Cubic		$a = b = c$; $\alpha = \beta = \gamma = 90°$

In order to describe planes and vectors in a crystal lattice, a notational system called the Miller indices exists. These indices are determined during XRD analysis and further describe the structure of a material analysed. Graphite has a hexagonal crystal system due to its aromatic molecular structure and is described by the cell parameters displayed in the fifth row of Table 1-5. Other crystal systems may exist within a graphite sample as perfect order in a specific crystal system is unlikely.

1-5 Flame retardants

1-5.1 Ignition and combustion

To ignite and sustain a flame there must be three key components present namely a fuel source, oxygen and an ignition source. The ignition source provides the activation energy to start oxidation. For a flame to sustain combustion, fuel and oxygen is required. Once the flame has been ignited the heat of reaction provides energy to the system which allows it to continue burning. At this point an ignition source is no longer needed.

1-5.2 Introduction to flame retardants

Flame retardants are additive chemicals or solid media which give resistance to ignition or inhibit the spread of flame in a medium. The medium for flame retardants can include textiles, coatings, thermosets, thermoplastics. In recent years, flame retardants have become essential additions to most polymers. This is due to the increased use of polymers in a wide variety of applications where flame retardant behaviour is favourable. The following are some examples of flame retardants (Davis & Huggard, 1996; Smith, 1984):

- Minerals such as aluminium hydroxide, borates and phosphorus compounds.
- Organohalogen compounds such as organochlorides, brominated polymers and antimony compounds.
- Organophosphorus compounds such as organophosphates, phosphonates and phosphinates.
- Halogen phosphorus compounds such as chlorophosphates.
- Exfoliating media such as vermiculite clays and EG.

1-5.3 Mechanisms of flame retardant action

In Table 1-5, some of the mechanisms of action for flame retardant media are discussed (Smith, 1984). An IFR is "a coating or component that swells up when heated thus protecting the material underneath or sealing a gap in the event of a fire" (Oxford dictionaries, 2011). One should note that an IFR has the flame retardant property of thermal shielding as defined in Table 1-5.

Table 1-5: Some flame retardant mechanisms

Property	Mechanism
Endothermic degradation	Heat is removed from the substrate via endothermic break down of compounds at high temperatures.
Gas phase radical quenching	Propagation of oxidation is slowed by producing radical halogens (due to thermal degradation) which have much lower energy than hydrogen and hydrate radicals.
Dilution of gas phase	Combustible gases are diluted by inert gases such as CO_2 and water vapour (released during thermal degradation) slowing the reaction rate of oxidation.
Thermal shielding	An insulation barrier is created between the polymer and the flame. This can either occur through charring of the polymer due to intumescent additives or via creation of an exfoliated surface.

1-5.4 Intumescent flame retardants

An IFR can generally be described as a substance which expands when exposed to a flame to form a foam barrier. Commercially available IFRs include components such as ammonium polyphosphate, pentaerythritol, melamine and EDAP. When a material undergoes combustion the flame retardant will form a char foam layer at the surface of the material to protect it (Shen & Schilling, 2012).

This foam creates a barrier between a flame and the IFR substrate which causes a thermal shielding effect and decreases transfer of oxygen to the flame both of which decrease the ability of the flame to be sustained. This causes a flame to burn at lower temperatures, to burn more slowly and even results in self-extinguishing in some cases.

1-6 Expandable Graphite

EG is a GIC with the ability to exfoliate when heated above a certain expansion onset temperature (T_O). EG may also be called graphite bisulfate $[C_{24}]^+ [HSO_4]^-$.

EG can be produced according to the method explained in section 2.3.2 i.e. chemically or via electrochemical methods where EG is produced through anodic oxidation of graphite in the presence of sulfuric acid. When studying EG or GIC production on a fundamental level, an electrochemical approach is much more attractive as it requires no addition of oxidants, is an easier method to optimise and delivers product with a lower excess ash and sulfur content. For a more in depth study on both galvanostatic synthesis and potentiostatic synthesis of graphite bisulfate (EG) one may consult Leshin, Sorokina and Avdeev (2004).

Non-intercalated graphite itself has some inherent exfoliation ability which occurs when heat and shear is applied. EG is a relatively inexpensive flame retardant compared to most industrial flame retardants used at this time. Although no definitive proof exists to validate this belief, the following is the believed mechanism of expansion for EG:
When the expansion onset temperature is reached, the bonds between the intercalant molecules and the graphite medium start to deteriorate and the distance between two consecutive layers increases. At this point the cross-plane interactions are removed and the GIC rapidly increases in volume due to the release of CO_2 and SO_2 gas within the GIC (Celzard *et al*, 2005). The release of gas within the medium increases the pressure between the intercalated layers sufficient to push the layers apart, parallel to the crystallographic c-axis, resulting in an exfoliated string shape (Greinke, 2003).

When a GIC is rapidly heated above T_O, irreversible exfoliation results and the GIC volume can increase by up to 300 times (Zou *et al*, 2009). Contrary to this, Celzard *et al* (2005) observed unique reversible exfoliation behaviour under certain conditions. This is due to the reduced heating rates and the fact that an insufficient maximum temperature is reached. At slow heating rates, the vaporisation in the GIC occurs at a much slower rate and lower pressures are produced between layers, resulting in lower exfoliation.

Equations 1-3 and 1-4 were formulated in order to calculate the dimensions of an exfoliated successfully intercalated EG layer (Zou *et al*, 2009).

$$A = 2\,\pi \cdot r \cdot h \tag{1-3}$$

$$V = \pi \cdot r^2 \cdot h \tag{1-4}$$

The symbols in equations 1-3 and 1-4 represent the following in the case of EG.

Symbol	Compound
h	Distance between two consecutive exfoliated EG layers
r	Radius of semi-circular layer
A	Edge area of an exfoliated EG layer
V	Volume of an exfoliated EG layer

The symbol A represents the area at the side of an expanded layer through which the created gases can escape during and after expansion. It should be noted that the amount of pressure build-up that can occur is directly related to V. The dimensions of the GIC therefore determine the maximum pressure build-up in between layers which in turn determines the maximum expansion of the GIC (Zou *et al*, 2009).

Figure 1-7 indicates the comparison of neat and exfoliated EG obtained through scanning electron microscopy (SEM). These images indicate the explosive expansion delivered by EG flakes which can expand from a thickness of 10 – 40 μm to 1 – 4 mm. The images in Figure 1-7 were compiled by combining multiple SEM micrographs obtained at the same magnification using Adobe Photoshop in order to indicate the relative size difference before and after exfoliation.

In order to allow intumescent behaviour, EG must be placed within a polymer medium under conditions which prevent structural break-up of the EG. This entails using a temperature range that is as low as possible and allowing little or no mechanical agitation using rotary blades. A popular method which meets these requirements is the process of rotomoulding (Crawford, 1996) but many other methods exist. After EG is inserted into the polymer medium, the principle of its flame retardant action is simply intumescent swelling of the material, allowing EG strings to expand, creating an insulating barrier. This slows down the oxidation rate on the surface of the polymer, which retards combustion sufficiently to allow increased time for external firefighting action to be taken (Morgan & Wilkie, 2007).

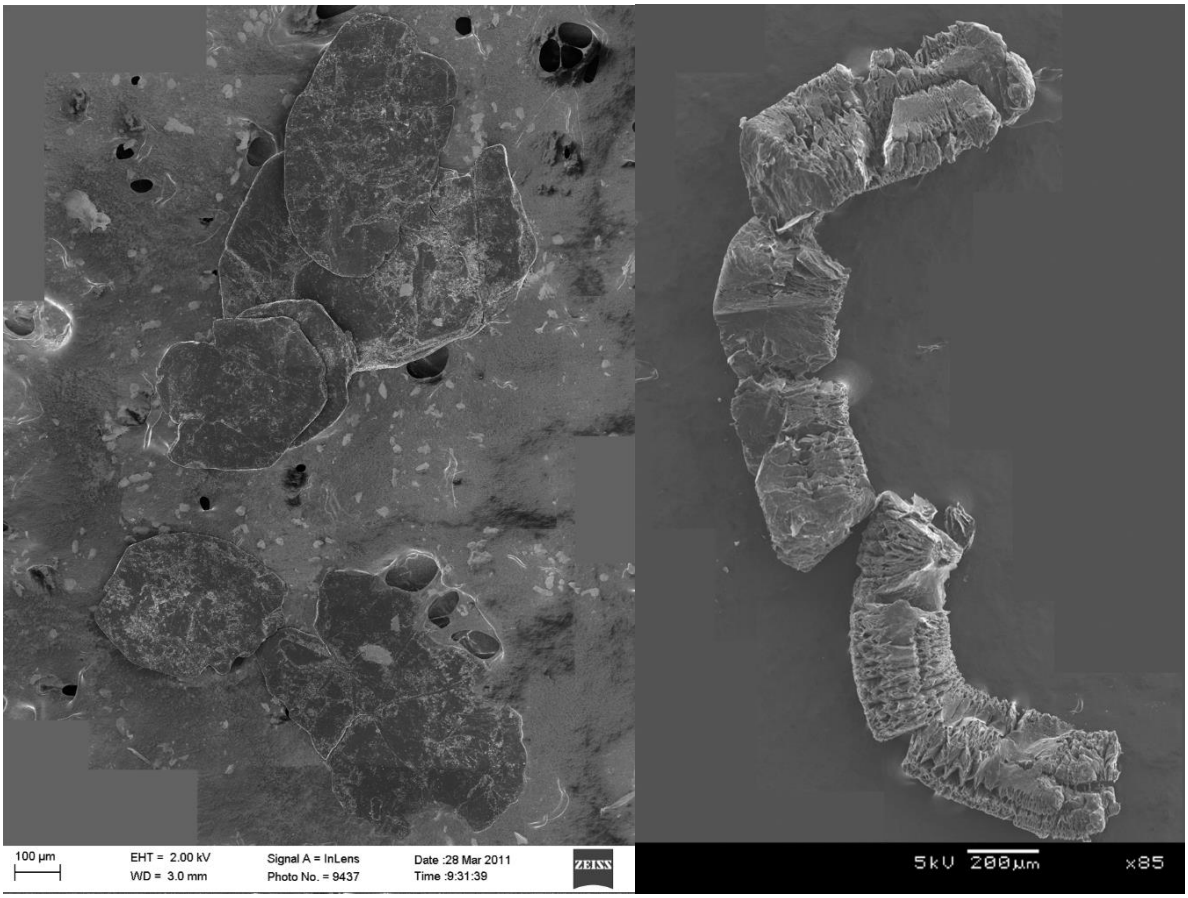

Figure 1-7: SEM micrographs of EG flakes and an expanded EG flake.

The major drawback of EG as a flame retardant is that it does not deliver uniform flame retardant behaviour in all directions. When EG expansion in a polymer medium is considered from below, gravity negatively affects the thermal shielding behaviour allowing higher oxidation rates at the bottom of the medium.

A recent study at the University of Pretoria utilised expandable graphite in a unique manner to produce a high quality novel graphite foam which this project contributed to (Focke *et al*, 2014b).

1-7 Characterisation methods for carbon materials

1-7.1 Overview of characterisation and testing techniques

Characterisation of a material allows one to fully quantify its mechanism of action and gives a greater understanding of the composition of the material. Throughout history, characterisation techniques have been employed to accurately identify the structure and properties of substances.

In the case of graphitic materials, characterisation is of utmost importance due to the wide variety of possible graphite origins, both natural and synthetic (Cunningham *et al*, 2005; Wissler, 2006; Zhao *et al*, 2006). A wide range of characterisation apparatus can be used to study graphite, but often only the behaviour relevant to the application of the material is studied. For this reason, only the techniques relevant to characterisation of GICs such as EG and its applications are mentioned in the sections that follow. GIC properties are dependent on the success and extent of intercalation achieved, and it is therefore important, when possible, to characterise both the raw graphite and altered material in order to determine the level of intercalation achieved.

1-7.2 Particle analysis techniques

Density, surface area and particle size measurement are all considered particle analysis techniques. In order to quantify the change in the structural parameters of an intercalated compound such as the GIC EG, it is important to characterise the structural parameters of both the unaltered graphite and the resulting GIC. This section discusses some of the techniques used to measure the density, surface area and particle size of a sample before and after an experiment such as intercalation has occurred. These properties also change significantly in EG when exfoliation occurs.

1-7.2.1 Particle density measurement

There is more than one type of material density that can describe a sample. The bulk density is the density of a volume of particles taking the inter-particle voids and the porosity of each particle into account. The skeletal density, or true density, of a material is the material density excluding the inter-particle voids and the particle porosity. The simplest form of density measurement is done by submerging a particle or set of particles in a fluid and measuring the volumetric displacement. Pycnometry is the general term for this type of measurement technique.

In modern pycnometers, a liquid, gas or even a solid powder can be used as the displaced medium. If the pores on a particle surface are larger than the particle/molecular size of the testing fluid used, then the true skeletal density is measured otherwise the measured density is only an approximation thereof. For this reason, the most popular pycnometry medium is helium gas which easily penetrates even the smallest pores. When one wants to measure the bulk density alone, a dry solid powder is used as the pycnometry medium (Ayral, Phalippou & Woignier, 1992).

1-7.2.2 Surface area measurement

Although liquid adsorption and many other surface area measurement techniques exist, gas adsorption is the most popular technique used today. An envelope surface area analyser (ESA) is a gas adsorption technique often used to determine the average particle size of a sample set of particles, by measuring the outside surface area alone. ESA utilises compressed air at room temperature within its apparatus as the adsorption gas (Sanders & Jena, 2000).

When the porous area of a material is desired, an ESA measurement does not suffice, but a technique called BET is often employed. Brunauer, Emmett and Teller developed and published a theory for surface area measurement in 1938. This theory is the basis for the surface area analysis technique BET, which measures not only the outside surface area of a particle but the internal area as well (Brunauer, Emmett & Teller, 1938).

As with all gas-adsorption surface-area-measurement techniques, BET employs the use of a gas with well-defined molecular dimensions for its analysis. BET uses compressed gas with a molecular size smaller than the pore size of a material. The most popular BET gas is nitrogen due to its inert properties and the fact that it is available at a high purity at a relatively low price.

In order to set up the equations used to calculate the BET surface area of a material, BET theory uses the following assumptions:

- It is possible for gas molecules to physically adsorb onto the entire surface of the layers within a particle and on the outside surface.
- Gas molecules adsorbed onto adjacent layers within the same sample do not interact.
- Gas molecules adsorbed onto a surface can be described by the Langmuir equation.

For BET to function, a clean particle surface is required, which is achieved by "outgassing" the particle at elevated temperature during the analysis procedure. The "outgassed" sample is then cooled under high vacuum in a liquid nitrogen bath. After cooling and pressurising the sample, the BET gas flows into the sample tube and moves towards the sample. Measurement data generated during analysis are reworked using a set of complex calculations, to determine the BET area. BET theory is complex but the analysis technique is relatively simple and applicable to a multitude of sample types and the results are highly reproducible (Brunauer *et al*, 1938). BET does however have some limitations (Groen, Peffer & Pérez-Ramírez, 2003), and when the pore size distribution of a graphite sample is desired, extremely complex equations and modelling approaches are often required (Lastoskie, Gubbins & Quirke, 1993).

1-7.2.3 Particle size distribution

The particle size distribution (PSD) of a sample of particles or flakes is the list of particle diameter values for the sample which can be represented in different ways dependant on the analysis technique used (Jillavenkatesa, Dapkunas & Lum, 2001).

The PSD of a sample is determined using particle size analysis techniques, of which several exist. Table 1-6 discusses some of the possible PSD analysis techniques and their performance when analysing graphite powders.

Table 1-6: PSD techniques

Technique	Method of analysis	Graphite use
Sieve analysis [a]	Set of sample particles are subjected to multiple sieves and vibrated	Minimum sieve size of 20 µm is often insufficient and graphite is generally difficult to sieve
Optical counting [a]	Using microscopic techniques, particle sizes can be visually measured using microscope scale	For large samples with wide size distribution such as graphites, technique can be very slow
Electro resistance counting [a]	Apparatus measures liquid conductivity (values relate to particle size) of a dispersed sample passing through an orifice	Effective for a range of sample types and especially for conductive samples such as graphites.

Sedimentation [a]	Terminal velocity theory is taken into account to relate settling time of a set of particles to their respective terminal velocities and particle sizes	Can be a lengthy technique and does not give accurate results for sample diameters lower than 1µm.
Laser diffraction [a]	A laser beam passes through a liquid dispersed sample and angles of diffracted light is measured and correlated to particle size.	A very popular method for many sample types including graphites.
Acoustic spectroscopy [a, b]	Also called ultrasound attenuation spectroscopy, it functions in a similar manner to laser diffraction but replaces light with ultrasound waves which are scattered and absorbed b	Can deliver more accurate results than laser diffraction but consists of a more expensive apparatus and more lengthy running times are often required.

[a] (Syvitski, 2007: 59-61) [b] (Dukhin & Goetz, 2004: 91-119)

Due to its widespread use and high accuracy, laser diffraction (which can also be called dynamic light scattering) is the most popular method for PSD determination. The underlying assumption for all PSD techniques is that a particle is spherical. When flake graphitic compounds are analysed using PSD a distribution similar to the one in Figure 1-8 is obtained. In this way, one can approximate the average particle diameter and thickness as both give rise to different light diffraction angles. PSD can be used to approximate the average thickness and diameter values of flake particles but is not perfectly accurate.

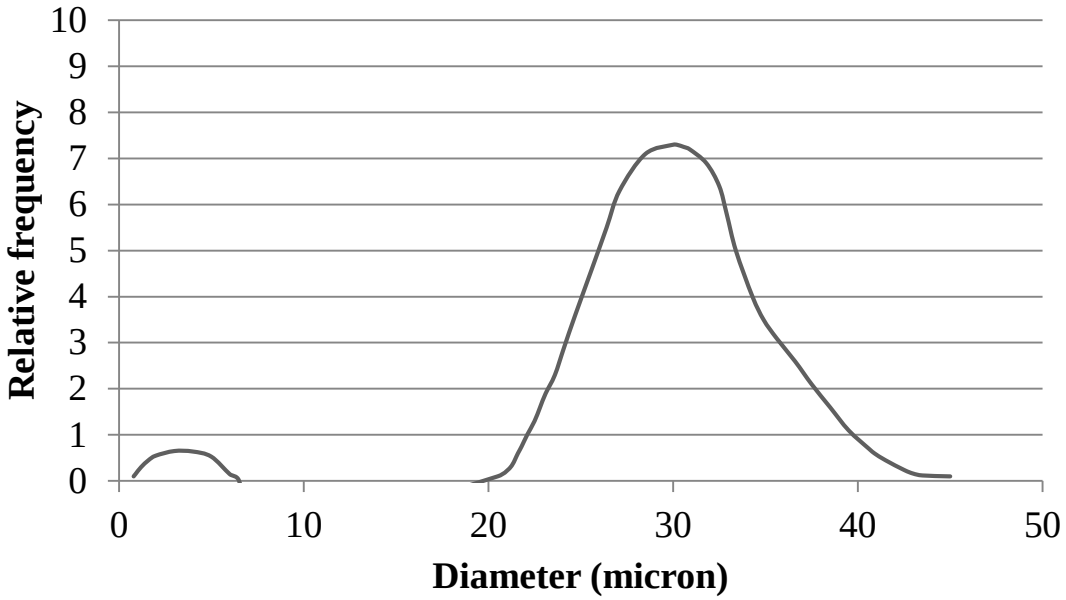

Figure 1-8: Sample graphite PSD result

1-7.3 Visual characterisation

1-7.3.1 Optical microscopy

Optical microscopy is the most simplified visual characterisation method that exists. When only macroscopic information is desired at lower magnifications, optical microscopy offers a quick and easy solution. For small samples such as flake graphites, this technique often delivers insufficient information and more advanced microscopy apparatus is used. As with most microscopy techniques, it is important that the samples be orientated perpendicular to the optical view direction as this delivers the best results. This is often difficult to achieve when analysing very small particles which tend to agglomerate.

1-7.3.2 Scanning electron microscopy

When higher magnifications are required, scanning electron microscopy (SEM) offers very good results. A basic scanning electron microscope can produce images of 60 000x magnification and up depending on the microscope used which allows one to visually inspect the surface and edges of a material more effectively. SEM generates images by bombarding the sample surface with a high energy electron beam and detecting the scattered electrons to produce a raster image of the bombarded area. For SEM to function, it is essential that the sample area be very conductive which is achieved by coating (sputter coat) non-conductive samples with highly conductive metals or, more commonly, carbon which can receive and scatter electrons (Akamatsu *et al*, 2010; Braun *et al*, 2005: 113-140; McMullan, 1995).

SEM images are grey scale raster images in which the colour intensity can indicate either topography or impurity as follows (Warner *et al*, 2009):

- Darker colours indicate flat surfaces which absorb more electrons
- Lighter colours can indicate angled surfaces where a higher degree of electron scattering occurred
- Lighter areas can indicate surface impurities of heavy elements.
- Darker areas can indicate surface impurities of lighter elements.

1-7.3.3 Field emission scanning electron microscopy

In order to overcome some of the limitations of normal SEM, field emission scanning electron microscopy (FE SEM) was developed which can deliver higher resolution and higher magnification images than conventional SEM (McMullan, 1995). Using FE SEM, images at magnifications upwards of to 350 000x can be generated. FE SEM uses a field emission gun to produce higher energy electron beams at lower diameters than the conventional SEM electron gun (Klusek, Datta & Kozlowski, 2003). FE SEM allows observations at a nano scale with the same reproducible results as conventional SEM. A drawback of FE SEM is that operation at very high magnification occurs at very low voltages, allowing limited surface penetration (Pawley, 1997).

1-7.3.4 Transmission electron microscopy

Transmission electron microscopy (TEM) generates extremely high magnification images at a molecular or atomic scale. In TEM, very thin samples are analysed by a high energy electron beam which shines through the sample, picking up scattered electrons on the opposite side of the sample. This technique, though ineffective for powders, can be used to analyse thin slivers removed from a graphite surface using a low thickness diamond cutter. The popularity of this technique is increasing at a rapid rate, and is commonly applied for all manner of samples today (Müller, Aebi & Engel, 2008).

1-7.4 Atomic and crystal structure characterisation

If one has a good understanding of both the crystal structure and physical molecular groups contained in a compound, it is possible to fully characterise the structure of a sample. This section discusses three of the most popular analysis techniques which can be used to gather this information.

1-7.4.1 X-ray diffraction

XRD is the best technique for determining the structural parameters and symmetries present within the crystal structure of GICs (Dresselhaus *et al*, 1981). XRD can deliver quantitative or qualitative results dependant on the testing conditions. When only qualitative results are desired, samples can be placed in a preferred orientation but this does not allow one to take all lattice orientations into account. When samples are milled into a powder form, it is possible to observe all orientations of the same lattice and quantitative results can be measured. Qualitative results are sufficient to determine a change in the d-spacing between two GIC layers allowing one to gauge the success of intercalation.

During XRD analysis a beam of x-rays strike the sample and are diffracted in multiple directions. At this point, diffracted rays undergo both constructive and destructive interference. This takes place as displayed in Figure 1-9.

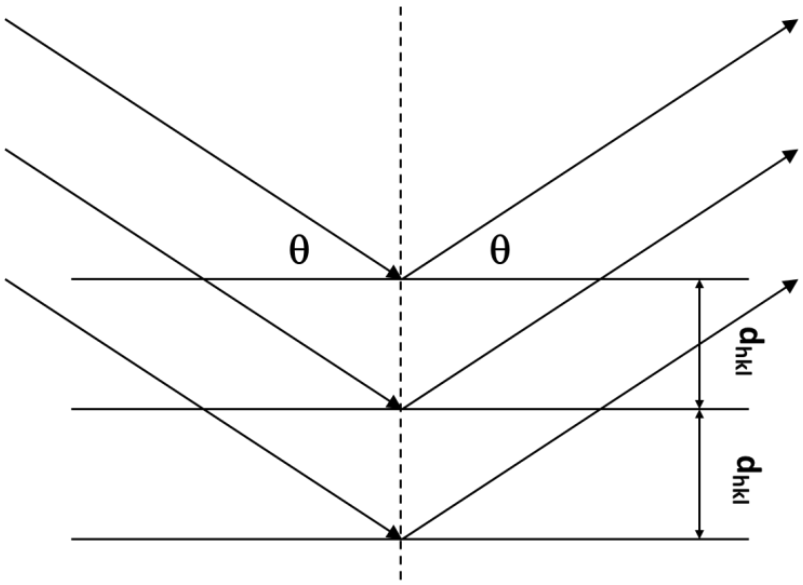

Figure 1-9: X-Ray scattering on a crystalline sample

The intensities and angles of these rays are then measured and used to determine the 3-dimensional angles and dimensions of the crystallographic unit cells which describe the sample. In order to calculate these values, Bragg's law (Parthasarathy, Sreedhar & Chetty, 2006), represented by equation 1-5, is used:

$$2d_{hkl} \sin\theta = n\lambda \tag{1-5}$$

The Symbols in equation 1-5 represent the following:

Symbol	Meaning
d_{hkl}	Distance between two diffracting lattice planes
θ	Angle of the incident beam
n	An integer value
λ	Beam wavelength employed

Figure 1-10 displays a sample XRD output for a crystal analysed between θ = 87° and θ = 96° with both Kα and Kβ peaks present for two distinct peaks.

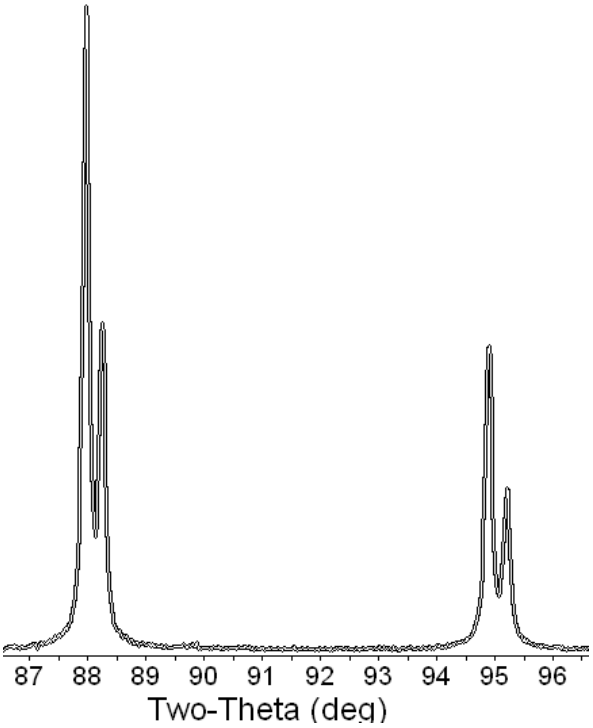

Figure 1-10: Sample XRD output over a range of theta values

Using the angles at which peaks were measured, one can determine which Miller indices each peak represents. The relative intensities of peaks which correspond to the same unit cell can be used to calculate the dimensions of the unit cell. This process can be repeated over a wide range of incident angles to quantitatively analyse the crystal structure of the entire sample. This process is not always accurate as peaks often coincide with one another and cannot always be separated (Parthasarathy *et al*, 2006).

1-7.4.2 Raman spectroscopy

Although similar, Raman scattering and absorption scattering are not to be confused with one another. Absorption of energy from a photon excites the atoms within a molecule to a discrete energy level above ground state. When the molecule returns to its ground state, it releases a photon (fluorescence) which can be detected. With Raman, excitation changes the vibrational and rotational state alone and releases photons when it returns to its original state. The energy of the photons released in this manner is measured and their wavelengths recorded. Raman spectroscopy operates in the visible to ultraviolet wavelength range alone, allowing measurements within a limited range of excitation wavelengths. The light employed utilises electromagnetic radiation to achieve excitation (Lyon *et al*, 1998; Murty & Seshadri, 1942).

The shift in wavelength between the emitted beam and a wavelength recorded is called the Raman shift wave number. The peak wavelengths detected in this manner indicate the rotational and vibrational states of the molecules contained within a sample. Wavelengths and Raman intensity generated in this manner are generally plotted against one another in what is called the Raman spectra of a sample. The Raman spectra of a sample can then be compared to a database to determine the meaning of each peak. Each wavelength is characteristic of a specific functional group and allows identification of the functional groups present in a sample. This allows one to determine to some degree what the complete molecular structure of a compound is (Dresselhaus *et al*, 2010). Raman spectroscopy can deliver results that are either quantitative or qualitative depending on the testing conditions and the composition of the sample tested. These results can be very inaccurate however, when there are high levels of surface impurities adsorbed onto a sample (Nikiel & Jagodzinski, 1993).

1-7.4.3 Fourier transform infrared spectroscopy

Fourier transform infrared spectroscopy (FTIR) is a method similar to Raman spectroscopy, but it utilises IR light wavelengths for excitation. The detection apparatus employed in FTIR is very complex and difficult mathematical techniques such as Fourier transformation mathematics are required to change the measured data into wave-number data and determine the absorption of light achieved at each wavelength. Generally, the level of absorption at a certain wavelength is characteristic of a specific atom or molecule, giving each compound a unique spectral response. After analysis, the obtained spectra can be analysed according to a database, to determine which compounds are present in the sample. FTIR also allows identification of some of the bonds present in a material as their spectra are also characteristic of the atoms present, their hybridisation state and their bond type (McCool, Murphy & Tripp, 2006; Sudha *et al*, 2011). FTIR and Raman spectroscopy function very well together as they operate in different wavelength regions, allowing amalgamation of results and better characterisation of a sample (Chen *et al*, 2013).

1-7.5 Compositional analysis

A multitude of compositional analysis techniques exist that allow one to determine the atomic composition of a sample. Having this information provides a much better understanding not only of the main building blocks of the sample structure but also of the trace elements present. If an engineered material does not function in the manner intended, the deviation can often be attributed to the trace elements contained within the compound. Some elements, even in trace amounts, can vastly change the properties of a material making compositional analysis techniques an essential part of the characterisation process.

1-7.5.1 Inductively coupled plasma – mass spectrometry

ICP-MS uses argon plasma at extremely high temperature (>10000 K) to completely ionise a sample. The argon plasma is generated by a high frequency induction coil. The individual ions generated are then sent through a mass spectrometer which has been calibrated according to standard concentrations of the elements which one wants to measure. MS measures the charge for each of the ions measured and relates this to the concentration of said compound in the sample (Jarvis, Gray & Houk, 2003: 135).

1-7.5.2 X-ray fluorescence

Fluorescence is defined as the phenomenon where an atom or molecule is subjected to radiation of a certain amount of energy which excites said molecules or atoms which then release radiation with a different amount of energy when the electrons relax to a more stable orbital. In x-ray fluorescence (XRF) a sample is bombarded with high energy x-rays which excite the molecules in the sample as with Raman spectroscopy and FTIR but in this case measures the characteristic secondary fluorescence (x-ray) emission from the sample. This fluorescence is released as demonstrated in Figure 1-11.

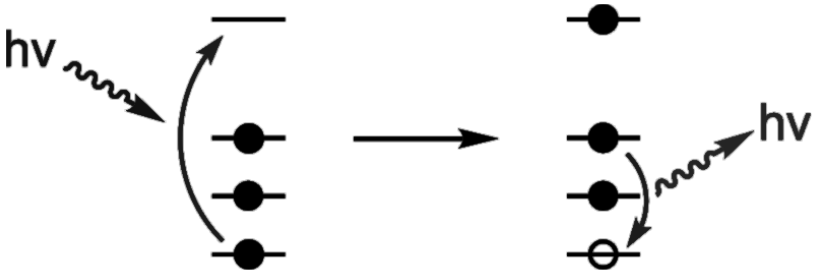

Figure 1-11: X-ray fluorescence generation during XRF analysis

This analysis technique allows measurement at a depth below 100 micron, into the sample surface, with variation according to X-ray incident wavelength and energy. It is therefore essential that the sample surface be clean of surface impurities which can negatively influence the accuracy of results or give results uncharacteristic of the entire sample (Brundle, Evans & Wilson, 1992).

XRF generally allows identification of atoms of greater size than oxygen preventing complete atomic characterisation but the low detection limit of XRF (in the ppm range) makes it a powerful characterisation technique for bulk analysis (Beckhoff *et al*, 2006).

1-7.5.3 Elemental analysis - gas chromatography coupled with conductivity measurement

One can determine the carbon (C), hydrogen (H), nitrogen (N) and sulfur (S) elemental composition of a compound by using the following method: first one measures the charge conductivity over a sample, which is influenced by the amount of each of the aforementioned atoms contained within the sample. One then combusts the sample at a low mass and very high temperature in order to fully oxidise and disperse the atoms contained within the sample into a gaseous form. This gas is fed through Gas chromatography (GC) or less commonly MS, which analyses the gas to give a breakdown of the atomic content.

When coupled together, these 2 techniques can give very accurate results and allow a partial elemental characterisation to be done (Perry & Green, 2007: 8-62). This technique is useful when analysing GICs and the graphites they are comprised of as the ratio between these elements, particularly between C and S, can change to a large degree during intercalation, especially with EG.

1-7.5.4 Energy dispersive x-ray spectroscopy

Energy dispersive x-ray (EDX) spectroscopy functions in a very similar manner to XRF in that it creates excitation in the molecules of a sample and measures the energy emitted when the molecules return to their ground states. The mechanism of excitation and detection is quite different though. High energy electrons in an electron beam bombard the sample and excite the atoms in the sample, ejecting an electron from an electron shell.

An electron from one of the other shells falls into the position of the ejected electron, and depending on the shell which it falls from, releases a characteristic alpha (α) wave as indicated in Figure 1-12. The α waves emitted from the sample are detected and compared to a database to identify the atomic composition of the sample (Feng, Bhatia & Barry, 2002).

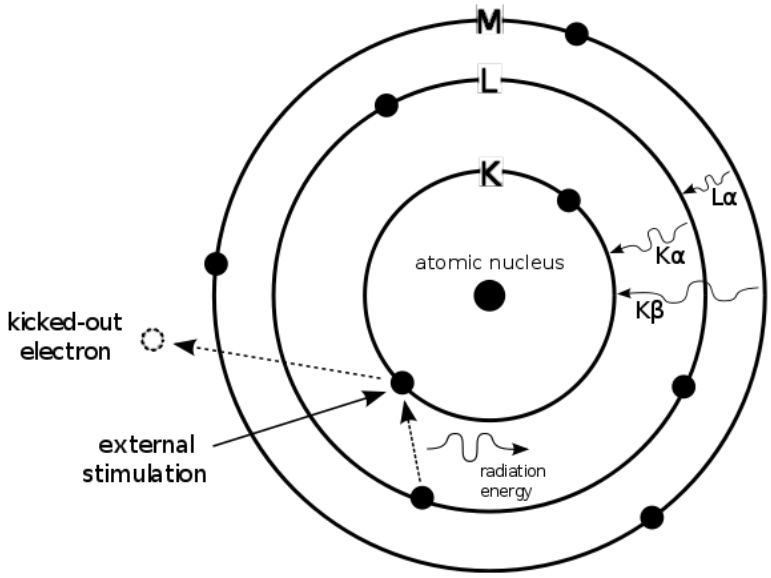

Figure 1-12: X-ray emission on an atomic scale in EDX analysis

EDX is generally combined with SEM, as both methods utilise similar hardware. When one switches to EDX operation on a SEM, one simply has to increase the operating voltage and identify regions on the sample for EDX analysis. The electron beam bombards each of the areas selected and utilises computer software to identify the elements detected. An example of an EDX spectrum is displayed in Figure 1-13.

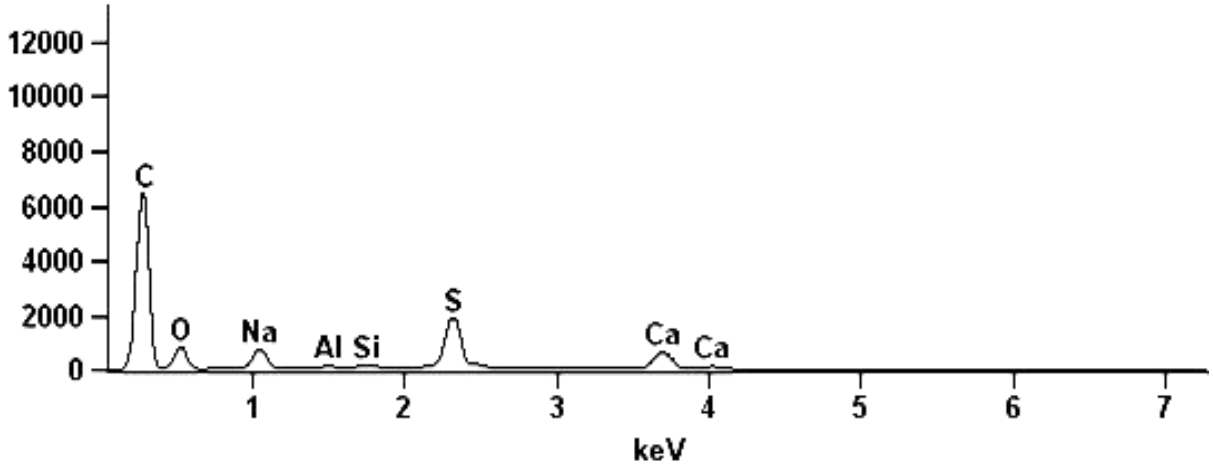

Figure 1-13: Example EDX spectrum

1-7.6 Thermal analysis techniques

Thermal analysis techniques allow one to measure physical changes in a sample subjected to a specific thermal profile. One can characterise the thermal properties of a sample using these techniques by varying testing conditions and observing the results of such changes. In this section, two of the most powerful thermal analysis techniques are discussed.

1-7.6.1 Thermomechanical analysis

Thermomechanical analysis (TMA) allows one to determine the thermal expansion onset temperature of EG, making it one of the most important analysis techniques in the characterisation of EG. TMA, as with most thermal analysis techniques including thermogravimetric analysis, occurs at a thermal ramp rate pre-set by the operator. TMA allows one to measure certain mechanical properties of a sample such as thermal expansion as a function of temperature (Reinheimer, Wenzel & Muenzenberger, 2009). A small amount of sample is generally used (ca. 8 mg) and a small load force (set by the user in Newtons) is applied to the sample through the probe used (e.g. a macro-expansion probe).

During EG thermal analysis, the use of a TMA macro-expansion probe is employed to measure the physical thickness of the sample. The temperature in the test chamber is also continuously monitored using a thermocouple. When EG is heated above T_O, expansion occurs according to the mechanisms mentioned in section 2.5.

The TMA continuously records this change in sample thickness and the corresponding sample temperature where this change occurs. Typically, TMA results are graphically displayed as a comparison of sample expansion ratio to temperature. The expansion ratio at any point can be calculated by division of the sample thickness by the original sample thickness. The smaller the increments of increased temperature, the more accurate the results will be. T_O for the sample can be graphically determined in the manner displayed in Figure 1-14. The results obtained can also be plotted as the derivative in order to show changes in the gradient of sample length versus temperature more clearly.

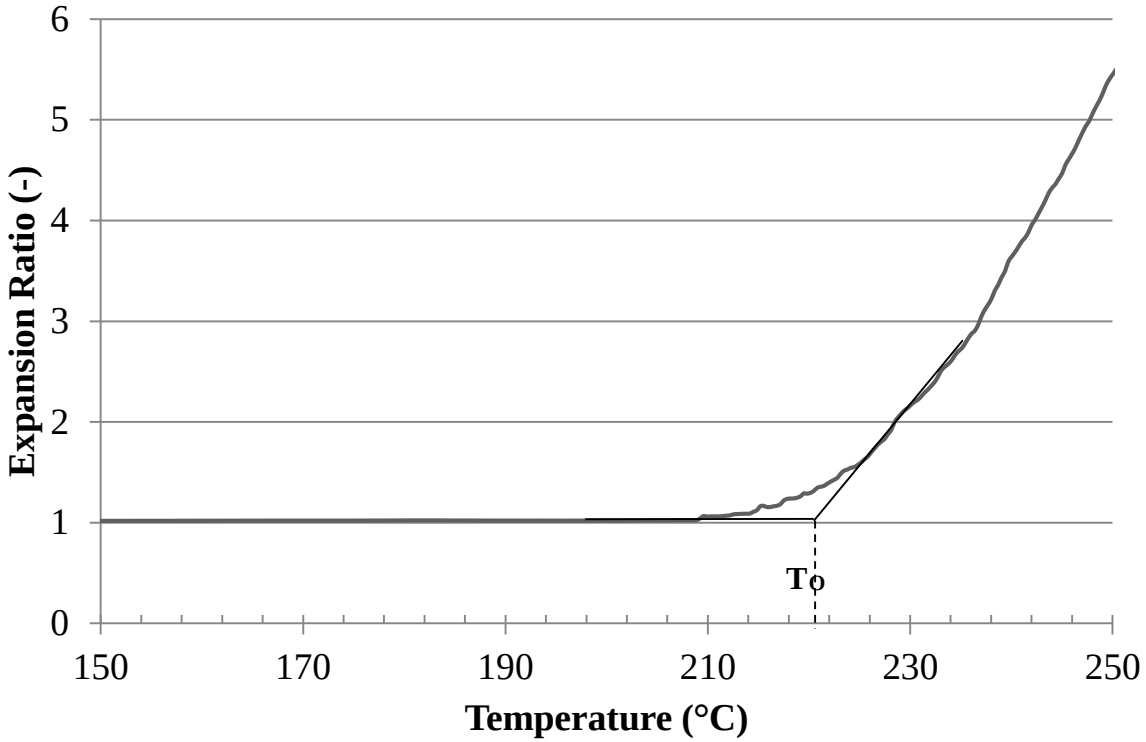

Figure 1-14: Sample EG TMA graphical results

1-7.6.2 Thermogravimetric analysis

Thermogravimetric analysis (TGA) allows one to measure changes in the mass of a sample as a function of temperature changes preselected by the operator. The sample analysed is placed within a temperature controlled furnace during analysis and a chosen gas is pumped at a low flowrate through the test chamber. By selecting the appropriate analysis gas medium, one can allow oxidation under inert, atmospheric or a multitude of other conditions (Soares *et al*, 1997).

During TGA, sample temperature is monitored using a well-placed thermocouple and sample mass is accurately measured through a calibrated counterweight. Continuous measurements are taken over the entire analysis period and stored.

TGA can be used to determine the water content of a sample, the ash percentage after full combustion and a multitude of other characteristic information about a sample. If one analyses an EG sample for instance, one can determine the following information:

- mass loss after all water contained in the sample is evaporated
- mass loss after complete expansion of the EG
- mass remaining after complete oxidation (ash content of sample) which relates directly to the mass fraction inorganic impurities in the sample.

Chapter 2: Characterisation of commercial expandable graphite flame retardants

Foreword

This chapter contributed to the publication:

- *Characterization of commercial expandable graphite flame retardants (Focke et al, 2014a)*

This chapter and publication acknowledges contributions from the following persons:

- *Walter Wilhelm Focke, Heinrich Badenhorst, Washington Mhike, Dewan Lombaard*

Executive summary

Thermal analysis and other techniques were employed to characterise two EG samples. The expansion onset temperatures of the EG samples were ca. 220 °C and 300 °C respectively. The key finding is that the commercial products are not just pure GICs with sulfuric acid species intercalated as guest ions and molecules in between intact graphene layers. A more realistic model is proposed where graphite oxide-like layers are also randomly interstratified in the graphite flakes. These graphite oxide-like layers comprise highly oxidised graphene sheets which contain many different oxygen-containing functional groups. This model explains the high oxygen to sulfur atomic ratios found in both elemental analysis of the neat materials and in the gas generated during the main exfoliation event.

Keywords: graphite, expandable graphite, characterisation, graphite oxide

2-1. Introduction

Natural flake graphite is a layered mineral made up of stacked graphene sheets of covalently bonded carbon atoms (Chung, 2002a; Wissler, 2006). Due to the anisotropic nature of graphite it possesses high but non-uniform electrical conductivity. It is high in the in-plane direction but much lower in the direction perpendicular to the graphene layers (Chung, 2002a).

Graphite oxide (GO) is a highly oxidised and disordered form of graphite that contains carbon, oxygen, and hydrogen in variable ratios (Chua, Sofer & Pumera, 2012; Chung, 2002a; Dreyer *et al*, 2010; Hummers Jr & Offeman, 1958). It is synthesised by exposing flake graphite to concentrated sulfuric acid in conjunction with strong oxidisers such as nitric acid or potassium permanganate (Chua *et al*, 2012; Hummers Jr *et al*, 1958). Mermoux and Chabre (1989) contend that GO is obtained via hydrolysis of an intermediary compound formed through over-oxidation of a GIC. GO retains the lamellar structure of the parent graphite but with a much larger and irregular basal spacing (d_{002} between 0.562 nm and 0.902 nm (Nakajima, Mabuchi & Hagiwara, 1988)) owing to the presence of oxygen-containing groups (Hummers Jr *et al*, 1958). The nature of GO is not well defined but it is believed that it has enol, keto and epoxy functional groups randomly attached to the graphene sheets (Dreyer *et al*, 2010). Depending on the synthesis method, the oxygen content can range from 44 wt.% to 56 wt.% and the carbon to oxygen ratio from about 1.0 to 1.6 (Chua *et al*, 2012; Hummers Jr *et al*, 1958). Owing to the highly oxidised nature of the graphene sheets, GO is able to act as an insulator (Chung, 2002a).

GICs possess guest molecules inserted (intercalated) between the graphite layers (Dresselhaus *et al*, 1981). The graphite layers in these complex materials remain largely intact with the guest molecules or atoms (X) located in between graphene layers. The actual composition varies on a layer by layer basis as not every layer becomes intercalated. This phenomenon is called staging and a stage *n* compound will have *n* graphite layers with no guests in between them for each intercalated layer. In other words, the stage number *n* is simply the number of graphene layers sandwiched between successive intercalant layers.

This means that in a Stage 1 (or first stage) compound the graphite layers and intercalant layers alternate perfectly. Such compounds may be described by the formula XC_y.

Graphite bisulfate is a Stage 1 lamellar compound (d-spacing of 0.397 nm) which possesses a blue hue (Inagaki, 1966; Rüdorff, 1959). The composition of the Stage 1 compound is stated as $C_{24}^{+}\cdot HSO_4^{-}\cdot 2H_2SO_4$ (Leshin *et al*, 2004; Sorokina *et al*, 2005). Graphite bisulfate may be produced electrochemically (Leshin *et al*, 2004) or by dipping natural graphite in concentrated sulfuric acid with sufficient nitric acid to oxidise the graphite to prepare it for intercalation (Inagaki, 1966).

Graphite bisulfate, however, is highly unstable and decomposes if a small amount of water is added to the acid or if the blue compound is exposed to air. One may observe the breakdown of graphite bisulfate exposed to moist air over time by following the change in its XRD patterns. Ultimately, breakdown of graphite bisulfate results in a residue with a very broad XRD reflection at a d-spacing of 0.339 nm (Inagaki, 1966). It appears to be a mixture of various higher stages of sulfuric acid intercalated graphite. Hennig (1951) suggested that the composition of the degraded residue can be approximated by $C_n^{+}\cdot HSO_4^{-}\cdot 4H_2SO_4$ with impurities distributed in a state of high disorder.

Industrial-scale synthesis of EG utilises liquid-phase graphite – sulfuric acid reactions in the presence of strong chemical oxidants such as $KMnO_4$, HNO_3 and H_2O_2 (Sorokina *et al*, 2007). At this scale it is, in effect, produced in a similar fashion to GO. The parallels between the production methods for GO and graphite bisulfate imply the possibility that both compounds may be formed during expandable graphite production.

According to Camino *et al* (2001b), EG is equivalent to a staged version of a graphite-sulfuric acid salt, i.e. the graphene layers all remain intact while bisulfate ions are intercalated between these layers. Talanov, Melezhik and Chuiko (1993), however, suggests that EG is obtained via hydrolysis of graphite bisulfate, implying that it is a less well-ordered material than its graphite bisulfate progenitor.

The key property of EG is its tendency to exfoliate when heated to high temperatures beyond a characteristic expansion onset temperature. During exfoliation it expands rapidly in a worm-like manner to form vermicular graphite with a low density (Chung, 1987; Chung, 2002a; Wissler, 2006). The exfoliation process is an endothermic event and the expansion follows ideal gas law behaviour. According to Chung (1987) the origin of this process lies in the vaporisation of the intercalant.

EG and its exfoliated form may be used in numerous applications (Chung, 1987). These include gaskets; seals and packings; fire extinguisher agents; thermal insulators; electrodes; for the production of high thermal conductivity graphite sheets; etc. (Chung, 1987).

EG may act as an IFR for some polymers (Chen & Wang, 2010; Nakagawa, 2006; Schartel *et al*, 2003; Seefeldt, Braun & Wagner, 2012; Weil, 2011; Weil *et al*, 2008) with polyethylene (Qu & Xie, 2003b) and polyurethane foams being the primary substrates for EG (Camino *et al*, 2001b; Nakagawa, 2006).

EG possesses similar in-plane electrical conductivity to natural flake graphite (Zheng, Lu & Wong, 2004). This means that it could impart both antistatic and thermal conductivity (Mortazavi *et al*, 2013) in addition to flame retardant properties to polymers (Mhike & Focke, 2013). Natural graphite and EG therefore possess the ability to impart both electrical and thermal conductivity into their polymer substrates while also improving flame retardant properties. This investigation and its associated projects aim to explore the use of these additives in a variety of applications ranging from flame retardants to heat storage materials (Focke *et al*, 2014c; Kruger *et al*, 2014; Mhike *et al*, 2013; Mhike *et al*, 2012). The specific objective of this particular study was to perform a comprehensive characterisation of two commercial EG grades used in industrial polymer applications. The aim was to gain a better understanding of the true nature of EG grades used in industry. Finally, this communication complements previous studies that have investigated the thermal properties of graphite bisulphate (Leshin *et al*, 2004; Skoropanov *et al*, 1985).

2-2. Experimental

2-2.1 Materials

Two grades of EG, ES 250 B5 (onset temperature 220°C) and ES170-300A (onset temperature 300°C), were obtained from Qingdao Kropfmuehl Graphite (China). Milled natural Zimbabwean flake graphite was supplied by BEP Bestobell (South Africa). Exfoliated graphite forms were prepared at a temperature of 600 °C by placing the EG powder samples in a Thermopower electric furnace.

2-2.2 Particle size, BET surface and density determination

The graphite particle size distributions were determined with a Mastersizer Hydrosizer 2000MY (Malvern Instruments, Malvern, UK). The specific surface areas of the graphite powders were determined. BET surface areas were measured on a Micromeritics Flowsorb II 2300 and a Nova 1000e BET instrument in N_2 at 77 K. Densities were determined on a Micrometrics AccuPyc II 1340 helium gas pycnometer.

2-2.3 Thermogravimetry

TGA was performed using the dynamic method on a Mettler Toledo A851 TGA / SDTA instrument. About 5 mg powder was placed in an open 150 µL alumina pan. Temperature was scanned from 25 to 1000 °C at a scan rate of 10 °C/min with air or N_2 flowing at a rate of 50 mL/min

2-2.4 Composition of evolved gases

Approximately 50 g samples of EG were placed in a graphite crucible. They were heated in a Thermal Technologies® high temperature graphitising furnace. The temperature was ramped up at a rate of 1 °C/min starting from 100 °C and ending at 600 °C. Helium was passed through the furnace at a flow rate of 0.1 L/min. A Teledyne PEM9004 portable emissions analyser was used to determine the concentration of SO_2 in the flue gas stream as a function of temperature.

The overall composition of the gases evolved during exfoliation was determined as follows:

Approximately 3 g samples of EG were placed in a sealed reaction vessel in a Thermopower furnace. The temperature was ramped up at a rate of 5 °C/min starting from 100 °C and ending at 600 °C. A sample gas bag was connected to the reactor purge line. The gases emitted from the process were trapped in SKC Flexifilm gas bags. Gas analysis was performed using GC by a SANAS accredited laboratory.

2-2.5 Graphite composition determinations

Elemental analysis was performed on a Thermo Scientific Flash 2000 CHNS Elemental Analyser with the furnace temperature set at 900 °C. The sulfur content was also checked using an Eltra CS-580 analyser.

The elemental composition of the inorganic part of the graphite powders was also measured using XRF analysis performed using a wavelength-dispersive spectrometer (ARL 9400XP+ XRF). The samples were prepared as pressed powder briquettes and introduced to the spectrometer. The powders were also ground in a tungsten carbide milling vessel and roasted at 1000°C for determination of the loss on ignition.

2-2.6 Ion exchange

EG grade ES250 B5 (43.2 g) was successively suspended in fresh portions of ca. 150 g of 27.4 wt.% diammonium phosphate (DAP) solution. The suspension was left to stand for one day before the EG was separated by filtration for further suspension in a fresh portion of the DAP solution. This procedure was repeated four times. After the final treatment, the graphite was thoroughly washed with deionised water. The recovered liquid filtrates and wash water were analysed for sulfate and phosphate to determine the amount of sulfate ions exchanged and the quantity of phosphate ions intercalated.

2-2.7 Thermomechanical analysis

Thermal expansion measurements were conducted on a TA Instruments Q400 Thermo Mechanical Analyser. Sufficient powder was placed in an alumina sample pan such that the bed height was between 35 µm and 40 µm. The flake expansion behaviour was measured with a flat-tipped standard expansion probe using an applied force of 0.02 N. The temperature was scanned from 30 °C to 1000 °C at a scan rate of 10 °C/min in nitrogen atmosphere. The expansion relative to the original powder bed height was reported.

2-2.8 X-Ray diffraction

XRD diffraction patterns were recorded using a Bruker D8 Advance powder diffractometer fitted with a Lynx eye detector. Measurements were performed in the 2θ range 15 - 120° with a 0.04° step size and a counting time of 0.2 s. The interlayer spacing, d_{002}, calculated using the Bragg equation, was used as an indicator for the extent of ordering.

2-2.9 Raman spectroscopy

The Raman spectra were recorded with a T64000 series II triple spectrometer system from HORIBA Scientific, Jobin Yvon Technology using the 514.3 nm laser line of a coherent Innova®70 Ar^+ laser with a resolution of 2 cm^{-1} in the range 1200 to 1700 cm^{-1}. The samples were recorded in a backscattering configuration with an Olympus microscope attached to the instrument (using a LD 50x objective). The laser power was set at 6 mW and a nitrogen-cooled CCD detector was used. The accumulation time was 120 s and the spectra were baseline corrected with using LabSpec software.

2-2.10 Scanning electron microscopy

Graphite morphologies were studied using a JEOL JSM 5800LV SEM for low resolution micrographs and an ultrahigh resolution FE SEM (HR FE SEM Zeiss Ultra Plus 55) for high resolution micrographs. An InLens detector at an acceleration voltage of 1 kV was used to ensure maximum resolution of surface detail. No electrically-conductive coating was applied to the graphite particles. Microanalysis was performed with a Thermo Scientific NanoTrace X-ray detector. This analysis was performed with the microscope magnification at 750× and an accelerating voltage of 20 kV.

2-3. Results

2-3.1 Graphite particle characteristics

Figure 2-1 shows the particle size distribution of the various graphite types used. The d_{50} particle size of the natural flake graphite was almost five times lower than that of the two expandable graphite grades. The d_{10}, d_{50}, and d_{90} particle sizes, BET surface area, and densities of the different graphite samples are presented in Table 2-1.

The surface area of the ES170-300A EG samples increased by a factor of twenty two when it expanded during heat treatment at 600 °C. The surface area of the neat ES250 B5 could not be determined however, as it started to exfoliate during BET measurement attempts. The substantial increase in surface area of the EG after exfoliation is attributed to the accordion-like exfoliation of the material which exposes a much larger area of the graphitic structure that is exposed during this expansion.

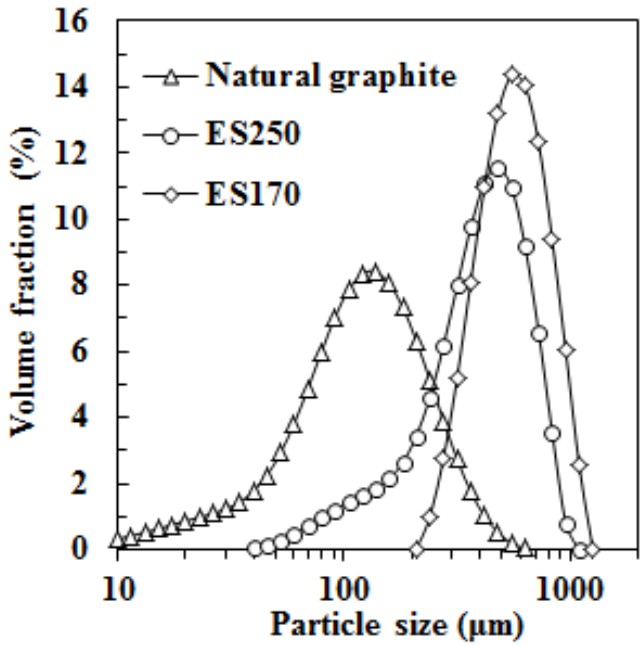

Figure 2-1: Particle size distribution of the various graphite samples

Table 2-1: Physical properties of graphite powders

Graphite type	D_{10}, µm	D_{50}, µm	D_{90}, µm	Surface area, m^2 / g	Density, g / cm^3
Zimbabwean graphite	37.5	112	241	3.72 ± 0.70	2.34 ± 0.01
ES 250 B5	306	517	803	n.d.	2.08 ± 0.01
ES 250 B5 (expanded)	-	-	-	22.4 ± 2.8	-
ES170-300A	313	533	807	0.66	2.23 ± 0.01
ES170-300A (expanded)	-	-	-	14.84 ± 0.14	-

Figure 2-2 indicates the flake-like nature of the natural and expandable graphite. The EG samples in Figure 2-2 have worm-shaped, accordion-like structures. Slit-shaped gaps between the graphite platelets are clearly visible in the high resolution micrographs.

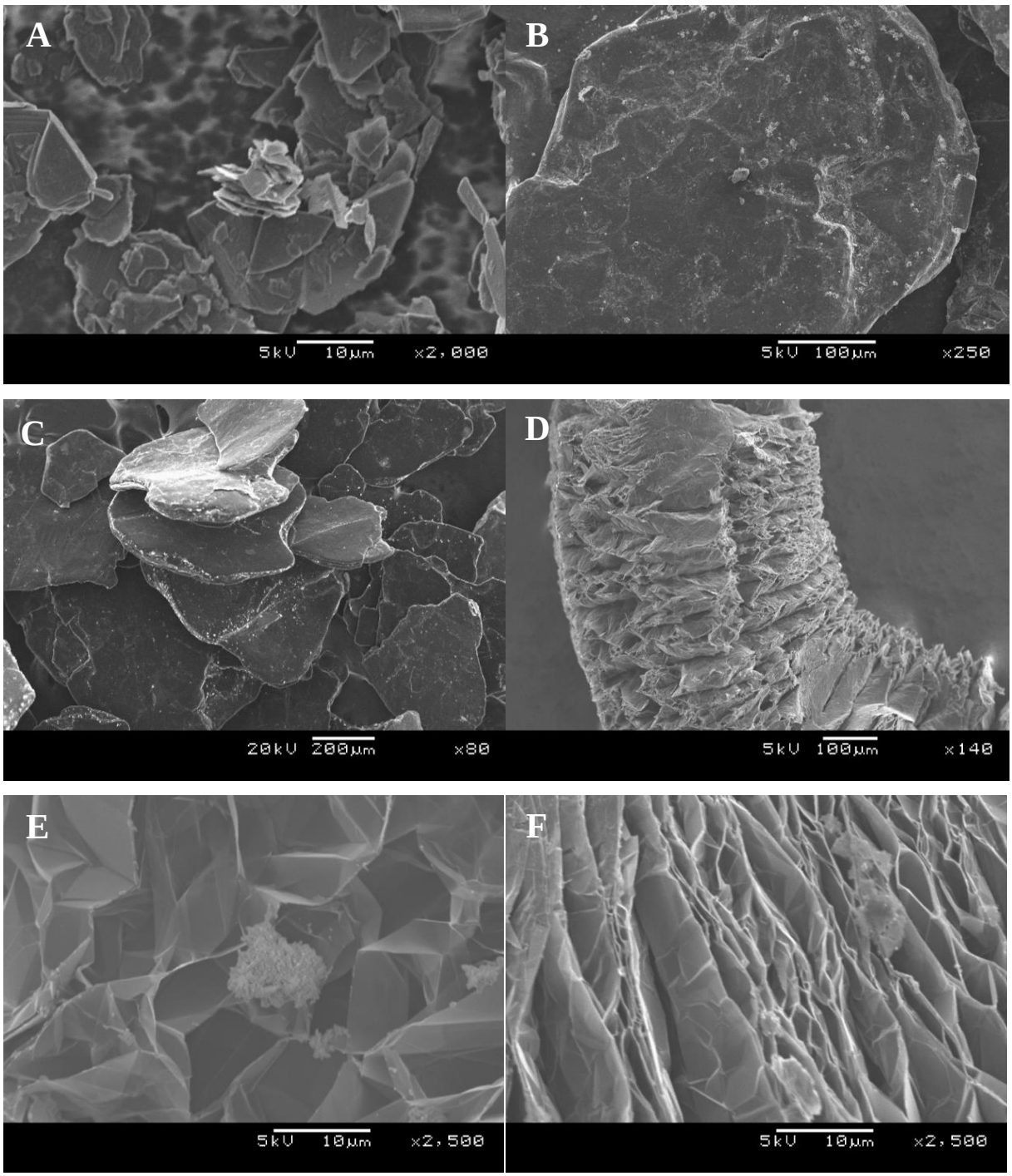

Figure 2-2. SEM micrographs of and graphite samples: (A) Natural Zimbabwean graphite; (B) Expandable graphite ES250 B5; (C) Expandable graphite ES170-300A; (D) Expanded graphite ES250 B5 (low resolution), (E) Expanded graphite ES170-300A (high resolution), and (F) Expanded graphite ES250 B5 (high resolution)

The microstructures of the expanded worms are built up of distorted graphite sheets. It is possible to consider these worms to be comprised of several discrete flake remnants with a thickness distribution. Owing to their very high aspect ratios, the average thickness of these sheets can be estimated from the BET surface area using equation 2-1.

$$t = 2/\rho A \qquad (2\text{-}1)$$

Where:

t is the average sheet thickness in m

ρ is the density in kg . m^{-3}

A is the BET surface area in m^2 . kg^{-1}.

Note that equation 2-1 neglects the edge surface area of the flakes. Applying this equation to the EG samples yields average flake thicknesses of 40 nm and 60 nm for ES250 B5 and ES170-300A respectively. This confirms the nanostructured nature of the expanded worms.

2-3.2 Thermogravimetry

Figure 2-3 shows the TGA mass loss curves for the EG samples in nitrogen. This two-step exfoliation event observed for the ES250 B5 but not for the ES170-expanda300A is attributed to the differences between these materials and their gaseous release mechanisms discussed in section 2-4. Expansion onset occurs at 190 °C and the DTG peaks (not shown) occur at 205 °C and 407 °C. In contrast, the ES170-300A TGA trace indicates a single-step exfoliation event with an onset temperature above 250 °C and a DTG peak at 296 °C in the TGA. At 600 °C the ES250 and the ES170 samples have lost 15.3 wt.% and 7.3 wt.% respectively. At higher temperatures all samples oxidised and rapidly lost mass. However, there are significant differences in the oxidative stability. The thermal stability increased in the order ES250 < ES170 < natural graphite. One may note that the natural graphite does not undergo a major mass loss event as it is a very stable compound. The minor losses incurred may be attributed to the loss of moisture and minor oxidation due to the interaction of oxygenated groups that are bound to the edges of the graphite layers.

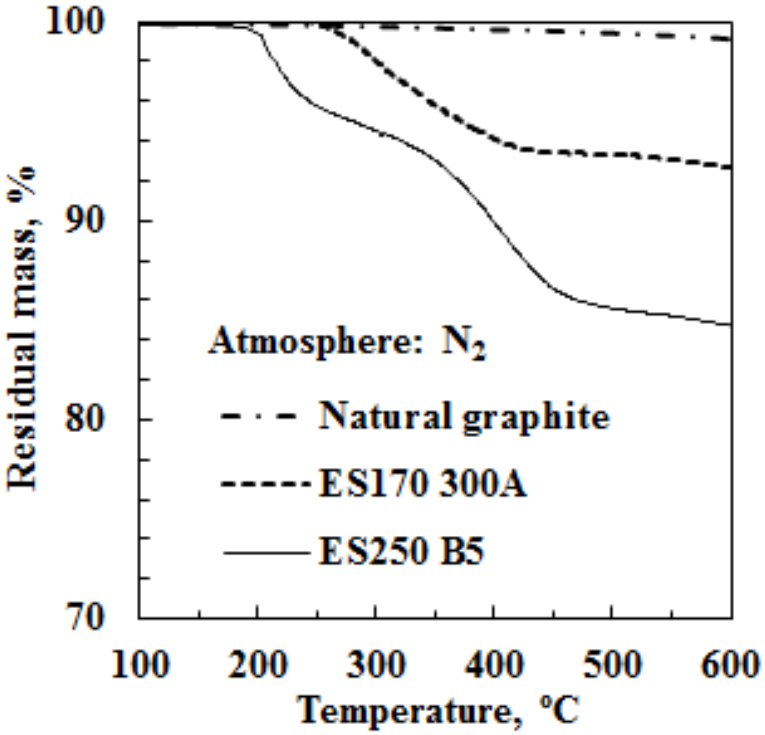

Figure 2-3: TGA traces in air for the three graphite samples

2-3.3 Composition of evolved gases

Camino *et al* (2001b) postulated that a redox reaction between the H_2SO_4 and graphite generates the blowing gases in EG:

$$C + 2H_2SO_4 \rightarrow CO_2 + 2H_2O + 2SO_2$$

Scheme 2-I. Redox reaction postulated by Camino *et al* (2001b) for the blowing gases responsible for the exfoliation of EG.

Indeed, Figure 2-4 shows that SO_2 is evolved during the exfoliation of EG samples in the graphitising furnace. Note that the onset temperature for SO_2 release was lower for ES250 than for ES170. The latter also released significantly less SO_2 during exfoliation. This figure displays two discrete gaseous release curves for ES250 and ES170 respectively indicating sample variance.

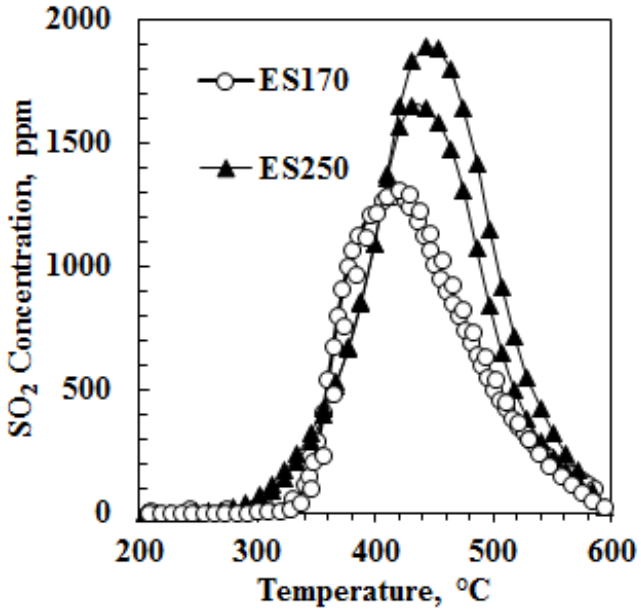

Figure 2-4: Sulfur dioxide release as a function of temperature for the two EG samples

Table 2-2 gives the overall composition of the gases collected during these experiments. They were collected in the temperature interval 100 °C to 600 °C. Table 2-2 also reports selected atomic ratios. The main constituents in order of decreasing importance are carbon dioxide > carbon monoxide > sulfur dioxide. This observation does not agree with the reaction mechanism posed in Scheme 2-I which suggests that two mole SO_2 should be released for every mole of CO_2. Furthermore, if the graphite samples only contained intercalated sulphate ions, the expected oxygen to sulfur ratio would be four. However, the observed ratios are much higher, twenty seven times for ES250 and three times higher for ES170.

Table 2-2: Overall composition of the gases evolved up to 600 °C in volume fractions. The atomic ratios of the evolved gases are also stated

Component	ES250 B5	ES170-300
CO_2	0.848 ± 0.260	0.442 ± 0.008
CO	0.135 ± 0.022	0.432 ± 0.017
SO_2	0.017 ± 0.003	0.126 ± 0.005
O / S	108	12
C / S	57	7.0
O / C	1.9	1.8

2-3.4 Graphite composition determinations

Table 2-3 reports the elemental analysis results and Table 2-4 the XRF data. Note that the sulfur content of ES250 B5 is higher than that of ES170-300A. The interesting observations are that a significant percentage of the sulfur is retained and that the carbon content increased following exfoliation at 600 °C. The data also indicate that the EG contained significant amounts of oxygen. Indeed, the elemental analysis indicates oxygen contents of 12.3 wt.% and 8.4 wt.% for ES250 and ES170 respectively. Following exfoliation at 600 °C the oxygen contents of the residues is significantly lower, i.e. 2.2 wt.% and 2.3 wt.% respectively.

Table 2-3. Elemental analysis of the graphite samples. Accuracy estimated as ± 0.3 wt.%

Composition, wt.%	C	H	S	O[1]	Ash[2]
ES 250 B5	77.4 ± 1.9	1.02 ± 0.09	4.0 ± 0.7	12.3 ± 1.6	5.3 ± 0.2
ES 250 B5 (expanded)	86.9 ± 3.7	0.76 ± 0.15	3.9 ± 0.5	2.2 ± 3.0	6.3 ± 0.1
ES170-300A	82.5 ± 0.2	0.49 ± 0.06	3.1 ± 0.7	8.4 ± 0.6	5.4 ± 1.2
ES170-300A (expanded)	88.3 ± 0.0	0.64 ± 0.04	2.7 ± 0.5	2.3 ± 0.5	6.0 ± 1.4

[1] By difference; [2] From TGA results

Table 2-4. XRF results with composition indicated as wt.%

Zimbabwe graphite	**SiO_2**	**TiO_2**	**Al_2O_3**	**Fe_2O_3**	**MnO**	**MgO**	**CaO**
	3.19	0.04	1.55	1.23	0.01	0.70	0.59
	Na_2O	**K_2O**	**SO_3**	**Co_3O_4**	**S**	**Rest**	
	0.05	0.20	0.05	*<0.01*	0.13	92.20	
ES250 B5	**SiO_2**	**TiO_2**	**Al_2O_3**	**Fe_2O_3**	**MnO**	**MgO**	**CaO**
	1.20	0.03	0.49	0.21	0.29	0.45	0.18
	Na_2O	**K_2O**	**SO_3**	**Co_3O_4**	**S**	**Rest**	
	0.81	0.18	7.60	0.08	*<0.01*	88.45	
ES170-300A	**SiO_2**	**TiO_2**	**Al_2O_3**	**Fe_2O_3**	**MnO**	**MgO**	**CaO**
	1.06	0.02	0.63	0.10	0.03	0.16	1.58
	Na_2O	**K_2O**	**SO_3**	**Co_3O_4**	**S**	**Rest**	
	0.48	0.07	6.06	*<0.01*	*<0.01*	89.67	

Detailed examination of the elemental analysis data in combination with the TGA data indicate that 85 % and 75 % of the oxygen, initially present, volatilised during the exfoliation of respectively the ES250 and ES170 EGs up to 600 °C. Considering the composition of the evolved gases and using the amounts of oxygen as the link, total mass losses of 14.8 wt.% and 10 wt.% were calculated for the exfoliation process. Considering the scatter in the experimental data, this compares favourably with the actual mass losses recorded in the TGA experiments (15.3 wt.% and 7.3 wt.% for ES250 and ES170 respectively).

The sulfur content of ES250 B5 (4.0 wt.%) translates into 12.1 wt.% SO_4 assuming that all of the sulfur is initially present as sulfate. Repeated washing with deionised water recovered 1.6 wt.% sulfate while the exhaustive ion exchange experiment removed 8.4 wt.% sulfate and replaced it with DAP in the EG. This indicates that most of the sulfur is indeed present as exchangeable sulfate ions consistent with sulfate intercalated graphite.

EDS analysis confirmed the presence of sulfur in both the neat and the exfoliated EG samples. However, in the latter case the sulfur was strongly associated with calcium. This suggests the formation of calcium sulfate or sulfide during the exfoliation process and explains why part of the sulfur is retained. However, the concentration of alkali and alkaline earth metals found by XRF was too low to explain the retention of all of the sulfur in the form of sulfate or sulfide salts. This means that sulfur must also be retained in the graphite matrix, perhaps acting as sulfide bridges that neutralise dangling carbon bonds at holes and the edges of graphene sheets. Furdin (1998) postulated that some of the sulfur might even be retained in its elemental form.

XRF results revealed that the inorganic content of the Zimbabwean flake graphite was about 8 wt.%. The main impurities appeared to be silica and clay minerals. According to the XRF results, the apparent carbon content of the two EG samples were both about 89 wt.%. These values are higher than those obtained from the elemental analysis because this value did not take into account the oxidised nature of the graphite samples. The XRF results provide hints regarding the way the two EG samples were made. Unlike ES170, ES250 contains manganese and potassium suggesting the $KMnO_4$ was used as an oxidant in its manufacture.

2-3.5 Thermomechanical analysis

A key property of EG is the ability to exfoliate over a narrow temperature range. Figure 2-5 shows the expansion behaviour of the graphite samples as characterised by TMA. The onset temperatures for the ES250 and ES170 were about 225 °C and 300 °C respectively. The ES250 showed a greater expansion most likely due to the larger volume of gas released by this grade during the exfoliation event.

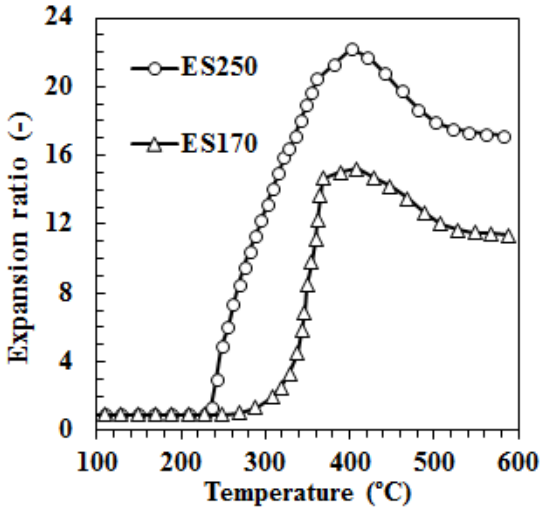

Figure 2-5: Thermomechanical characterisation of the exfoliation process in the two EG samples

2-3.6 X-Ray Diffraction (XRD)

Figure 2-6 shows XRD diffractograms for the two EG samples and compares them to the diffractogram for the natural graphite. Table 2-5 lists the d-spacing calculated from the positions of the main reflections observed in the diffractograms. The d-spacing for the natural graphite was 0.335 nm. The diffractograms of both EG samples in their neat and their expanded forms showed a peak (or at least a shoulder) that corresponded approximately to the same d-spacing. This is evidence for at most partial sulphate intercalation, i.e. the flakes also contain unreacted graphite layers. The neat EG samples featured an additional reflection located at a slightly lower angle. This corresponds to the sulfuric acid-intercalated graphite phase. Comparing the reflections in the two diffractograms suggests that this phase has a higher prevalence in ES250 than in ES170. After exfoliation, the reflections associated with this phase disappear completely and only a pure graphite reflection is evident.

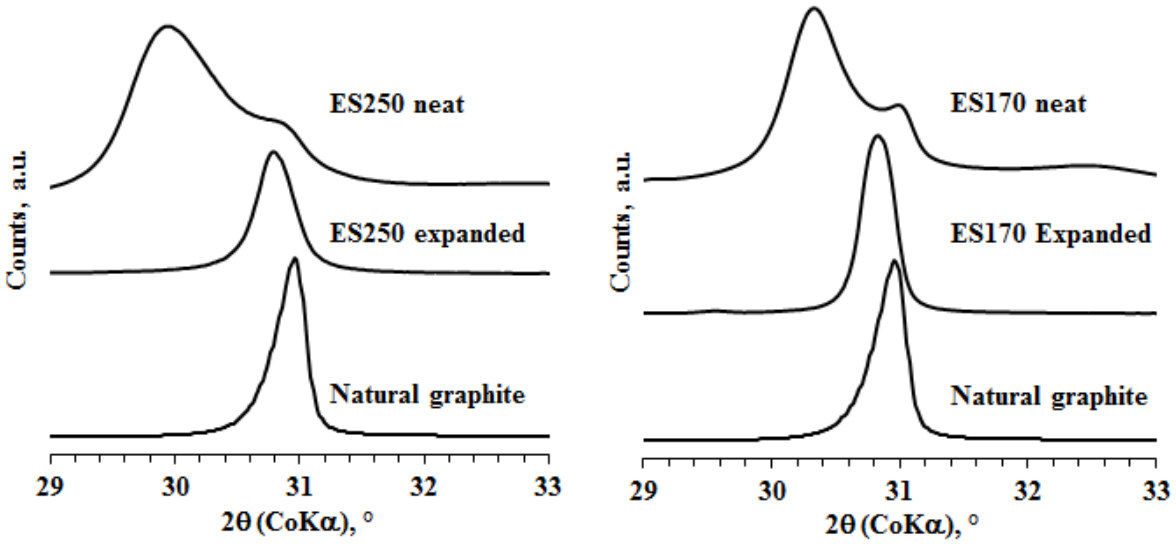

Figure 2-6: XRD patterns for the various states (neat and exfoliated) of the graphite samples compared to natural Zimbabwe graphite

Table 2-5. XRD d-spacing values and Raman I_D/I_G ratios

Sample	XRD d, nm	Raman I_D / I_G
Natural graphite	0.335	0.12
ES250 5B	0.347	0.20
	0.647	
ES250 Expanded	0.337	0.13
ES170-300A	0.342	0.26
	0.335	
	0.609	
ES170 Expanded	0.337	0.10

The XRD pattern for ES250 features another very broad reflection with a peak at $2\theta = 15.91°$ corresponding to a d-spacing of 0.65 nm. A similar reflection occurs in the XRD pattern for ES170. It is located at $2\theta = 16.90°$ corresponding to a d-spacing of 0.61 nm. The broad nature of these reflection and their peak locations are consistent with the presence of a GO phase. Expanded XRD patterns for the neat materials are also displayed in Figure A-11-1 in Appendix A-11.

2-3.7 Raman spectroscopy

Figure 2-7 shows Raman spectra. The Raman spectrum of the natural graphite exhibits a characteristic strong G band at 1580 cm^{-1} which is attributed to the vibration of sp^2-bonded carbon atoms in the two-dimensional hexagonal lattice. It also features a weak D band at 1349 cm^{-1} which is caused by the graphite edges or by imperfections. The Raman spectra of the EG samples exhibit a typical graphite-like pattern (Figure 2-7). Table 2-5 reports the I_D / I_G peak intensity ratios for the natural graphite and the neat as well as exfoliated EG samples. Lower values for this ratio indicate increased ordering (Tuinstra & Koenig, 1970). Thus the apparent ordering of the graphite improves on exfoliation. Botas *et al* (2012) reported peak intensity ratios for GO of I_D / I_G ≈ 0.9. This indicates that the disorder in the EG samples is not as severe as in GO.

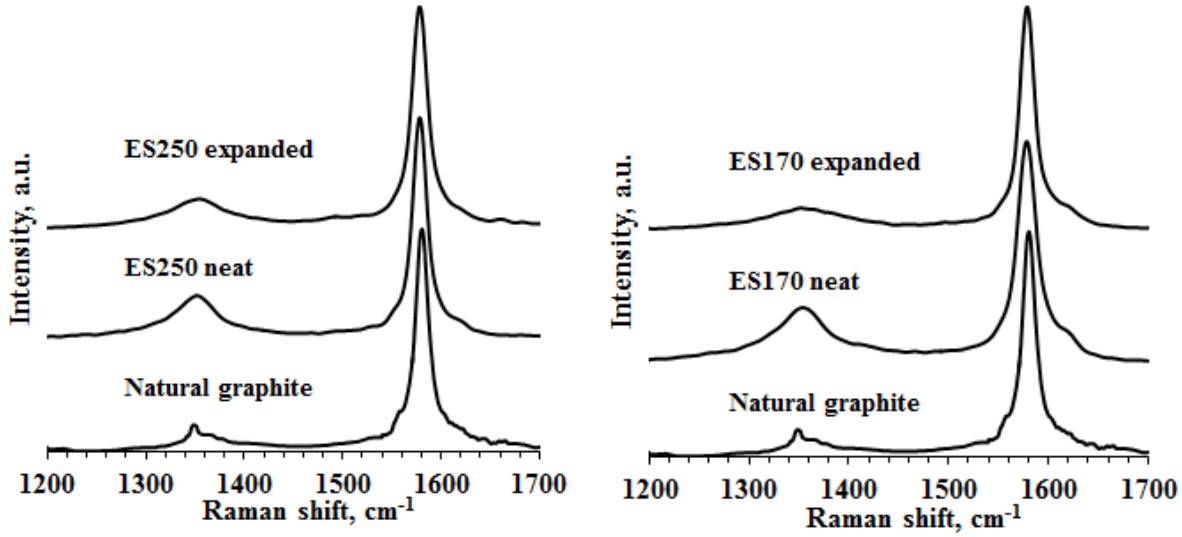

Figure 2-7: Raman spectra for the various states (neat and exfoliated) of the graphite samples compared to natural Zimbabwe graphite

2-4. Discussion

Natural graphite is a highly crystalline material (Wissler, 2006) formed through a range of complex geological processes which can result in a wide variety of morphologies. However, flake natural graphite is predominantly formed during the creation of metamorphosed siliceous or calcareous sediments (Luque *et al*, 1998). A recent extensive investigation on natural flake graphite by Dr Heinrich Badenhorst at the University of Pretoria (very similar to the materials under consideration in this study) concluded that the flakes are comprised of polygonised stacks of interlinked crystals as seen from an angle in Figure 2-9A (Badenhorst, 2014).

Dr Badenhorst consulted on this discussion and developed figures 2-8 and 2-9 which coincide with the extensive theory on graphite oxidation he developed (Badenhorst, 2014). The morphology is the result of complex crystal growth phenomena during flake formation. Disclinations and elastic instabilities lead to crystal growth along macrospirals which interlink the entire structure whilst polygonised blocks develop independently (Kvasnitsa, Yatsenko & Jaszczak, 1999). The dominant flaw in this structure is a type of prismatic edge dislocation which is better described as a region of slip misalignment. This represents a discontinuity in the crystal structure and is a very likely the point of attack for oxidants. This discontinuous layered stacking is clearly visible in Figure 2-8. The flaws where oxidation and intercalation may commence are indicated by the white arrows while the regions of overarching connectivity are represented by the red arrows.

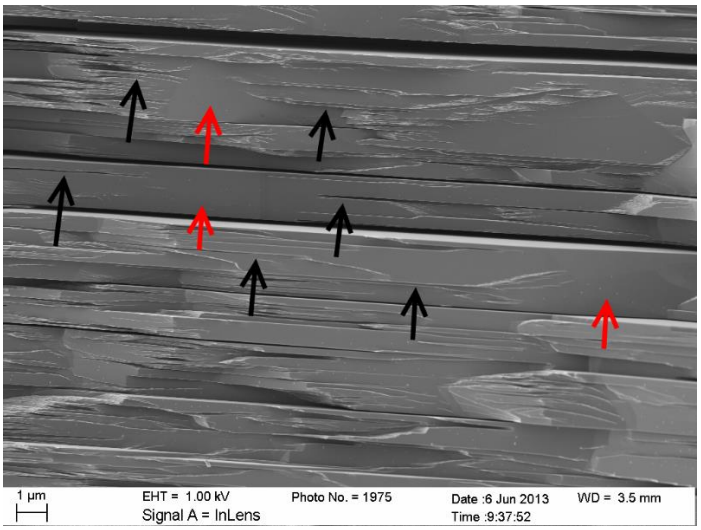

Figure 2-8: An edge view of a natural graphite flake.

Consider now what may happen during the manufacture of EG. As the oxidant molecules penetrate such a flaw, the entire plane on both sides of the flaw may become heavily oxidised, to the point of resembling GO. This is due the similar levels of oxidant concentrations used to produce intercalated graphite and GO (Chua *et al*, 2012). This is confirmed by the very high oxygen to carbon ratio measured for the intercalated graphite materials. It is also likely that this degradation will lead to weakening of the adjacent layers, leading to further attack in the regions adjacent to these flaws. This will lead to regions of highly oxidised GO sandwiched between regions of relatively pristine crystallinity.

The presence of considerable regions of homogenously intercalated graphite is demonstrated by the XRD traces in Figure 2-6. XRD reflections consistent with both GO and sulfuric acid-intercalated phases are found. The oxygen to carbon ratio for GO may be as high as 1:1 (Chua *et al*, 2012). The values for the EG grades were not as high due to the presence of regions where the graphite was not oxidised. The postulated progression of oxidation and intercalation is shown schematically in Figure 2-9. It is important to note that regions of overarching connectivity still exist, linking the entire flake together.

GO is thermally unstable. It deflagrates at above 200 °C with the formation of carbon monoxide, carbon dioxide, water, and an amorphous, soot-like carbon (Rüdorff, 1959; Talyzin *et al*, 2009). It is therefore plausible that the GO phase participates in the exfoliation of EG. Upon heating, the regions of GO vaporise, producing large amounts of oxidised gas that is trapped in localised pockets. These gas pockets expand within the interlinked flake structures leading to the accordion like structures visible in Figure 2-2D. When the flake edges of the exfoliated graphite are examined, sheets with thicknesses exceeding those expected from the BET are also observed (Figures 2-2F). The ash content of the two EG grades is the same and so is the oxygen to sulfur ratio. There are, however, two clear differences that could hold a key to the higher thermal stability of the ES170-300A when compared to the ES250 B5.

The sulfur content of the former is lower and it contains significantly less transition metal impurities, i.e. iron and manganese. It is possible that the catalytic activity of the latter may be responsible for the lower thermal stability.

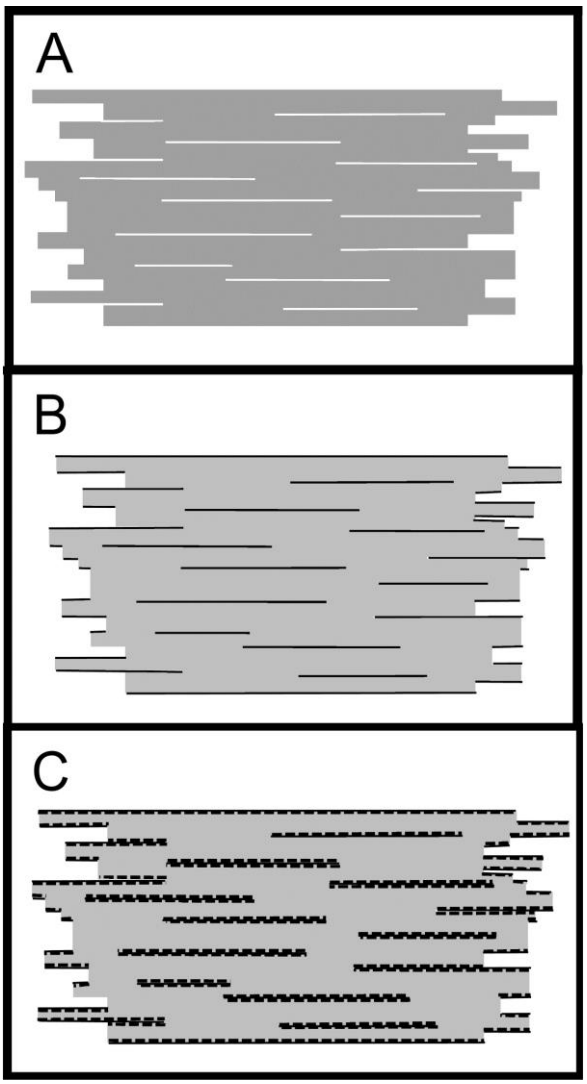

Figure 2-9: Postulated progression of oxidation and intercalation in natural graphite flakes.

A. Neat flake showing flaws.
B. Flaws provide internal access and facilitate intercalation.
C. the flaws also provide easy access to water and more oxidant facilitating the conversion to GO at internal sites

2-5. Conclusions

Two commercial EG samples and natural flake graphite were characterised. These EG samples were fabricated by treating natural graphite flakes with oxidants such as nitric acid and potassium permanganate in the presence of sulfuric acid. Elemental analysis revealed that the low onset temperature EG and the high onset temperature EG contained 3.03 wt.% and 2.27 wt.% sulfur respectively. The expansion onset temperatures were determined by thermomechanical analysis. They were ca. 225 °C and 300 °C respectively. Both samples released a mixture of carbon dioxide, carbon monoxide and sulfur dioxide during exfoliation. The composition of the evolved gases and the elemental analysis results indicate that the two samples contained more than twice the amount of oxygen expected if the EG samples were true GICs with sulfuric acid units as guest ions or molecules. However, exhaustive ion exchange with diammonium phosphate confirmed that the majority of the intercalated sulfate ions were exchangeable.

The present results are consistent with a model that assumes that the EG flakes contain both crystalline and disordered regions. The former comprise graphite layers randomly interstratified with sulfuric acid intercalated graphite layers while the latter can be described as a graphite oxide-like phase. The clearest evidence for the presence of the GO phase found through analysis comes from the broad amorphous XRD reflection consistent with d-spacing values near 0.60 – 0.65 nm. Further evidence to support this theory was found through elemental analysis, which revealed high oxygen content in the EG and high oxygen to sulfur and carbon to sulfur ratios. This pattern repeats in the evolved gases. Raman spectra further indicated a transformation from a state of higher disorder to a more ordered state during exfoliation of EG. Upon rapid heating, the oxygen-containing functional groups of the GO phase also degrade and volatilise as carbon dioxide or carbon monoxide. This explains the high oxygen to sulfur ratio of the extruded gas. Only part of the sulfur originally present is released as sulfur dioxide in the blowing gas. Some may be retained as inorganic sulfides but most probably serve to nullify dangling carbon bonds at defects and graphene edges.

Chapter 3: Development and production of flame retardants

Foreword

This chapter acknowledges contributions from the following persons:

- *Walter Wilhelm Focke and Albert Roberson*

Additional SEM micrographs for the developed flame retardants and the EG used are displayed in Appendix A-2.

Executive summary

The aim of this study was to synthesise two IFRs. The first compound was the well-established IFR, EDAP and the second was a novel compound designed as a phosphate containing IFR whose fire properties were unknown. These compounds were mixed with EG and exposed to an open flame to tentatively determine whether these compounds are compatible with EG for use in binary flame retardant systems. Both these compounds were successfully produced at high quality and achieved the further aim of cohesively covering and bonding EG strings. The results from this study indicate the utility of these compounds as individual flame retardants and potential binary flame retardants.

Keywords: flame retardants; intumescent flame retardants; ethylenediamine phosphate

3-1. Introduction

In recent years plastic has become one of the most popular piping materials. Plastic piping is widely used on chemical plants and in mines where there is a high risk of fire. This is a huge hazard to these industries as the plastic used throughout such installations are a fuel source which burns rapidly. To remedy this, flame retardants such as IFRs are added to slow down combustion of the plastic if exposure to a flame should occur.

In order to test EG in binary systems with other IFRs it was essential to first conduct a scoping trial and ascertain whether the materials synthesised or selected can indeed aid cohesion of expanded EG as desired.

The objective of this study was to synthesise EDAP and a novel flame retardant namely 3,5-diaminobenzoic acid phosphate (DABAP). These materials are then tested to ascertain their purity and are burnt in contact with EG to test their bonding and intumescent capabilities. Once successful, these materials can then be produced at a larger scale in later phases for further testing and use in the main experimental compounding and fire testing phases.

Experimental synthesis was conducted on a laboratory scale.

3-2. Experimental

3-2.1 Materials

3-2.1.1 Preliminary synthesis of EDAP

EDAP is an IFR commonly used in industry. “It is self-intumescent and does not require a char-forming synergist” (Krems Chemie Chemical Services). The raw materials used when producing EDAP are very expensive and production of industrial quality EDAP requires extensive cooling and milling of the product. The chemical properties of EDAP are given in Table 3-1.

Table 3-1: Properties of EDAP

Molecular Weight	158.09 g / gmol
Density	800 g / L
Water Solubility (20 °C)	5 g/ 100 mL
pH (saturated @ 20 °C)	7

The chemicals orthophosphoric acid [7664-38-2] and ethylenediamine [107-15-3], chemicals used during the synthesis of EDAP were sourced from Merck. The preliminary synthesis procedure for EDAP production was as follows: preliminary synthesis was done at a small scale in order to test whether the media reacts as expected. The reaction details of this experiment are displayed in Table 3-2. The reaction mechanism displayed in Scheme 3-I was used to synthesise the EDAP product

$$C_2N_2H_6(s) + H_3PO_4(aq) \rightarrow C_2N_2H_9PO_4(s) + H_2O(aq)$$

Scheme 3-I. Phosphorification of ethylenediamine to produce EDAP

Table 3-2: Preliminary EDAP production results

Material	EDAP	Filtrate from EDAP production
Mass (g)	16.74	149.12
pH	-	8.83
Colour Observed	White	Light orange
Yield (%)	66.62	-

EDAP is a low density crystal that is very soluble in water. The liquid is alkaline as some of the EDAP cannot be filtered out and stays in solution. The yield for this experiment was 66.62 %. The expected pH was 8. To prevent the production temperature from reaching EDAP's degradation temperature, an ice bath was used to cool the beakers and liquids. The reaction occurred over a long period of time.

For this experiment 12.02 g of EDA was used and 19.60 g of orthophosphoric acid. 500 g of ice was used in the ice bath. The pH and mass of the liquid obtained through filtration was also measured. This production method was revised for large scale production to improve the lower than expected yield achieved due to high filtration losses.

After the success of this test, the production of ca. 1000 g of the EDAP product was desired for compounding purposes. This larger scale synthesis and further characterisation of this compound are reported in Chapter 5. A full characterisation of the fire performance of this compound as FR in polyethylene on its own and in combination with EG is also contained within this section and continues in Chapter 6.

3-2.1.2 Preliminary synthesis of DABAP

3,5-Diamino benzoic acid, although not normally utilised for flame retardant applications was tested as an additive in a PhD project (Labuschagne, 2003) completed prior to this project. It was theorised that modification of this compound to produce a phosphate salt would produce good fire performance as phosphate amide groups often produce intumescent behaviour (Hu, Wang & Wang, 2013).

The chemically pure chemicals 3,5-diaminobenzoic acid [535-87-5], ammonium dihydrogen phosphate [7722-76-1] and hydrochloric acid [7647-01-0] were sourced from Sigma-Aldrich, Protea Chemicals and Merck respectively and these chemicals were used to produce DABAP.

The synthesis procedure for DABAP production was as follows:
Small scale preliminary synthesis was undertaken to test whether the media reacts as expected. The initial results for DABAP production at a small scale are displayed in Table 3-3.

Table 3-3: Preliminary DABAP production results

Material	DABAP	Filtrate from DABAP synthesis
Mass (g)	15.14	569.56
pH	-	7.79
Colour Observed	Silver	Dark orange
Yield (%)	80.52	-

DABAP is a very low density powder that is fairly soluble in water. As expected, prior to crystallisation, the liquid product had a pH close to neutral, meaning that the reagents reacted to a high conversion level. The DABA was measured as 15.22 g and 500 g of ice was used for cooling. A 0.1 mole hydrochloric acid ampoule was then added after which 11.50 g of ammonium dihydrogen phosphate was added. The pH and mass of the filtrate was measured.

To promote a protonation reaction of one of the amine groups instead of an exothermic hydrolysis and phosphorification of the alcohol group an ice bath was used to maintain a decreased reaction temperature.

The proposed mechanism for the synthesis of DABAP is displayed in Scheme 3-II while Scheme 3-III is the mechanism which would occur in the absence of cooling. Scheme II is akin to the reaction observed by Chowdary, Enturi and Sandhya Rani (2011) when reacting potato starch and anhydrous di-sodium hydrogen orthophosphate at elevated temperatures. Scheme II represents the esterification of benzoic acid to form an amino phosphate ester group. Scheme 3-II is preferred as the resulting chemical formula more closely matches the structure of IFRs such as EDAP. This scheme was pursued in the hope that an IFR with a high propensity for charring would result.

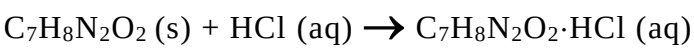

$$C_7H_8N_2O_2\,(s) + HCl\,(aq) \rightarrow C_7H_8N_2O_2{\cdot}HCl\,(aq)$$

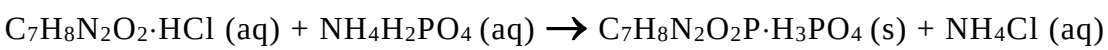

$$C_7H_8N_2O_2{\cdot}HCl\,(aq) + NH_4H_2PO_4\,(aq) \rightarrow C_7H_8N_2O_2P{\cdot}H_3PO_4\,(s) + NH_4Cl\,(aq)$$

Scheme 3-II. Synthesis of the phosphate salt of 3,5-diaminobenzoic acid

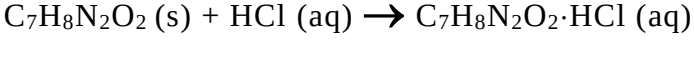

$$C_7H_8N_2O_2\,(s) + HCl\,(aq) \rightarrow C_7H_8N_2O_2{\cdot}HCl\,(aq)$$

$$NH_4H_2PO_4\,(aq) \leftrightarrow NH_4^+\,(aq) + H_2PO_4^-\,(aq)$$

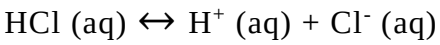

$$HCl\,(aq) \leftrightarrow H^+\,(aq) + Cl^-\,(aq)$$

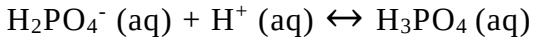

$$H_2PO_4^-\,(aq) + H^+\,(aq) \leftrightarrow H_3PO_4\,(aq)$$

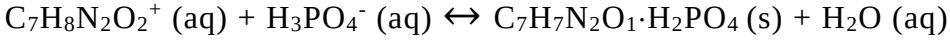

$$C_7H_8N_2O_2^+\,(aq) + H_3PO_4^-\,(aq) \leftrightarrow C_7H_7N_2O_1{\cdot}H_2PO_4\,(s) + H_2O\,(aq)$$

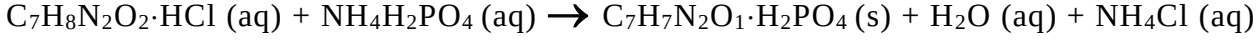

$$C_7H_8N_2O_2{\cdot}HCl\,(aq) + NH_4H_2PO_4\,(aq) \rightarrow C_7H_7N_2O_1{\cdot}H_2PO_4\,(s) + H_2O\,(aq) + NH_4Cl\,(aq)$$

Scheme 3-III. Phosphorification of 3,5-diaminobenzoic acid

After the success of this test, the production of ca. 1000 g of the DABAP product was desired for compounding purposes. The results of this production and the characterisation of the product are reported in chapter 4. A full characterisation of the fire performance of this compound as a flame retardant in polyethylene on its own and in combination with EG is also contained within this section and continues in chapters 5 and 6.

3-3. Results

3-3.1 Quantification of synthesised EDAP quality and bonding ability

In order to quantify the quality of the laboratory produced EDAP prior to upscaling of the process, the sample was compared to an industrially produced sample of high purity.

3-3.1.1 Raman and FTIR

Raman and FTIR were identified as key test methods for this comparison as they would clearly identify the chemical composition of the sample and would indicate crystallinity if the peaks obtained were sharp and well deconvoluted (Narayanan, 1948). Figure 3-1 and 3-2 display the results of Raman and FTIR respectively. Figure 3-1 and 3-2 clearly indicate that the laboratory produced EDAP was produced at high purity and measures up well to industrially produced EDAP in terms of molecular structure.

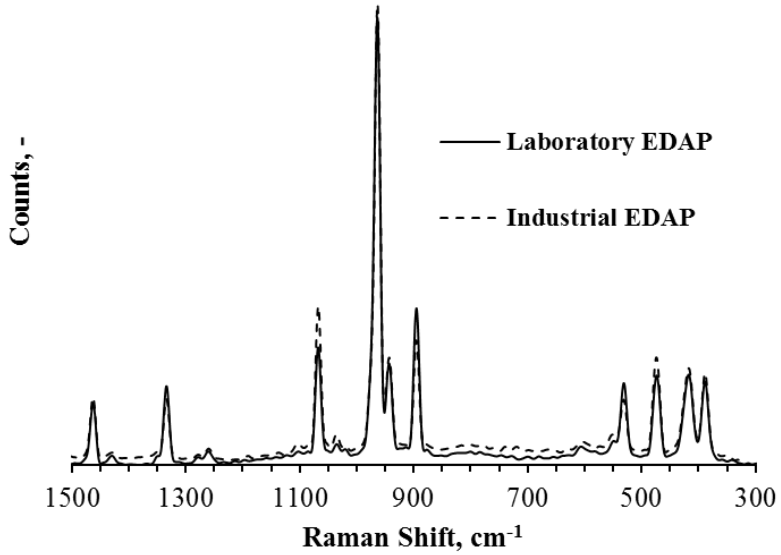

Figure 3-1: Raman spectrum for EDAP

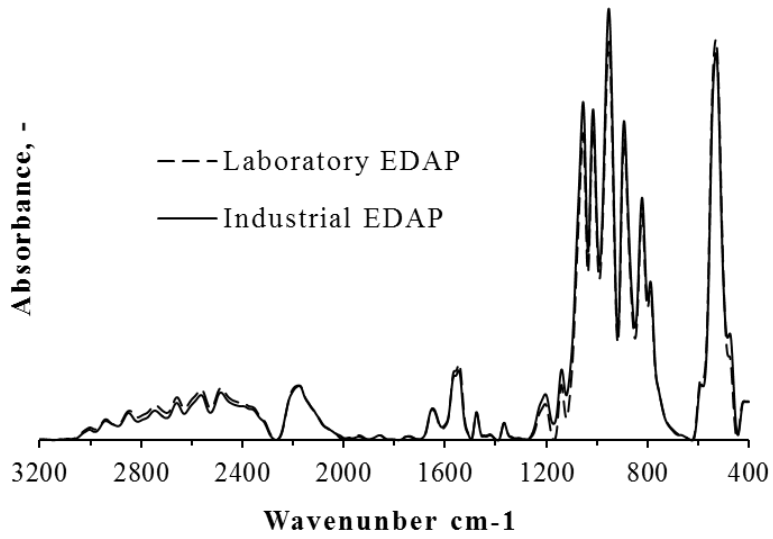

Figure 3-2: FTIR spectrum for EDAP

3-3.1.2 Scanning electron microscopy

The FE SEM micrograph displayed in Figure 3-3 indicates the crystalline structure of the milled EDAP samples. 3 wt.% silica was added to EDAP to promote easier milling of the EDAP produced.

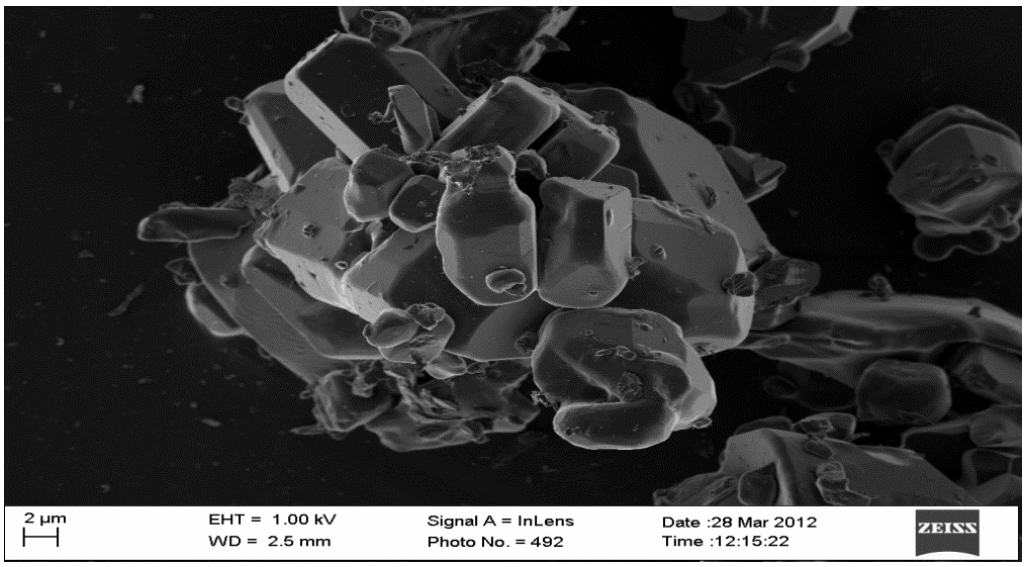

Figure 3-3: FE SEM pictures of laboratory produced EDAP

EDAP and EG powder was mixed together and placed in a crucible and exposed to an open flame instigating expansion of both materials. Visual inspection showed that the EDAP and EG strings stuck together. A FE SEM micrograph of the resulting media is displayed in Figure 3-4. This micrograph indicates that the EDAP covers the surface of the expanded EG structure indicating that the media expanded together with EDAP covering and bonding adjacent strings together.

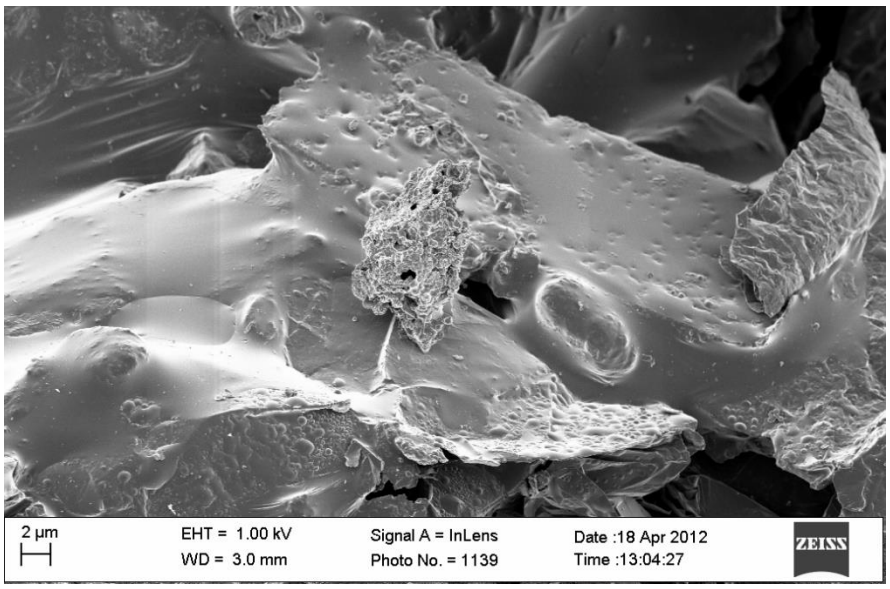

Figure 3-4: FE SEM results for EDAP with EG burned together

EDAP is further characterised and its fire performance in binary systems with EG is reported in chapter 5 in greater detail.

3.3.2 Quantification of synthesised DABAP quality and bonding ability

The Raman and FTIR scans of DABAP are reported in Chapter 4. Figure 3-5 indicates the microstructure of the DABAP at high magnification obtained using FE SEM.

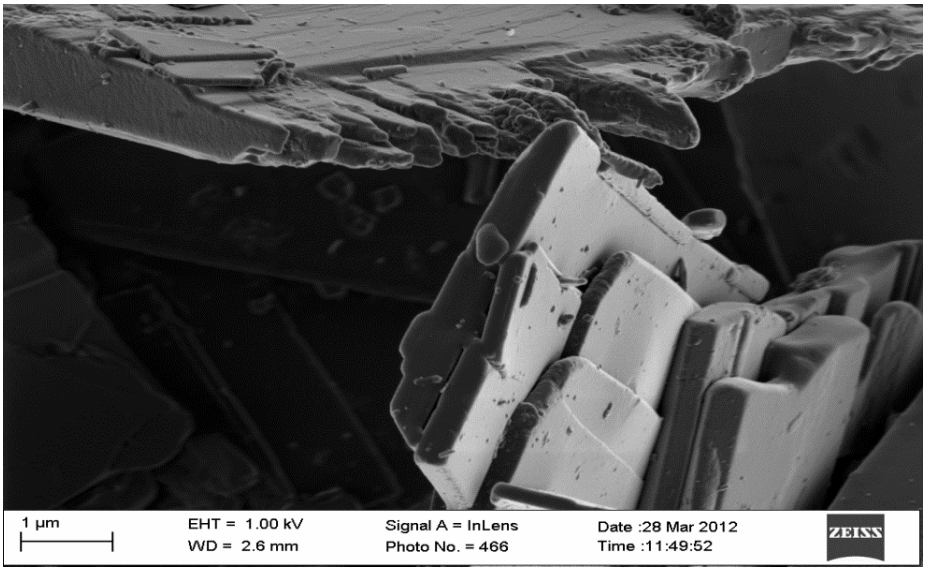

Figure 3-5: FE SEM of DABAP crystals

DABAP and EG powder was mixed together and placed in a crucible and exposed to an open flame instigating expansion of both materials. Visual inspection showed that the DABAP and EG strings stuck together. A SEM micrograph of the resulting media is displayed in Figure 3-6B while Figure 3-6A shows the edges of pure expanded EG. Figure 3-7 shows that DABAP covered EG flake edges as they expanded together.

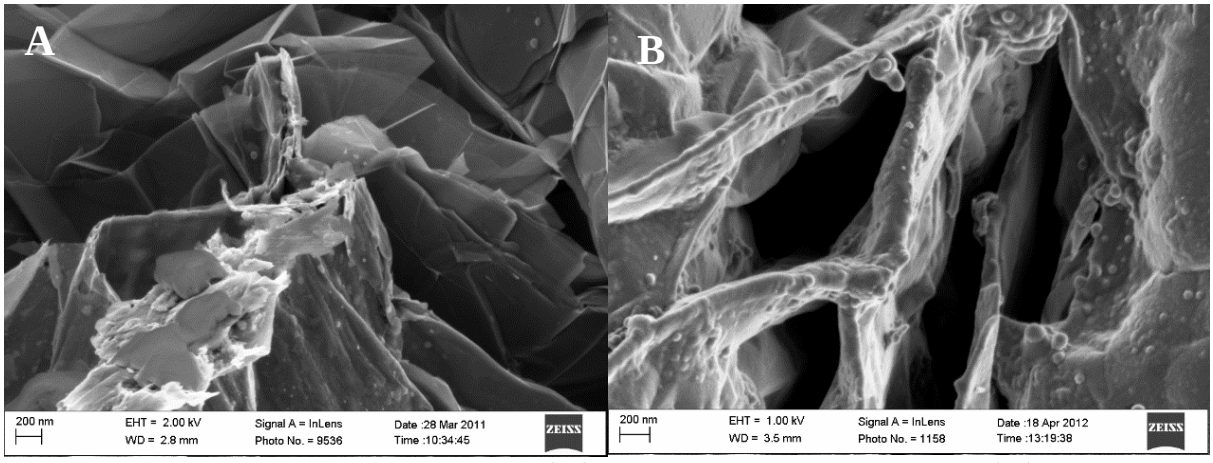

Figure 3-6: SEM micrographs of (A) neat expanded EG and (B) expanded EG and 3,5-diamino benzoic acid phosphate (DABAP) crystals

Figure 3-7 displays another SEM micrograph of the bonding of EG and DABAP

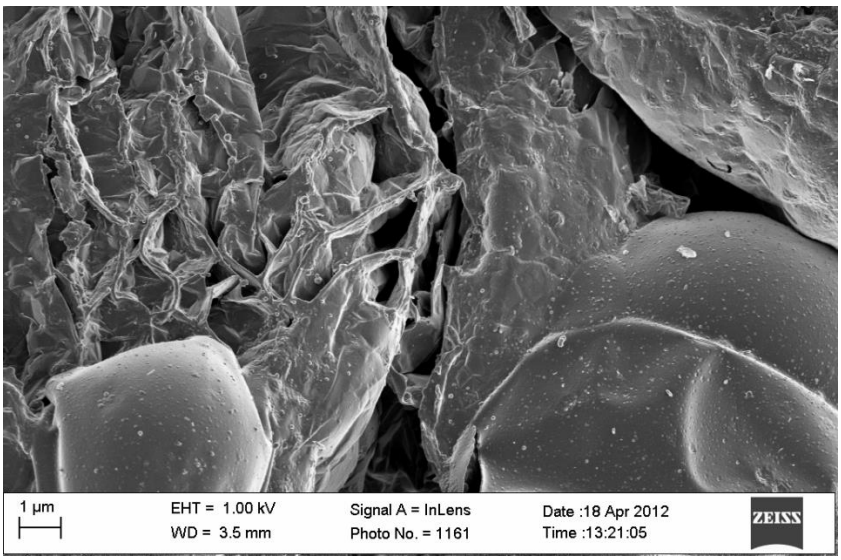

Figure 3-7: FE SEM results for DABAP with EG burned together

DABAP is further characterised in Chapter 4 and its fire performance is reported in Chapters 4 and 5.

3-4. Conclusions

The phosphate salt of 3,5-diaminobenzoic acid and ethylenediamine was successfully obtained. Both these materials react as desired when exposed to an open flame, by softening, expanding and eventually charring. Moderate yields were obtained and it is believed that these yields may be further improved upon for larger scale production. The EDAP produced was tested against a pure sample and proved to be of high crystallinity and purity. Fire testing of each compound with EG coupled with FE SEM post analysis indicated that both compounds bond and coat the EG strings fairly well as desired.

Chapter 4: Cone calorimeter fire performance of low temperature expandable graphite and a novel flame retardant

Foreword

This chapter contributed to the publication:

- *Polyethylene flame retarded with expandable graphite and a novel intumescent additive (Focke et al, 2014c)*

This chapter and publication acknowledges contributions from the following persons:

- *Walter Wilhelm Focke, Washington Mhike, Albertus Taute, Albert Roberson and Osei Ofosu*
- See appendix A-10 for the apparatus used for cone calorimetric testing and table A-10-1 which indicates some of the multitude of properties cone calorimetry can measure.

Executive summary

A novel intumescent additive was synthesised by neutralising 3,5-diaminobenzoic acid hydrochloride salt with ammonium dihydrogen phosphate. This compound, which melts at 257 °C, decomposes concurrently to release carbon dioxide gas. The flame retardant performance of this compound as a primary flame retardant and in combination with EG was evaluated by cone calorimetry. Cone calorimeter results revealed that addition of 10 wt.% EG alone lowers peak heat release rate of carbon black-pigmented polyethylene from 710 ± 109 $kW.m^{-2}$ to 342 ± 15 $kW.m^{-2}$, while addition of 27 wt.% of the novel intumescent lowered it to 400 ± 16 $kW.m^{-2}$. Combinations of these two additives were able to decrease the peak heat release rate even further. Furthermore, the novel intumescent additive reduced the flame out time from 773 ± 307 s to 537 ± 69 s although all other EG containing samples increased it.

Keywords: intumescent flame retardants; cone calorimetry; expandable graphite

4-1. Introduction

Polyethylenes are a family of commodity polymers (HDPE, LDPE, and LLDPE) primarily used as packaging materials. They are also used to fabricate moulded products such as battery boxes, air conditioning ducting, pipes and cable sheathing. Polyethylenes feature high heats of combustion and have a low propensity for char formation (Weil *et al*, 2008). As a result, these products present a potential fire hazard in certain applications, such as deep-level underground mining. Cone calorimetry presents a modern method for measuring the ignition time, heat release rate, combustion products and other flammability characteristics of polymer samples. This fire testing instrument determines the transient heat release rate by measuring transient oxygen consumption rate in the exhaust gases. According to Babrauskas and Peacock (1992) the heat release rate is the most important single variable in characterising the "flammability" of products and thus the fire hazard they may pose. Among the more widely used polymers, pure polyethylenes feature the highest heat release capacities and heat release rates in cone calorimeter tests (Dasari *et al*, 2013a).

It is therefore necessary for critical applications to flame retard polyethylene products with flame retardant additives. A wide range of effective additives are available (Dasari *et al*, 2013a; Weil *et al*, 2008). Recent studies have highlighted the utility of EG, IFRs and their synergistic combinations which improve the fire behaviour of polyethylene (Han, Li & Zhao, 2007a; Pang & Song, 2012a; Qu *et al*, 2003b; Sun *et al*, 2013b; Weil *et al*, 2008; Xie & Qu, 2001c; Xie & Qu, 2001d). Intumescent additives cause the materials to swell when exposed to fire or heat to form a carbonaceous foam residue that acts as a heat insulator and a physical barrier to the transport of oxygen and pyrolysis products (Camino *et al*, 1989; Dasari *et al*, 2013a; Lewin, 1999b; Wang *et al*, 2005).

EG is actually a partially oxidised, intercalated form of graphite containing intercalated guest species (e.g. sulfuric acid anions) in between the stacked graphene layers (Camino *et al*, 2001b; Furdin, 1998). A key property of EG is its tendency to exfoliate explosively, i.e. expand rapidly in a worm-like manner when heated to high temperatures (Chung, 1987; Chung, 2002a; Wissler, 2006). When this occurs at the surface of a polymer, the low density vermicular graphite that is formed provides a protective barrier similar to that generated by conventional intumescent additives.

According to Han *et al* (2007a) and Xie *et al* (2001c) better fire properties are possible with combinations of EG and other IFRs. Despite this, only a few such combinations have been explored to date. Therefore, this communication reports on the synthesis and characterisation of a novel IFR additive for use as a primary IFR and in combination with EG. The unique aspect of these two additives is that they both feature relatively high thermal stabilities. This could make them useful in applications where the polymer conversion requires high processing temperatures, e.g. rotomoulding. The fire performance of these additives in LDPE, on their own and in combinations, was studied using cone calorimeter fire testing.

4-2. Experimental

4-2.1. Materials

The chemicals 3,5-diamino benzoic acid [535-87-5], ammonium dihydrogen phosphate [7722-76-1] and hydrochloric acid [7647-01-0] were sourced from Sigma-Aldrich, Protea Chemicals and Merck respectively. Sasol Polymers supplied the LDPE in powder and pellet form. It was injection moulding grade LT019 with density 0.919 g.cm^{-3} and MFI 20.5 g / 10 min @ 190 °C / 2.16 kg. Carbon black grade N660 was sourced from Ferro Industrial Products. The EG grade ES170-300A, with a high expansion onset temperature, was sourced from Qingdao Kropfmuehl, China. The d_{10}, d_{50}, and d_{90} particle sizes were 313 µm, 533 µm and 807 µm respectively (Mastersizer Hydroliser 2000, Malvern Instruments, Malvern, UK). The density was 2.23 ± 0.01 g.cm^{-3} and the surface area in the pre-expanded form was 0.66 m^2.g^{-1} (Nova 1000e BET in N_2 at 77K).

4-2.2. Synthesis of DABAP

Scheme 4-I (Section 4-3.1) shows the reaction details. The synthesis procedure was as follows: seven moles of 3,5-diamino benzoic acid (1065 g) was weighed out into a large glass container placed in an ice bath which contained ca. 500 g crushed ice. Seven ampules of concentrated hydrochloric acid (containing 1 mol HCl each) were added drop wise to the 3,5-diamino benzoic acid container which was continuously stirred and maintained at a temperature below ambient.

At this stage the solution developed a dark brown colour, most likely due to oxidation of a minor portion of the 3,5-diamino benzoic acid. Next, seven moles (805 g) ammonium dihydrogen phosphate powder was added slowly to the reaction mixture with continued stirring. During this procedure the colour of the liquid phase changed from brown to orange. The final pH was 7.8. The precipitated silver-white crystals were recovered using vacuum filtration. The filter cake was first washed with distilled water and then with acetone. The resulting filter cake was oven dried at 50 °C for 12 h and milled into a fine powder. The yield was 95 %. More detail on the DABAP production is provided in appendix A-3.

4-2.3. Preparation of the polyethylene compounds

Polyethylene compounds containing EG and / or DABAP were compounded on a 28 mm co-rotating intermeshing twin screw laboratory extruder (L/D = 16) at a screw speed of 140 - 220 rpm. The compounder's screw design comprised intermeshing kneader elements with a forward transport action. The four extrusion processing stage temperatures, feed to die, were set at 120 °C, 175 °C, 175 °C and 180 °C respectively. The extruded strands were granulated and pressed into flat sheets in a hot press set at 180 °C. The final sheet dimensions were 100 mm × 100 mm × 3.2 ± 0.1 mm. A polyethylene compound containing 3 wt.% carbon black (N660) was prepared in a similar way. This compound was used as the reference sample for cone calorimeter testing. The compound containing 27 wt.% DABAP also contained 3 wt.% carbon black. This maintained a consistent range of dark product sheets as delivered for all EG containing compounds, in order to ensure comparable heat absorption during cone calorimeter testing.

4-2.4. Characterisation and analysis

FTIR spectra were recorded on a PerkinElmer Spectrum RX FT-IR, coupled with a computer using Spectrum v5.0.1 software, with a scan resolution of 2.0 cm^{-1}. A total of 32 interferograms were collected for each sample applying single beam radiation in an ATR configuration.

The compositions of the graphite particles and the DABAP were determined through XRF analysis performed using a wavelength-dispersive spectrometer (ARL 9400XP+ XRF). The samples were prepared as pressed powder briquettes and introduced to the spectrometer. The powders were ground in a tungsten carbide milling vessel and roasted at 1000°C for determination of the loss on ignition.

SEM images were obtained using an ultrahigh resolution field emission SEM (HR FE SEM Zeiss Ultra Plus 55) with an InLens detector at acceleration voltages of as low as 1 kV to ensure maximum resolution of surface detail. No electro-conductive coating was applied on the graphite particles.

4-2.5. Thermal analysis

Differential scanning calorimetry (DSC) data were obtained on a Perkin Elmer PYRIS Diamond DSC. The temperature was scanned from 30 °C to 370 °C at a scan rate of 10 °C min^{-1} with nitrogen flowing at a rate of 50 $mL.min^{-1}$.

TGA was performed using the dynamic method on a TA Instruments SDT Q600 instrument. About 7 mg of sample was placed in a 50 µL alumina pan with an alumina lid. Temperature was scanned from 50 °C to 900 °C at a scan rate of 10 °C min^{-1} with gas flowing at a rate of 50 $mL.min^{-1}$.

Thermal expansion measurements were conducted on a TA instruments Q400 Thermo Mechanical Analyzer. Sufficient EG powder was placed in an alumina sample pan such that the bed height was between 35 µm and 40 µm. The flake expansion behaviour was measured with a flat-tipped standard expansion probe using an applied force of 0.02 N.
The temperature was increased from 30 °C to 1000 °C at a scan rate of 10 $°C.min^{-1}$ in a nitrogen atmosphere. The expansion relative to the original powder bed height was reported. The same procedure was used to determine the softening point of the DABAP using a thin tipped penetration probe. In this case however, the applied force was 0.01 N, the temperature was scanned from 30 °C to 500 °C at a scan rate of 4 $°C.min^{-1}$ and the starting sample height was 229 µm.

4-2.6. Cone calorimeter flammability testing

The ISO 5660-1 standard was followed in performing the cone calorimeter tests using a Dual Cone Calorimeter (Fire Testing Technology (UK) Ltd.). Three specimens of each composition were tested and average values are reported. The sheet dimensions were 100 mm × 100 mm × 3.2 mm. They were placed horizontally on aluminium foil and exposed perpendicularly from above to an external heat flux of 35 kW.m^{-2}.

4-3. Results and discussion

4-3.1. Characterisation

The synthesis yielded the phosphate salt of 3,5-diamino benzoic acid as shown by the reactions of Scheme 4-I. It is expected that one of the amine functional groups of 3,5-diamino benzoic acid became protonated by the phosphoric acid while the other remained a free amine (that nevertheless participates in hydrogen bonding). The FTIR spectrum shown in Figure 4-1 is consistent with these assertions.

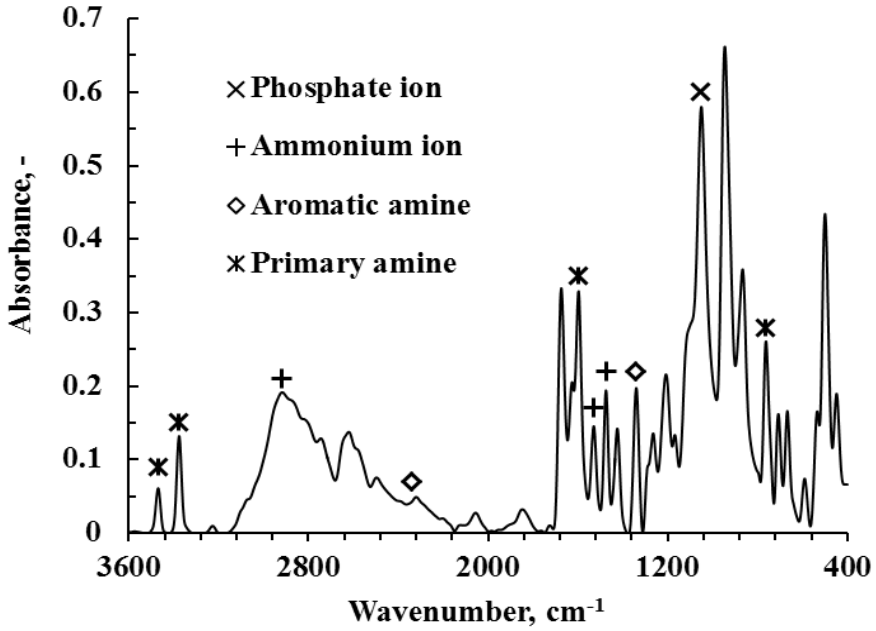

Figure 4-1: FTIR spectrum for DABAP

The presence of a free primary aromatic amine is indicated by the two bands located at 3469 cm^{-1} and 3377 cm^{-1} which are characteristic of the N–H stretching vibrations in primary amines. The sharp band at 1600 is due to the N–H bending vibration in primary amines.

The band at 1340 cm^{-1} is characteristic of the C–N stretch of aromatic amines. Finally, the sharp peak at 763 cm^{-1} is consistent with the N–H wagging vibration of primary amines. The band at 1050 cm^{-1} is attributed to the phosphate ion. The broad band with a peak at 2917 cm^{-1} is consistent with the presence of a primary ammonium ion (N–H stretch). The primary ammonium ion N–H bending vibrations are indicated by the two bands located at 1530 cm^{-1} and 1475 cm^{-1} (Coates, 2000).

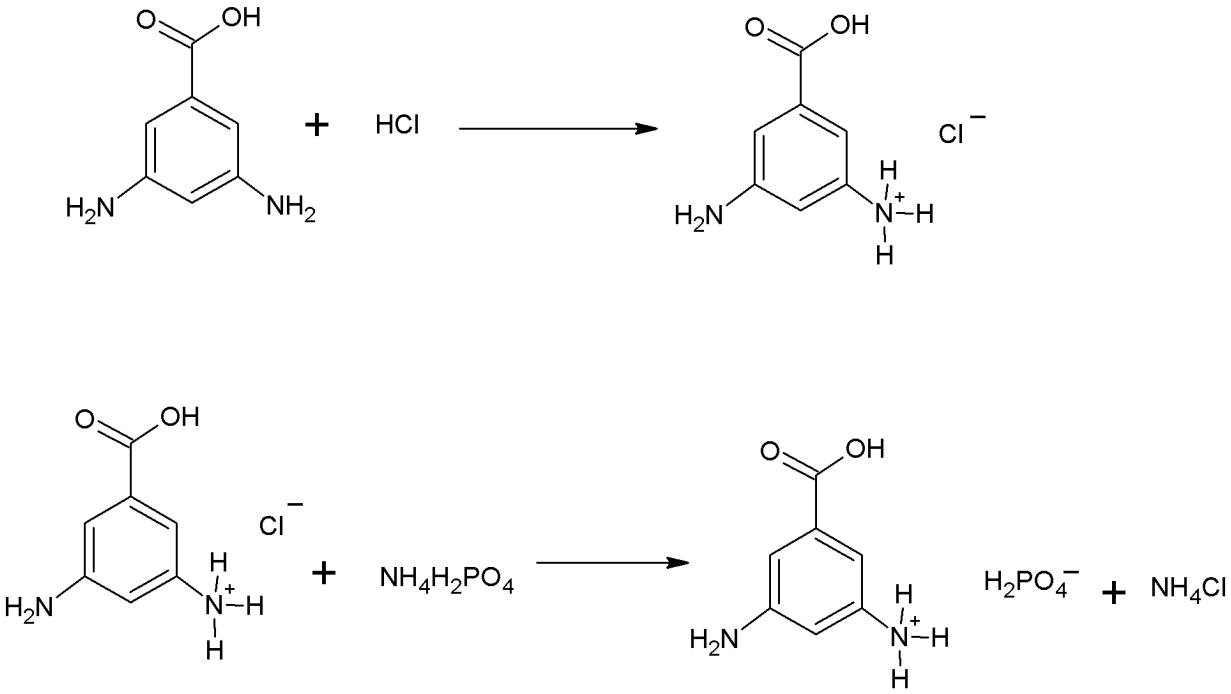

Scheme 4-I. Synthesis of the phosphate salt of 3,5-diaminobenzoic acid phosphate

Table 4-1 reports the XRF results for DABAP and the EG. According to the XRF results, the apparent P_2O_5 content of DABAP is 25.47 % whereas the theoretical value is 28.37 %.

The chlorine content suggests co-crystallisation of the chloride salt of 3,5-diamino benzoic acid. Both samples contain some inorganic impurities. In DABAP the source is probably the technical grade ammonium dihydrogen phosphate that was used. The EG contains intercalated sulfuric acid moieties and as expected the XRF results revealed the presence of a significant amount of sulfur. However, the graphite sample also contains other inorganic impurities. The main impurity elements were silicon and aluminium suggesting that the precursor graphite may have been contaminated with clay minerals.

Table 4-1: XRF results with composition indicated as wt.%

ES170-300A	**SiO_2**	**TiO_2**	**Al_2O_3**	**Fe_2O_3**	**MnO**	**MgO**	**CaO**
	1.06	0.02	0.63	0.10	0.03	0.16	1.58
	Na_2O	**K_2O**	**SO_3**	**Co_3O_4**	**S**	**Rest**	
	0.48	0.07	6.06	*<0.01*	*<0.01*	89.67	
DABAP	**Fe_2O_3**	**MgO**	**Na_2O**	**P_2O_5**	**SO_3**	**Cl**	**Rest**
	0.05	0.04	0.29	25.47	0.02	0.68	73.46

Figure 4-2A and 4-2B show the SEM micrographs of the DABAP crystals and the flake-like nature of EG respectively. One may note here that EG flakes are orders of magnitude larger.

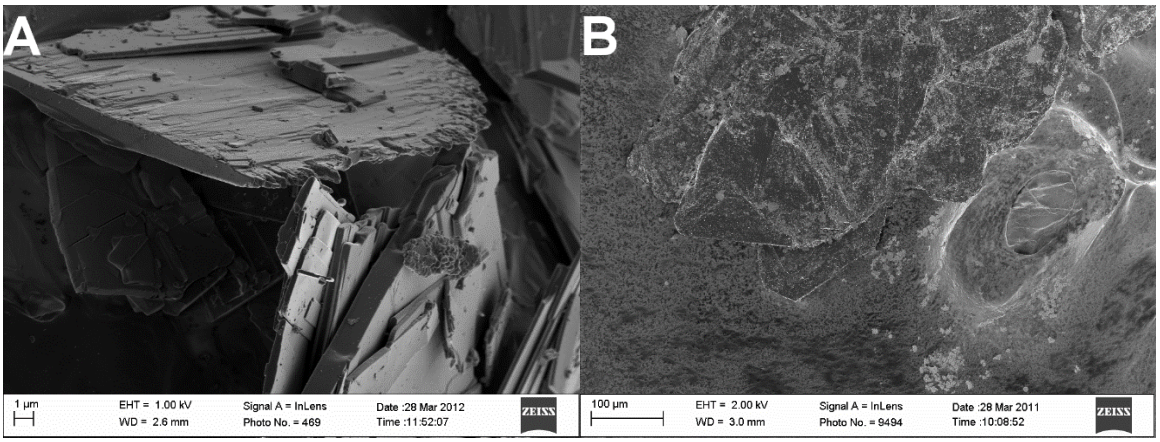

Figure 4-2: SEM micrographs of (A) 3,5-diaminobenzoic acid phosphate crystals and (B) EG flakes.

4-3.2. Thermal analysis

Figure 4-3 shows the TGA mass loss curve and the differential thermogravimetry (DTG) curves for DABAP obtained in N_2, together with the TGA trace for the EG obtained in nitrogen and air (Temperature was scanned from 25 °C to 900 °C at a scan rate of 10 °C.min^{-1} with gas flowing at a rate of 50 mL.min^{-1}). The mass loss for the EG in air occurs in two steps. The first step corresponds to the gas released during the exfoliation event. This step is also observed in a nitrogen atmosphere. The mass loss in air and nitrogen at 600 °C amounts to 10 wt.% and 7 wt.% respectively. The second step corresponds to the oxidation of graphite residue. The mass loss for the DABAP occurs in four steps.

The minor mass loss (1.17 %) below 200 °C probably reflects the loss of moisture. Thereafter a steep mass loss (ca. 15.5 %) event occurs with an onset temperature of 254 °C. This probably reflects the loss of CO_2 due to the decarboxylation of the DABAP. The theoretical mass loss for decarboxylation is 17.6 %. Mass loss continues and reaches the third peak value at a temperature of 446 °C. We attribute this to the char-forming decomposition reaction that also releases ammonia gas. The pyrolysis of the char that is formed continues as the temperature is raised. It reaches a maximum rate at 860 °C. At 900 °C, the carbonised char residue that remains represents just above 27 % of the initial DABAP mass.

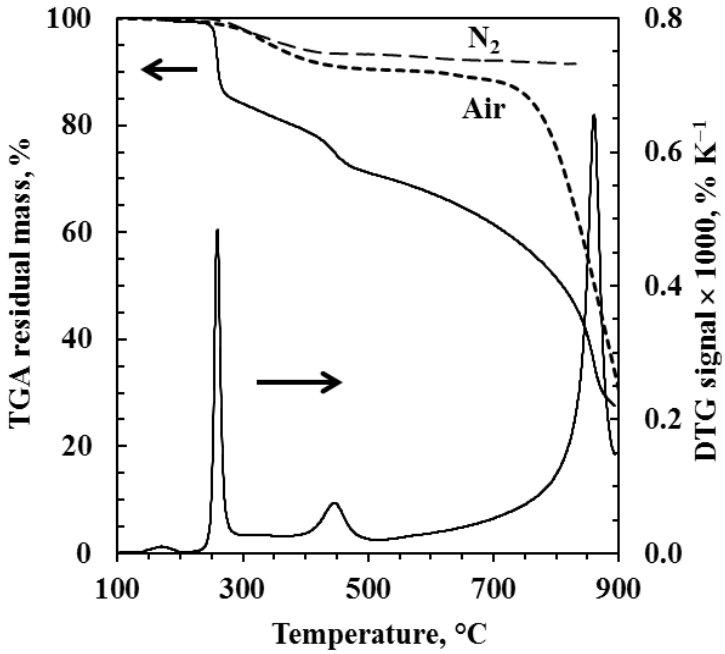

Figure 4-3: TGA and DTG curves for DABAP obtained in N_2 and TGA traces for the EG in air and in nitrogen (dotted lines)

Figure 4-4 shows the DTA curves together with the TGA trace for DABAP (obtained at a scan rate of 10 °C min^{-1} with N_2 gas flowing at a rate of 50 mL min^{-1}). It is clear from this figure that all the mass loss events seen in the TGA are associated with endothermic events.

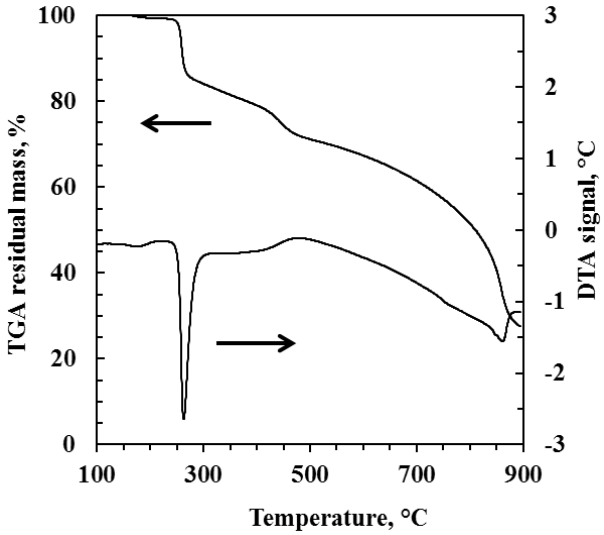

Figure 4-4: TGA and DTA curves for DABAP

A sharp endothermic peak with an onset temperature of 257 °C is displayed in the DSC scan in Figure 4-5(obtained with N_2 gas flowing at a rate of 50 mL min^{-1}. The temperature scan rates were 10 °C min^{-1} and 4 °C min^{-1} respectively). The shape and the corresponding enthalpy change of 624 kJ kg^{-1} are reminiscent of a melting event. The TMA curve in Figure 4-5 indicates softening of the material at this temperature. The melting of DABAP, with simultaneous thermal decomposition commences at about 257 °C.

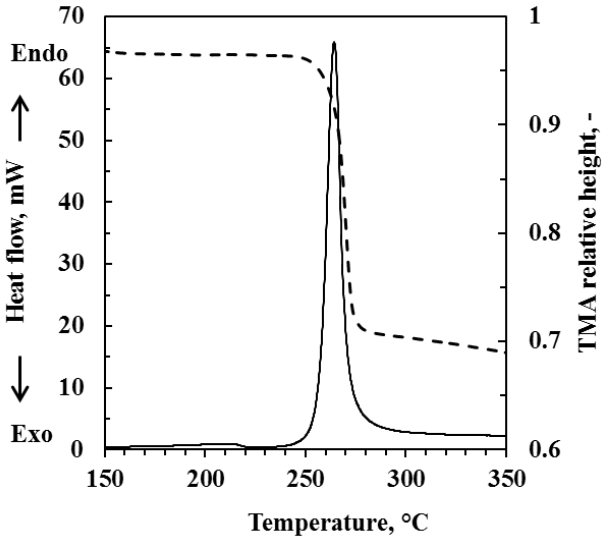

Figure 4-5: DSC and TMA curves for DABAP

The key property of EG in flame retardant applications is the ability to exfoliate within a narrow temperature range. Figure 4-6 compares the TMA expansion performance of the EG sample with the behaviour of DABAP.

The exfoliation onset temperature of the EG was ca. 300 °C. It is clear that the DABAP softened well before the onset of the EG expansion which promotes expansion of EG through DABAP thus increasing the thermal barrier thickness. A penetration probe was used for the DABAP and a flat-tipped standard expansion probes was used for the EG. The applied force was 0.01 N for the DABAP and 0.02 N for the EG. The temperature was scanned at rates of 4 °C min^{-1} and 10 °C min^{-1} respectively.

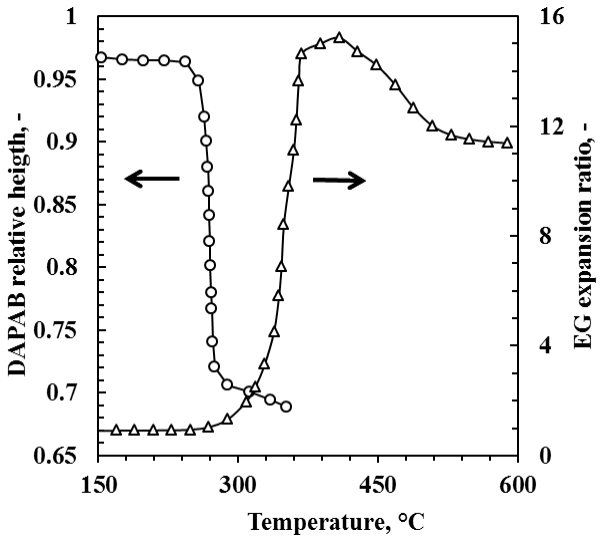

Figure 4-6: Thermomechanical characterisation of the softening of DABAP and the exfoliation process of the EG in a nitrogen atmosphere

4-3.3. Flammability

The cone calorimeter results are presented in Figures 4-7 to 4-13 and these results are summarised in Table 4-2. The sample sheets for all cone calorimeter samples were backed by aluminium foil and their dimensions were 100 mm x 100 mm x 3.2 mm. They were mounted horizontally and exposed to an external heat flux of 35 $kW.m^{-2}$ from above. Figure 4-7 shows representative heat release rate (HRR) curves obtained from the cone calorimeter tests. These curves indicate the substantial reduction in the pHRR achieved through use of flame retardants.

The HRR curves for the flame retarded samples display plateauing behaviour, also known as thermally thick behaviour opposed to the thermally thin behaviour observed for non-flame retarded LDPE.

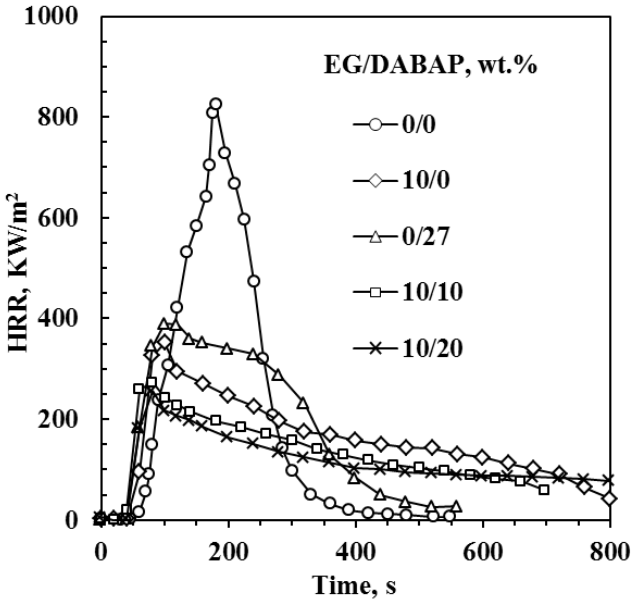

Figure 4-7: Cone calorimeter heat release rate curves for the polyethylene compounds with EG and DABAP

Figures 4-8 reports average values for the total heat release (tHR) and the pHRR. Unexpectedly the tHR value measured was lowest for the carbon black-pigmented polyethylene, hereafter referred to as neat polyethylene (Table 4-2). It was 90 ± 18 $MJ.m^{-2}$ for the neat polyethylene and 103 ± 3 $MJ.m^{-2}$ for the compound with 27 wt.% DABAP. Intermediate values were measured for the other compounds.

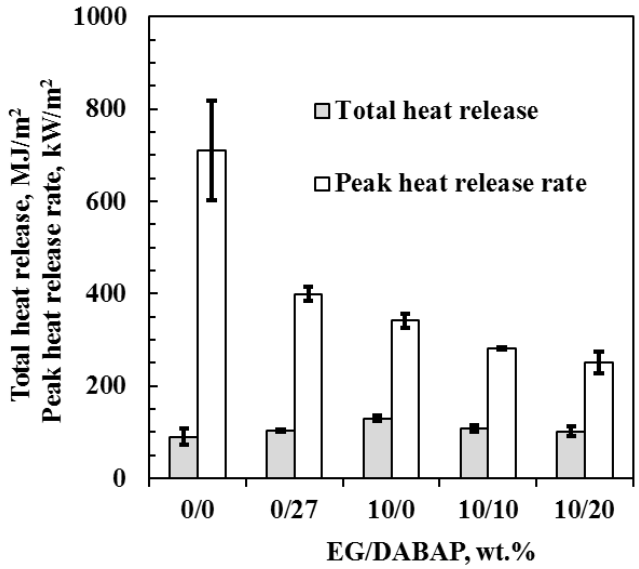

Figure 4-8: Cone calorimeter peak heat release rates and total heat release for the polyethylene compounds with EG and DABAP

All the neat samples ignited and flamed for extended periods of time. The heat release curves for the neat polyethylene compound exhibited the shape characteristic of a thermally thin sample (Schartel & Hull, 2007). Thermally thin samples are identified by a sharp peak in their HRR curves as the whole sample is pyrolysed at once. HRR curves characteristic of thermally thick, char-producing samples show a sudden rise to a plateau value (Schartel *et al*, 2007). The HRR curves for the flame retarded samples approached this shape. They showed a rapid rise after ignition followed by a slower, downward taper. The HRR curve for the 27 wt.% DABAP compound showed a third phase where a faster decay in the HRR occurred. All the flame retarded samples expanded during the fire test but expansion was more pronounced in the samples containing EG. Figure 4-8 shows the effect of adding both EG and DABAP on the pHRR and the THR. The pHRR results are also tabulated in Table 4-2.

The pHRR for the neat polyethylene was 710 ± 109 kW m^{-2}. The best result was obtained from 10 wt.% EG plus 20 wt.% DABAP (252 ± 24 $kW.m^{-2}$) but even the addition of 10 wt.% EG alone reduced the value to 342 ± 15 $kW.m^{-2}$. Table 4-2 shows that the 10 wt.% EG compound is more effective at reducing the pHRR than the 27 wt.% DABAP compound. The improved fire performance with respect to the pHRR is attributed to the formation of a heat-insulating protective barrier at the solid surface. This limited heat transfer to the substrate and thus slowed down the rate of thermal degradation.

Figure 4-9 confirms that the addition of the EG reduced the mass loss rate (MLR). This can be attributed to the expansion of the intercalated graphite which forms a low density layer of loose worm like structures at the surface. Visual inspection of the residues showed that the DABAP containing compounds formed a denser charred foam layer at the polymer interface.

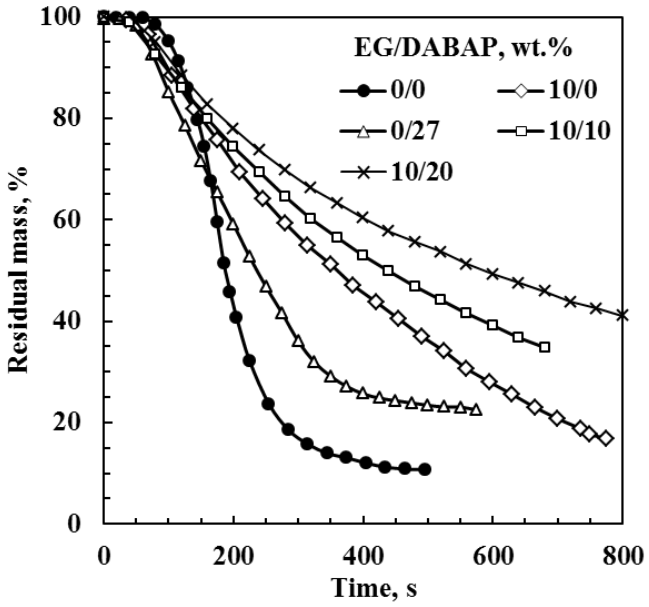

Figure 4-9: Cone calorimeter mass loss curves for the polyethylene compounds with EG and DABAP

Table 4-2: Cone calorimeter data summary

		EG/DABAP, wt.%				
Property	**Units**	**0/0**	**10/0**	**0/27**	**10/10**	**10/20**
Time to ignition (t_{ign})	s	58 ± 3	46 ± 1	33 ± 5	39 ± 3	41 ± 1
Time to *pHRR*	s	177 ± 6	92 ± 3	105 ± 13	72 ± 6	75 ± 0
Time to flame out	s	773 ± 307	869 ± 68	537 ± 69	993 ± 46	1124 ± 106
Total heat release (*tHR*)	MJ m^{-2}	90 ± 18	130 ± 5	103 ± 3	109 ± 7	102 ± 10
Peak heat release rate (*pHRR*)	kW m^{-2}	710 ± 109	342 ± 15	400 ± 16	282 ± 3	252 ± 24
MAHRE	MJ m^{-2}	316 ± 47	199 ± 13	276 ± 12	168 ± 6	146 ± 7
FIGRA	kW $m^{-2}s^{-1}$	4.01 ± 0.52	3.73 ± 0.09	3.86 ± 0.68	3.95 ± 0.37	3.36 ± 0.32
$pHRR/t_{ign}$	kW $m^{-2}s^{-1}$	12.2 ± 2.2	7.38 ± 0.41	12.4 ± 2.7	7.31 ± 0.55	6.15 ± 0.71

Table 4-2 lists the ignition and flame out times for the various samples. Addition of the flame retardants increased the propensity of the material to ignite. The time to ignition (t_{ig}) was 58 ± 3 s for the neat polyethylene and 46 ± 1 s for the compound containing 10 wt.% EG but decreased to 33 ± 5 for the compound containing 27 wt.% DABAP. The lower ignition times are tentatively attributed to rapid decomposition of the IFRs occurring at a lower temperature than for the neat polymer. This suggests that more flammable volatiles are release at an earlier stage in sufficient quantities to allow ignition to occur.

The time to flame out showed considerable variability as outlined in Table 4-2. It was 773 ± 307 for the neat polyethylene, reduced to 539 ± 69 for the 27 wt.% DABAP compound. All other compounds had a longer time to flame out. The reduction found in the DABAP samples may be attributed to its strong charring nature displayed during thermal degradation. For the other samples however, the increase in time to flame out may be attributed to the extended time period during which the thermal barrier counteracts the energy applied. This leads to a plateaued heat release over a longer period with the thermal layer ignited in part throughout the thermal event. For all flame retarded samples there was a marked increase in the tHR. This may be attributed, in part, to the extended plateaued heat release curves of these samples and, in part, to the exothermic nature of the intumescing event of DABAP and the thermal conductivity and glowing behaviour in EG.

Figure 4-10 compares the smoke production rates (SPR) of the composites with that for the neat polyethylene. All the compounds containing EG showed very similar performance with a considerable reduction in smoke generation. Adding DABAP lowered the peak smoke production rate but the total amount of smoke released was higher. A potential explanation is as follows: the rate of smoke reduction is reduced owing to the barrier properties of the char layer that forms on the surface. However, ultimately more smoke is released because the aromatic additive itself has a greater tendency to produce smoke than the aliphatic polymer matrix.

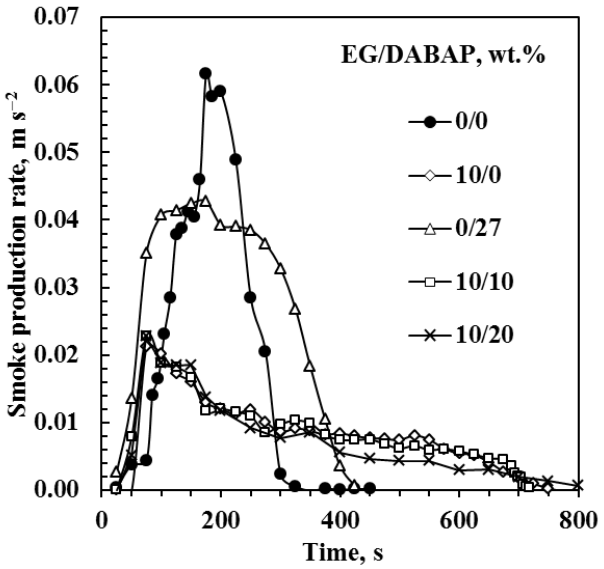

Figure 4-10: Cone calorimeter smoke production curves for the polyethylene compounds with EG and DABAP

Figure 4-11 and Figure 4-12 show the CO_2 and CO release rate curves. The observed trends for CO_2 mirror those observed for the HRR (Figure 4-7) almost perfectly. This is expected as the heat release rate correlates with the oxygen consumption and hence the rate of CO_2 production. The curves for CO are more complex especially in the case of the 27 wt.% DABAP compound. The cause for this behaviour is not currently understood but it could be related to the particular way DABAP decomposes under simulated fire scenarios. Although the peak rate of CO release was higher for the neat polyethylene, the total amount produced by the additive containing compounds appears to be higher. However, this is not significant as the CO production rate was almost two orders of magnitude lower than that of CO_2.

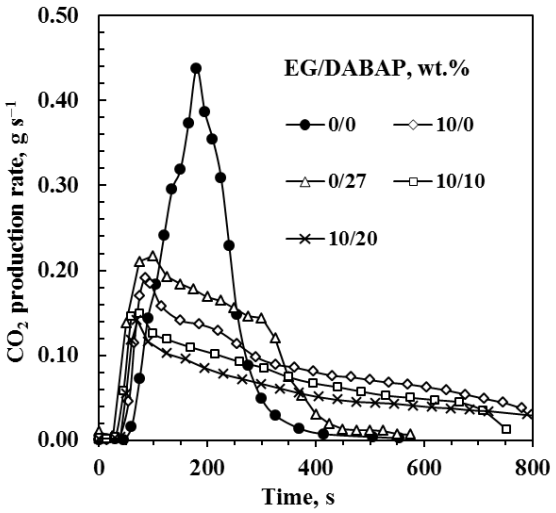

Figure 4-11: Cone calorimeter CO_2 production curves for the polyethylene compounds with EG and DABAP

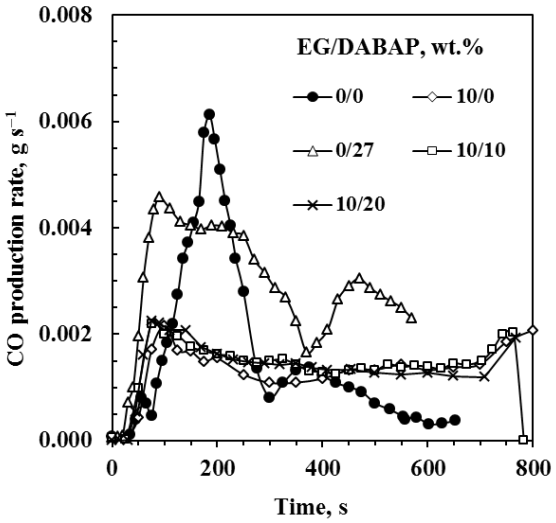

Figure 4-12: Cone calorimeter CO production curves for the polyethylene compounds with EG and DABAP

The fire growth rate (FIGRA) and the maximum average rate of heat emission (MAHRE) are indices that may be used to interpret cone calorimeter data (Sacristán *et al*, 2010; Schartel *et al*, 2007). The MARHE parameter is defined as the peak value of the cumulative heat emission divided by time (Sacristán *et al*, 2010). It provides a measure of the propensity for fire development under real scale conditions (Sacristán *et al*, 2010).

The FIGRA is an estimator for the fire spread rate and size of the fire whereas the MARHE guesstimates the tendency of a fire to develop.(Sacristán *et al*, 2010) The FIGRA is determined as

$$FIGRA = pHRR/time\ to\ pHRR \quad (4\text{-}1)$$

Table 4-2 lists the FIGRA and MAHRE indices. A marked reduction of up to 50 % relative to the neat polyethylene was observed for the MAHRE measured for the 10 wt.% EG / 20 wt.% DABAP combination. The FIGRA values, although somewhat reduced, did not differ markedly from those of the neat polyethylene.

The parameters that are pertinent to fire hazards are the fire load and flame spread (Schartel *et al*, 2007). The Petrella plot is an attempt to gauge the magnitude of the fire hazard posed (Petrella, 1994; Schartel *et al*, 2007). It is a plot of the total heat evolved *tHR* (as fire load) against $pHRR/t_{ig}$ (as a fire growth index). For a material to be effectively flame retarded both the fire load and the fire growth index should assume low values. Figure 4-13 shows a Petrella plot for the present formulations.

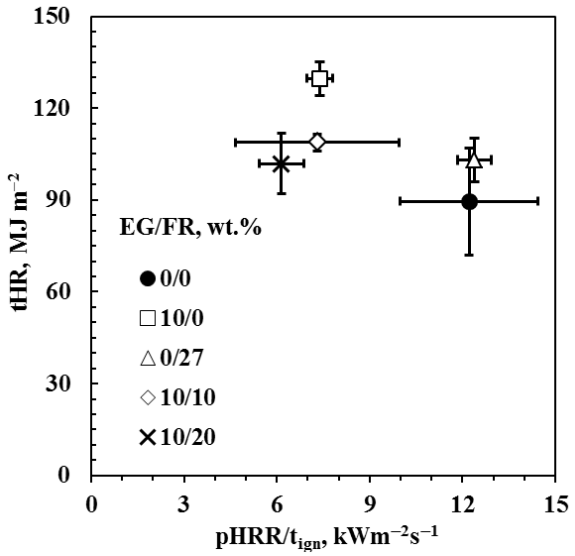

Figure 4-13: Petrella plot[21] for the polyethylene compounds with EG and DABAP

Except for the 27 wt.% DABAP compound, all the other flame retarded compounds showed a decrease in the $pHRR/t_{ig}$ parameter but a slight increase in the heat load. The former performed slightly worse than the neat polyethylene according to both Petrella parameters. The reason for this is that the reduction in the time to ignition was larger than the reduction in pHRR. The overall heat load was also higher than that of the neat polyethylene.

4-4. Conclusions

The phosphate salt of 3,5-diaminobenzoic acid was obtained by a facile precipitation reaction. This compound has a relatively high thermal stability. It softens and melts at 257 °C and simultaneously decomposes with rapid mass loss up to ca. 17 wt.% observed just above this temperature. This is attributed to a decarboxylation reaction that releases CO_2. The thermal decomposition proceeded stepwise at higher temperatures and resulted in a char yield of ca. 27 wt.% at 900 °C.

The flame retardant performance of this compound on its own, and in combination with a high thermal-stability EG, was evaluated by cone calorimetry. Polyethylene containing 5 wt.% carbon black was used as reference. Cone calorimeter results revealed that adding 10 wt.% EG lowered the pHRR of carbon black-pigmented polyethylene from 710 ± 109 $kW.m^{-2}$ to 342 ± 15 $kW.m^{-2}$, while the compound containing 27 wt.% of the intumescent and 3 wt.% carbon black lowered it to 400 ± 16 $kW.m^{-2}$. Combinations of these two additives decreased the pHRR even further.

The intumescent additive reduced the flame out time from 773 ± 307 s to 537 ± 69 s while all other samples containing EG increased it. On the other hand, the addition of the EG had a much greater effect on reducing smoke emission.

All present additives caused a marginal decrease in the FIGRA fire index. The sample containing 10 wt.% EG in combination with 20 wt.% intumescent DABAP caused a staggering reduction of 50% in the MAHRE value. The Petrella plot (Figure 4-13), an alternative measure of the flame retarding ability of a compound, indicated only marginal performance differences between the formulations tested.

Chapter 5: Cone calorimeter fire performance of low and high temperature expandable graphite in binary systems with ethylenediamine phosphate and 3,5-diaminobenzoic acid phosphate to determine optimal synergistic combinations

Foreword

This chapter contributed to the publication:

- *Cone calorimeter study of polyethylene flame retarded with expandable graphite and intumescent flame retardant additives (Kruger et al, 2014)*

This chapter and publication acknowledges contributions from the following persons:

- *Walter Wilhelm Focke, Washington Mhike, Albertus Taute, Albert Roberson and Osei Ofosu*

See appendix A-10 for the apparatus used for cone calorimetric testing and table A-10-1 which indicates some of the multitude of properties cone calorimetry can measure.

Executive summary

Polyethylene was flame retarded with an IFR at 27 wt.% and EG at 10 wt.% either on its own or in combination with 10 wt.% or 20 wt.% of the intumescent. Two grades of each flame retardant type were used. They differed primarily with respect to the onset temperature for exfoliation (commercially sourced EG types) or decomposition (intumescence).

The latter were the high-decomposition-onset-temperature intumescent 3,5-diaminobenzoic acid phosphate and the commercially available low-decomposition-onset-temperature EDAP. The fire performance of pressed sheets with a nominal thickness of 3.2 mm was tested in a cone calorimeter at a radiant flux of 35 $kW.m^{-2}$.

The best char yields were obtained with compositions containing 3,5-diaminobenzoic acid phosphate. Despite this, the best fire overall performance was realised using EDAP, together with the low-exfoliation-onset-temperature EG. Formulations based on this intumescent compound ignited later, reached the pHRR earlier, and also burned longer irrespective of the EG grade used. This can be attributed to the formation, at the burning surface, of a more cohesive char with better thermal and mass transfer barrier properties. This explains why compositions based on EDAP as intumescent outperformed those containing 3,5-diaminobenzoic acid phosphate in terms of the pHRR and other important fire indices.

Keywords: expandable graphite; exfoliation; intumescent flame retardant; thermal analysis; cone calorimeter

5-1. Introduction

Polyethylene is used to fabricate melded goods such as battery boxes and air ventilation ducting, as well as extruded products such as pipes and cable sheathing. These products are used extensively in deep-level underground mining applications. Polyethylene has a high heat of combustion and a low propensity for char formation (Weil *et al*, 2008). As a result, these products present a potential fire hazard which is of particular concern in confined space mining applications. It is therefore necessary to flame retard polyethylene products with suitable additives for critical applications. A wide range of effective flame retardants are available (Dasari *et al*, 2013a; Weil *et al*, 2008). Some studies have highlighted the utility of EG, IFRs and their synergistic combinations which improve the fire behaviour of polyethylene (Han *et al*, 2007c; Pang *et al*, 2012a; Qu *et al*, 2003b; Sun *et al*, 2014; Weil *et al*, 2008; Xie *et al*, 2001c; Xie *et al*, 2001d).

Intumescent additives swell when exposed to fire or heat. They form a carbonaceous foam residue on the surface that acts as a heat insulator and a physical barrier to the transport of oxygen and pyrolysis products (Camino *et al*, 1989; Dasari *et al*, 2013a; Lewin, 1999b; Wang *et al*, 2005).

EG is a partially oxidised, intercalated form of graphite. It contains intercalated guest species (e.g. sulfuric acid anions) in between the stacked graphene layers (Camino *et al*, 2001b; Furdin, 1998). A key property of EG is its tendency to exfoliate explosively, i.e. to expand rapidly in a worm-like manner when heated to high temperatures (Chung, 1987; Chung, 2002a; Wissler, 2006). When this occurs at an upward facing surface of a polymer, a loose cover of "fluffy" vermicular graphite is deposited. This provides a protective barrier similar to that generated by conventional intumescent additives. However, unlike the foam coating generated by conventional IFRs, this cover is weakly bonded to the polymer surface and there is no cohesion between adjacent EG worms. This leads to poor performance when the fire is associated with strong convection currents or when a sample is exposed to a flame from below.

Cone calorimetry is a modern method for measuring the t_{ig}, HRR, combustion products and other flammability characteristics of polymer samples. This fire testing method determines the transient HRR by measuring transient oxygen consumption rate in the exhaust gases. According to Babrauskas *et al* (1992) the HRR is the most important single variable in characterising the flammability of products and thus the fire hazard they may pose. Among the more widely used polymers, polyethylene features the highest heat release capacity and the highest HRR in cone calorimeter tests (Dasari *et al*, 2013a).

According to Han *et al* (2007c) and Xie *et al* (2001c) superior fire properties are possible with combinations of EG and other IFRs. However, only a few such combinations have been explored to date. Therefore, this contribution considered two EG grades and two IFRs as additives for polyethylene. The two grades in each category differed primarily with respect to their decomposition onset temperatures. The fire performance of these additives, on their own and in selected combinations, was studied using cone calorimeter fire testing. A key objective was to determine whether adding an IFR to an EG flame retarded compound can improve cohesion of the exfoliated graphite layer to the polymer surface and cohesion between individual EG worms.

5-2. Experimental

5-2.1. Materials

Sasol Polymers supplied the low density polyethylene in powder and pellet form. It was injection moulding grade LT019 with density 0.919 g cm^{-3} and MFI 20.5 g / 10min @ 190 °C / 2.16 kg. Carbon black grade N660 was sourced from Ferro Industrial Products. The EG grades ES170-300A (with a high expansion onset temperature) and ES250 B5 (low expansion onset temperature) were sourced from Qingdao Kropfmuehl, China. The d_{10}, d_{50}, and d_{90} particle sizes of these two grades were 306 µm, 517 µm, 803 µm and 313 µm, 533 µm and 807 µm respectively (Mastersizer 2000, Malvern Instruments, Malvern, UK). The densities were 2.08 ± 0.01 $g.cm^{-3}$ and 2.23 ± 0.01 $g.cm^{-3}$ respectively.

The surface area of ES170-300A, in the pre-expanded form, was 0.66 $m^2.g^{-1}$ (Nova 1000e BET in N_2 at 77K). The surface area of ES250 B5 could not be determined by BET as it started to exfoliate when measurement was attempted.

The phosphate salt of 3,5-diaminobenzoic acid was synthesised using the procedure previously described in chapter 3 (Focke *et al*, 2014c). EDAP is available for commercial scale use (from Thor in the US and UK, Krems Chemie (Austria), Westman Chemical (India), and also from Chinese manufacturers. The EDAP was synthesised as follows: a quantity of 420.7 g ethylenediamine was weighed into a 5 L beaker. This beaker was placed in 1.5 kg of crushed ice. Next a total of 807 g 85 % technical phosphoric acid was added dropwise, stirring continuously. The precipitated crystals were recovered by vacuum filtration. They were washed once with cold water and then with acetone and left to dry under ambient conditions. The yield was 0.98 kg EDAP (88.6 %). More detail on the EDAP production is provided in appendix A-3.

5-2.2. Preparation of the polyethylene compounds

Polyethylene compounds containing EG and / or IFRs were compounded on a 28 mm co-rotating intermeshing twin screw laboratory extruder (L / D = 16) at a screw speed of 140 - 220 rpm. The extruder screw design comprised intermeshing kneader elements with a forward transport action. The four extrusion processing stage temperatures, feed to die, were set at 120 °C, 175 °C, 175 °C and 180 °C respectively. The extruded strands were granulated and the pellets were air-dried. A polyethylene compound containing 5 wt.% carbon black (N660) was prepared in a similar way. This compound was used as the reference sample for cone calorimeter testing. The compounds containing 27 wt.% intumescent additives (EDAP or DABAP) also contained 3 wt.% carbon black. This maintained a consistent range of dark product sheets as delivered for all EG containing compounds. This was done to ensure comparable absorption of IR radiation during cone calorimeter testing.

Test specimens for cone calorimeter testing were prepared by pressing the pellets into flat sheets in a hot press set at 180 °C. These sheets were prepared at sheet dimensions of 100 mm × 100 mm × 3.2 ± 0.1 mm.

5-2.3. Characterisation and analysis

SEM images were obtained using an ultrahigh resolution FE SEM (HR FE SEM Zeiss Ultra Plus 55) with an InLens detector at acceleration voltages of as low as 1 kV to ensure maximum resolution of surface detail. No electro-conductive coating was applied on the graphite particles.

SEM micrographs of the temperature driven dynamic EG exfoliation processes were also obtained using a SEM (FEI QUANTA 200 ESEM) fitted with a heating stage. The graphite flakes were placed inside a crucible and mounted in the heating stage. They were viewed at 200x magnification. The pressure was 0.5 kPa, voltage 20 kV, spot size 6 - 7 and a working distance of 16 – 20 mm. Temperature was ramped at 20 °C min^{-1}.

5-2.4. Thermal analysis

TGA was performed using the dynamic temperature scan method. Two different instruments, a TA Instruments SDT Q600 and a Mettler Toledo TGA 850e instrument, were employed. Typically, about 10 - 15 mg of sample was placed in an open 50 µL alumina pan. Sample size was reduced to below 5 mg for intumescent materials such as EG which were placed in 150 µm alumina sample holders covered with lids (pin hole) to ensure containment of solids. Temperature was scanned from below 50 °C to 900 °C at a scan rate of 10 °C.min^{-1} with gas (nitrogen or air) flowing at a rate of 50 mL.min^{-1}.

DSC data was obtained on a Perkin Elmer PYRIS Diamond DSC. The temperature was scanned from 30 °C to 370 °C at a scan rate of 10 °C.min^{-1} with nitrogen flowing at a rate of 50 mL.min^{-1}.

Thermal expansion measurements were conducted on a TA instruments Q400 Thermo Mechanical Analyzer. Sufficient EG powder was placed in an alumina sample pan such that the bed height was between 35 µm and 40 µm. The flake expansion behaviour was measured with a flat-tipped standard expansion probe using an applied force of 0.005 N. The temperature was scanned from 30 °C to 600 °C at a scan rate of 10 °C.min^{-1} in a nitrogen atmosphere. The expansion relative to the original powder bed height was reported.

5-2.5. Cone calorimeter flammability testing

The ISO 5660-1 standard was followed in performing the cone calorimeter tests using a Fire Testing Technology Dual Cone Calorimeter. Three specimens of each composition were tested and average values are reported. The sheet dimensions were 100 mm × 100 mm × 3.2 mm. They were placed horizontally on aluminium foil and exposed perpendicularly from above to an external heat flux of 35 kW.m^{-2}.

5-3. Results and discussion

5-3.1. Characterisation

A comprehensive characterisation of the EG samples was previously reported (Focke *et al*, 2014a). These commercial additives were fabricated by treating natural graphite flakes with oxidants such as nitric acid and potassium permanganate in the presence of sulfuric acid. Elemental analysis revealed that the low onset temperature EG (ES250) and the high temperature onset EG (ES170) contained 3.03 wt.% and 2.27 wt.% sulfur respectively. The expansion onset temperatures, determined by thermomechanical analysis, were ca. 225 °C and 300 °C respectively. Both samples released a mixture of carbon dioxide, carbon monoxide and sulfur dioxide during the exfoliation process (Focke *et al*, 2014a). The SEM micrograph in Figure 5-1A shows the morphology of the EDAP powder particles. The flake-like morphology of the DABAP crystals is shown in Figure 5-1B. The EG particles also had a flake-like nature but the flakes were much larger (Focke *et al*, 2014a).

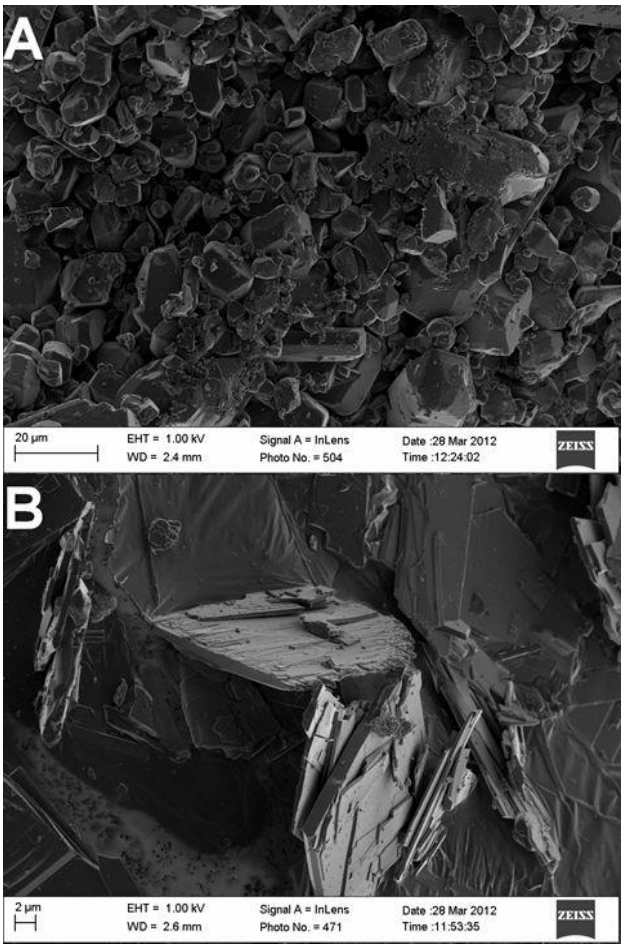

Figure 5-1: FE SEM micrographs of the (A) EDAP powder and (B) the diaminobenzoic acid phosphate crystals (DABAP).

Figure 5-2 shows micrographs of the expanded graphite samples taken in the environmental scanning electron microscopy (ESEM). Both samples yielded vermicular residues. The expansion of the low temperature EG resulted in worms with a fairly regular cross-section. However, those derived from the high temperature EG were highly irregular in shape.

According to the manufacturer, the volume expansion of the low and high temperature EGs were at least 250 $mL.g^{-1}$ and 170 $mL.g^{-1}$ respectively.

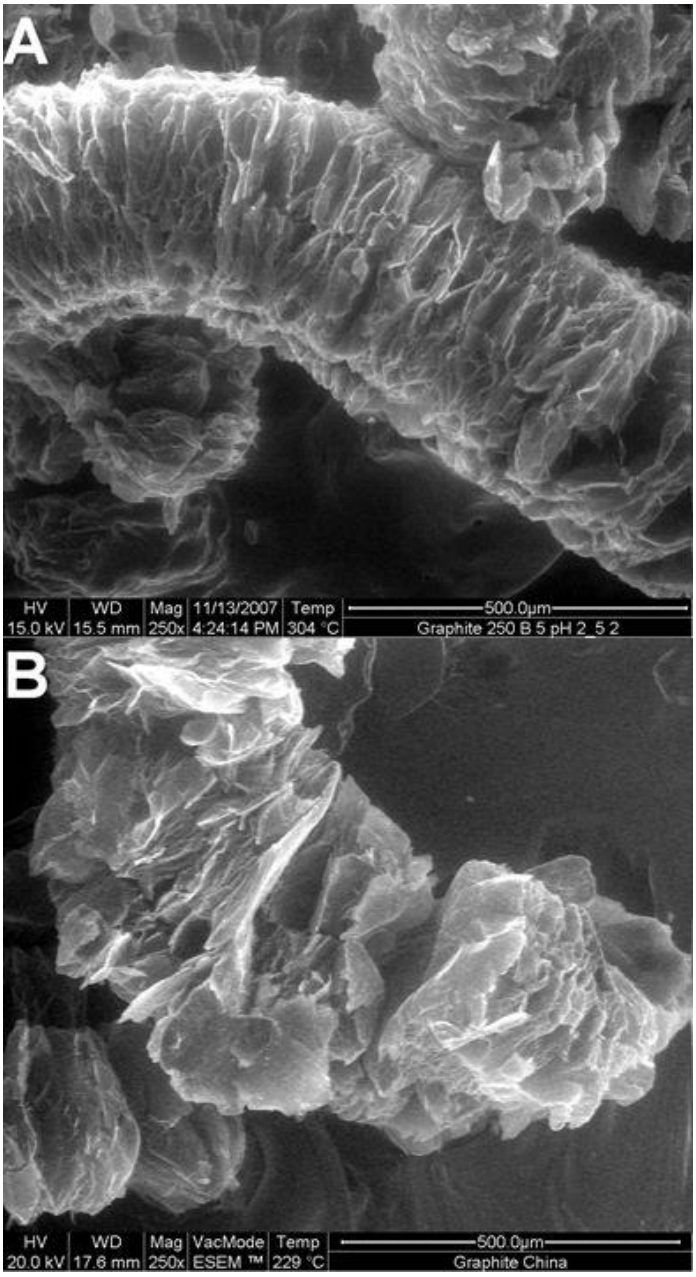

Figure 5-2: Micrographs of the expanded graphite samples after exfoliation in the ESEM. (A) Low onset temperature EG (ES250 B5) and (B) high onset temperature EG (ES170-300A).

5-4. Thermal analysis

The key property of EG in flame retardant applications is the ability to exfoliate when exposed to high heat. Figure 5-3 shows the TMA expansion traces obtained in N_2 and the TGA mass loss curves obtained in air for the EG samples. Apart from a minor mass loss associated with a moisture content of ca. 1 %, the mass loss for the high exfoliation onset temperature EG (ES170) occurred in two steps. The first corresponds to the gas released during the exfoliation event. It commenced at ca. 280 °C and reached a peak mass loss rate at ca. 310 °C. The mass loss associated with the exfoliation reached ca. 10 % at 600 °C. The second mass loss event corresponds to the oxidation of graphite residue. Less than 6 % of the graphite sample remained at 900 °C.

The low exfoliation onset temperature EG (ES250) showed four mass loss steps. There was a minor mass loss below 150 °C indicating a moisture loss of ca. 0.5 %. This was followed by a second mass loss event that started at 210 °C and reached a peak mass loss rate at 226 °C and resulted in an additional mass loss of 4.5 % (total mass loss of 5 %). The TMA traces indicated that this second mass loss event was associated with the expansion of the EG. The third mass loss event commenced at 361 °C and peaked at 408 °C resulting in a further mass loss of 11% (total mass loss of 16%) by 600 °C. The TMA trace indicates that this mass loss was connected with a secondary gas release that ultimately led to the full exfoliation of the graphite. The final step corresponded to oxidation of the graphite residue and a similar char residue remained at 900 °C. In summary, the exfoliation onset temperatures were ca. 210 °C and 280 °C for ES250 and ES170 respectively. ES170 appears to follow a single stage exfoliation. In contrast, both the TMA and TGA curves in Figure 5-3A show that ES250 featured a two-stage exfoliation. In the TMA and TGA experiments the temperature was scanned to 600 °C and 900 °C respectively at a scan rate of 10 °C.min^{-1} with gas flowing at a rate of 50 mL.min^{-1}. In the TMA experiment, a flat-tipped standard expansion probe was used and the applied force was 0.005 N.

The reason for the observed behaviour is not known at this stage but is believed to be related to the characteristic differences between ES250 and ES170 discussed in chapter 2. DSC results (not shown) indicated that the exfoliation, in both samples, is endothermic in nature.

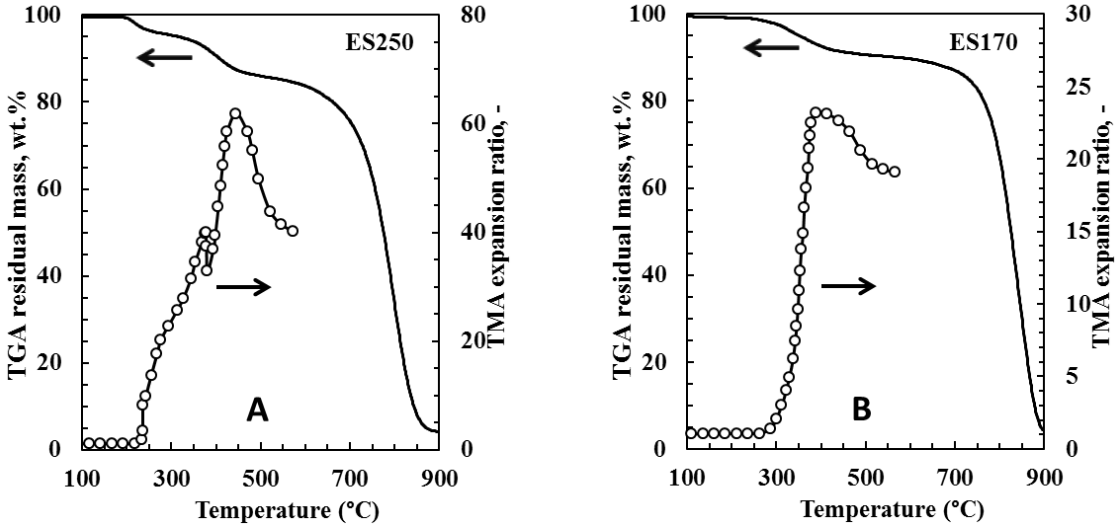

Figure 5-3: TGA (in air) and TMA (in nitrogen) curves for (A) the low exfoliation onset temperature EG (ES250) and (B) the high exfoliation onset temperature EG (ES170)

Figure 5-4 shows TGA and DSC curves for the two IFRs recorded in an air atmosphere. The DSC curve (Figure 5-4D) indicates that mass loss for the DABAP occurred in four steps. TGA and DSC Temperature was scanned to 900 °C at a scan rate of 10 °C min^{-1} with air flowing at a rate of 50 mL min^{-1}.

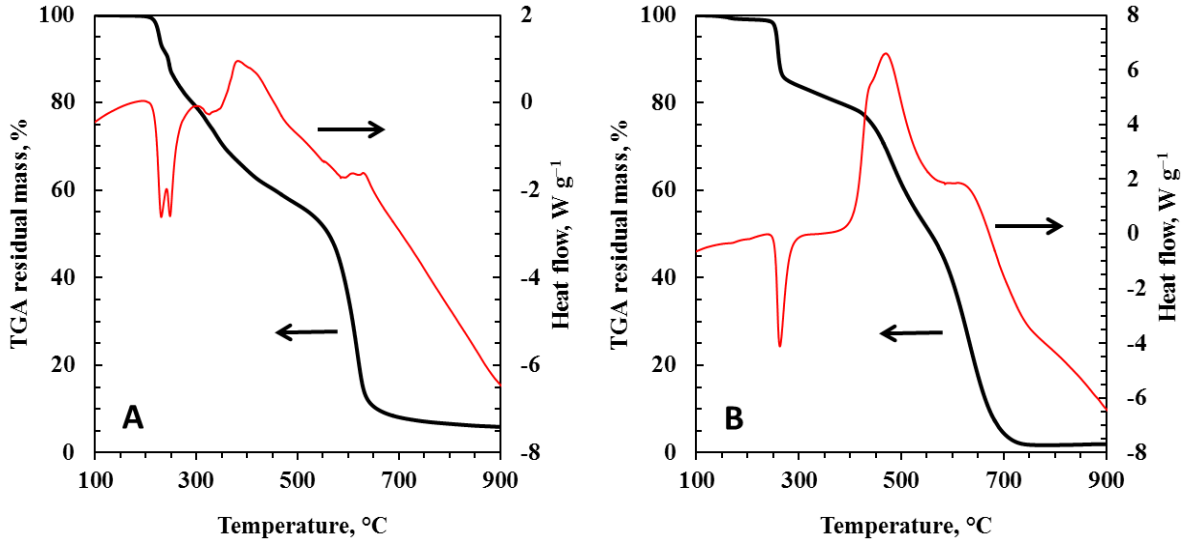

Figure 5-4: TGA (thick line) and DSC (thin red line) curves for (A) EDAP and (B) 3,5-diaminobenzoic acid phosphate

The minor mass loss (1 %) below 200 °C probably reflects the loss of moisture. Starting at a temperature of about 225 °C, an event associated with a steep mass loss (ca. 16 %) occurred. This probably reflects the loss of CO_2 due to the decarboxylation of the DABAP. The theoretical mass loss for decarboxylation is 17.6 %. Mass loss continued and next reached another peak value at a temperature of 465 °C. The DSC curve in Figure 5-4B indicates that this reaction was exothermic, whereas all the others mass loss steps were endothermic in nature. However, in a nitrogen atmosphere this step was endothermic, most likely due to the char-forming decomposition reaction also releasing ammonia gas. The pyrolysis of the char continued as the temperature was raised. It reached a maximum rate at ca. 622 °C and was complete by about 750 °C. The carbonised char residue that remained represented just above 2 % of the initial DABAP mass.

The DSC curve (Figure 5-4A) indicates that the decomposition route for the EDAP was significantly more complicated. The melting and decomposition of this additive commences just above 200 °C. It is characterised by two sharp DSC peaks located at ca. 225 °C and 245 °C. The first is attributed to the onset of melting and the second to an endothermic decomposition reaction.

Multiple peaks are observed between 280 °C and 480 °C. Their number and positions vary with each scan. This suggests that they are associated with the erratic release of gaseous products during the on-going char-forming decomposition reactions. The well-defined DTG peak located at ca. 615 °C is associated with the air oxidation reaction. The DSC curve in Figure 5-4A indicates that this reaction is exothermic whereas all the others are endothermic in nature. The carbonised char residue remaining at 900 °C was only about 6 %.

5-5. Cone calorimeter fire testing

The cone calorimeter results are summarised in Table 5-1 and 5-2 and are presented in Figures 5-5 to 5-11. The summarised data in Table 5-1 includes time to ignition (t_{ig}), time to flame out (t_{fo}), total heat release (tHR), residual mass, total smoke release (TSR) and peak specific extinction area (SEA).

All cone calorimeter test sample sheets were backed by aluminium foil and their dimensions were 100 mm × 100 mm × 3.2 ± 0.1 mm. They were exposed horizontally to an external heat flux of 35 kW m^{-2}. All the samples ignited and flamed for a short period of time. Table 5-1 lists the ignition and flame out times for the various samples. The time to ignition (t_{ig}) was 58 ± 3 s for the neat polyethylene and 46 ± 1 s for the compound containing 10 wt.% EG but decreased to 33 ± 5 for the compound containing 27 wt.% DABAP. For other samples the addition of the flame retardants increased the propensity of the material to ignite. See Table 5-1 for these values.

Table 5-1: Cone calorimeter data summary

	t_{ig} s	t_{fo} s	*tHR* MJ/m²	Residue wt.%	*TSR*×10⁻³ m²/m²	Peak *SEA*×10⁻³ m²/kg
Polyethylene (5 wt.% CB)	58.3 ± 2.5	773 ± 307	90 ± 18	8.3 ± 3.2	0.73 ± 0.14	1.6 ± 1.4
ES250 (10 wt.%)	45.7 ± 1.5	1049 ± 12	119 ± 14	18.5 ± 0.3	0.53 ± 0.01	1.6 ± 1.0
ES170 (10 wt.%)	46.3 ± 0.6	869 ± 68	130 ± 15	12.8 ± 0.1	0.71 ± 0.05	1.7 ± 0.5
EDAP (27 wt.%)	41.3 ± 0.6	878 ± 190	103 ± 8	26.1 ± 2.7	1.45 ± 0.19	4.0 ± 0.9
DABAP (27 wt.%)	33.0 ± 5.2	537 ± 69	103 ± 3	22.4 ± 0.5	1.33 ± 0.03	1.8 ± 0.9
ES250/EDAP (10/10 wt.%)	45.3 ± 1.2	1046 ± 17	109 ± 12	26.3 ± 0.4	0.72 ± 0.01	1.5 ± 0.3
ES250/DABAP (10/10 wt.%)	37.7 ± 0.6	1172 ± 48	117 ± 17	27.8 ± 0.4	0.62 ± 0.02	3.5 ± 1.1
ES170/EDAP (10/10 wt.%)	43.3 ± 1.2	878 ± 48	105 ± 3	21.8 ± 0.3	0.94 ± 0.07	3.6 ± 0.9
ES170/DABAP (10/10 wt.%)	38.7 ± 2.5	993 ± 46	109 ± 7	23.4 ± 1.6	0.77 ± 0.04	1.5 ± 0.7
ES250/EDAP (10/20 wt.%)	46.7 ± 2.5	948 ± 20	100 ± 9	29.5 ± 1.0	0.68 ± 0.02	1.3 ± 0.3
ES250/DABAP (10/20 wt.%)	37.7 ± 1.5	1138 ± 24	99 ± 10	30.6 ± 1.3	0.72 ± 0.06	2.1 ± 1.8
ES170/EDAP (10/20 wt.%)	46.3 ± 1.5	866 ± 28	109 ± 12	26.6 ± 1.0	0.88 ± 0.09	2.5 ± 1.0
ES170/DABAP (10/20 wt.%)	41.0 ± 1.0	1124 ± 106	102 ± 10	31.6 ± 2.1	0.65 ± 0.02	3.2 ± 1.3

The times to ignition were shorter for the flame retarded compounds. This phenomenon is attributed to the lower thermal stability of the additives relative to the neat polymer and destabilisation of the polymer by the presence of the additives. Support for this contention was provided by TGA (Focke *et al*, 2014a). Addition of the flame retardants resulted in the initiation of mass loss at lower temperatures. This implies that flammable volatiles could have been released at an earlier stage in the fire tests.

The time to flame out showed considerable variability. It was 773 ± 307 s for the neat polyethylene. It was longer for all flame retarded samples except for the 27 wt.% DABAP compound where it was reduced to 539 ± 69 s.

The heat release curves for the black-pigmented polyethylene compound exhibited the shape characteristic of a thermally thin sample (Schartel *et al*, 2007). Thermally thin samples feature a sharp peak in their HRR curves as the whole sample is pyrolysed at once. HRR curves characteristic of thermally thick, char-producing samples show a sudden rise to a plateau value (Schartel *et al*, 2007). The HRR curves for the flame retarded samples approached this shape. They showed a rapid rise after ignition followed by a slower, downward taper in the HRR. The HRR curve for the 27 wt.% DABAP compound showed a third phase where a faster decay in the HRR occurred. All the flame retarded samples expanded during the fire test but expansion was more pronounced in the samples containing EG.

Figure 5-5 shows representative HRR curves and Figure 5-6 reports pHRR from the cone calorimeter tests. The pHRR for the neat polyethylene was 710 ± 109 kW m^{-2}.

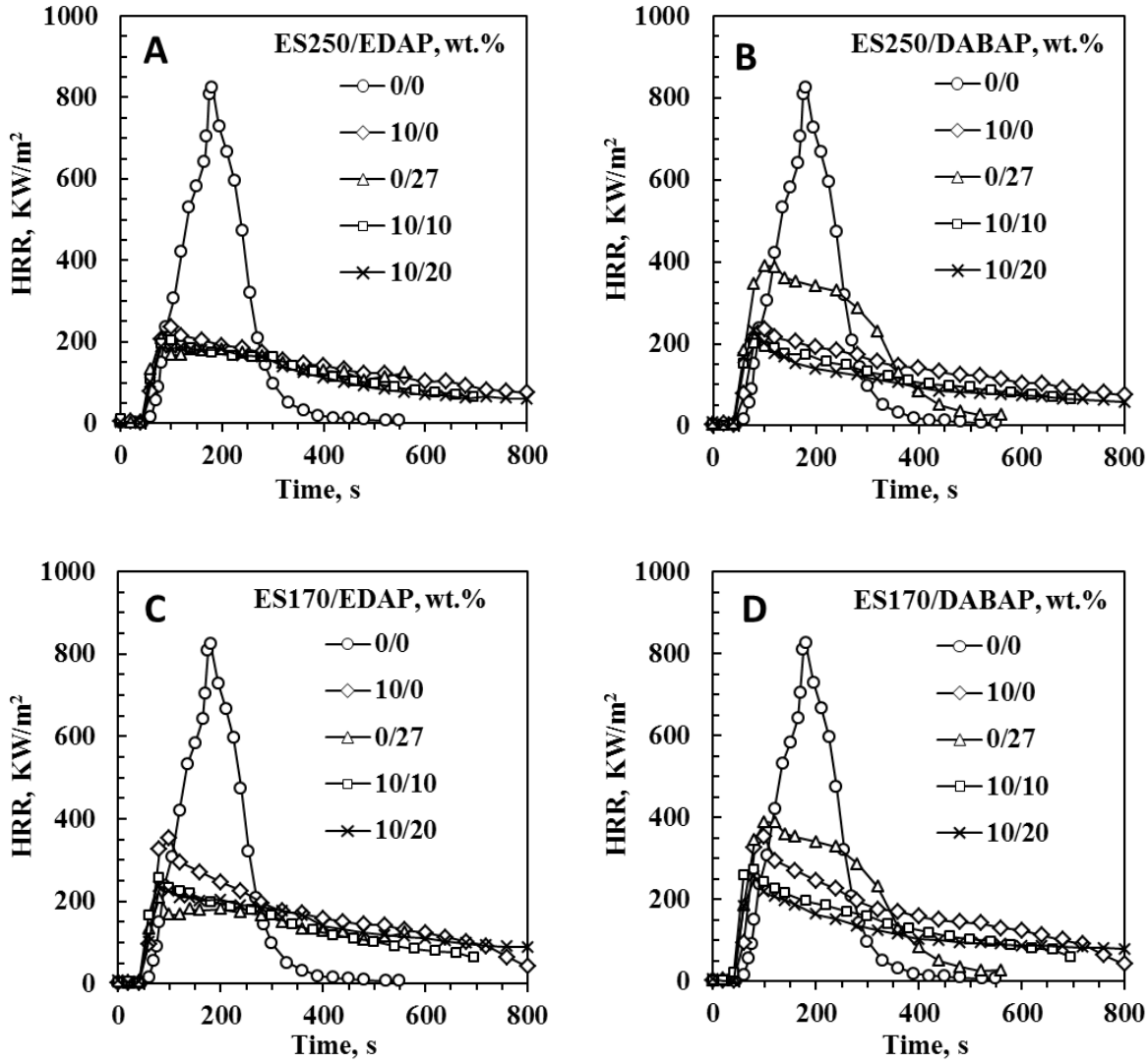

Figure 5-5: Cone calorimeter heat release rate curves for the various compounds. (A) Low exfoliation onset temperature EG (ES250) with EDAP. (B) ES250 with diaminobenzoic acid phosphate (DABAP). (C) High exfoliation onset temperature EG (ES170) with EDAP. (D) ES170 with DABAP

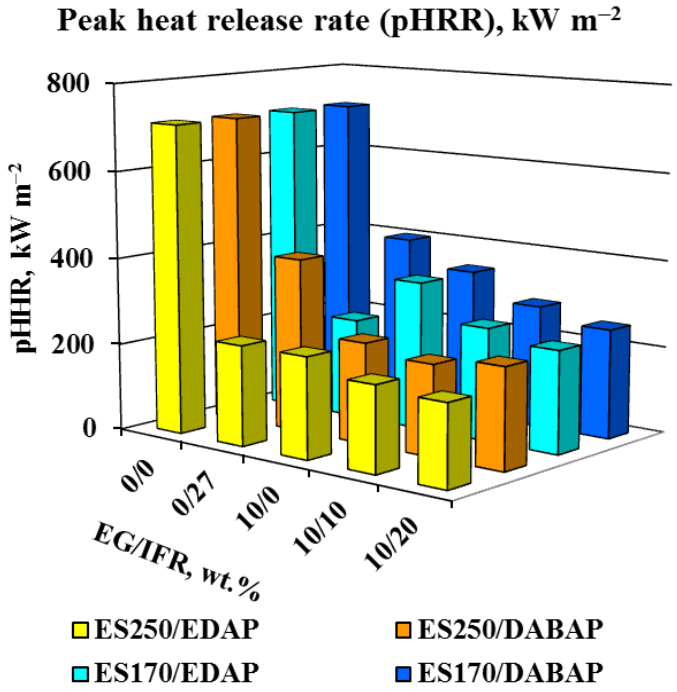

Figure 5-6: Cone calorimeter peak heat release rates for polyethylene flame retarded with different EG grades and IFRs

Figure 5-5 and Table 5-2 shows that all 10 wt.% EG compounds were more effective at reducing the pHRR than the 27 wt.% DABAP compound. The 10 wt.% EG, 20 wt.% DABAP compound reduced the pHRR to 231 ± 11 kW.m^{-2}. However, this is about the same as the value achieved by the compound with 10 wt.% ES250 alone. The best pHRR reduction result was obtained with the 10 wt.% ES 250 plus 20 wt.% EDAP (187 ± 1 kW.m^{-2}) compound. Table 5-2 presents pHRR, time to peak heat release rate (t-PHRR), MAHRE, FIGRA and the fire growth index (pHRR/t_{ign}).

Table 5-2: Cone calorimeter data summary

Quantity	***pHRR***	***t-pHRR***	***MAHRE***	***FIGRA***	***pHRR/t*$_{ign}$**
Sample (Composition)	**kW m^{-2}**	**s**	**kW m^{-2}**	**kW m^{-2}s^{-1}**	**kW m^{-2}s^{-1}**
Polyethylene (5 wt.% CB)	710 ± 109	177 ± 6	317 ± 47	4.0 ± 0.5	12 ± 2
ES250 (10 wt.%)	231 ± 7	97 ± 3	154 ± 6	2.4 ± 0.1	5.1 ± 0.2
ES170 (10 wt.%)	342 ± 15	92 ± 3	199 ± 13	3.7 ± 0.1	7.4 ± 0.4
EDAP (27 wt.%)	230 ± 5	73 ± 3	149 ± 6	3.1 ± 0.2	12 ± 3
DABAP (27 wt.%	400 ± 16	105 ± 13	276 ± 12	3.9 ± 0.7	12 ± 3
ES250/EDAP (10/10 wt.%)	197 ± 10	97 ± 8	141 ± 1	2.1 ± 0.2	5.6 ± 0.3
ES250/DABAP (10/10 wt.%)	209 ± 8	80 ± 0	142 ± 6	2.6 ± 0.1	5.6 ± 0.3
ES170/EDAP (10/10 wt.%)	260 ± 6	77 ± 3	173 ± 6	3.4 ± 0.2	6.0 ± 0.2
ES170/DABAP (10/10 wt.%)	282 ± 3	72 ± 6	168 ± 6	4.0 ± 0.4	7.3 ± 0.6
ES250/EDAP (10/20 wt.%)	187 ± 1	128 ± 53	141 ± 2	1.6 ± 0.7	6.1 ± 0.4
ES250/DABAP (10/20 wt.%)	231 ± 11	78 ± 3	136 ± 3	3.0 ± 0.2	6.1 ± 0.4
ES170/EDAP (10/20 wt.%)	235 ± 2	97 ± 29	167 ± 1	2.6 ± 0.6	5.1 ± 0.1
ES170/DABAP (10/20 wt.%)	252 ± 24	75 ± 0	146 ± 7	3.4 ± 0.3	6.2 ±0.7

Parameters that are pertinent to fire hazards are the fire load and the flame spread (Schartel *et al*, 2007). The fire load is the total amount of heat that can be generated by a flammable material if it is ignited. In the cone calorimeter this index is quantified by the tHR. The tHR value measured was lowest for the carbon black-pigmented polyethylene at 90 ± 18 MJ m^{-2}. Owing to the large uncertainty in the experimental tHR values, the observed differences between this sample and the other samples tested were not statistically significant.

Flame spread is not directly measured in a cone calorimeter. The FIGRA and the fire growth index ($pHRR/t_{ig}$) proposed by Petrella (1994), can be used as proxy estimators for the flame spread (Schartel *et al*, 2007). The FIGRA can usually be determined from equation 5-1.

$$\text{FIGRA} = \text{pHRR/time to pHRR} \tag{5-1}$$

An important index used to interpret cone calorimeter data is the MAHRE (Sacristán *et al*, 2010; Schartel *et al*, 2007). The MAHRE parameter is defined as the peak value of the cumulative heat emission divided by time (Sacristán *et al*, 2010). It provides a measure of the propensity for fire development under full scale conditions (Sacristán *et al*, 2010).

Table 5-2 lists the time to pHRR together with the FIGRA, MAHRE and fire growth indices. For a material to be effectively flame retarded, the indices should all assume low values. Table 5-2 shows that all the flame retarded compounds did indeed achieve the required reductions relative to the neat carbon black pigmented polymer. The effect of composition on the MAHRE index is illustrated in Figure 5-7. The value for the reference compound was 317 ± 47 $kW.m^{-2}$. The two IFRs at 27 wt.% gave a marginal reduction. All other compounds showed a reduction in the MAHRE of more than 50% relative to the neat polyethylene. The best result was obtained with the 10 wt.% ES250 + 20 wt.% DABAP combination.

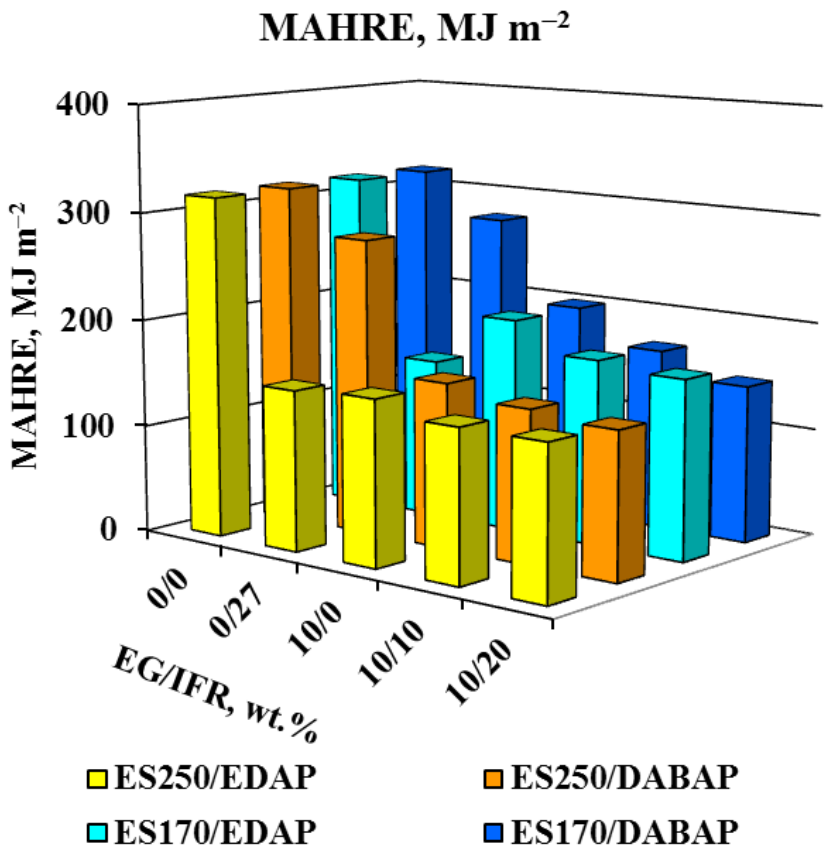

Figure 5-7: Cone calorimeter *MAHRE* for polyethylene flame retarded with different EG grades and IFRs

The *FIGRA* data are plotted in Figure 5-8. The *FIGRA* value for the black pigmented polyethylene was 4.0 ± 0.5 kW.m^{-2}s^{-1}. Using only DABAP or ES170 as flame retardants made very little difference to the value of this index. The ES250 EG grade was very effective in reducing the *FIGRA* but the best results were achieved with the 10 wt.% ES250 + 20 wt.% EDAP compound. The *FIGRA* for this combination was only 40 % of the value for the reference compound.

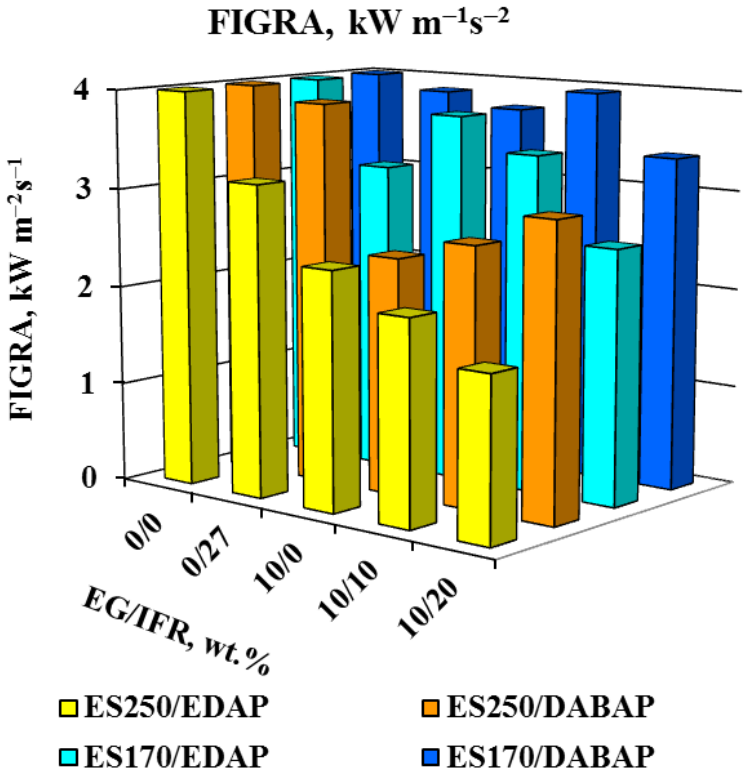

Figure 5-8: Cone calorimeter *FIGRA* for polyethylene flame retarded with different EG grades and IFRs

Figure 5-9 and Table 5-2 show that, barring the two IFR additives at 27 wt.%, all flame retarded compounds decreased the $pHRR/t_{ig}$ parameter. The reason for the poor performance of the IFRs was their short ignition times (Table 5-1). These times were shortened in proportion to the degree of reduction in pHRR of said compounds. The lowest value for the fire growth index was $pHRR/t_{ig}$= 5.1 kW.m^{-2}s^{-1} while that for the neat polymer was 12 1 kW.m^{-2}s^{-1}. These were achieved by the 10 wt.% ES250 compound and the compound containing 10 wt.% ES250 + 20 wt.% EDAP.

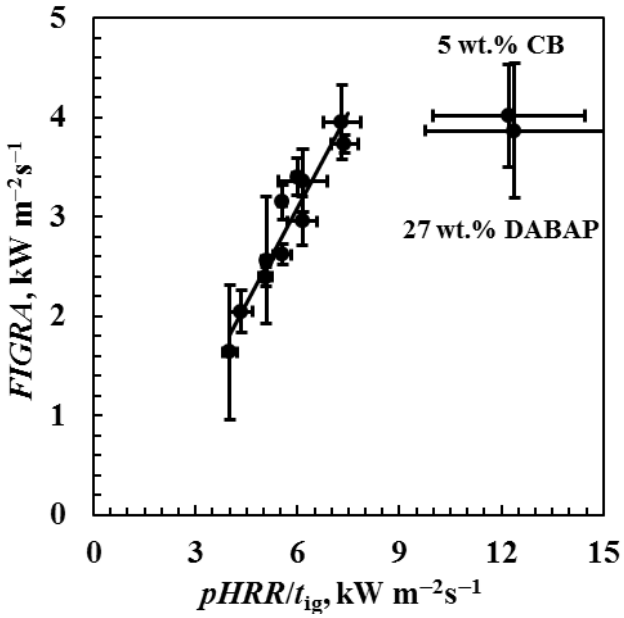

Figure 5-9: Relationship between the *FIGRA* and the $pHRR/t_{ig}$ index for the present flame retarded compounds.

As previously mentioned, both the FIGRA and the fire growth index ($pHRR/t_{ig}$) are considered to be potential estimators for the flame spread (Schartel *et al*, 2007). This implies that these two parameters should be linearly correlated. These two parameters are plotted against one another in Figure 5-9. If the reference polyethylene compound, and the compound containing 27 wt.% DABAP, are not included, it reveals that the two parameters are correlated.

The improved fire performance, with respect to the various fire indices, is attributed to the formation of heat-insulating protective barriers at the solid surface exposed to the radiant heat. These layers limited heat transfer to the substrate which slowed down the rate of thermal degradation of the polymer. This, in turn, reduced the rate at which volatile fuel was released. This phenomenon led to decreased material consumption, or mass loss, during fire testing of the flame retarded samples. This is confirmed by the higher residue values listed in Table 5-1.

The smoke generated by fires reduces visibility and this can significantly affect life safety in underground mining applications (Perera & Litton, 2011). Figure 5-10 compares the total smoke release (TSR) during the flaming phase of the cone calorimeter tests of the composites with that for the neat polyethylene. In general, adding an IFR only lowered the peak smoke production rate but the total amount of smoke released increased significantly.

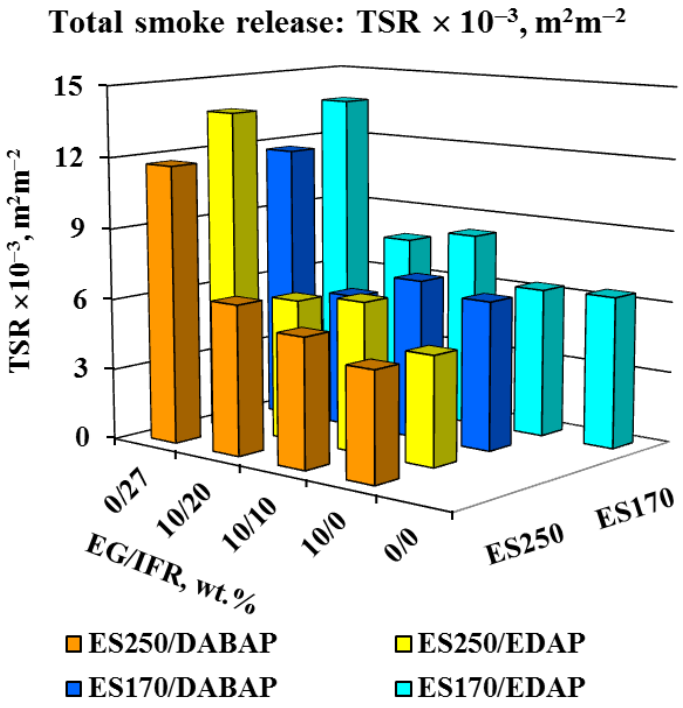

Figure 5-10: Cone calorimeter total smoke release for polyethylene flame retarded with different EG grades and IFRs

The decrease in the peak smoke release rate is attributed to the surface barrier generated by intumescence which reduces the rate of combustion. The overall increase is attributed to the lower molar mass and consequently higher volatility of the IFRs. The 27 wt.% DABAP compound produced the highest amount of smoke. This is possibly due to the aromatic nature of this compound which facilitates soot formation. All the compounds containing EG showed very similar performance with a considerable reduction in smoke generation. These results indicate that EGs are powerful suppressants of the smoke, including smoke produced by the intumescent additives. These observations may be explained as follows: the expanded graphite flakes do not decompose to contribute to smoke creation. Instead, the high surface area of the porous layer of exfoliated graphite worms formed at the top of the sample probably absorbs smoke particles emitted by the rest of the material.

In fire deaths the influence of heat is considered to be of minor importance. Mortality is invariably caused by toxic gases (Babrauskas *et al*, 1992) with carbon monoxide as primary culprit and carbon dioxide of secondary importance (Gormsen, Jeppesen & Lund, 1984; Hirschler, 1994).

The observed trends for CO_2 release rates mirrored those observed for the *HRR* (Figure 5-6) almost perfectly. However, Figure 5-11 shows that the measured CO release rate curves were more complex. Although the peak rate of CO release was higher for the neat polyethylene, the total amount produced by the IFR containing compounds appeared to be slightly higher. However, the CO emissions were significantly lower with the two compounds containing 10 wt.% EG. This suggests that the decomposition of the EGs does not result in significant CO generation in comparison to the IFRs. In addition, the lower rate of fuel generation from the decomposition of the polymer may have resulted in a leaner flame and thus more complete combustion with lower carbon monoxide content in the exhaust gases.

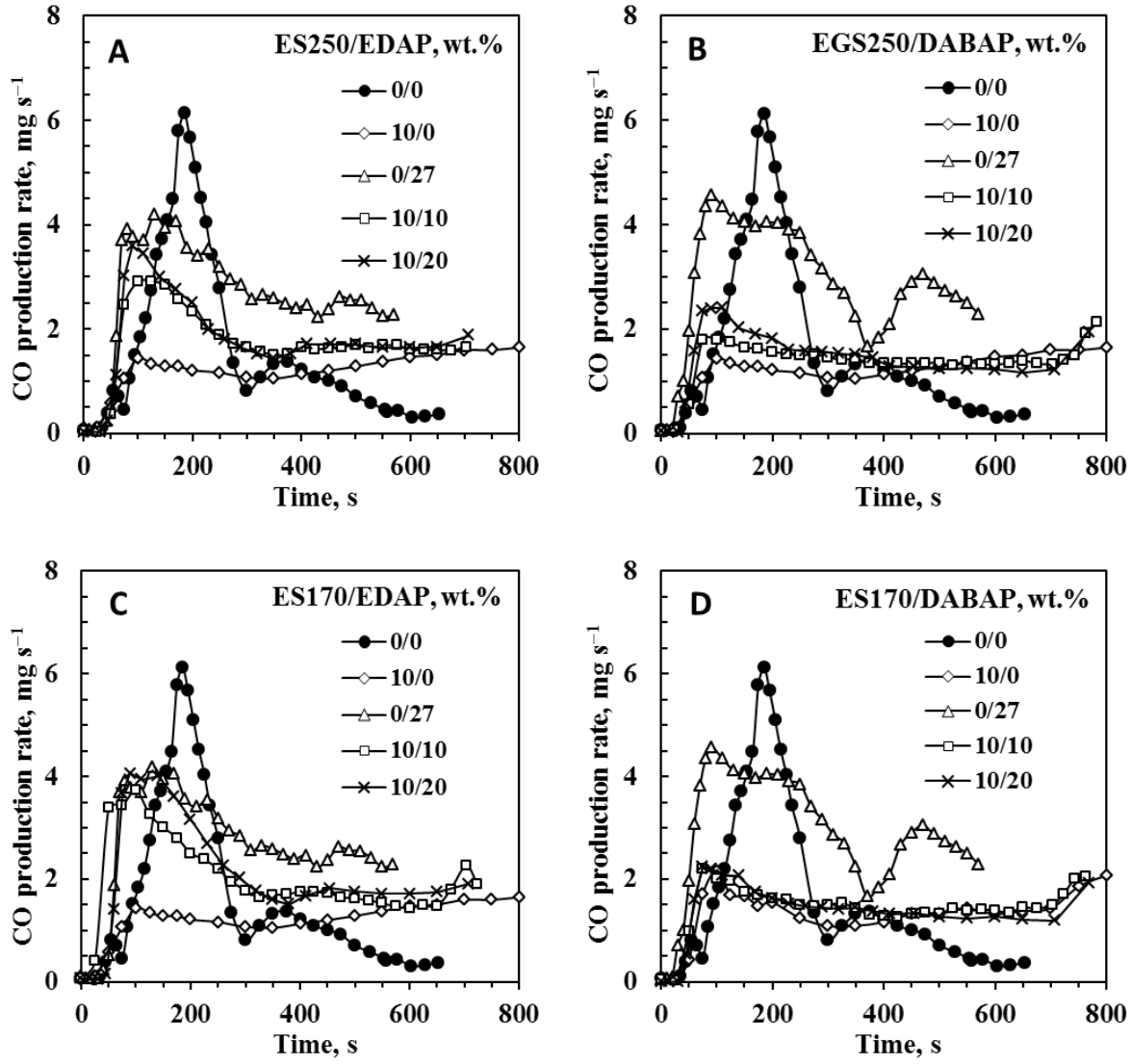

Figure 5-11: Cone calorimeter CO production curves for the various compounds. A. Low exfoliation onset temperature EG (ES250) with EDAP. B. ES250 with diaminobenzoic acid phosphate (DABAP). C. High exfoliation onset temperature EG (ES170) with EDAP. D. ES170 with DABAP

Compositions containing EDAP outperformed those containing DABAP in terms of the fire indices and the pHRR. The EDAP formulations ignited later but still reached their pHRR earlier but burned for a longer period of time. This was true irrespective of the EG grade used. In contrast, the opposite was true with respect to the mass of the char residue that remained following a cone test. These results indicate that comparable DABAP formulations showed a better char yield.

Figure 5-12 shows FE SEM micrographs of the microstructure of chars obtained by exposing 1:1 (mass basis) mixtures of ES250 with EDAP or DABAP after exposure to an open flame.

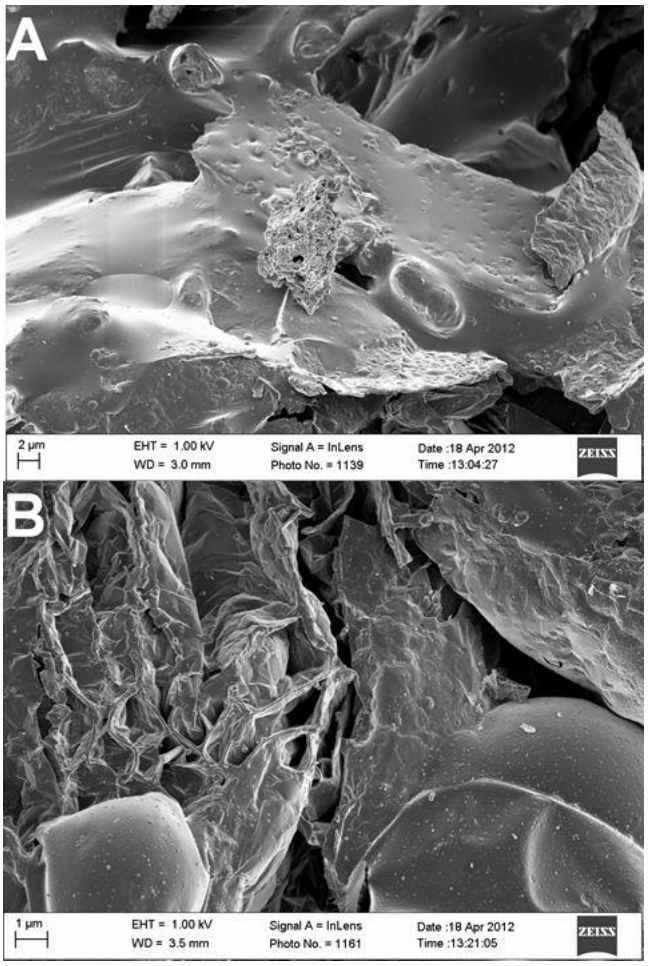

Figure 5-12: SEM micrographs of the expanded EG microstructures obtained by exposing 1:1 mass ratio mixtures of ES250 with either (A) EDAP or (B) DABAP.

These pictures should be compared with those in Figure 5-2 which show the uncoated accordion-like surface of the expanded worms. Careful inspection of these and several other micrographs showed that EDAP formed a more cohesive coating on the EG flake edges than DABAP did. The reason for the improved performance of the EDAP systems may therefore be found in the superior integrity of the intumescent char layer that formed at the surface of the test samples as they expanded together. Further confirmation was obtained by visual inspection of the cone calorimeter chars. These also indicated that EDAP as an IFR resulted in char residues with a greater cohesion.

5-6. Conclusions

The effectiveness of two EG grades and two IFRs was evaluated. Pressed sheets with a nominal thickness of 3.2 mm were tested in a cone calorimeter at a radiant flux of 35 kW.m^{-2}. A polyethylene compound pigmented black with 5 wt.% carbon black was used as the reference material. The compositions of the flame retarded compounds were as follows: 0/27, 10/0, 10/10, and 10/20 wt.% intumescent/EG.

The pHRR of the carbon black-pigmented polyethylene reference material was 710 ± 109 kW m^{-2}. All the flame retarded compounds significantly decreased the pHRR. It was lowered to 231 ± 7 kW.m^{-2} and 230 ± 5 kW.m^{-2} in the presence of 10 wt.% EG with a low exfoliation onset temperature and 27 wt.% EDAP respectively. The lowest value was 187 ± 1 kW.m^{-2} obtained with a compound containing 10 wt.% EG and 20 wt.% EDAP. The best char yield was obtained with compositions containing the high decomposition onset temperature intumescent 3,5-diaminobenzoic acid phosphate. Despite this, the best fire performance was realised using the low-decomposition-onset-temperature EDAP together with the low-exfoliation-onset-temperature EG. Formulations based on this intumescent compound also ignited later and reached the pHRR earlier, but also burned for a longer time. This was true irrespective of the EG used. It is speculated that this can be attributed to the formation, at the burning surface, of a more cohesive char with better thermal and mass transport barrier properties. This would explain why compositions based on EDAP outperformed those containing 3,5-diaminobenzoic acid phosphate in terms of the pHRR and other important fire indices.

These results indicate that the low expansion onset temperature EG is most compatible with EDAP, as the onset and mechanism of expansion and intumescence respectively are well matched between these compounds. Furthermore, it is surmised that all binary compounds studied showed synergistic fire behaviour, resulting in far superior fire behaviour compared to their individual flame retarded counterparts. The intumescent additives increased the total smoke release and retained high CO production rates whereas with both the EG grades the emission of both was suppressed. This possibly indicates strong smoke suppressing potential in EG.

Chapter 6: Studying the thermal properties of polyethylene flame retarded with intumescent flame retardant additives through conventional and novel fire testing methods

Foreword

This chapter contributed to the submitted journal article under review:

- *Thermal properties of polyethylene flame retarded with expandable graphite and intumescent flame retardant additives (Kruger et al, 2016)*

This chapter and acknowledges contributions from the following persons:

- *Walter Wilhelm Focke, Washington Mhike, Albert Roberson and Albertus Taute*

Executive summary

The aim of this study was to obtain binary EG containing systems which improve upon the thermal barrier properties of EG alone, creating more cohesive thermal barriers which deliver uniform fire retardation. EDAP, an industrial flame retardant, was selected and another phosphate based intumescent flame retardant was developed. This selection was made in pursuit of the positive cohesive intumescent abilities of phosphate based flame retardants. A series of LDPE compounds flame retarded by various concentrations (10-27% by weight) of EDAP and 3,5-diamino benzoic acid phosphate (DABAP) and low expansion onset temperature EG were prepared. Open flame fire testing indicated that addition of the flame retardants generally caused a decrease in the measured time to ignition with the exception of all binary configurations during vertical open flame exposure.

Laser pyrolysis and open flame fire testing supported by video and IR camera data capture and analysis was conducted to measure sample flame retardant performance across many performance criteria. All fire tests indicated synergistic flame retardant behaviour in EG-EDAP systems.

Cone calorimeter results indicated that EG delivers very good smoke suppressing abilities. Laser pyrolysis and cone calorimeter testing increased mass loss resistance in all binary flame retarded systems. Generous reductions in the average HRR of the binary samples were obtained, due to spread of the heat release over a much broader time scale. This also resulted in increased time to flame out.

IR and video data from open flame fire tests indicated cohesive bonding of EG strings and uniform thermal shielding properties in all binary systems. All binary systems delivered flame retardation that exceeded all single flame retardant compounds. All binary flame retarded samples were also able to withstand increased temperatures before initiation of ignition, burn through or sag occurred. Both binary flame retardant system types delivered good resistance to ignition, while all EDAP containing binary systems prevented sample burn through, maintaining structural integrity of samples until eventual melting of the polymer media occurred.

Keywords: Expandable graphite; exfoliation; intumescent flame retardant; thermal analysis; cone calorimeter; laser pyrolysis

6-1. Introduction

Polymer flame retardant technology is constantly evolving and the search for more effective flame retardants is ongoing. Parallel to this search there is a desire to find cheaper alternative flame retardants which deliver the same level of performance.

The GIC EG also known as graphite bisulphate (Leshin *et al*, 2004) is a popular intumescent flame retardant because of its high availability and relatively low price. EG, when incorporated into a polymer medium, is an effective thermal shielding flame retardant which has a UL-94 V-0 fire rating when used at 10% content by mass. This property is due to its exfoliation behaviour which can result in volumetric increases of up to 300 times the original volume. This occurs via intumescent swelling of the polymer media, which creates an insulating barrier (Greinke, 2003; Zou *et al*, 2009). This insulating barrier slows the oxidation rate on the surface of the polymer, sufficiently increasing the combustion time of the media to allow increased time for external fire-fighting action to be taken (Morgan *et al*, 2007).

Large scale fire testing was conducted by the Institute of Applied Materials at the University of Pretoria a few years previous to the commencement of this project. These tests indicated that, at a large scale, EG delivered reduced flame retardation when exposed to a flame from below. This reduced thermal shielding at the bottom of the medium is believed to be due to negative gravitational effects. It was theorised that EG would deliver good synergistic flame retardant behaviour when used in binary systems with other intumescent flame retardants as they could create a cohesive barrier, negating the aforementioned gravitational effects.

In order to test this theory 2 compounds were synthesised at a large scale: EDAP, a compound which has a UL-94 V-0 fire rating when used at a 25-30% content, and a novel phosphate based intumescent and charring agent. Both these phosphate containing compounds were selected due to phosphorus' well known flame retardant abilities. Phosphorus based flame retardants have been used for many a decade as a polymer flame retardant and binary systems of EG and phosphorus containing compounds have been studied to some degree by researchers in the past (Modesti *et al*, 2002).

What sets this study apart is its aim: to strengthen the weaknesses of EG while using lower amounts of the secondary compounds than they individually require to deliver effective flame retardant behaviour. The success of such binary systems will allow production of cheaper flame retarded polymers for a wide range of applications where fire risk is prevalent. LDPE was used as the flame retarded polymer media for this study.

To gauge the level of flame retardant performance of a polymeric compound a wide range of techniques have been developed. The most popular methods historically were measurement of the limiting oxygen index (LOI) and the UL-94 fire rating of a sample (Smith, 1984). In recent years however, cone calorimetric testing has dominated and become a well-accepted standard due to its ability to measure an extremely wide range of variables, including HRR, specific extinction area (SEA) and SPR (Wang *et al*, 1993). The results of cone calorimeter tests provide a good comparison of the flame retardant performance of multiple samples across multiple variables. For this reason, cone calorimetry has been used to set a number of flame retardant standards across the last decade (Alongi, Frache & Gioffredi, 2011; Peacock & Braun, 1999; Zhu *et al*, 2001).

Although cone calorimetry is a highly effective technology, it remains costly and is available sparsely. A cheaper set of alternative methods was therefore sought. For this purpose, laser pyrolysis coupled with novel continuous mass loss monitoring was used and an open flame fire testing method was developed which allows horizontal and vertical fire testing. These methods were developed in parallel and the efficacy of each fire testing method was assessed against cone calorimeter fire testing. Similarities in the results of these alternative methods and cone calorimetry would indicate their utility as cheaper alternatives for preliminary testing of multiple small specimens before large scale tests are required.

6-2. Experimental

6-2.1. Materials

6-2.1.1 Polymeric materials

Powder and pellet form low density polyethylene (LDPE) of injection moulding grade LT019 (0.919 g.cm^{-1} density, MFI = 20.5 g / 10min @ 190 °C / 2.16kg) was sourced from Sasol polymers and used in the production of all compounds for fire testing. The methods and conditions employed in processing this material are reported in section 3.3.

6-2.1.2 Flame retardants

Two different grades of EG were sourced from Qingdao Kropfmuehl Graphite (China / Hauzenberg, Germany). The first was low expansion onset temperature (220 °C) grade ES 250 B5. The d_{10}, d_{50}, and d_{90} particle sizes of this low expansion onset temperature grade were 315 µm, 548 µm and 987 µm respectively (Mastersizer 2000, Malvern Instruments, Malvern, UK). The ES 250 B5 flake density before expansion was 2.08 ± 0.002 g cm^{-3} and the surface area in the expanded form was 22.380 m^2 g^{-1} ± 2.295 (Nova 1000e BET in N_2 at 77 K). The second grade of EG used was ES 170-300A, a high expansion onset temperature grade EG (300 °C). The d_{10}, d_{50}, and d_{90} particle sizes of this low expansion onset temperature grade were 313 µm, 533 µm and 807 µm respectively (Mastersizer 2000, Malvern Instruments, Malvern, UK). The ES 170-300A flake density before expansion was 2.236 ± 0.01 g cm^{-3} with a surface area in its flake and expanded form of 14.84 ± 0.1 m^2 g^{-1} and ca. 0.66 m^2 g^{-1} respectively (Nova 1000e BET in N_2 at 77 K).

Two other flame retardants were used in this study. The first was the well-known and widely used industrial IFR EDAP. EDAP was produced at a laboratory scale for compounding and characterisation purposes using the method reported in section 3-2.1.1 and 5-2.1. The characterisation results for this compound were compared to those of the laboratory produced sample in order to verify that the lab EDAP was of adequate quality.

The second flame retardant used was a novel charring agent and intumescent compound synthesised for this study. This compound is a phosphate salt of 3,5-diaminobenzoic acid which has been named DABAP. This compound was produced using the method reported in section 3-2.1.2 and 4-2.2. The phosphate salts of ethylenediamine and of 3,5-diaminobenzoic acid were synthesised using the procedures previously described by Focke et al (Focke *et al*, 2014c; Kruger *et al*, 2014).

6-2.1.3 Other materials

This section includes outlines other materials used during this study (excluding equipment).

Carbon black grade N660 was sourced from Ferro Industrial Products and was used in compounding.

Milled natural Zimbabwean flake graphite (henceforth referred to as flake graphite) was supplied by BEP Bestobell (South Africa).

6-2.2. Preparation of the polyethylene compounds

Polyethylene compounds containing EG and/or the IFRs DABAP or EDAP were compounded on a 28 mm co-rotating intermeshing twin screw laboratory extruder (L/D = 16) at a screw speed of 140-220 rpm. The compounder's screw design comprised intermeshing kneader elements with a forward transport action. The four extrusion processing stage temperatures, feed to die, were set at 120 °C, 175 °C, 175 °C and 180 °C respectively. The first stage of production involved compounding using powder LDPE well mixed with powder EDAP and/or DABAP. The latter 3 compounds in Table 6-1 were extruded and the extruded strands were then granulated and air dried. Combinations of these compounds and compound CB01 in Table 6-1 were used to produce the primary flame retarded formulations studied.

Table 6-1: First compounds produced

Sample code	Sample Content	Source
CB01	10 wt.% Carbon black (CB) in LDPE	Ferro Industrial Products (N660)
EG01	30 wt.% EG in LDPE	Self-compounded
EDAP01	30 wt.% EDAP in LDPE	Self-compounded
DABAP01	30 wt.% DABAP in LDPE	Self-compounded

A dark sample colour was maintained for all fire testing compounds by adding 5 wt.% carbon black (N660) to all non EG containing compounds. Dark test samples automatically resulted in EG containing samples. Maintaining dark sample colour ensures comparable heat absorption from IR radiation during cone calorimetry and laser pyrolysis experiments. A reference compound which contained 5 wt.% carbon black (N660) alone was prepared and used as reference sample in all testing.

Test specimens for cone calorimeter testing were prepared by pressing the pellets into flat sheets in a hot press set at 180 °C. These sheets were prepared at sheet dimensions of 100 mm × 100 mm × 3.2 ± 0.1 mm.

A round ASTM D5420 drop impact testing disc mould (ca. 68.5 mm disc diameter, 2.93 ± 0.02 mm disc thickness) was selected for the second set of fire tests where samples were exposed to an open flame. These discs were injection moulded directly on an Engel EC088. The final set of fire testing required ca. 50 µm of each test compound. These samples were cut from the well homogenised drop impact discs and prepared for testing.

6-3. Characterisation and analysis

6-3.1. Scanning electron microscopy

FE SEM images were obtained using an ultrahigh resolution FE SEM (HR FE SEM Zeiss Ultra Plus 55) with an InLens detector at acceleration voltages of as low as 1 kV to ensure maximum resolution of surface detail. No electro-conductive coating was applied on the graphite particles.

SEM micrographs of the temperature driven dynamic EG exfoliation processes were also obtained using a SEM (FEI QUANTA 200 ESEM) fitted with a heating stage. The graphite flakes were placed inside a crucible and mounted in the heating stage. They were viewed at 200x magnification. The pressure was 0.5 kPa, voltage 20 kV, spot size 6-7 and a working distance of 16 – 20 mm. Temperature was ramped at 20 °C min^{-1}.

6-3.2. Thermogravimetry

TGA was performed using the dynamic temperature scan method. Two different instruments, a TA Instruments SDT Q600 and a Mettler Toledo TGA 850e instrument were employed. Typically, approximately 10 - 15 mg of sample was placed in an open 50 µL alumina pan. Sample size was reduced to below 5 mg for intumescent materials such as EGs which were placed in 150 µm alumina sample holders and covered with lids (pin hole) to ensure containment of solids. Temperature was scanned from below 50 °C to 900 °C at a scan rate of 10 °C min^{-1} with gas (nitrogen or air) flowing at a rate of 50 $mL.min^{-1}$.

6-3.3. Thermomechanical analysis

Thermal expansion measurements were conducted on a TA instruments Q400 Thermo Mechanical Analyzer. Sufficient EG powder was placed in an alumina sample pan such that the bed height was between 35 µm and 40 µm. The flake expansion behaviour was measured with a flat-tipped standard expansion probe using an applied force of 0.005 N. The temperature was scanned from 30 °C to 600 °C at a scan rate of 10 °C min^{-1} in a nitrogen atmosphere. The expansion relative to the original powder bed height was reported.

6-3.4. Differential scanning calorimetry

DSC data was obtained on a Perkin Elmer PYRIS Diamond DSC. The temperature was scanned from 30 °C to 370 °C at a scan rate of 10 °C.min^{-1} with nitrogen flowing at a rate of 50 mL.min^{-1}.

During DSC, a test sample in a sample pan and an identical empty pan were placed in two identical spots in the machine with or without lids. In this technique a specific temperature profile is selected and the energy flowing into or out of the sample and the empty reference is measured and subtracted from one another. The difference in heat flow between the sample and the reference sample is used to determine the heat flow profile of the sample which is plotted and analysed.

When the sample undergoes a phase change (solid to liquid, recrystallisation, etc.) there will be a rapid positive or negative change in the energy flow of the sample which, when plotted, will indicate the specific change. Further, one may study and compare the energy of the endothermic and exothermic phase changes of different materials.

6-3.5. Open flame fire testing

Samples with a mass of ca. 40 µm, cut from injection moulded discs, were placed in 6.3 mm diameter alumina pans for laser pyrolysis studies. Mass loss was recorded with a Perkin-Elmer TGA 4000 thermogravimetric analyzer under quiescent conditions, i.e. the gas flow was shut down. First the samples were heated to 200 °C and kept at this temperature for ca. 20 min in order to melt the compounds and completely fill the area of the pans. This allowed removal of non-homogeneity in the polymeric media and allowed the samples to settle into a flat surface. These samples were allowed to cool for 10 minutes which proved sufficient for the small sample size used. These samples were then heated to 100 °C at 10 °C.min^{-1} and exposed to laser energy generated by a class-4 CO_2 laser. The beam power was set at 2 W. This exposure and temperature was maintained for at least 30 min. Three specimens of each composition were tested and average values are reported.

Open flame fire tests were conducted on the injection-moulded circular discs in two different configurations. In the first configuration (Figure 6-1 A) the test specimens were mounted horizontally and exposed to a 4 cm butane flame at 45° from below. IR footage was recorded perpendicular to the sample surface at a distance of 20 cm from above the sample. In the second configuration (Figure 6-1 B) the sample discs were mounted vertically and exposed to a 4 cm butane flame perpendicular to the sample surface. IR footage was recorded at a 45° angle to the sample surface at a distance of 20 cm from behind each sample. Note that the IR camera and open flame source are always oriented at a 45° angle to one another to prevent damage to the IR measurement apparatus due to face-on exposure to the hottest point of the flame.

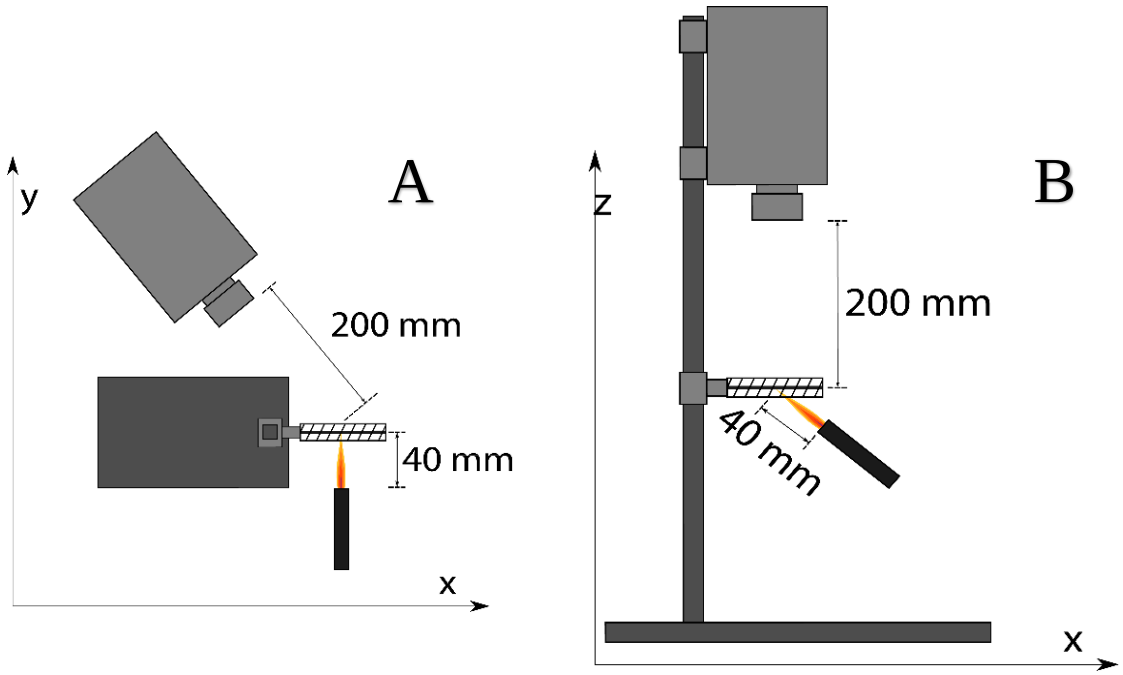

Figure 6-1: Diagrammatic representation of (A) Horizontal and (B) Vertical configurations used for open flame fire testing.

The temperature profiles shown were measured along a line through the flame impingement point and were recorded by the IR camera. These curves were extracted from the recorded IR footage. The temperature profiles are also shown for time instants just after initiation of sagging, ignition or burn-through occurred. The profiles measured indicate the temperature variation from the left side to the right side of the sample, passing approximately through the center of the sheet where the flame impinged.

6-3.6. Laser pyrolysis

Samples with a mass of ca. 40 µm, cut from injection moulded discs, were placed in 6.3 mm diameter alumina pans for laser pyrolysis studies. Mass loss was recorded with a Perkin-Elmer TGA 4000 thermogravimetric analyzer under quiescent conditions, i.e. the gas flow was shut down. First the samples were heated to 200 °C and kept at this temperature for ca. 20 min in order to melt the compounds and completely fill the area of the pans. This allowed removal of non-homogeneity in the polymeric media and allowed the samples to settle into a flat surface. These samples were allowed to cool for 10 minutes which proved sufficient for the small sample size used.

These samples were then heated to 100 °C at 10 °C min^{-1} and then exposed to laser energy generated by a class-4 CO_2 laser. The beam power was set at 2 W. This exposure and temperature was maintained for at least 30 min. Three specimens of each composition were tested and average values are reported.

6.3.7. Cone calorimeter flammability testing

The ISO 5660-1 standard was followed in performing the cone calorimeter tests using a Dual Cone Calorimeter (Fire Testing Technology (UK) Ltd.). Three specimens of each composition were tested and average values are reported. The sheet dimensions were 100 mm × 100 mm × 3.2 mm. They were placed horizontally on aluminium foil and exposed perpendicularly from above to an external heat flux of 35 $kW.m^{-2}$.

6-4. Results and discussion

6-4.1. Characterisation

A comprehensive characterisation of the commercial EG was previously reported in chapter 2 (Focke *et al*, 2014a). This flame retardant additive was fabricated by treating natural graphite flakes with an oxidant in the presence of sulfuric acid. The expansion onset temperature, as determined by TMA, was ca. 225 °C. The EG released a mixture of carbon dioxide, carbon monoxide and sulfur dioxide during the exfoliation process (Focke *et al*, 2014a).

The SEM micrograph in figure 6-2A shows the morphology of the EDAP powder particles. The flake-like morphology of the DABAP crystals is shown in figure 6-2B. The EG particles also had a flake-like nature but the flakes were much larger (Focke *et al*, 2014a). Figure 6-3 shows micrographs of the vermicular residues of the expanded graphite sample taken in the ESEM. The expansion of the low temperature EG resulted in "worms" with a fairly regular cross-section. According to the manufacturer, the volume expansion of the EG was at least 250 mL g^{-1}.

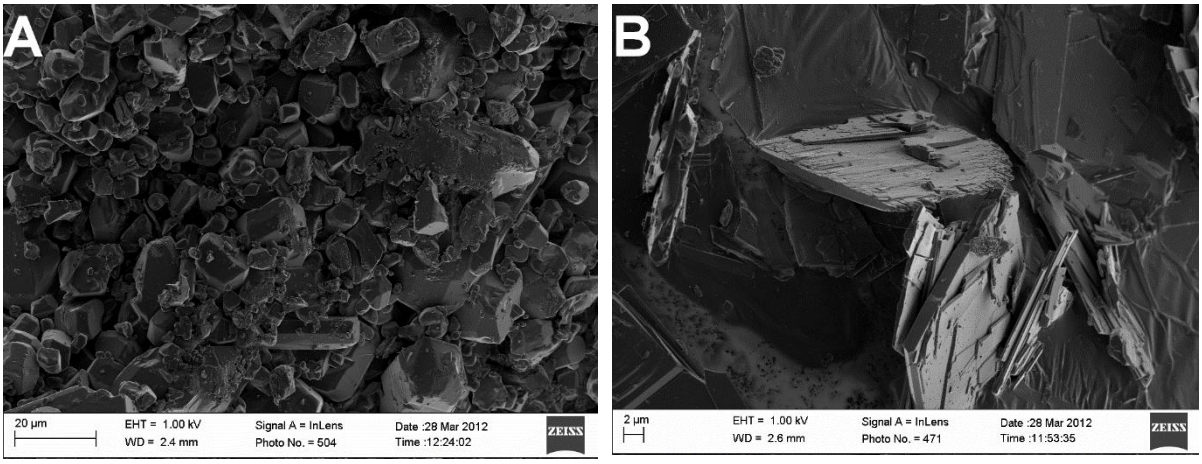

Figure 6-2: FE SEM micrographs of the (A) EDAP powder and (B) the diaminobenzoic acid phosphate crystals (DABAP).

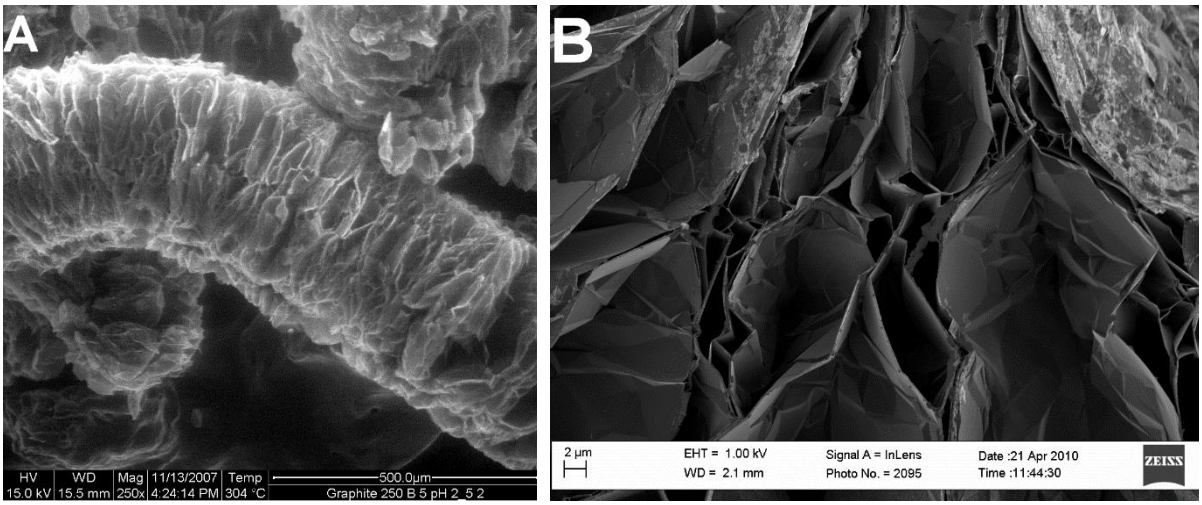

Figure 6-3: Micrographs of the expanded graphite after exfoliation in (A) the ESEM and (B) a close up view taken with the FE SEM.

6-4.2. Thermal analysis of the flame retardant additives

The key property of EG in flame retardant applications is the ability to exfoliate within a narrow temperature range. Figure 6-4 shows the TMA expansion trace obtained in N_2 and the TGA mass loss curve obtained in air for the EG. In the TMA and TGA experiments the temperature was scanned to 600 °C and 900 °C respectively at a scan rate of 10 °C min^{-1} with gas flowing at a rate of 50 mL min^{-1}. In the TMA experiment, a flat-tipped standard expansion probe was used with an applied force of 0.005 N.

The EG showed four mass loss steps when heated in air. There was a minor mass loss below 150 °C indicating moisture loss of ca. 0.5%. This was succeeded by a second mass loss initiated at 210 °C which reached a peak mass loss rate at 226 °C. This event was associated with an additional mass loss of 4.5% (total mass loss of 5 %). The TMA traces indicated that this second mass loss event is associated with expansion of the EG. The third mass loss event commenced at 361 °C, peaked at 408 °C and contributed at a further mass loss of 11% (total mass loss of approximately 16%) by 600 °C.

The TMA trace indicates that this mass loss was connected with a second gas release that ultimately lead to the full exfoliation of the graphite. The apparent contractions in the TMA curves are attributed to the loss of gas pressure after the exfoliation events, i.e. the applied pressure from the TMA probe was able to compress the “fluffy” exfoliated graphite layer that was formed. The final mass loss event started at 705 °C and peaked at 798 °C, corresponding to the oxidation of the graphite residue. The residual mass at 900 °C was 4.2%. Both the TMA and TGA curves in Figure 6-3 show that the EG underwent a two-stage exfoliation. This is likely due to the separate release in ES250 of gasses related to intercalated molecules oxidising and graphite oxide layer groups’ reacting respectively. DSC results presented in chapter 4 (Focke *et al*, 2014c) indicated that both exfoliation events are endothermic in nature.

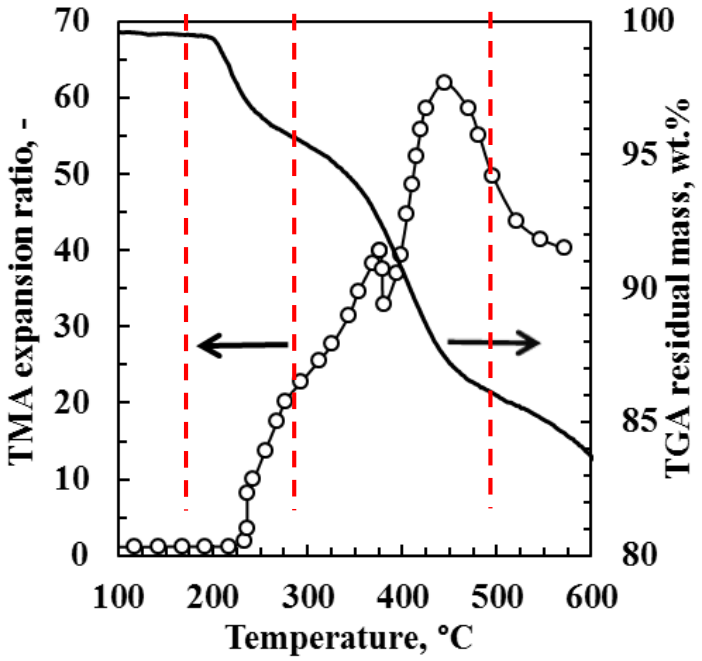

Figure 6-4: TGA (in air) and TMA (in nitrogen) curves for the low exfoliation onset temperature EG

Figure 6-5 shows TGA and DTG curves for the two IFRs recorded in an air atmosphere. Temperature was scanned to 900 °C at a scan rate of 10 °C min^{-1} with air flowing at a rate of 50 mL min^{-1}. The DTG curve indicates that mass loss for the DAPAB occurred in four steps. The minor mass loss (1 %) below 200 °C probably reflects the loss of moisture. Starting at a temperature of about 225 °C, an event associated with a steep mass loss (ca. 16 %) occurred. This probably reflects the loss of CO_2 due to the decarboxylation of the DABAP. The theoretical mass loss for decarboxylation is 17.6 %. Mass loss continued and reached another peak value at a temperature of 465 °C. The DSC curves (not shown) indicated that this reaction is exothermic whereas all the other mass loss steps are endothermic in nature. However, in a nitrogen atmosphere this step was also endothermic. This is attributed to a char-forming decomposition reaction that also released ammonia gas. The pyrolysis of the char continued as the temperature was raised. It reached a maximum rate at ca. 622 °C and was complete by about 750 °C. The carbonised char residue that remained represented just above 2% of the initial DABAP mass.

A DSC scan indicated a sharp endothermic peak with an onset temperature of 257 °C reminiscent of a melting event (chapter 4) (Focke *et al*, 2014c). Additionally TMA indicated softening of the material at this temperature (Focke *et al*, 2014c). This means that the melting of DABAP commenced with simultaneously thermal decomposition.

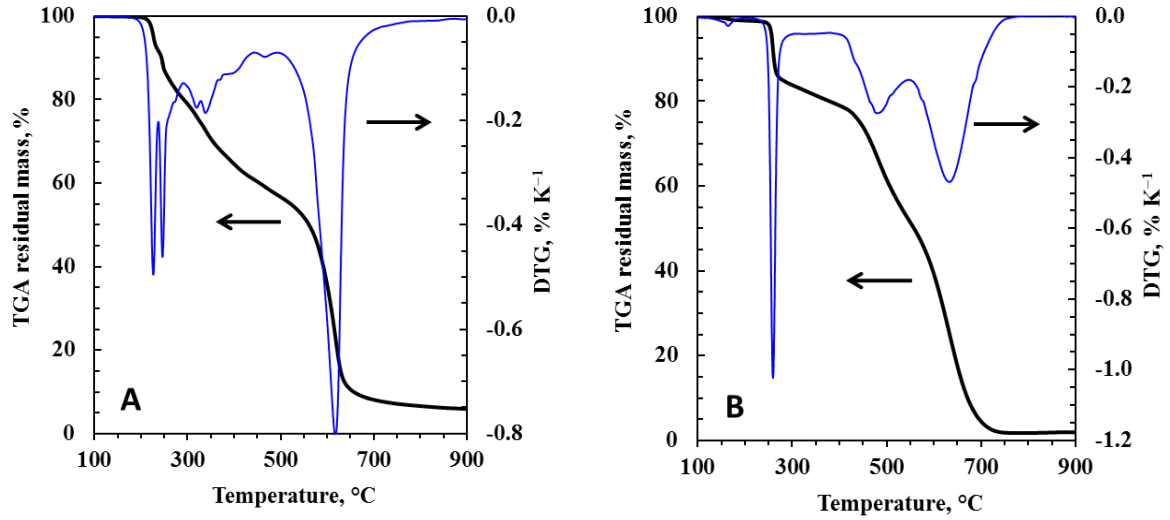

Figure 6-5: TGA (thick line) and DTG (thin blue line) curves for (A) EDAP and (B) 3,5-diaminobenzoic acid phosphate

The DTG curve in figure 6-5A indicates that the decomposition of the EDAP was significantly more complicated. The melting and decomposition of this additive commences just above 200 °C. Melting and decomposition is characterised by two sharp DTG peaks located at 225 °C and 245 °C respectively. This is attributed to a reaction that also released ammonia gas. Multiple peaks are observed between 280 °C and 480 °C. Their number and positions vary with each scan. This suggests that the peaks are associated with the erratic release of gaseous products during the on-going char-forming decomposition reactions. The well-defined DTG peak located at ca. 615 °C is associated with the air oxidation reaction. The DSC curve (not shown) indicates that this reaction is exothermic whereas all the others are endothermic in nature. The carbonised char residue remaining at 900 °C is only about 6 %.

Figures 6-6 to 6-8 represent the DSC results for all the single and dual flame retardant compounds as well as neat LDPE and the 5 % CB reference compound. One may note from these results that the addition of any of the flame retardants tested significantly reduced the melting and crystallisation temperatures. This reduction is favourable for processing but generally unfavourable for flame retardance of the material. In this case however the intumescent behavior of the material generally prevents polymer flow of melted media. The results do however indicate a large increase in the solidification temperature of each compound which is very favourable for polymer processing of the compounds.

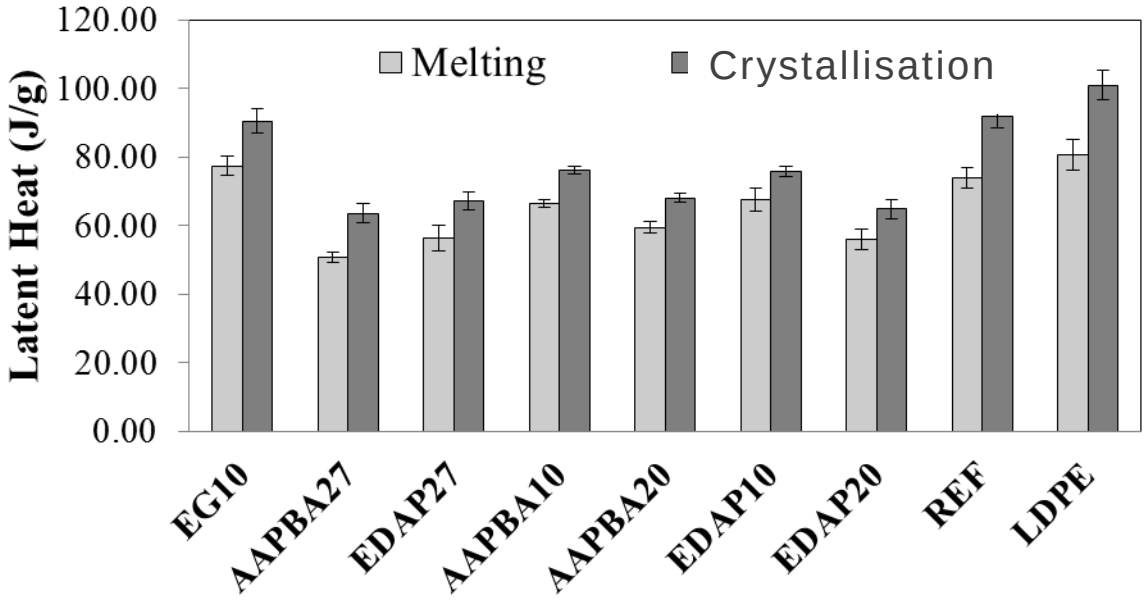

Figure 6-6: DSC latent values for the compounded flame retarded materials

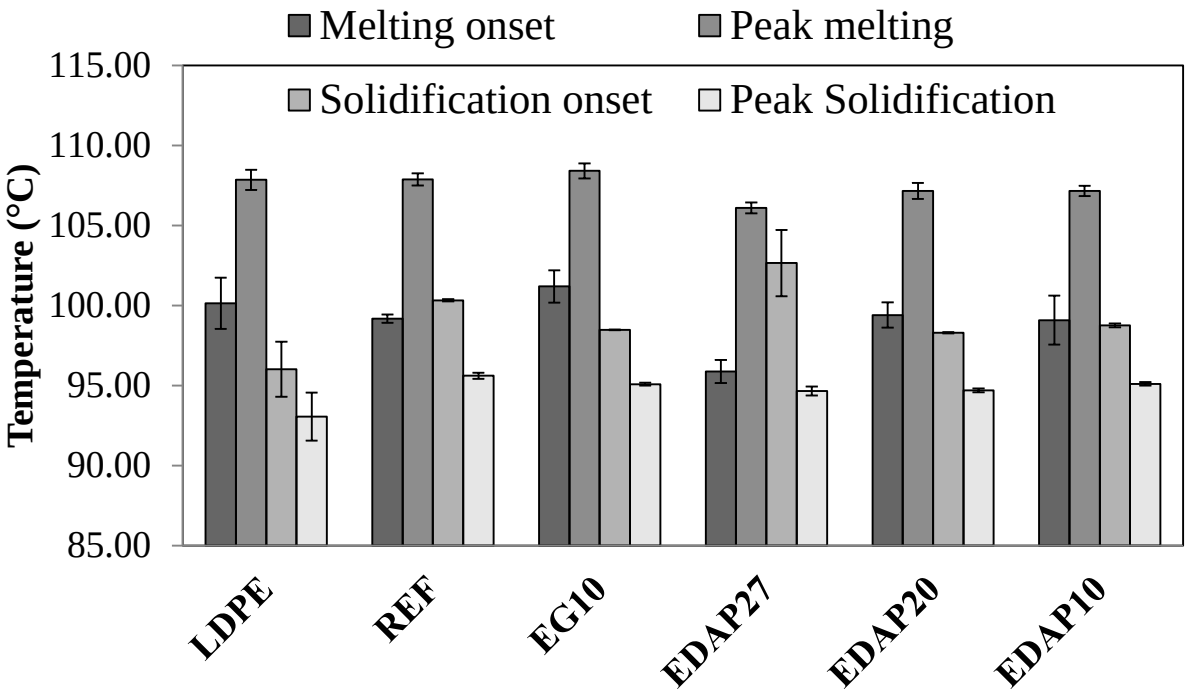

Figure 6-7: Onset and peak temperatures for melting and crystallisation obtained using DSC – Part 1

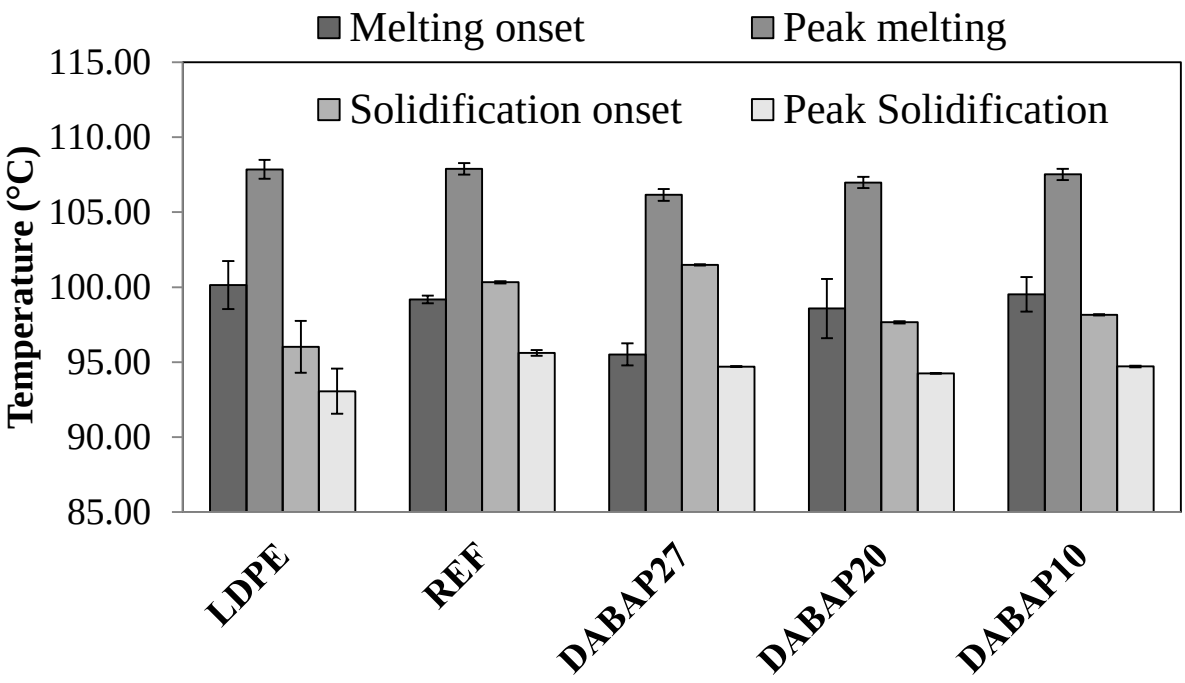

Figure 6-8: Onset and peak temperatures for melting and crystallisation obtained using DSC – Part 2

6-4.3. Thermal analysis of the flame retarded compounds

Figure 6-9 shows TGA results for the flame retarded polyethylene compounds recorded in a nitrogen atmosphere. Temperature was scanned to 600 °C at a scan rate of 10 °C min^{-1} with nitrogen flowing at a rate of 50 mL min^{-1}. The pyrolysis of the neat polyethylene (containing 5 wt.% carbon black) commenced at ca. 260 °C. The material volatilised completely and virtually no residue was left by 600 °C. Addition of the flame retardants resulted in the initiation of mass loss at lower temperatures. This phenomenon is caused by the lower thermal stability of the additives relative to the neat polymer. The compound containing 10 wt.% EG showed enhanced overall mass loss up to a temperature of ca. 410 °C. It would appear that the presence of the EG destabilised the polymer. However, beyond this temperature all compounds show a lower mass loss than the neat black pigmented polyethylene. The residue remaining at 600 °C is similar for the samples containing at least some IFR. It exceeds 15 % but is less than 20 %. Just below 7% residue remained at 600 °C for the compound with 10 wt.% EG.

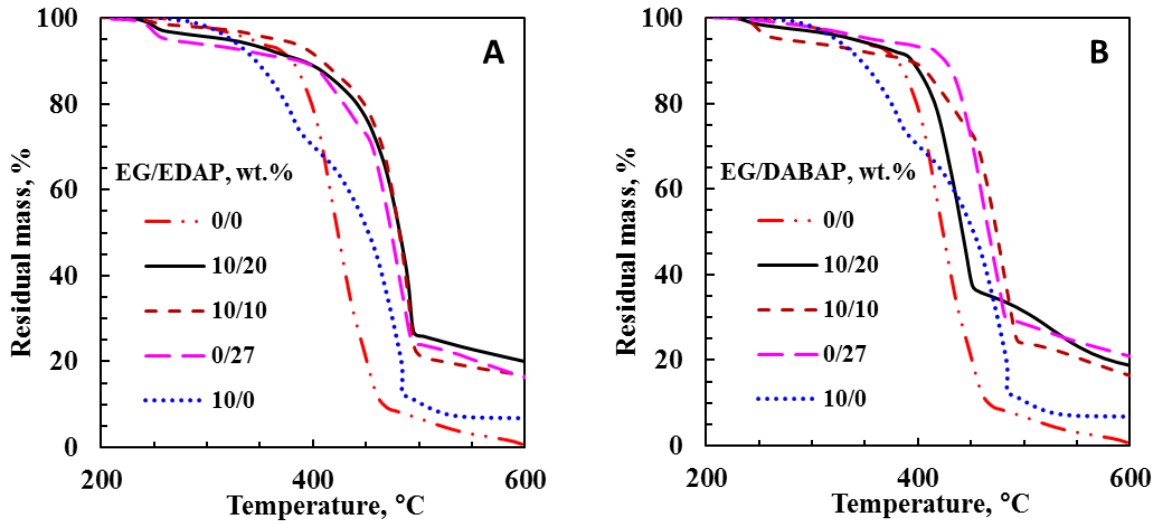

Figure 6-9: TGA pyrolysis of polyethylene compounds of EG with (A) EDAP and (B) 3,5-diaminobenzoic acid phosphate

6-4.4. Fire testing

6-4.4.1 Introduction

The results from the different novel fire tests follow. Further information is available in the appendices as follows:

- Appendix A-5 and A-6 display alternative representations of the open flame fire testing results with discussion of said results in Appendix A-7.
- Appendix A-8 displays some of the equipment used during IR measurement and a screenshot of the IR video obtained for the triplicate of each sample tested. Figures A-8-4 and A-8-5 displays the exceptional results obtained for one of the binary flame retardants tested showing very clearly the success of the project in creating cohesive thermal barriers from EG containing flame retarded systems.
- Appendix A-9 displays the thermal barriers achieved for the laser pyrolysis samples tested and shows the low variance achieved in the mass loss curves for the multiple samples tested in triplicate, indicating that the figures in the section that follows are a good representation of the results obtained.

6-4.4.2. Open flame tests

Figure 6-10 shows the open flame test results for the carbon black pigmented polyethylene and the compound containing 10 wt.% each of EG and EDAP. Samples were mounted horizontally and the flame was applied from below as in figure 6-1B. The temperature profiles shown were measured along a line through the flame impingement point and were recorded by the IR camera at selected time intervals. These curves were extracted from the recorded IR footage. The temperature profiles are also shown for time instants just after initiation of sagging, ignition or burn-through occurred. The profiles displayed indicate the temperature variation from the left side to the right side passing approximately through the center of the sheet where the flame impinged.

The profiles for the non-flame retarded sheet quickly develops a sharp temperature peak that results in ignition within a short period of time (15.4 s for this sample). A hole opened up in the sheet less than three seconds later. The strange shape of the temperature profile obtained at 19.3 s is an artifact of the hole that burned into the sheet. By comparison the temperature profiles for the flame retarded sample are flatter at similar times. The polymer is heated over a larger area owing to the shielding effect of the intumescent layer that forms. The temperature eventually reached values that exceed the melting point of material causing a softening that resulted in sagging. Only then did ignition occur. Table 6-2 summarises the open flame test data.

Figures 6-10A and 6-10B show linear temperature profiles for the vertical test specimen after 16 s of open flame exposure from below. The 4 cm butane flame was applied from below at a 45° angle. The IR camera was positioned above and recorded the top surface temperature as a function of time and position. The profiles displayed indicate the temperature variation from left to the right of the samples passing through the centre where the flame impinged the sheet. One may note that the single flame retardant systems and the neat polymer each deliver a sharper temperature curve around the point of flame exposure. All the binary flame retarded systems lowered the local increase at the point of flame exposure due to continuous intumescence and formation of an effective thermal barrier at this point. This effect spreads the heat towards the perimeter of the test specimen, lowering the chance of burn through at similar exposure times.

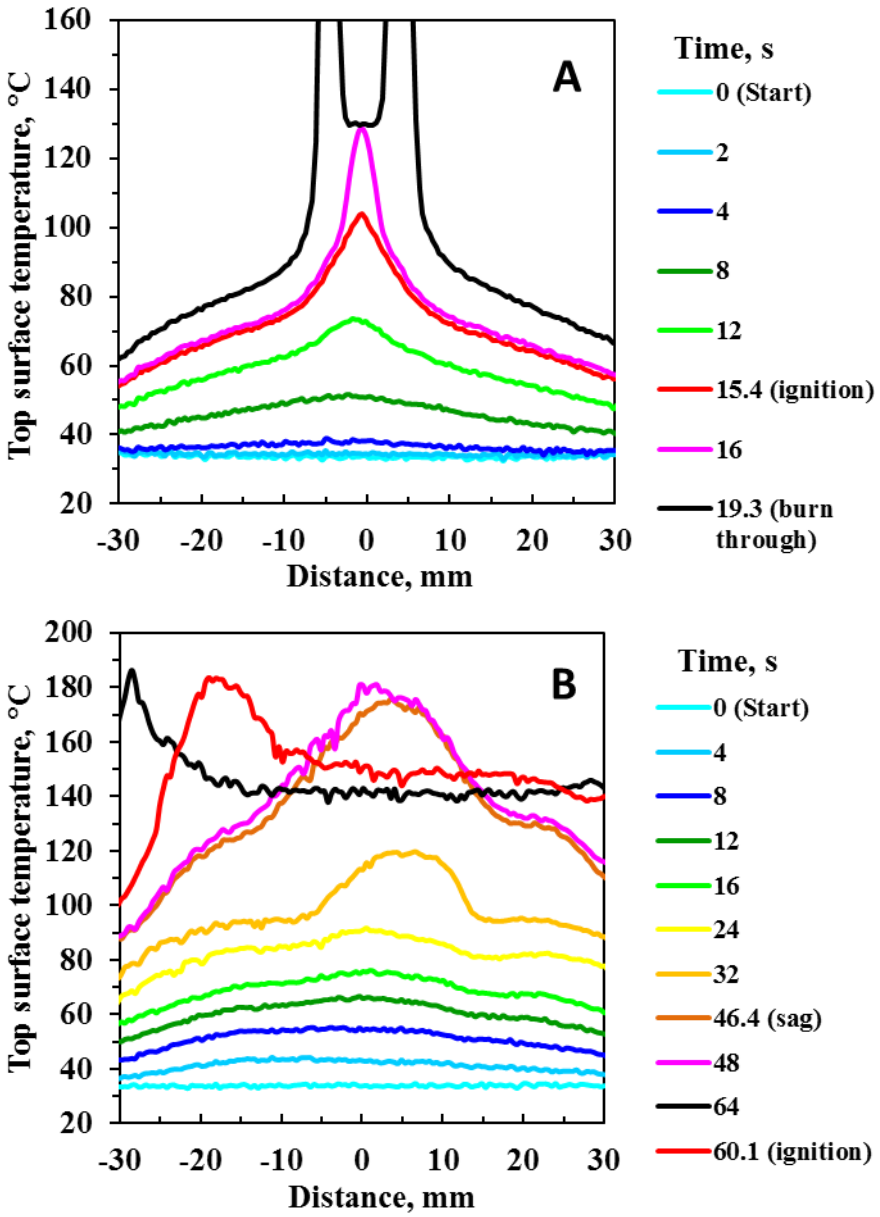

Figure 6-10: Representative open flame temperature profiles measured by IR camera with the sample disc in a horizontal position for (A) Polyethylene with 5 wt.% carbon black and (B) Polyethylene with ES250/EDAP at 10/10 wt.%

Figure 6-11C and 6-11D show linear temperature profiles for the horizontal test specimen exposed to open flame normal to the sample surface for 16 seconds. Horizontally mounted test specimens were exposed to the flame held at 45 degrees from below while IR footage was recorded perpendicular to sample surface at a distance of 20 cm from sample. Vertically mounted specimens were exposed with the flame perpendicular to the sample surface. IR footage was recorded on the top sample surface at a 45 degree angle at a distance of 20 cm from each sample.

The profiles displayed indicate the temperature variation from the bottom of the samples to the top of the samples from left to right. These results indicate a sharper peak for the non-flame retarded sample. The 27 wt.% DABAP samples showed a further increase in surface temperature towards the top point of the exposed samples. This was caused by increased radiant heat absorption in the DABAP sample of the heat which rose across the sample surface from the point of flame exposure. Addition of EG prevented this heat absorption due to the increased thermal barrier delivered by the binary samples. A more peaked temperature curve was measured for the horizontal samples while the vertical samples maintained a bell curve shape. This phenomenon may be attributed to the formation of a thicker thermal barrier around the point of exposure. This barrier lowers the spread of heat to the immediate surrounding area, causing temperature increases above the point of exposure in the non-foamed region of the sample alone.

Increased temperature maxima were measured across the first 8 seconds of exposure to the flame in the 10 wt.% EG and 27 wt.% DABAP samples. The rate of temperature increase in these samples then slowed as intumescence increased and the barrier performance reached a thermally thick level of performance. The binary systems were able to reach this level of performance earlier reducing the maximum temperature reached as heat was conducted away from the point of flame exposure across the thermal barrier. The temperature in the non-flame retarded sample increased at a much higher rate at the point of exposure due to the continuous reduction in sample thickness due to polymer flow and droplet formation.

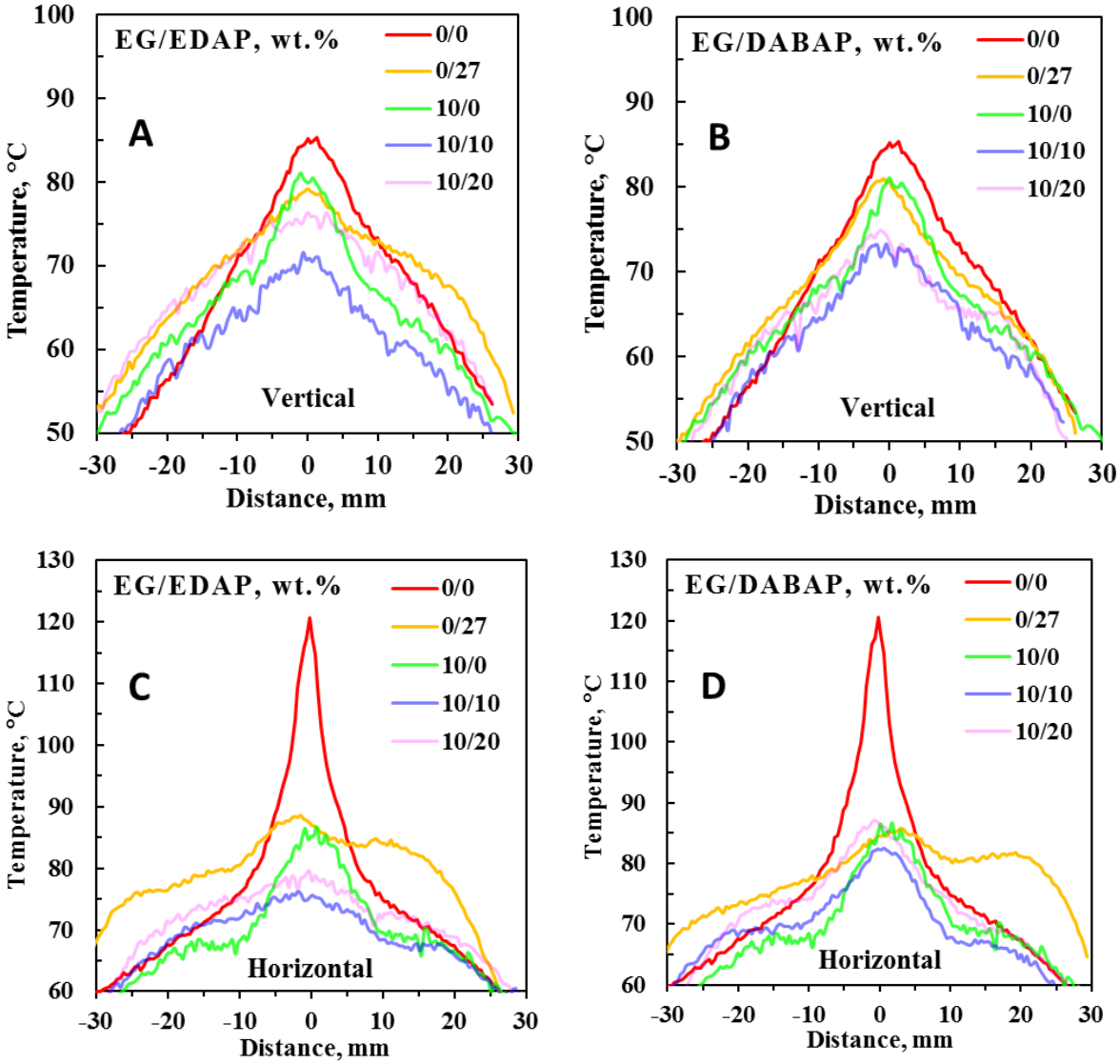

Figure 6-11: Open flame test temperature profiles from top to bottom right (vertical discs) or from left to right (horizontal discs) after 16 of disc seconds of exposure to 4 cm butane flame

Table 6-2 lists the ignition and flame out times during open flame fire testing for the various samples and all other fire behaviour for the open flame fire tests.

Table 6-2: Open flame fire testing summary

		ES250/EDAP, wt.%				
Property	**Units**	**0/0**	**10/0**	**0/27**	**10/10**	**10/20**
Vertical open flame						
Time to ignition (t_{ign})	s	22 ± 1	18 ± 11	11 ± 1	-	-
Time to sag initiation	s	-	27 ± 1	27 ± 3	25 ± 0	25 ± 0
Time to burn through	s	20 ± 1	37 ± 1	34 ± 0	n.a.	n.a.
Polymer flow / Droplets	Y / N	Y	N	N	N	N
Horizontal open flame						
Time to ignition (t_{ign})	s	16 ± 2	33 ± 2	29 ± 4	*58 ± 2	*51 ± 4
Time to sag initiation	s	-	-	39 ± 4	48 ± 2	40 ± 3
Time to burn through	s	20 ± 0	35 ± 0	39 ± 3	n.a.	n.a.
Polymer flow / Droplets	Y / N	Y	N	N	N	N
		ES250/DABAP, wt.%				
Property	**Units**	**0/0**	**10/0**	**0/27**	**10/10**	**10/20**
Vertical open flame						
Time to ignition (t_{ign})	s	22 ± 1	18 ± 11	13 ± 2	12 ± 0	11 ± 1
Time to sag initiation	s	-	27 ± 1	31 ± 1	24 ± 0	24 ± 0
Time to burn through	s	20 ± 1	37 ± 1	34 ± 0	51 ± 1	n.a.
Polymer flow / Droplets	Y / N	Y	N	N	N	N
Horizontal open flame						
Time to ignition (t_{ign})	s	16 ± 2	33 ± 2	19 ± 1	27 ± 1	30 ± 3
Time to sag initiation	s	-	-	34 ± 2	33 ± 10	40 ± 7
Time to burn through	s	20 ± 0	35 ± 0	29 ± 1	40 ± 5	45 ± 0
Polymer flow / Droplets	Y / N	Y	N	N	N	N

*Ignition only occurred after sagging occurred

Figure 6-12 displays the ignition and burn through times for the horizontal and vertical flame tests. Sample discs were either mounted horizontally and exposed to a 4 cm butane flame at 45 degrees from below or vertically and exposed to the same flame perpendicular to the surface. Data points coloured black indicate a sample for which the flame failed to burn through. Omission of a peak in these graphs indicates that no ignition whatsoever occurred.

During vertical and horizontal fire testing all flame retarded samples prevented dripping and even polymer flow across the sample. EDAP delivered extremely effective burn through prevention abilities, at times even blocking burn through during singular use of EDAP. All binary EDAP containing samples blocked burn through when exposed to vertical and horizontal flame attack. Although slightly less effective at fire retardation than EDAP when used alone, DABAP delivers burn through prevention at 20 % loading with EG and good flame retardant properties throughout all tests.

Addition of the flame retardants increased the propensity of the material to ignite with the exclusion of the binary systems containing EG and EDAP. EDAP and EG showed exceptional performance in open flame fire testing preventing ignition in all flame retarded samples tested. These compounds only ignited when the edge of the material was exposed to the test flame when the sample, after extended exposure, reached the melting temperature of the polymer and sagged, exposing the top edge of the samples. Very good bonding of loose EG strings is observed with EDAP and DABAP binary use. EDAP binary systems showed the most cohesive thermal barrier formation which resulted in excellent fire retardation as a result. All flame retarded samples prevented polymer flow.

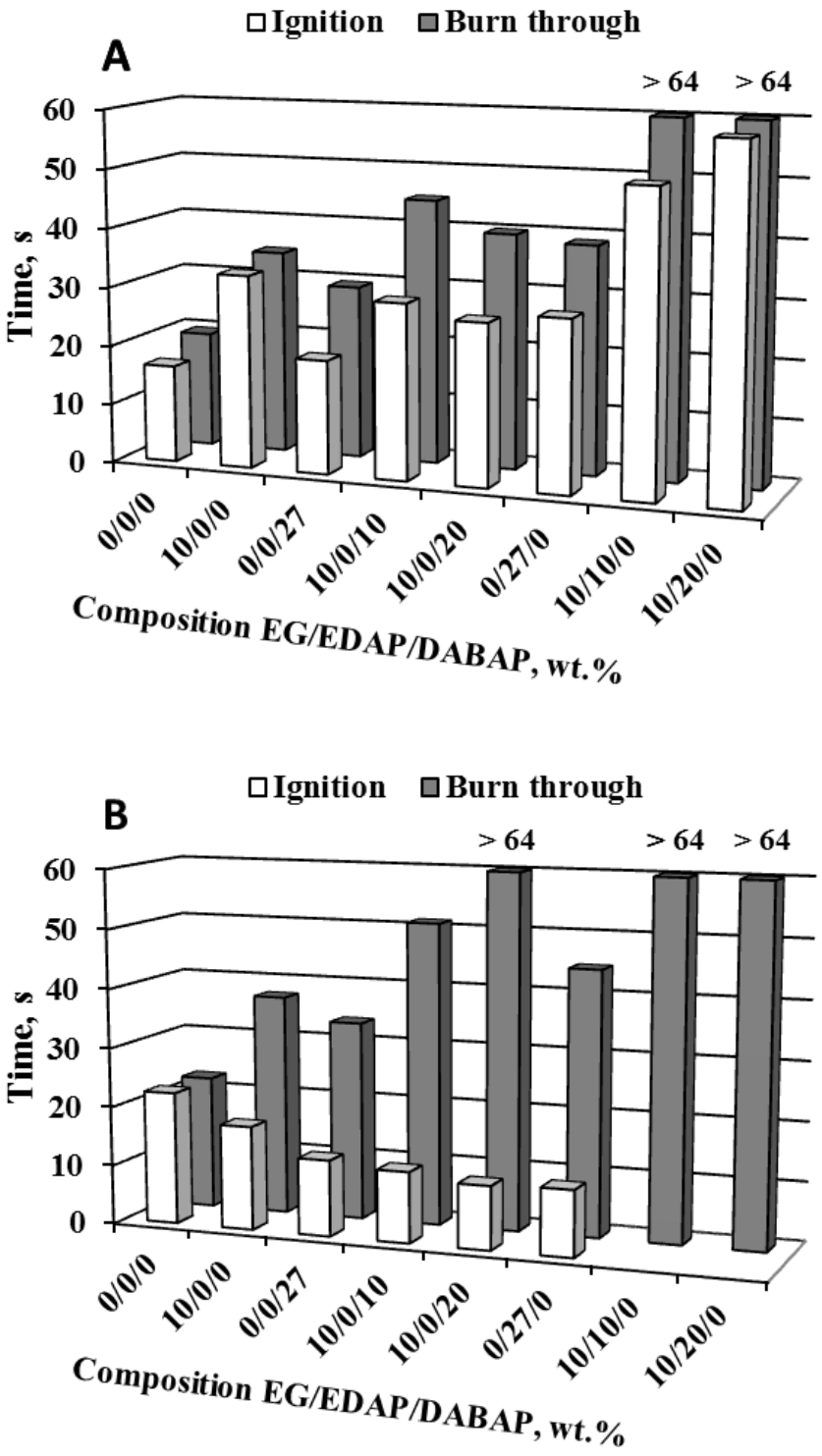

Figure 6-12: Ignition and burn through times for (A) horizontal and (B) vertical flame tests.

6-4.4.3. TGA laser pyrolysis

Figure 6-13 displays the sample temperature as a function of time for the laser pyrolysis tests. Figure 6-14 displays the mass loss as a function of time for the laser pyrolysis tests. The laser power was set at 2 W and the initial sample temperature was 100 °C.

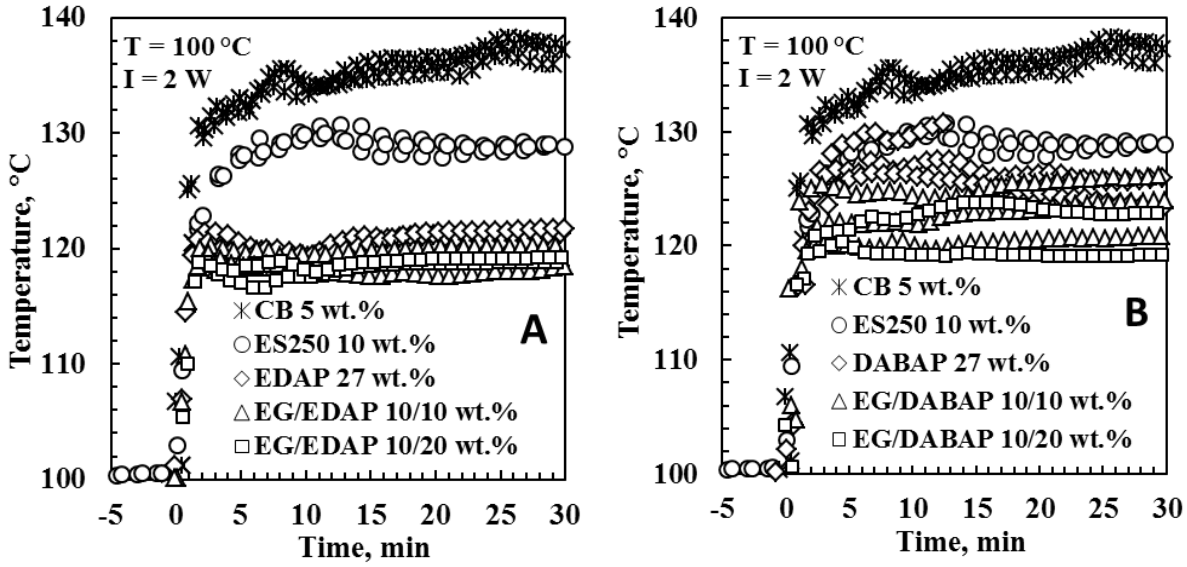

Figure 6-13: TGA-laser pyrolysis temperature curves for combinations of EG with (A) EDAP and (B) DABAP

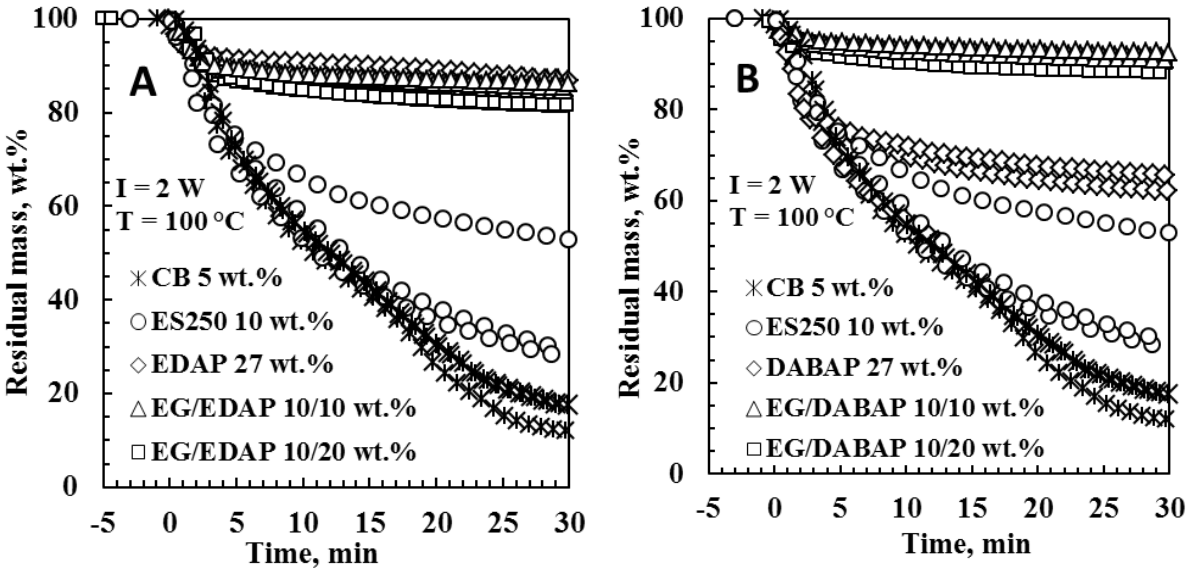

Figure 6-14: TGA-laser pyrolysis mass loss curves for combinations of EG with (A) EDAP and (B) DABAP

When comparing the temperature and residual mass loss curves for the different samples one may note a direct connection between temperature reached and residual mass. This trend indicates that samples with improved mass loss resistance also prevent said samples from reaching higher temperatures by resisting energy transfer through the fire barrier to the polymeric material below where the temperature probe was located. Furthermore, there is very good synergism between DABAP and EG as all DABAP binary systems outperform both the 27 wt.% DABAP and the 10 wt.% EG systems by a very large margin. The 27 wt.% EDAP system outperforms the 27 wt.% DABAP system in all respects. Interestingly, the best results are achieved by the 10/10 wt.% EG/DABAP system although EDAP binary systems outperform DABAP systems in other fire tests.

6-4.4.4. Cone calorimeter fire testing

A detailed analysis of the cone calorimeter results is presented in chapters 3,4 and 5 and in publications by Kruger *et al* (2014). Table 6-2 and Figure 6-15 summarise information pertinent to the present discussion. The sample sheets were backed by aluminium foil and their dimensions were 100 mm × 100 mm × 3.2 mm. They were exposed horizontally to an external heat flux of 35 kW.m^{-2}. Figure 6-15 confirms that the addition of the EG reduced the MLR. This can be attributed to the expansion of the intercalated graphite which forms a low density layer of loose, worm like structures at the surface. DABAP containing compounds formed a denser charred foam layer at the polymer interface.

In cone calorimeter testing (Table 6-3) the time to ignition (t_{ig}) was 58 ± 3 s for the neat polyethylene and 46 ± 1 s for the compound containing 10 wt.% ES250 but decreased to 33 ± 5 s for the compound containing 27 wt.% DABAP. These values mirror the pattern observed in open flame fire testing. See table 6-3 for other values.

Table 6-3 reveals that the time to flame out showed considerable variability. It was 773 ± 307 for the neat polyethylene, 539 ± 69 for the 27 wt.% DABAP compound but was longer than both these times for all other compounds.

Table 6-3: Cone calorimeter data summary

	t_i, s	t_{fo}, s	t-pHRR, s	pHRR, kW m^{-2}	Residue, wt.%
Polyethylene (5 wt.%CB)	58.3 ± 2.5	773 ± 307	177 ± 6	710 ± 109	8.3 ± 3.2
ES250 (10 wt.%)	45.7 ± 1.5	1049 ± 12	97 ± 3	231 ± 7	18.5 ± 0.3
EDAP (27 wt.%)	41.3 ± 0.6	878 ± 190	73 ± 3	230 ± 5	26.1 ± 2.7
DABAP (27 wt.%)	33.0 ± 5.2	537 ± 69	105 ± 13	400 ± 16	22.4 ± 0.5
ES250/EDAP (10/10 wt.%)	45.3 ± 1.2	1046 ± 17	97 ± 8	197 ± 10	26.3 ± 0.4
ES250/DABAP (10/10 wt.%)	37.7 ± 0.6	1172 ± 48	80 ± 0	209 ± 8	27.8 ± 0.4
ES250/EDAP (10/20 wt.%)	46.7 ± 2.5	948 ± 20	128 ± 53	187 ± 1	29.5 ± 1.0
ES250/DABAP (10/20 wt.%)	37.7 ± 1.5	1138 ± 24	78 ± 3	231 ± 11	30.6 ± 1.3

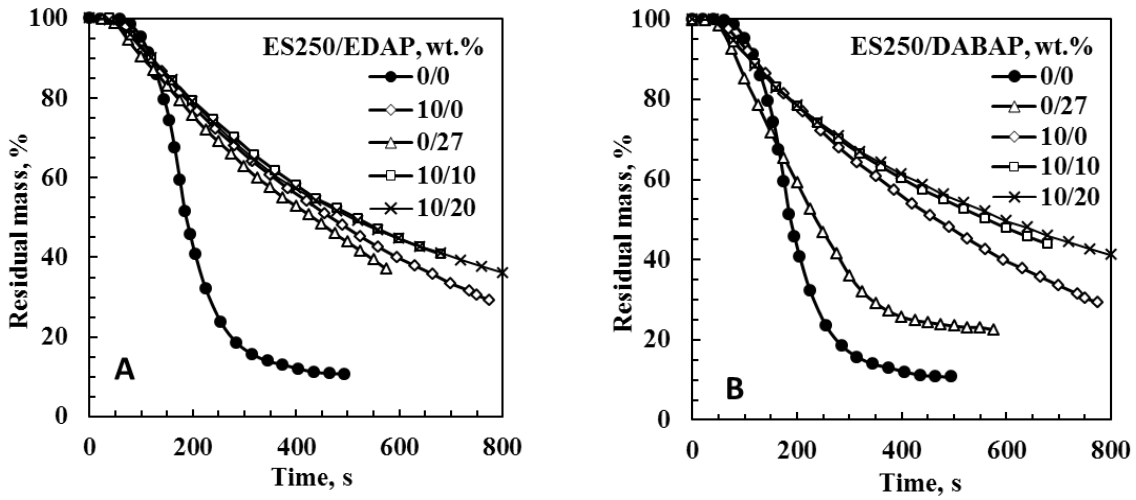

Figure 6-15: Cone calorimeter mass loss curves for the polyethylene compounds with EG and EDAP

6-5 Conclusions

Observations and analysis of the open flame and pyrolysis fire testing conducted showed that cohesive bonding of EG strings to cause uniform fire behaviour was achieved successfully for all binary systems. All binary systems delivered fire retardation exceeding any single flame retardant systems. Both binary flame retardant types delivered good resistance to ignition, with all EDAP containing binary systems preventing sample burn through completely while maintaining structural integrity of samples until eventual melting of the polymer media occurs. Analysis of IR camera data obtained for all open flame fire tests indicates that all binary flame retarded samples were able to withstand higher temperature before ignition, burn through or sag of the polymer is initiated. This may be attributed to a reduction of the temperatures at the polymer surface itself due to effective thermal barrier formation.

10% EG combined with both 10 % DABAP and 10 % EDAP delivered satisfactory results offering more economical and more effective flame retardant alternatives to the 25 - 30 % EDAP loaded compounds currently in use industrially.

Laser pyrolysis at 50 MW/m^2 (similar energy to a well-developed large scale fire) of small samples indicate increased flame retardant performance in the same samples indicated by open flame fire testing and cone calorimeter testing results, making it a viable and less expensive prototype fire test before large scale fire tests are considered. Synergistic fire retardation effects could be identified in laser pyrolysis results showing that both types of binary flame retarded systems delivered better results than their single compound flame retarded counterparts in terms of % mass loss. The same synergism was identified in both other fire testing methods.

In cone calorimeter testing synergistic effects were obtained in terms of reductions in smoke production driven by EG (effective smoke suppressant) and a large decrease in the average HRR of all binary flame retarded samples. Similar trends were obtained for the reduction in residual mass % during laser pyrolysis and open flame fire testing indicated strengths in the same compounds as well.

Chapter 7: Overall project conclusions and recommendations

EG and the phosphate salt of 3,5-diaminobenzoic acid and ethylenediamine were used to flame retard injection moulding grade polyethylene with a low propensity for char formation and a high heat of combustion. EDAP and 3,5-diaminobenzoic acid phosphate were tested alone, in the polymer substrate and in binary combinations with EG. Polyethylene containing 5 wt.% carbon black was used as reference.

Cone calorimetry, laser pyrolysis and open flame fire testing coupled with IR and optical footage was utilised to measure the fire properties of the compounds produced.

Thermal analysis highlighted the 2 step expansion and 4 step oxidative decomposition of the low expansion onset temperature (ca. 210 °C) EG. Both phosphate compounds underwent a complex four stage decomposition with EDAP, releasing ammonia gas and expanding explosively, while 3,5-diaminobenzoic acid phosphate released CO_2 producing an effective charring effect.

Open flame fire testing indicated that the addition of a second flame retardant to an EG containing system caused the temperature profile around the point of flame exposure to be flattened and indicated good heat dispersal to the edges of the test specimens. This effect also caused a decrease in the maximum temperature reached at any specific exposure time when compared to the single flame retardant and non-flame retarded compounds. This in turn extends the time to failure. In the case of the 10 wt.% / 20 wt.% EG/DABAP system and both binary EDAP systems, burn through was prevented completely with the compounds only failing once their melting points were exceeded.

All flame retarded compounds prevented polymer flow but in some cases increased the propensity of the compounds to ignite. Interestingly, the best result was observed for the 10 wt.% / 10 wt.% EG/EDAP system which delivered the best ignition and burn through resistance and produced the lowest temperature profile. This indicates possible synergism between EG and EDAP at this content which outperforms both the 10 wt.% EG and 27 wt,% EDAP systems which both meet a UL-94 V-0 fire rating.

The common trend between the barrier properties delivered and the temperature reached was further reinforced by the laser pyrolysis results which also indicated that configurations which lower the maximum temperature reached deliver increased mass loss resistance. Laser pyrolysis indicated increased performance in both 10 wt.% / 10 wt.% binary compounds over their 10wt.% / 20 wt.% counterparts, further reinforcing the results obtained from open flame fire testing.

The results obtained from open flame fire testing and laser pyrolysis mirror those obtained from cone calorimeter testing indicating the utility of these methods as low cost alternatives for preliminary fire testing.

The success of this project has contributed to produce EG flame retarded PVC (Focke *et al*, 2013) and it the author's hope that these results will lead to a number of novel EG applications in future.

It is recommended, in light of the successful results of this study, that the synergistic binary flame retardant systems be explored further, tested in large scale fire tests and be put forward as an alternative for industrial IFRs currently used. Furthermore, the good parity between the results from the novel fire testing methods and those from the cone calorimeter tests, indicate that these novel low cost methods should be used for all future scoping of new formulations.

8. References

Aihara, J-I, Yamabe, T and Hosoya, H (1994), "Aromatic character of graphite and carbon nanotubes", *Synthetic Metals*, **64**(2-3), 309-313.

Akamatsu, K, Kaneko, D, Sugawara, T, Kikuchi, R and Nakao, S-i (2010), "Three Preparation Methods for Monodispersed Chitosan Microspheres Using the Shirasu Porous Glass Membrane Emulsification Technique and Mechanisms of Microsphere Formation", *Industrial & Engineering Chemistry Research*, **49**(7), 3236-3241.

Alongi, J, Frache, A and Gioffredi, E (2011), "Fire-retardant poly(ethylene terephthalate) by combination of expandable graphite and layered clays for plastics and textiles", *Fire and Materials*, **35**(6), 383-396.

Ashcroft, NW and Mermin, ND (1976), *Solid State Physics*, Saunders College, New York.

Ayral, A, Phalippou, J and Woignier, T (1992), "Skeletal density of silica aerogels determined by helium pycnometry", *Journal of Materials Science*, **27**(5), 1166-1170.

Babrauskas, V and Peacock, RD (1992), *Heat Release Rate: The Single Most Important Variable in Fire Hazard*, in *Fire Safety Developments and Testing: Toxicity--Heat Release--Product Development--Combustion Corrosivity*, Ponte vedra beach, Lancaster, (Eds), October 20-25 1990, pp. 255-272.

Badenhorst, H (2014), "Microstructure of natural graphite flakes revealed by oxidation: Limitations of XRD and Raman techniques for crystallinity estimates", *Carbon*, **66**, 674-690.

Beckhoff, B, Kanngießer, B, Langhoff, N, Wedell, R and Wolff, HH (2006), *Handbook of Practical X-Ray Fluorescence Analysis*, Springer, London.

Botas, C, Alvarez, P, Blanco, C, Santamaria, R, Granda, M, Ares, P, Rodriguez-Reinoso, F and Menendez, R (2012), "The effect of the parent graphite on the structure of graphene oxide", *Carbon*, **50**(1), 275-282.

Braun, D, Cherdon, H, Rehahn, M, Ritter, H and Voit, B (2005), *Polymer Synthesis: Theory and Practice: Fundamentals, Methods, Experiments*, Springer, New York.

Brunauer, S, Emmett, PH and Teller, E (1938), "Adsorption of Gases in Multimolecular Layers", *Journal of the American Chemical Society*, **60**(2), 309-319.

Brundle, CR, Evans, CA, Jr. and Wilson, S (1992), "Surfaces, Interfaces, Thin films", in *Encyclopedia of Materials Characterisation*, Fitzpatrick, L (Ed.), Butterworth-Heinemann, Boston.

Callister, WD, Jr. (2007), *Materials Science and Engineering: An Introduction*, John Wiley & Sons, New York.

Camino, G, Costa, L and Martinasso, G (1989), "Intumescent fire-retardant systems", *Polymer Degradation and Stability*, **23**(4), 359-376.

Camino, G, Duquesne, S, Delobel, R, Eling, B, Lindsay, C and Roels, T (2001a), *Mechanism of Expandable Graphite Fire Retardant Action in Polyurethanes*, in "Fire and Polymers", American Chemical Society, 90-109.

Camino, G, Duquesne, S, Delobel, R, Eling, B, Lindsay, C and Roels, T (2001b), "Mechanism of expandable graphite fire retardant action in polyurethanes", Paper presented at *Fire and polymers: materials and solutions for fire prevention*.

Celzard, A, Marêché, JF and Furdin, G (2005), "Modelling of exfoliated graphite", *Progress in Materials Science*, **50**(1), 93-179.

Chen, L and Wang, YZ (2010), "A review on flame retardant technology in China. Part I: Development of flame retardants", *Polymers for Advanced Technologies*, **21**(1), 1-26.

Chen, X, Huo, L, Jiao, C and Li, S (2013), "TG–FTIR characterization of volatile compounds from flame retardant polyurethane foams materials", *Journal of Analytical and Applied Pyrolysis*, **100**(0), 186-191.

Chowdary, KPR, Enturi, V and Sandhya Rani, A (2011), "Preparation and evaluation of starch phosphate- A new modified starch as a disintegrant in tablet formulations", *International Journal of Chemical Sciences*, **9**(2), 889-899.

Chua, CK, Sofer, Z and Pumera, M (2012), "Graphite Oxides: Effects of Permanganate and Chlorate Oxidants on the Oxygen Composition", *Chemistry-a European Journal*, **18**(42), 13453-13459.

Chung, DDL (1987), "Exfoliation of graphite", *Journal of Materials Science*, **22**(12), 4190-4198.

Chung, DDL (2002a), "Review Graphite", *Journal of Materials Science*, **37**(8), 1475-1489.

Chung, DDL (2002b), "Review: Graphite", *Journal of Materials Science*, **37**(8), 1475-1489.

Coates, J (2000), "Encyclopedia of Analytical Chemistry", in *Encyclopedia of Analytical Chemistry*, Meyers, RA (Ed.), John Wiley & Sons, Chichester.

Crawford, RJ (1996), "Recent advances in the manufacture of plastic products by rotomoulding", *Journal of Materials Processing Technology*, **56**(1–4), 263-271.

Cunningham, N, Lefèvre, M, Dodelet, J-P, Thomas, Y and Pelletier, S (2005), "Structural and mechanical characterization of as-compacted powder mixtures of graphite and phenolic resin", *Carbon*, **43**(15), 3054-3066.

Dasari, A, Yu, Z-Z, Cai, G-P and Mai, Y-W (2013a), "Recent developments in the fire retardancy of polymeric materials", *Progress in Polymer Science*, **38**(9), 1357-1387.

Dasari, A, Yu, ZZ, Cai, GP and Mai, YW (2013b), "Recent developments in the fire retardancy of polymeric materials", *Progress in Polymer Science*, **38**(9), 1357-1387.

Davis, J and Huggard, M (1996), "The technology of halogen-free flame retardant phosphorus additives for polymeric systems", *Journal of Vinyl and Additive Technology*, **2**(1), 69-75.

Dittrich, B, Wartig, K-A, Hofmann, D, Mülhaupt, R and Schartel, B (2013), "Flame retardancy through carbon nanomaterials: Carbon black, multiwall nanotubes, expanded graphite, multi-layer graphene and graphene in polypropylene", *Polymer Degradation and Stability*, **98**(8), 1495-1505.

Dogan, M and Bayramli, E (2010), "Effect of Boron-Containing Materials on the Flammability and Thermal Degradation of Polyamide 6 Composites Containing Melamine", *Journal of Applied Polymer Science*, **118**(5), 2722-2727.

Dresselhaus, MS and Dresselhaus, G (1981), "Intercalation compounds of graphite", *Advances in Physics*, **51**(1), 1-186.

Dresselhaus, MS, Jorio, A, Hofmann, M, Dresselhaus, G and Saito, R (2010), "Perspectives on Carbon Nanotubes and Graphene Raman Spectroscopy", *Nano Letters*, **10**(3), 751-758.

Dreyer, DR, Park, S, Bielawski, CW and Ruoff, RS (2010), "The chemistry of graphene oxide", *Chemical Society Reviews*, **39**(1), 228-240.

Dukhin, AS and Goetz, PJ (2004), *Ultrasound for Characterizing Colloids*, in "Concentrated Dispersions", American Chemical Society, Amsterdam, 91-119.

Feng, B, Bhatia, SK and Barry, JC (2002), "Structural ordering of coal char during heat treatment and its impact on reactivity", *Carbon*, **40**(4), 481-496.

Focke, WW, Badenhorst, H, Mhike, W, Kruger, HJ and Lombaard, D (2014a), "Characterization of commercial expandable graphite fire retardants", *Thermochimica Acta*, **584**, 8-16.

Focke, WW, Badenhorst, H, Ramjee, S, Kruger, HJ, Van Schalkwyk, R and Rand, B (2014b), "Graphite foam from pitch and expandable graphite", *Carbon*, (0).

Focke, WW, Kruger, HJ, Mhike, W, Taute, A, Roberson, A and Ofosu, O (2014c), "Polyethylene flame retarded with expandable graphite and a novel intumescent additive", *Journal of Applied Polymer Science*, 8.

Focke, WW, Muiambo, H, Mhike, W, Kruger, HJ and Ofosu, O (2013), "Flexible PVC flame retarded with expandable graphite", *Polymer Degradation and Stability*, (0).

Foley, GMT, Zeller, C, Falardeau, ER and Vogel, FL (1977), "Room temperature electrical conductivity of a highly two dimensional synthetic metal: AsF5-graphite", *Solid State Communications*, **24**(5), 371-375.

Furdin, G (1998), "Exfoliation process and elaboration of new carbonaceous materials", *Fuel*, **77**(6), 479-485.

Gao, M and Zhang, H (1996), "Preparation of an amorphous fullerene film", *Physics Letters A*, **213**(3–4), 203-206.

Geim, AK and Novoselov, KS (2007), "The rise of graphene", *Nature Materials*, **6**(3), 183-191.

Giacovazzo, C, Monaco, HL, Artioli, G, Viterbo, D, Ferraris, G, Gilli, G, Zanotti, G and Catti, M (2002), *Fundamentals of Crystallography*, Oxford University Press, New York.

Gormsen, H, Jeppesen, N and Lund, A (1984), "The causes of death in fire victims", *Forensic Science International*, **24**(2), 107-111.

Greinke, RA (2003), "Intercalated graphite flakes exhibiting improved expansion characteristics and process therefor", *US Patent 6,669,919*, assigned to Advanced Energy Technology Inc., US.

Groen, JC, Peffer, LAA and Pérez-Ramírez, J (2003), "Pore size determination in modified micro- and mesoporous materials. Pitfalls and limitations in gas adsorption data analysis", *Microporous and Mesoporous Materials*, **60**(1–3), 1-17.

Han, Z, Li, Y and Zhao, H (2007a), "An investigation on synergistic effect of EG with IFR in polyethylene", 828-831.

Han, Z, Li, Y and Zhao, H (2007b), *An investigation on synergistic effect of EG with IFR in polyethylene*, (Eds), pp. 828-831.

Han, ZD, Dong, LM, Li, Y and Zhao, H (2007c), "A comparative study on the synergistic effect of expandable graphite with APP and IFR in polyethylene", *Journal of Fire Sciences*, **25**(1), 79-91.

Hannay, NB, Geballe, TH, Matthias, BT, Andres, K, Schmidt, P and Macnair, D (1965), "Superconductivity in Graphitic Compounds", *Physical Review Letters*, **14**(7), 225&226.

Hennig, G (1951), "The properties of the interstitial compounds of graphite. I. The electronic structure of graphite bisulfate", *The Journal of Chemical Physics*, **19**(7), 922-929.

Hirschler, MM (1994), "Fire retardance, smoke toxicity and fire hazard", Paper presented at *Flame retardants '94 British plastics federation*, 26-27 January, London.

Holleman, AF, Wiber, E and Wiberg, N (2001), *Inorganic Chemistry*, Acad. Press, San Diego.

Hu, X, Wang, D and Wang, S (2013), "Synergistic effects of expandable graphite and dimethyl methyl phosphonate on the mechanical properties, fire behavior, and thermal stability of a polyisocyanurate–polyurethane foam", *International Journal of Mining Science and Technology*, **23**(1), 13-20.

Hummers Jr, WS and Offeman, RE (1958), "Preparation of graphitic oxide", *Journal of the American Chemical Society*, **80**(6), 1339.

Inagaki, M (1966), "On the formation and decomposition of graphite-bisulfate", *Carbon*, **4**(1), 137-141.

Jarvis, KE, Gray, AL and Houk, RS (2003), *Handbook of Inductively Coupled Plasma Mass Spectrometry*, Viridian, United Kingdom.

Jillavenkatesa, A, Dapkunas, SJ and Lum, L-SH (2001), *Particle size characterization*, National Institute of Standards and Technology, Gaithersburg.

Kikkawa, S, Kanamaru, F, Koizumi, M, Rich, SM and Jacobson, A (2007), *Layered Intercalation Compounds*, in "Inorganic Syntheses", John Wiley & Sons, Inc., Published Online, 86-89.

Klusek, Z, Datta, PK and Kozlowski, W (2003), "Nanoscale studies of the oxidation and hydrogenation of graphite surface", *Corrosion Science*, **45**(7), 1383-1393.

Kruger, HJ, Focke, WW, Mhike, W, Taute, A and Roberson, A (2016), "Thermal properties of polyethylene flame retarded with expandable graphite and intumescent fire retardant additives", *Fire and Materials*, n/a-n/a.

Kruger, HJ, Focke, WW, Mhike, W, Taute, A, Roberson, A and Ofosu, O (2014), "Cone calorimeter study of polyethylene flame retarded with expandable graphite and intumescent fire-retardant additives", *Journal of Fire Sciences*, **32**(6), 498-517.

Kuilla, T, Bhadra, S, Yao, D, Kim, NH, Bose, S and Lee, JH (2010), "Recent advances in graphene based polymer composites", *Progress in Polymer Science*, **35**(11), 1350-1375.

Kvasnitsa, VN, Yatsenko, VG and Jaszczak, JA (1999), "Disclinations in unusual graphite crystals from anorthosites of Ukraine", *Canadian Mineralogist*, **37**, 951-960.

Labuschagne, FJWJ (2003), *Metal catalysed intumescence of polyhydroxyl compounds*, PhD, Thesis, University of Pretoria, Pretoria.

Lastoskie, C, Gubbins, KE and Quirke, N (1993), "Pore size heterogeneity and the carbon slit pore: a density functional theory model", *Langmuir*, **9**(10), 2693-2702.

Lee, S, Cho, D and Drzal, LT (2005), "Real-time observation of the expansion behavior of intercalated graphite flake", *Journal of Materials Science*, **40**(1), 231-234.

Leshin, VS, Sorokina, NE and Avdeev, VV (2004), "Electrochemical Synthesis and Thermal Properties of Graphite Bisulfate", *Inorganic Materials*, **40**(6), 649-655.

Lewin, M (1999a), "Synergistic and catalytic effects in flame retardancy of polymeric materials - an overview", *Journal of Fire Sciences*, **17**(1), 3-19.

Lewin, M (1999b), *Synergistic and catalytic effects in flame retardancy of polymeric materials : An overview*, Sage Publications, London, ROYAUME-UNI.

Luque, FJ, Pasteris, JD, Wopenka, B, Rodas, M and Barrenechea, JF (1998), "Natural fluid-deposited graphite; mineralogical characteristics and mechanisms of formation", *American Journal of Science*, **298**(6), 471-498.

Lyon, LA, Keating, CD, Fox, AP, Baker, BE, He, L, Nicewarner, SR, Mulvaney, SP and Natan, MJ (1998), "Raman spectroscopy", *Analytical Chemistry*, **70**(12), 341R-361R.

McCool, B, Murphy, L and Tripp, CP (2006), "A simple FTIR technique for estimating the surface area of silica powders and films", *Journal of Colloid and Interface Science*, **295**(1), 294-298.

McMullan, D (1995), "Scanning electron microscopy 1928–1965", *Scanning*, **17**(3), 175-185.

Mermoux, M and Chabre, Y (1989), "Formation of graphite oxide", *Synthetic Metals*, **34**(1-3), 157-162.

Mhike, W and Focke, WW (2013), "Surface Resistivity and Mechanical Properties of Rotationally Molded Polyethylene/Graphite Composites", *Journal of Vinyl & Additive Technology*, **19**(4), 258-270.

Mhike, W, Focke, WW, Mofokeng, JP and Luyt, AS (2012), "Thermally conductive phase-change materials for energy storage based on low-density polyethylene, soft Fischer-Tropsch wax and graphite", *Thermochimica Acta*, **527**, 75-82.

Modesti, M and Lorenzetti, A (2002), "Halogen-free flame retardants for polymeric foams", *Polymer Degradation and Stability*, **78**(1), 167-173.

Morgan, AB and Wilkie, CA (2007), *Flame Retardant Polymer Nanocomposites*, Wiley, New Jersey.

Mortazavi, B, Hassouna, F, Laachachi, A, Rajabpour, A, Ahzi, S, Chapron, D, Toniazzo, V and Ruch, D (2013), "Experimental and multiscale modeling of thermal conductivity and elastic properties of PLA/expanded graphite polymer nanocomposites", *Thermochimica Acta*, **552**, 106-113.

Müller, SA, Aebi, U and Engel, A (2008), "What transmission electron microscopes can visualize now and in the future", *Journal of Structural Biology*, **163**(3), 235-245.

Murty, GVLN and Seshadri, TR (1942), "Raman effect and hydrogen bonds", *Proceedings of the Indian Academy of Sciences - Section A*, **16**(4), 264-269.

Nakagawa, Y (2006), "Recent development of flame retardant polymeric materials containing expandable graphite", *Bulletin of Japan Association for Fire Science and Engineering*, **56**(2), 37-43.

Nakajima, T, Mabuchi, A and Hagiwara, R (1988), "A new structure model of graphite oxide", *Carbon*, **26**(3), 357-361.

Narayanan, PS (1948), "Raman spectrum of ammonium di-hydrogen phosphate", *Proceedings of the Indian Academy of Sciences - Section A*, **28**(5), 469-474.

Nikiel, L and Jagodzinski, PW (1993), "Raman Spectroscopic Characterization of the Oxidation of Nuclear-Grade Graphites", *Appl. Spectrosc.*, **47**(12), 2087-2092.

Oxford dictionaries (2011), "Intumescent", http://oxforddictionaries.com/definition/intumescent, [2011, November 4].

Pang, XY and Song, M (2012a), "Preparation and anti-flame capability of expandable graphite", Paper presented at *Material sciences and technology*, Xi'an.

Parthasarathy, G, Sreedhar, B and Chetty, TRK (2006), "Spectroscopic and X-ray diffraction studies on fluid deposited rhombohedral graphite from the Eastern Ghats Mobile Belt, India", *Current Science*, **90**(7), 995-1000.

Pawley, J (1997), "The development of field-emission scanning electron microscopy for imaging biological surfaces", *Scanning*, **19**(5), 324-336.

Peacock, RD and Braun, E (1999), *Fire safety of passenger trains - Phase 1: Materials evaluation (cone calorimeter)*, National Institute of Standards and Technology (Federal railroad administration), Gaithersburg, US.

Perera, IE and Litton, CD (2011), "A detailed study of the properties of smoke particles produced from both flaming and non-flaming combustion of common mine combustibles", Paper presented at *10th International Symposium on Fire Safety Science*, College Park, MD.

Perry, RH and Green, DW (2007), *Perry's Chemical Engineers' Handbook*, McGraw-Hill, New York.

Petrella, RV (1994), "The assessment of full-scale fire hazards from cone calorimeter data", *Journal of Fire Sciences*, **12**(1), 14-43.

Qu, B and Xie, R (2003a), "Intumescent char structures and flame-retardant mechanism of expandable graphite-based halogen-free flame-retardant linear low density polyethylene blends", *Polymer International*, **52**(9), 1415-1422.

Qu, BJ and Xie, RC (2003b), "Intumescent char structures and flame-retardant mechanism of expandable graphite-based halogen-free flame-retardant linear low density polyethylene blends", *Polymer International*, **52**(9), 1415-1422.

Reinheimer, A, Wenzel, A and Muenzenberger, H (2009), "Use of thermally expandable graphite intercalation compounds for producing fire- protection seals and method for their production", *US Patent 7,479,513 B2*, assigned to Hilti Aktiengesellschaft Germany.

Rüdorff, W (1959), "Graphite Intercalation Compounds", *Advances in Inorganic Chemistry and Radiochemistry*, **1**, 223-266.

Russell, NV, Gibbins, JR and Williamson, J (1999), "Structural ordering in high temperature coal chars and the effect on reactivity", *Fuel*, **78**(7), 803-807.

Sacristán, M, Hull, TR, Stec, AA, Ronda, JC, Galià, M and Cádiz, V (2010), "Cone calorimetry studies of fire retardant soybean-oil-based copolymers containing silicon or boron: Comparison of additive and

reactive approaches", *Polymer Degradation and Stability*, **95**(7), 1269-1274.

Sanders, H and Jena, A (2000), "A New Technique Provides Faster Particle Size Analysis at a Lower Cost Compared to Conventional Methods", http://www.pmiapp.com/publications/docs/CeramicIndus_anewtech.pdf [2011, February 09].

Schartel, B, Braun, U, Schwarz, U and Reinemann, S (2003), "Fire retardancy of polypropylene/flax blends", *Polymer*, **44**(20), 6241-6250.

Schartel, B and Hull, TR (2007), "Development of fire-retarded materials—Interpretation of cone calorimeter data", *Fire and Materials*, **31**(5), 327-354.

Seefeldt, H, Braun, U and Wagner, MH (2012), "Residue Stabilization in the Fire Retardancy of Wood-Plastic Composites: Combination of Ammonium Polyphosphate, Expandable Graphite, and Red Phosphorus", *Macromolecular Chemistry and Physics*, **213**(22), 2370-2377.

Shen, K and Schilling, B (2012), "Recent advantages with expandable graphite in intumescent flame retardant technology", http://www.nyacol.com/exgraphadv.htm, [2012, 13 May].

Skoropanov, AS, Bulgak, IA, Kizina, TA, Kurnevich, GI, Alfer, SA and Malei, LS (1985), "Graphite bisulfates thermal-analysis", *Thermochimica Acta*, **93**(SEP), 433-434.

Smith, JG (2008), *Organic Chemistry*, McGraw-Hill, Harvard.

Smith, T (1984), "Flame Retardants", *Hospital Development*, **12**(5), 14-15.

Soares, RW, Menezes, VJ, Fonseca, MVA and Dweck, J (1997), "Characterization of carbonaceous products by TG and DTA", *Journal of thermal analysis*, **49**(2), 657-661.

Sorokina, NE, Khaskov, MA, Avdeev, VV and Nikol'skaya, IV (2005), "Reaction of graphite with sulfuric acid in the presence of KMnO4", *Russian Journal of General Chemistry*, **75**(2), 162-168.

Sorokina, NE, Shornikova, ON and Avdeev, VV (2007), "Stability limits of graphite intercalation compounds in the systems graphite-HNO_3(H_2SO_4)-H_2O-$KMnO_4$", *Inorganic Materials*, **43**(8), 822-826.

Subrina, S, Kotchetkov, D and Balandin, AA (2009), "Graphene Heat Spreaders for Thermal Management of Nanoelectronic Circuits", *IEEE Electron Device Letters*, **30**(12), 1281.

Sudha, S, Sundaraganesan, N, Kurt, M, Cinar, M and Karabacak, M (2011), "FT-IR and FT-Raman spectra, vibrational assignments, NBO analysis and DFT calculations of 2-amino-4-chlorobenzonitrile", *Journal of Molecular Structure*, **985**(2–3), 148-156.

Sun, Z, Ma, Y, Xu, Y, Chen, X, Chen, M, Yu, J, Hu, S and Zhang, Z (2013a), "Effect of the particle size of expandable graphite on the thermal stability, flammability, and mechanical properties of high-density polyethylene/ethylene vinyl-acetate/expandable graphite composites", *Polymer Engineering and Science*.

Sun, Z, Ma, Y, Xu, Y, Chen, X, Chen, M, Yu, J, Hu, S and Zhang, Z (2013b), "Effect of the particle size of expandable graphite on the thermal stability, flammability, and mechanical properties of high-density polyethylene/ethylene vinyl-acetate/expandable graphite composites", *Polymer Engineering & Science*, n/a-n/a.

Sun, ZD, Ma, YH, Xu, Y, Chen, XL, Chen, M, Yu, J, Hu, SC and Zhang, ZB (2014), "Effect of the particle size of expandable graphite on the thermal stability, flammability, and mechanical properties of high-density polyethylene/ethylene vinyl-acetate/expandable graphite composites", *Polymer Engineering and Science*, **54**(5), 1162-1169.

Syvitski, JPM (2007), *Principles, Methods and Application of Particle Size Analysis*, Cambridge University Press, New York.

Talanov, VS, Melezhik, AV and Chuiko, AA (1993), "X-ray photoelectron study of the surface of expanded and expandable graphite", *Theoretical and Experimental Chemistry*, **28**(4), 273-276.

Talyzin, AV, Szabo, T, Dekany, I, Langenhorst, F, Sokolov, PS and Solozhenko, VL (2009), "Nanocarbons by High-Temperature Decomposition of Graphite Oxide at Various Pressures", *Journal of Physical Chemistry C*, **113**(26), 11279-11284.

Tuinstra, F and Koenig, JL (1970), "Raman Spectrum of Graphite", *The Journal of Chemical Physics*, **53**(3), 1126-1130.

Wang, JQ and Chow, WK (2005), "A brief review on fire retardants for polymeric foams", *Journal of Applied Polymer Science*, **97**(1), 366-376.

Wang, Z, Huang, P, Fan, WC and Wang, Q (1993), "Measurements on the fire behaviour of PVC sheets using the cone calorimeter", Paper presented at *3rd Asia-Oceania Symposium of Fire Science & Technology*, China.

Warner, JH, Schäffel, F, Rümmeli, MH and Büchner, B (2009), "Examining the Edges of Multi-Layer Graphene Sheets", *Chemistry of Materials*, **21**(12), 2418-2421.

Wehling, TO, Novoselov, KS, Morozov, SV, Vdovin, EE, Katsnelson, MI, Geim, AK and Lichtenstein, AI (2008), "Molecular doping of graphene", *Nano Letters*, **8**(1), 173-177.

Weil, ED (2011), "Fire-Protective and Flame-Retardant Coatings - A State-of-the-Art Review", *Journal of Fire Sciences*, **29**(3), 259-296.

Weil, ED and Levchik, SV (2008), "Flame retardants in commercial use or development for polyolefins", *Journal of Fire Sciences*, **26**(1), 5-43.

Wissler, M (2006), "Graphite and carbon powders for electrochemical applications", *Journal of Power Sources*, **156**(2), 142-150.

Xie, R and Qu, B (2001a), "Expandable graphite systems for halogen-free flame-retarding of polyolefins. I. Flammability characterization and synergistic effect", *Journal of Applied Polymer Science*, **80**(8), 1181-1189.

Xie, R and Qu, B (2001b), "Expandable graphite systems for halogen-free flame-retarding of polyolefins. II. Structures of intumescent char and

flame-retardant mechanism", *Journal of Applied Polymer Science*, **80**(8), 1190-1197.

Xie, RC and Qu, BJ (2001c), "Expandable graphite systems for halogen-free flame-retarding of polyolefins. I. Flammability characterization and synergistic effect", *Journal of Applied Polymer Science*, **80**(8), 1181-1189.

Xie, RC and Qu, BJ (2001d), "Expandable graphite systems for halogen-free flame-retarding of polyolefins. II. Structures of intumescent char and flame-retardant mechanism", *Journal of Applied Polymer Science*, **80**(8), 1190-1197.

Ying, Z, Lin, X, Qi, Y and Luo, J (2008), "Preparation and characterization of low-temperature expandable graphite", *Materials Research Bulletin*, **43**(10), 2677-2686.

Zhao, H, Liang, T, Zhang, J, Li, Z and Tang, C (2006), "Research on graphite powders used for HTR-PM fuel elements", *Rare Metals*, **25**(6), 347-350.

Zheng, W, Lu, XH and Wong, SC (2004), "Electrical and mechanical properties of expanded graphite-reinforced high-density polyethylene", *Journal of Applied Polymer Science*, **91**(5), 2781-2788.

Zhu, J, Uhl, FM, Morgan, AB and Wilkie, CA (2001), "Studies on the mechanism by which the formation of nanocomposites enhances thermal stability", *Chemistry of Materials*, **13**(12), 4649-4654.

Zou, L, Kang, F, Zheng, Y-P and Shen, W (2009), "Modified natural flake graphite with high cycle performance as anode material in lithium ion batteries", *Electrochimica Acta*, **54**(15), 3930-3934.

Appendix

A-1 – Ion Exchange

Preliminary rough results followed, some of which were reported by a student under my supervision. The original word document for this section was lost and unedited images follow:

2.5.6 Water analysis

Inductively Coupled Plasma Mass Spectrometry (ICP-MS) produces ions of the sample and analyses the ions by use of a Mass Spectrometer. Concentration of specific elements such as Boron and Phosphorus can be determined. As result, the degree of ion exchange can be calculated.

3 Experimental

3.1 Planning

To improve GIC's flame retarding properties, the following method was proposed: substitute the intercalated sulphate with ions possessing flame retarding elements such as phosphorus and boron (Prof. W.W. Focke). Four possible ion exchange compounds were chosen:

1. Di-ammonium phosphate ($(NH_4)_2HPO_4$)
2. Mono-ammonium phosphate ($NH_4H_2PO_4$)
3. Tetra borate ($Na_2B_4O_7.10H_2O$)

Distilled Water (H_2O) was chosen as the benchmark treatment liquid. The Ammonium phosphate compounds were chosen for their contribution of Phosphate (PO_4^{3-}(aq)) ions, Borax for Borate (BO_3^{3-}(aq)) ions. Each EG sample was exposed to its selected solution numerous times.

In order to validate analysis results for the treated samples one needs to determine the degree of ion exchange that occurred. One method that can prove ion exchange success is to perform a mass balance on the EG. If the intercalated sulphate ions were exchanged with heavier borate or phosphate ions, the mass of the dry EG should increase. By measuring the solution pH, one can determine whether ions left or entered the solutions. pH and mass readings were therefore taken at frequent intervals.

3.2 Preparation

Precipitation can lead to unwanted solids attaching to the EG outer surface instead of interring the layers. In order to prevent precipitation, the solubility limits in Table 1 were not exceeded.

Table 1: Solubility limits of chosen compounds (Green and Perry, 2007)

Compound	Solubility in 100 parts cold Water	Solubility temperature (deg C)
di-Ammonium phosphate (DAP)	131	15°C
mono-Ammonium phosphate (MAP)	22.7	0°C
Tetra Borate (Borax)	1.14	-

To ensure adequate exposure the EG was exposed to the solutions numerous times at a constant initial solution concentration. Solutions were prepared in 5 litre plastic containers and used throughout the experiment. The concentrations of the three solutions used are displayed in Table 2. The solution concentrations are well within the solubility limits.

Table 2: Initial concentrations were prepared with de-ionized Water (H_2O_D).

Compound	Concentration (g/g)[a]	Mass de-ionized Water (g)[b]
DAP	0.12157	4145.75
MAP	0.11983	4174.07
Borax	0.01065	2299.92

[a] Gram compound per gram de-ionized Water

[b] Gram de-ionized Water

Each solution was added to EG in a 500 millilitre glass bottle. The glass bottles and their corresponding lids were weighed. Table 3 shows the mass of the solutions and EG used.

Table 3: Mass solution added to mass EG.

	Mass (g)		Mass fraction
Compound	**Solution**	**EG**	**(g Solution/g EG)**
DAP	378.57	40.028	9.457
MAP	378.16	39.959	9.463
Borax	353.04	39.526	8.931
H_2O_D	327.5	41.301	7.929

3.3 Method

To ensure homogenous concentrations inside the glass bottles, a shaker (Labcon, 3100U) was used to stir the contents continuously. The shaker was set to 200 revolutions per minute. This speed prevents the EG from forming stagnant areas, ensuring an even distribution of particles. The contents were stirred for one day at a time. The solutions were separated from the EG using a fine mesh. An elastic band was used to secure the mesh around the opening of the glass bottle. The solution was then poured out into smaller containers, leaving the EG behind. This EG was repeatedly exposed to the initial solutions, using the same method. Repeated exposure ensures a possible saturation point that can be reached. All the solutions separated were weighed.

After the final separation, the wet EG was dried in an oven at 80°C. This temperature was chosen to effectively dry the EG whilst preventing expansion or damage. The dried EG was then weighed.

Samples of the separated solutions were sent to a company called Waterlab for testing. Tests were done for Phosphorus, Boron, Sulphate and Nitrogen as Nitrate. The following tests were performed: SEM, XRD, XRF, TMA and Elemental analysis.

Note below that a certain trend was expected in the final results. This trend did not occur however and due to inconclusive results from the liquid analysis and multiple other techniques this project phase was thus abandoned

4.8 Waterlab results

The following is expected from the latest waterlab results (not yet obtained):

- Sharp increase in sulphate concentration followed by a steady decrease.
- Steady decrease in boron concentration from borax solution until saturation is achieved.
- Same with phosphorus.
- Larger amount of ions exchanged (Dynamic exposure method, all the EG had contact with solution).

Table 6: Borax containing solutions separated after exposure to EG. Previous results based on stagnant exposure method, not all the EG were exposed to the same concentration of solution.

	Exposure time for borax solutions		
	1 day	**1 day**	**1 day**
Boron (mg/L)	1 884	1 383	1 413

Table 7: DAP containing solutions separated one day at a time after exposure to EG. These results are also based on the stagnant method

	Exposure time for DAP solutions			
Ions tested (mg/L)	**1 day**	**1 day**	**1 day**	**1day**
Sulphate as SO_4	6 943	7 416	7 011	5 277
Ortho Phosphate as Phosphorus	<0.2	<0.2	<0.2	<0.2

See Appendix A.5 for results on distilled water and initial DAP solution used.

The phosphorus test results in Table 7 were conducted for orthophosphate as phosphorus. However, pH results indicated that phosphorus in aqueous DAP solution is present as dihydrogen phosphate. This explains why no phosphorus was detected.

5. Conclusions

- No concrete evidence to support successful ion exchange.
- XRD results showed no difference in d-spacing.
- Mass EG increased after exposure to phosphorus containing compounds.
- Phosphorus and boron concentrations of solutions exposed decreased.
- EG was produced by using $KMnO_4$ as oxidising agent and H_2SO_4 as intercalate.
- Exposed EG appears to be more swollen than the unexposed EG when expanded.
- Phosphorus can be present as Dihydrogen phosphate in DAP solution or as orthophosphate in MAP solution.

A-2 - SEM

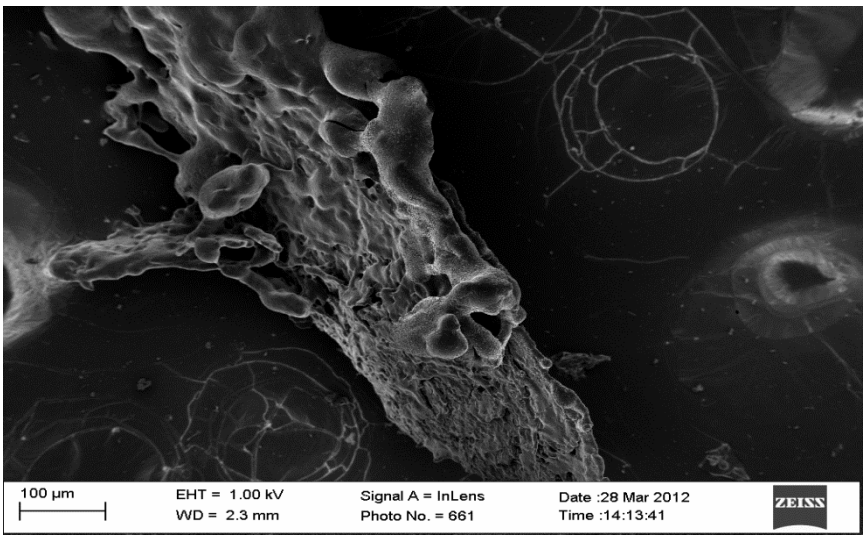

Figure A-2-1: Pictures taken by the FE SEM of foamed DABAP

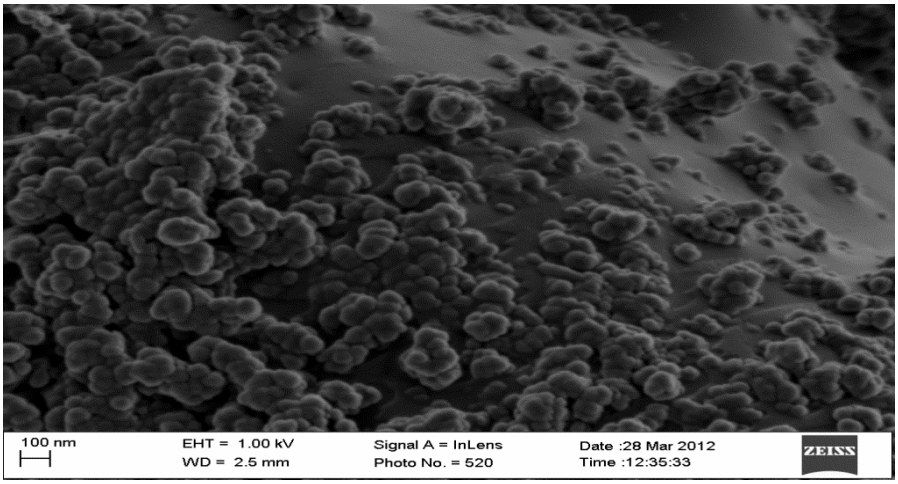

Figure A-2-2: Pictures taken by the FE SEM of foamed EDAP

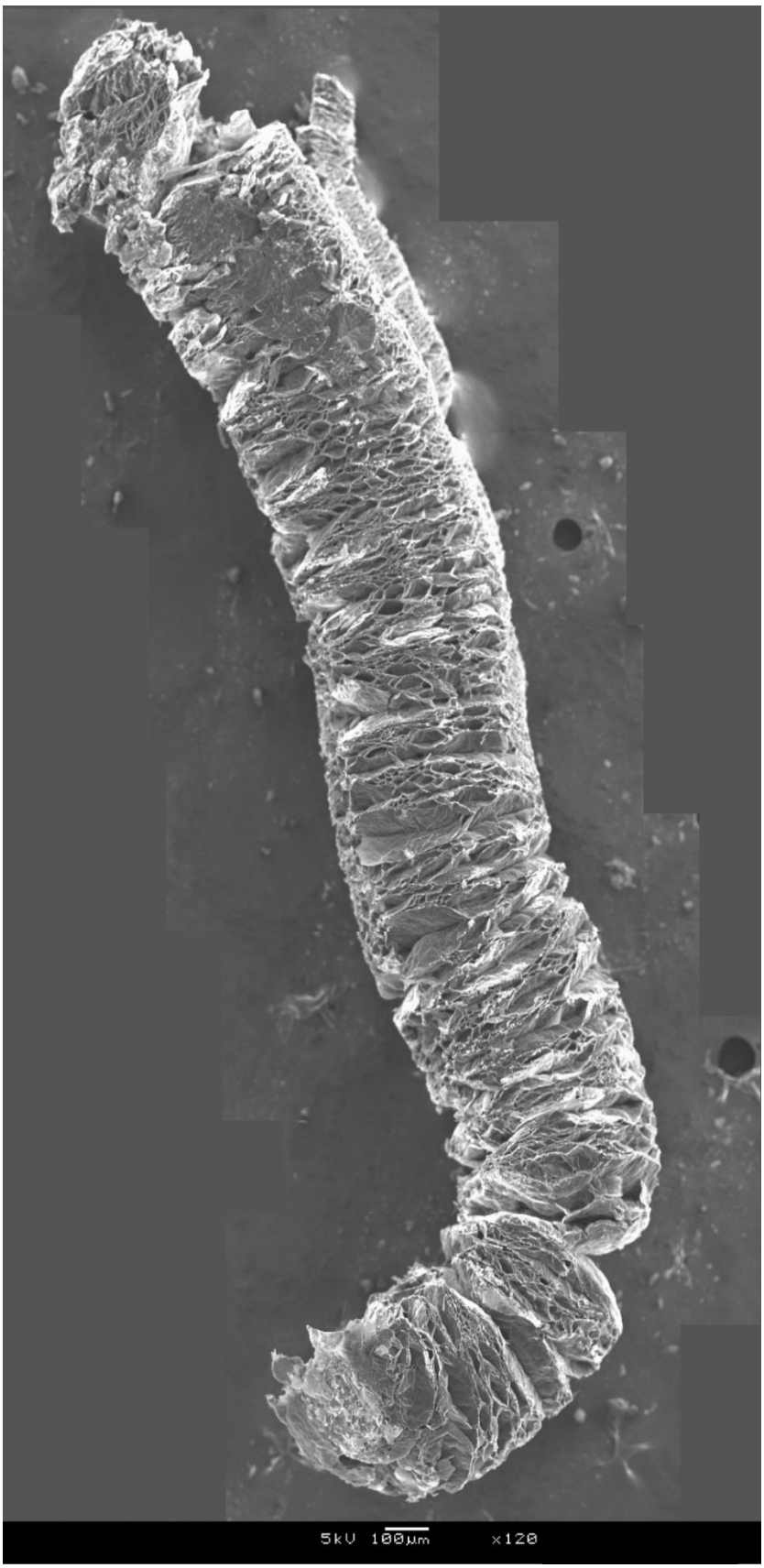

Figure A-2-3: 5800 SEM micrograph image of ES 250 created by combining multiple micrographs into one image

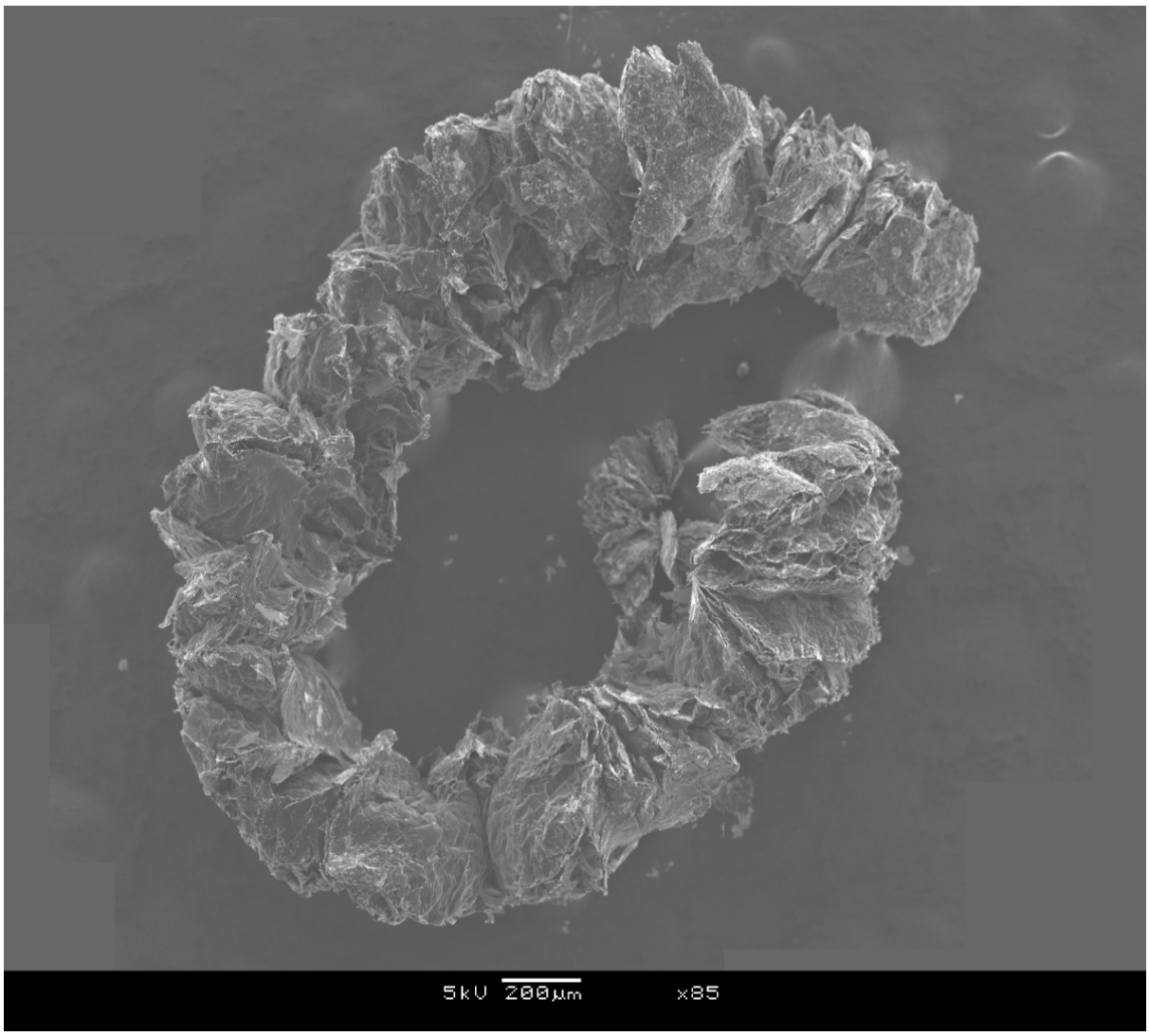

Figure A-2-3: 5800 SEM micrograph image of ES 170 B5 created by combining multiple micrographs into one image

Figure A-2-3: FE SEM micrograph image of ES 250 created by combining multiple micrographs into one image

A-3 – EDAP production

A-3.1Production

Seven moles of ethylenediamine (420.7 g pH 1.5) was weighed out into a 5 L glass container which was placed in an ice bath which contained ca. 1500 g crushed ice. A larger quantity of ice was employed to cool the EDAP synthesis reactions than that used for DABAP synthesis due to the extremely exothermic nature of the EDAP reactions. Seven moles of orthophosphoric acid was then added dropwise in the form of 807 g 85 % technical grade (pH 12) orthophosphoric acid (686g pure orthophosphoric acid content) to the EDA container which was continuously stirred and maintained at a temperature below ambient. During this procedure the colour of the liquid phase changed from colourless to yellow and produced white precipitated EDAP crystals. The final pH of the liquid solution was 8.83. The precipitated white crystals were recovered using vacuum filtration. The filter cake was first washed with distilled water and then with acetone. The resulting filter cake was left to dry at ambient conditions for 12 hours. Fumed silica was then added to the filter cake to a total of 3 wt.% to promote milling and lower agglomeration and the crystals were milled into a fine powder. The yield was 0.9805kg (88.6%).

A-4 – DABAP production

A-4.1Production

Seven moles of 3,5-diaminobenzoic acid (DABA) (1065 g) was weighed out into a large glass container placed in an ice bath which contained ca. 500 g crushed ice. The ice bath was used to maintain a decreased reaction temperature to promote a protonation reaction of one of the amine groups instead of an exothermic hydrolysis and phosphorification of the alcohol group.

Once the DABA containing glass container was submerged seven ampules of concentrated hydrochloric acid (1 mol HCl each) were added dropwise to the DABA container which was continuously stirred and maintained at a temperature below ambient. At this stage the solution developed a dark brown, near black colour, most likely due to oxidation of a minor portion of the DABA.

The measured pH at this stage was 2. After this addition all DABA powder was dissolved within the HCl as shown in the first step of scheme I. Next, seven moles (805 g) ammonium dihydrogen phosphate powder was added slowly to the reaction mixture with continuous stirring. During this procedure the colour of the liquid phase changed from brown to orange. The final pH was 7.8. The precipitated silver-white crystals were recovered using vacuum filtration. The filter cake was first washed with distilled water and then with acetone. The resulting filter cake was oven dried at 50 °C for 12 hours in a Thermopower electric furnace and milled into a fine powder. The yield was 1433g (95 %).

A-5 – DABAP open flame fire testing and cone calorimetry

Table A-5-1 lists all the time related open flame fire testing results for the vertical and horizontal fire tests using EG and DABAP combinations. The occurrence of polymer flow or formation of droplets is noted. Figures A-5-1 – A-5-6 display the results obtained from IR video analysis during open flame fire testing for DABAP-EG compounds.

Table A-5-1 Cone calorimeter and Open flame fire testing summary for EG-DABAP systems

			EG/DABAP, wt.%				
	Property	**Units**	**0/0**	**10/0**	**0/27**	**10/10**	**10/20**
Cone calorimetry	Time to ignition (t_{ign})	s	58 ± 3	46 ± 2	33 ± 5	38 ± 1	38 ± 2
	Time to flame out	s	773 ± 307	1049 ± 12	537 ± 69	1172 ± 48	1138 ± 24
Vertical open flame fire testing	Time to ignition (t_{ign})	s	22 ± 1	18 ± 11	13 ± 2	12 ± 0	11 ± 1
	Time to sag initiation (t_{ign})	s	-	27 ± 1	31 ± 1	24 ± 0	24 ± 0
	Time to burn through (t_{ign})	s	20 ± 1	37 ± 1	34 ± 0	51 ± 1	-
	Polymer flow / Droplets	Y / N	Y	N	N	N	N
Horizontal open flame fire testing	Time to ignition (t_{ign})	s	16 ± 2	33 ± 2	19 ± 1	27 ± 1	30 ± 3
	Time to sag initiation (t_{ign})	s	-	-	34 ± 2	33 ± 10	40 ± 7
	Time to burn through (t_{ign})	s	20 ± 0	35 ± 0	29 ± 1	40 ± 5	45 ± 0
	Polymer flow / Droplets	Y / N	Y	N	N	N	N

Figure A-5-1 indicates the maximum temperatures reached along the first 24 seconds of flame exposure for the vertically exposed samples. Test specimens were injection moulded and mounted horizontally and exposed to a 4 cm butane flame at 45 degrees from below each sample. IR footage was recorded perpendicular to sample surface at a distance of 20 cm from sample.

Increased temperature maxima are measured across the first 8 seconds of exposure to the flame in the 10 wt.% EG and 27 wt.% DABAP samples although the point temperature increase then slows as intumescence increases and the barrier performance reaches a thermally thick level of performance. The binary systems are able to reach thermally thick fire behaviour earlier reducing the maximum temperature reached as temperature is dissipated away from the point of flame exposure across the thermal barrier. The temperature in the non-flame retarded sample increases at a much higher rate at the point of exposure due to the continuous reduction in sample thickness at this point due to polymer flow and droplet formation.

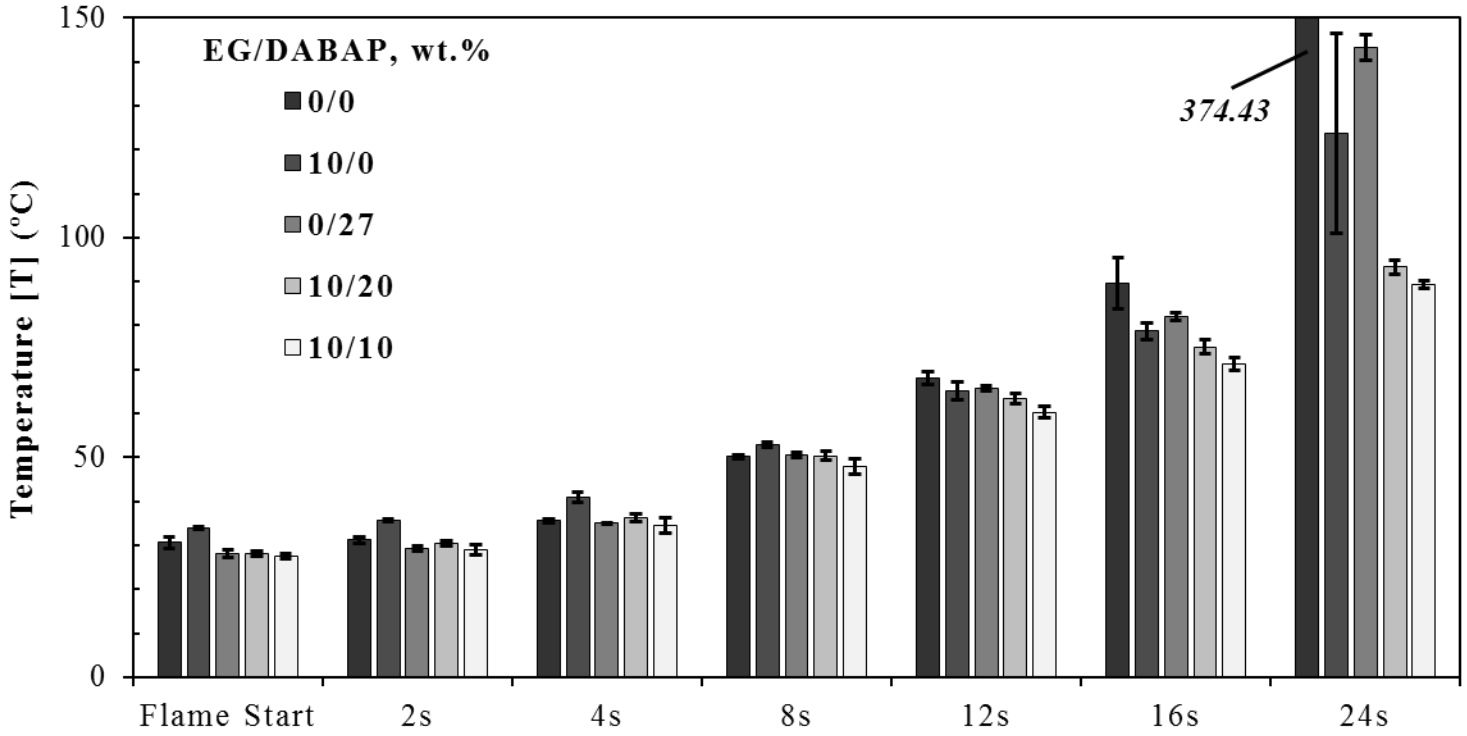

Figure A-5-1: Temperature profiles for vertically mounted flame retarded samples exposed to an open flame

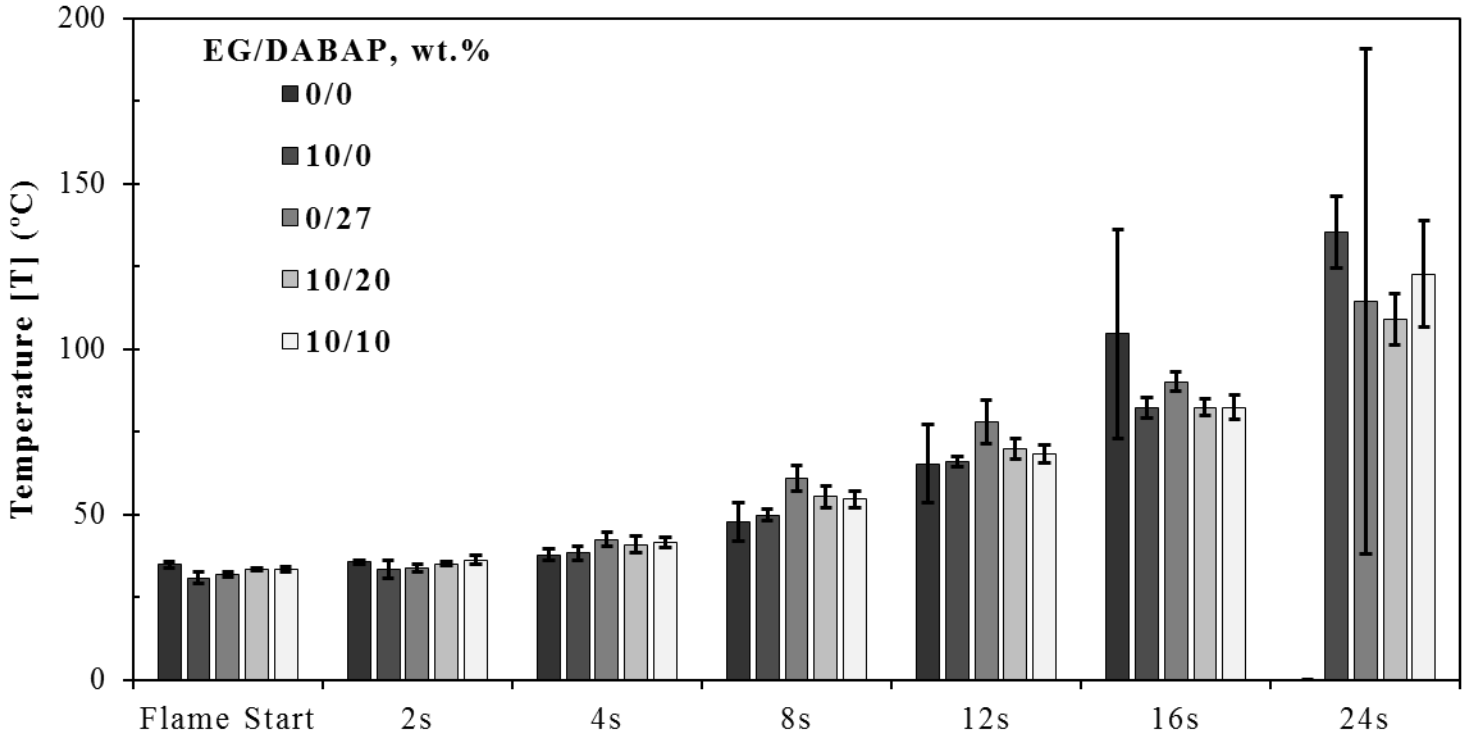

Figure A-5-2: Temperature profiles for horizontally mounted flame retarded samples exposed to an open flame

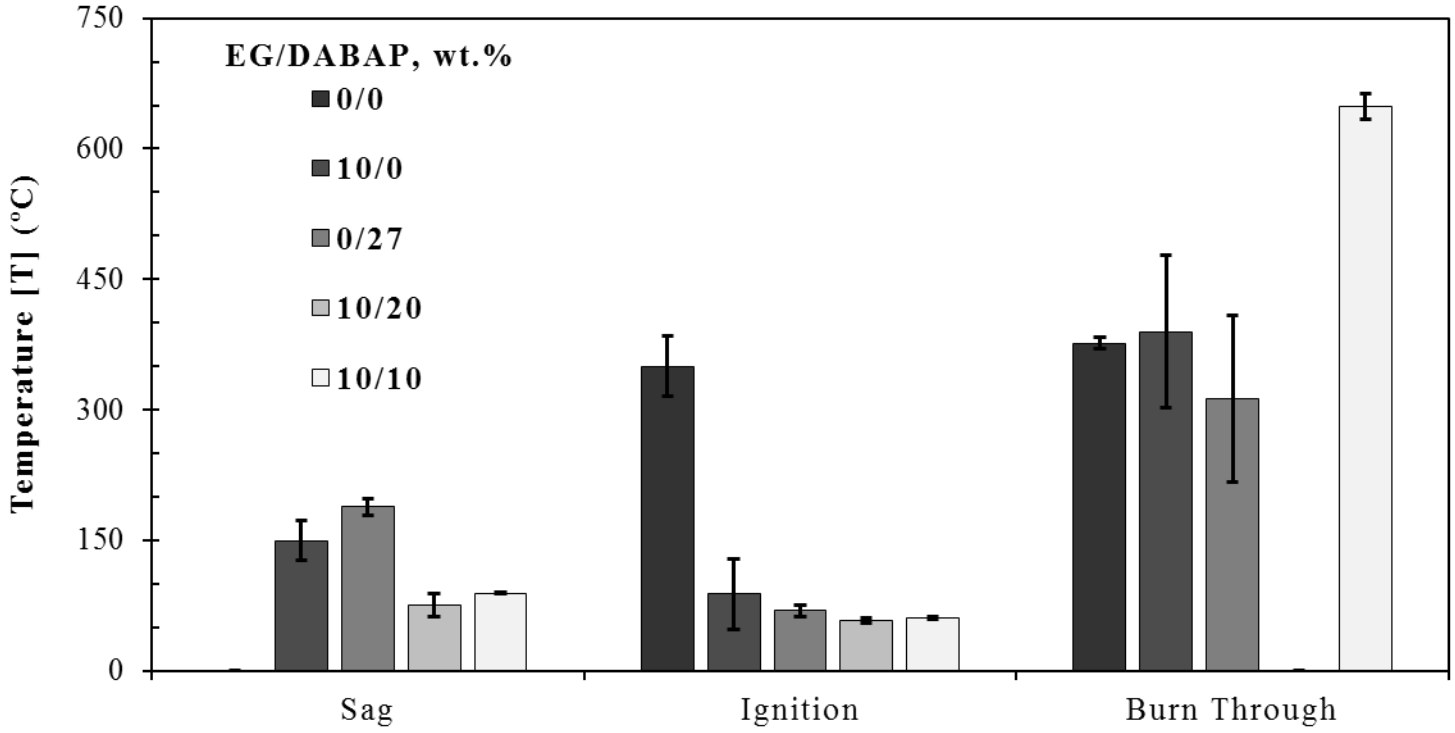

Figure A-5-3: Vertically mounted samples' maximum temperatures during initiation of sag, ignition and burn through when exposed to an open flame

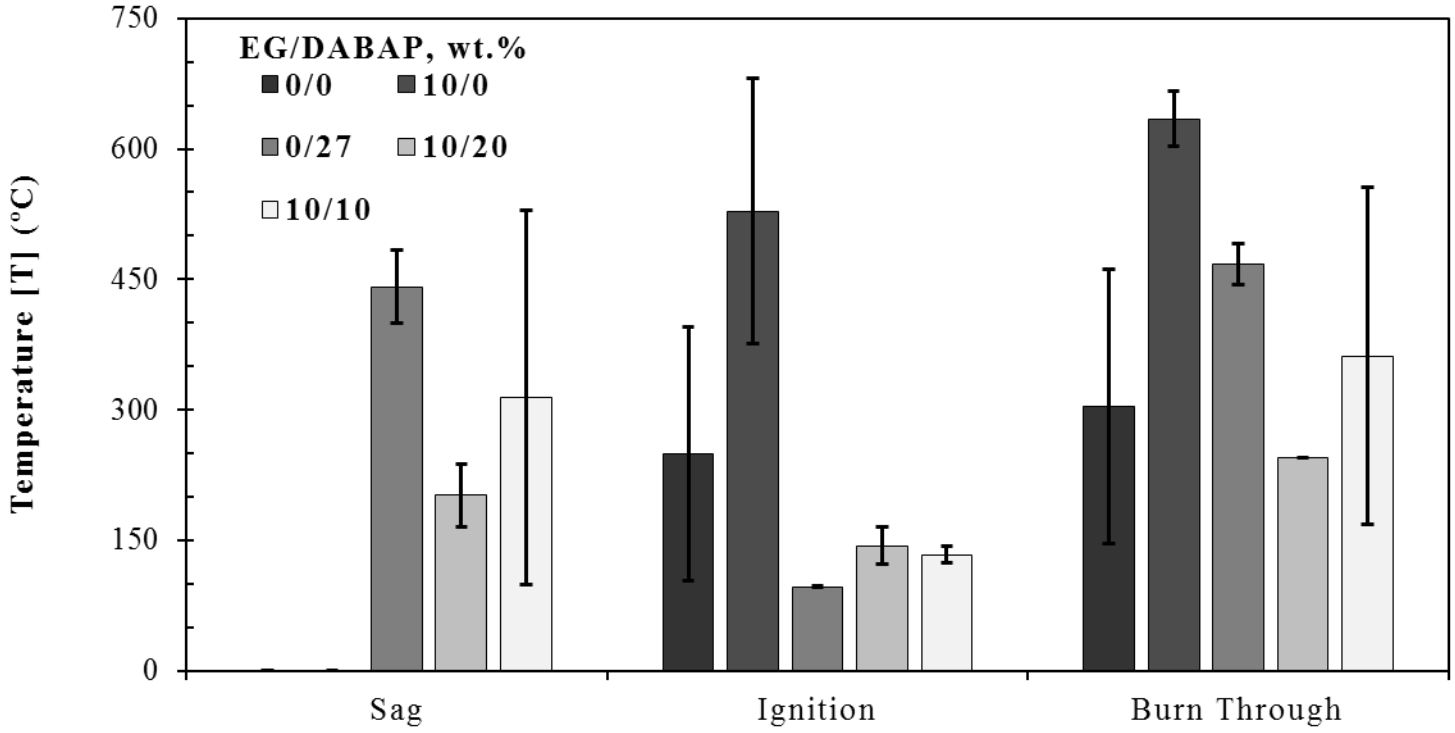

Figure A-5-4: Horizontally mounted samples' maximum temperatures during initiation of sag, ignition and burn through when exposed to an open flame

Figure 6-9 indicates linear temperature profiles for the vertically exposed test specimen exposed to open flame from below for 16 seconds. These curves were extracted from the recorded IR footage. One may note that the single flame retardant systems and the non-flame retarded sample each deliver a sharper temperature curve around the point of flame exposure. Contrary to this, the binary systems lower the local increase at the point of flame exposure due to continuous intumescence and formation of an effective thermal barrier at the centre. This spreads temperature further to the perimeter of the test specimen lowering the chance of burn through at similar exposure times.

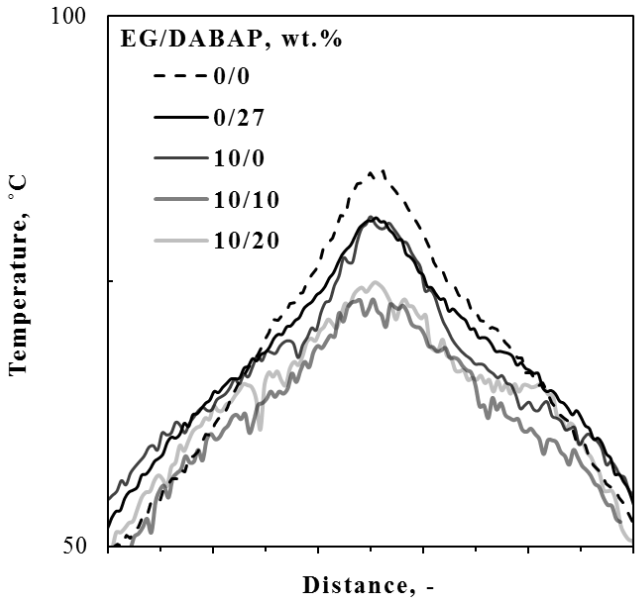

Figure A-5-5: Vertically mounted samples' linear temperature profiles from top to bottom of disc right to left after 16 seconds of exposure to flame

Figure A-5-6 indicates linear temperature profiles for the horizontally exposed test specimen exposed to open flame normal to the sample surface for 16 seconds. Test specimens were injection moulded and mounted vertically and exposed to a 4 cm butane flame perpendicular to the sample surface. IR footage was recorded at a 45 degree angle to sample surface at a distance of 20 cm from each sample. The profile displayed indicates the temperature profile from the bottom of the samples to the top of the samples from left to right.

The 27 wt.% DABAP samples show a further increase in surface temperature towards the top point of the exposed samples. This is caused by increased heat absorbance in the DABAP sample from the heat which rises from the point of exposure across the sample surface. Addition of EG prevents this heat absorption due to the increased thermal barrier delivered by the binary samples. The binary samples displayed a sharper temperature increase during these tests opposed to the vertically exposed samples. These samples formed thicker thermal expansion around the point of exposure which blocks the surrounding area further from the spreading heat as this is only able to spread vertically further away from the sample surface.

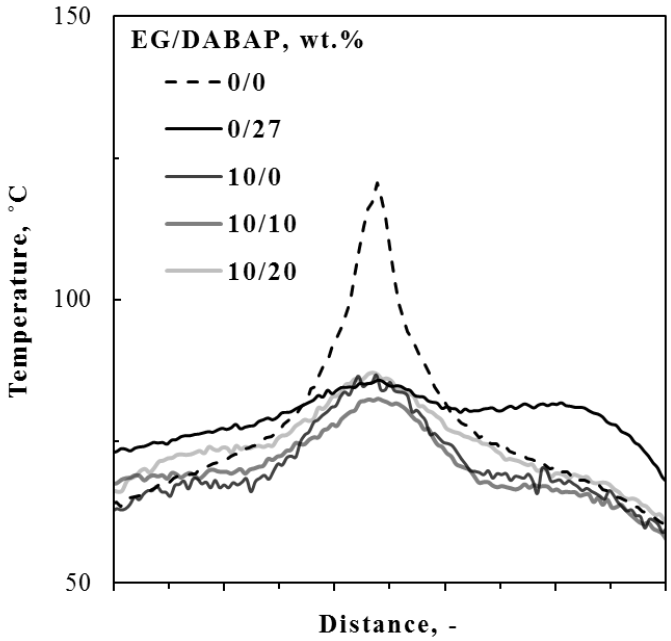

Figure A-5-6: Horizontally mounted samples' linear temperature profiles from top to bottom of disc right to left after 16 seconds of exposure to flame

A-6 – EDAP open flame fire testing and cone calorimetry

Table A-6-1 summarises the open flame fire testing results for EDAP EG systems summarised with key cone calorimeter results. Figures A-6-1 – A-6-6 display the results obtained from IR video analysis during open flame fire testing for EDAP-EG compounds.

Table A-6-1: Cone calorimeter and Open flame fire testing summary for EDAP-EG systems

			EG/EDAP, wt.%				
	Property	**Units**	**0/0**	**10/0**	**0/27**	**10/10**	**10/20**
Cone calorimetry	CC Time to ignition (t_{ign})	s	58 ± 3	46 ± 2	41 ± 1	45 ± 1	47 ± 2
	CC Time to flame out	s	773 ± 307	1049 ± 12	878 ± 191	1046 ± 17	948 ± 20
Vertical open flame fire testing	Time to ignition (t_{ign})	s	22 ± 1	18 ± 11	11 ± 1	-	-
	Time to sag (t_{ign})	s	-	27 ± 1	27 ± 3	25 ± 0	25 ± 0
	Time to burn through (t_{ign})	s	20 ± 1	37 ± 1	34 ± 0	-	-
	Polymer flow / Droplets	Y / N	Y	N	N	N	N
Horizontal open flame fire testing	Time to ignition (t_{ign})	s	16 ± 2	33 ± 2	29 ± 4	*58 ± 2	*51 ± 4
	Time to sag (t_{ign})	s	-	-	39 ± 4	48 ± 2	40 ± 3
	Time to burn through (t_{ign})	s	20 ± 0	35 ± 0	39 ± 3	-	-
	Polymer flow / Droplets	Y / N	Y	N	N	N	N

*Ignition only occurred after sagging occurred

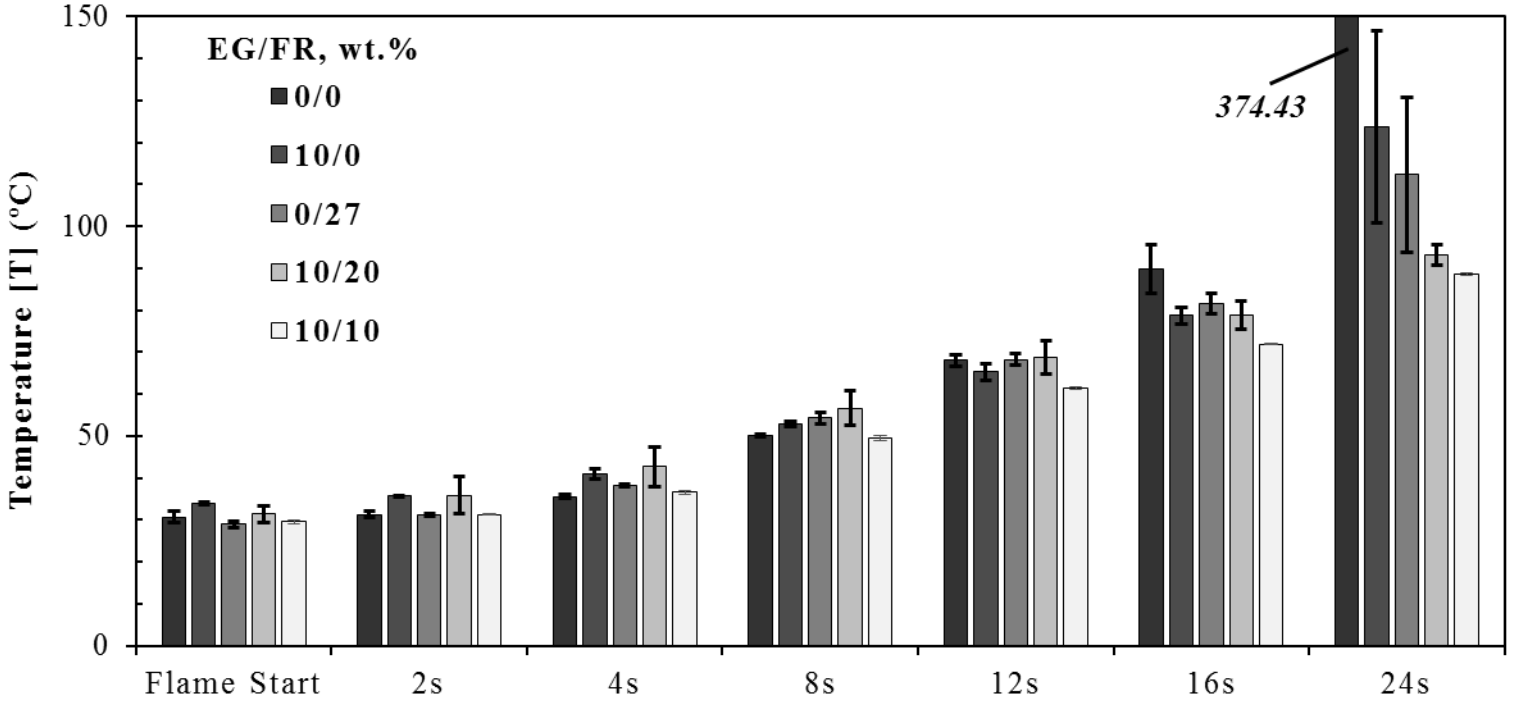

Figure A-6-1: Temperature profiles for vertically mounted flame retarded samples exposed to an open flame

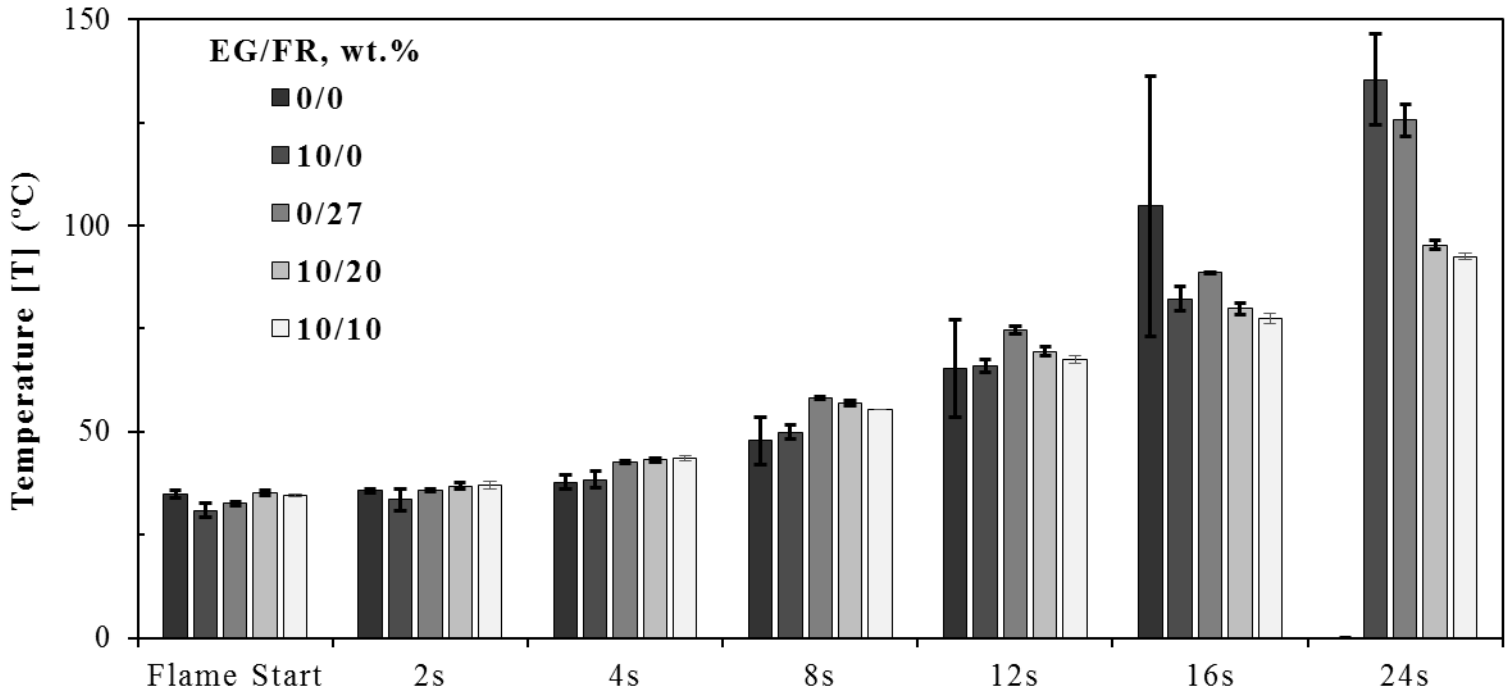

Figure A-6-2: Temperature profiles for horizontally mounted flame retarded samples exposed to an open flame

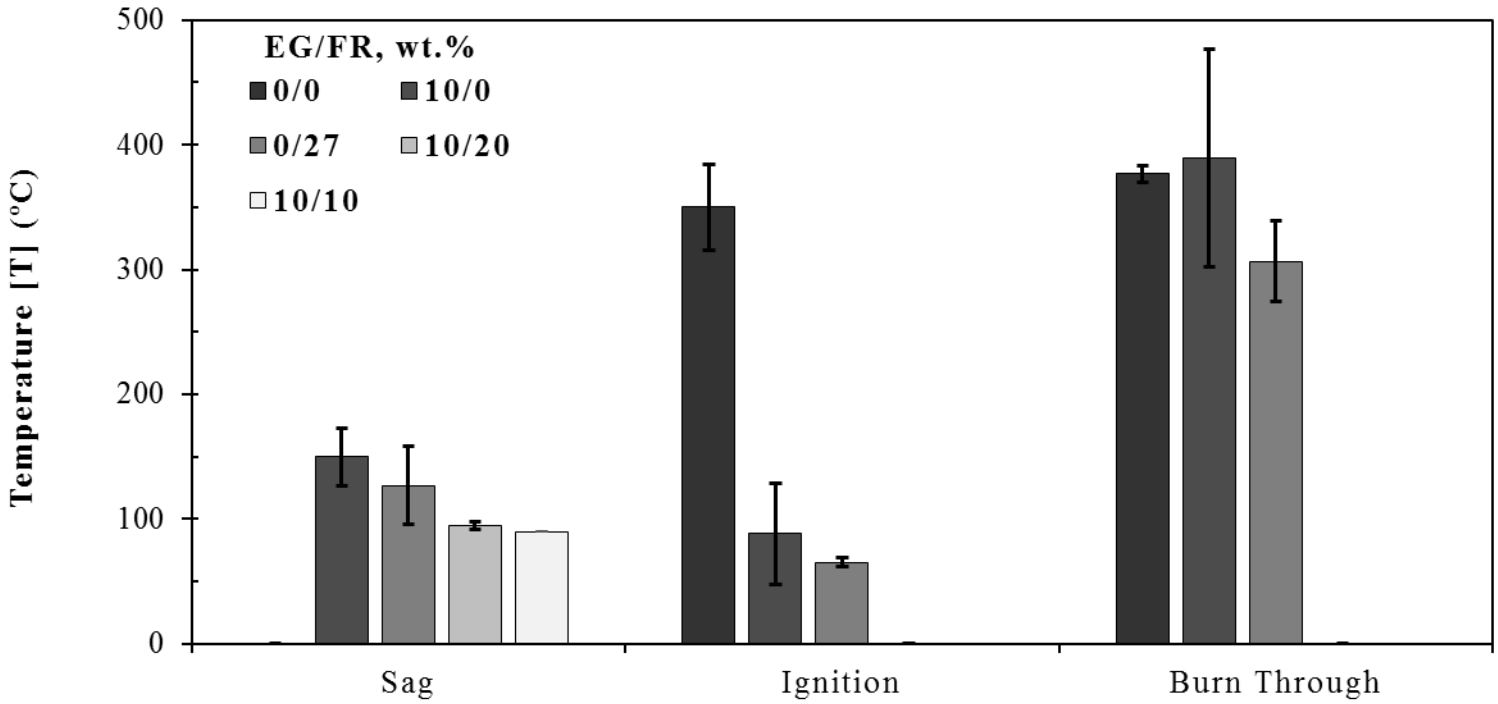

Figure A-6-3: Vertically mounted samples' maximum temperatures during initiation of sag, ignition and burn through when exposed to an open flame

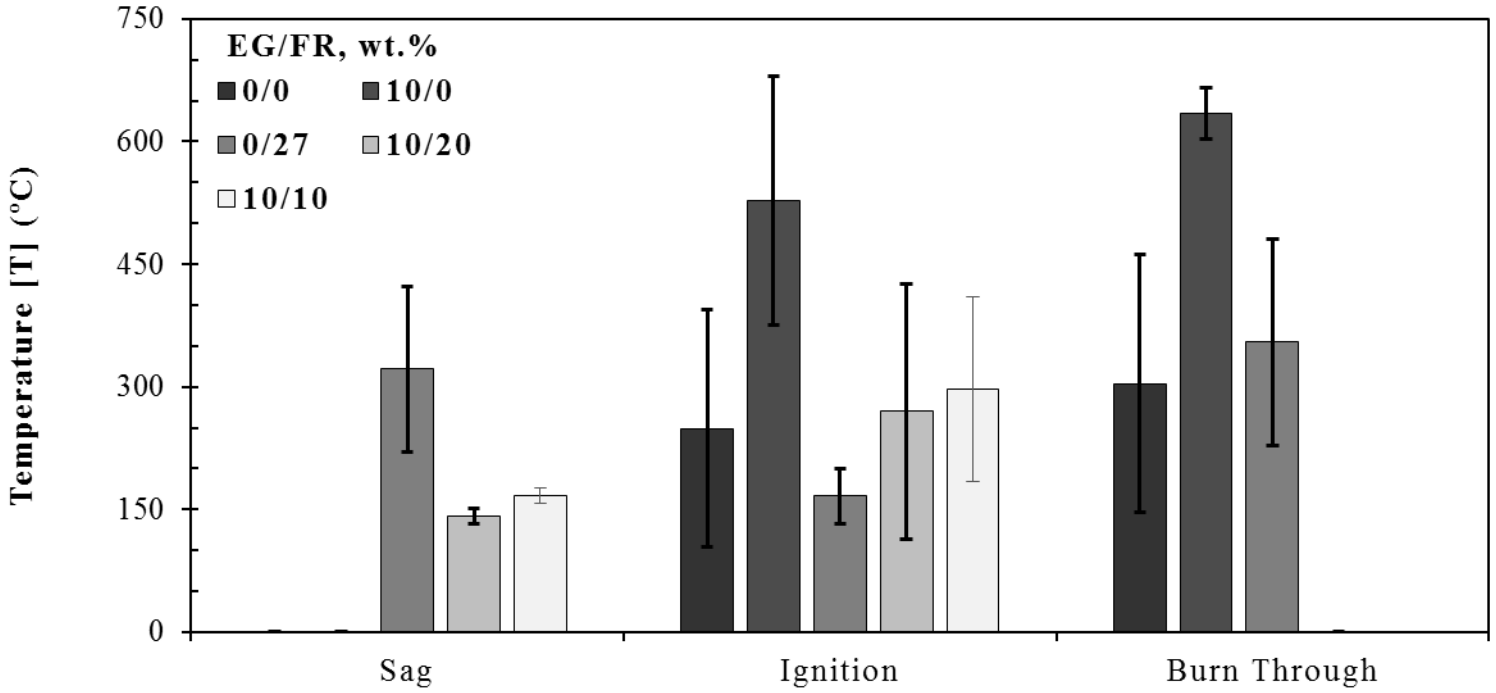

Figure A-6-4: Horizontally mounted samples' maximum temperatures during initiation of sag, ignition and burn through when exposed to an open flame

Figure A-6-5 indicates linear temperature profiles for the vertically exposed test specimens exposed to open flame from below for 16 seconds. Test specimens were injection moulded and mounted horizontally and exposed to a 4 cm butane flame at 45 degrees from below each sample while IR footage was recorded perpendicular to sample surface at a distance of 20 cm from sample. These curves were extracted from the recorded IR footage.

One may note that the single flame retardant systems and the neat polyethylene each deliver a sharper temperature curve around the point of flame exposure while the binary systems lower the local increase at the point of flame exposure due to continuous intumescence and formation of an effective thermal barrier at this point. This spreads temperature further to the perimeter of the test specimen lowering the chance of burn through at similar exposure times.

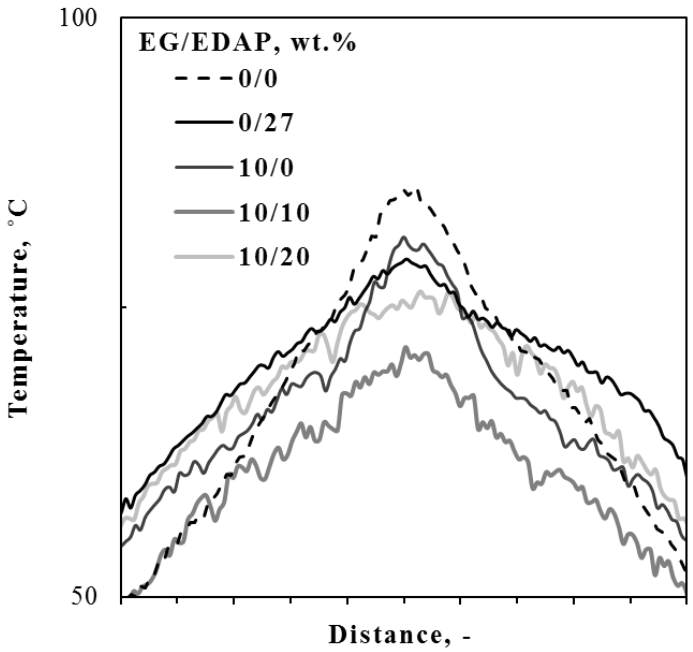

Figure A-6-5: Vertically mounted samples' linear temperature profiles from top to bottom of disc right to left after 16 seconds of exposure to flame

Figure A-6-6 indicates linear temperature profiles for the horizontally exposed test specimens exposed to open flame normal to the sample surface for 16 seconds. Test specimens were injection moulded and mounted vertically and exposed to a 4 cm butane flame perpendicular to the sample surface. IR footage was recorded at a 45 degree angle to sample surface at a distance of 20 cm from each sample. The profile displayed indicates the temperature profile from the bottom of the samples to the top of the samples from left to right.

These results indicate an even sharper peak for the non-flame retarded sample. The 27 wt.% DABAP samples show a further increase in surface temperature towards the top point of the exposed samples. This is caused by increased heat absorbance in the DABAP sample from the heat which rises from the point of exposure across the sample surface. Addition of EG prevents this heat absorption due to the increased thermal barrier delivered by the binary samples. The binary samples indicate a more peaked temperature curve during these tests as opposed to the vertically exposed samples due to formation of thicker thermal expansion around the point of exposure which blocks the surrounding area further from the spreading heat as this is only able to spread vertically further away from the sample surface.

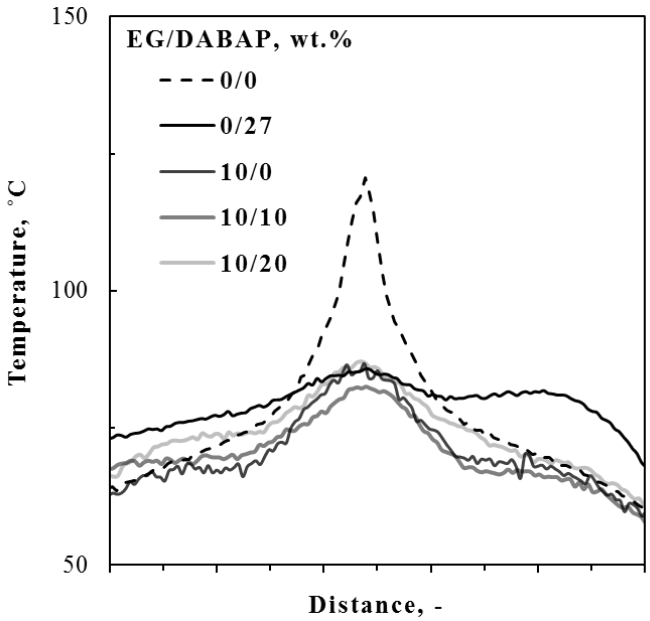

Figure A-6-6: Horizontally mounted samples' linear temperature profiles from top to bottom of disc right to left after 16 seconds of exposure to flame

A-7 – Open flame fire testing discussion and observations

During vertical and horizontal fire testing all flame retarded samples prevent formation of droplets and polymer flow across the samples containing EDAP delivering extremely good burn through prevention. In some cases blocking burn through during singular use of EDAP and always blocking burn through at 20% and 10% loading in the binary systems when exposed to vertical and horizontal flame attack. DABAP, although slightly less effective at fire retardation than EDAP when used alone, delivers burn through prevention at 20% loading with EG and good flame retardant properties throughout all tests.

EDAP and EG showed extremely good synergism in open flame fire testing preventing ignition in flame retarded samples tested. Very good bonding of loose EG strings is observed with EDAP and DABAP binary use. EDAP binary systems showed the most cohesive thermal barrier formation which yields excellent fire retardation as a result. All binary samples exceed the fire retarding properties of their single compound counterparts which is indicative of synergistic interactions. This indicates success at creating cohesive and more effective EG based thermal barriers and therefore success of the provisional aim.

Polymer flow was prevented in all flame retarded samples. As expected, the fire performance of the 10 wt.% EG compound was reduced when exposed to an open flame from below as opposed to horizontal exposure. The 27 wt.% DABAP compound showed similar performance to the 10 wt.% EG compound in both test types but their binary systems outperformed both these compounds. The binary compounds substantially increased the time before burn through occurs and the 10 wt.% EG – 20 wt.% DABAP completely prevented vertical burn through from below only heating up until full sag of the material occurred. The flame exposure time before complete sagging occurred was also increased in all binary systems. Where sag values are not listed, burn through occurred before sag initiation could occur.

Where burn through times are not listed, burn through was completely prevented and the samples increased in temperature until eventual sagging occurred. Results indicate

the best overall open flame fire resistance in the 10 wt % EG – 20 wt.% DABAP compound.

Table A-5-1 lists the ignition and flame out times for the various samples. Addition of the flame retardants increased the propensity of the material to ignite although overall fire performance was improved. The time to ignition (t_{ig}) was 58 ± 3 s for the neat polyethylene and 46 ± 1 s for the compound containing 10 wt.% EG but decreased to 33 ± 5 for the compound containing 27 wt.% DABAP. See Table A-6-1 for other values. Overall, the DABAP containing samples were more easily ignited.
The time to flame out showed considerable variability. See Table A-6-1. It was 773 ± 307 for the neat polyethylene, reduced to 539 ± 69 for the 27 wt.% DABAP compound and was longer than both these times for all other compounds.

During vertical and horizontal fire testing all flame retarded samples prevented dripping and even polymer flow across the sample. EDAP delivered extremely effective burn through prevention abilities, sometimes even blocking burn through entirely during singular use of EDAP. All binary EDAP containing samples and always blocking burn through at 20 % and 10 % loading in the binary systems when exposed to vertical and horizontal flame attack. DABAP, although slightly less effective at fire retardation than EDAP when used alone, DABAP delivers burn through prevention at 20 % loading with EG and good flame retardant properties throughout all tests.

Addition of the flame retardants increased the propensity of the material to ignite with the exclusion of the binary systems containing EG and EDAP. EDAP and EG showed exceptionally good synergism in open flame fire testing preventing ignition in all flame retarded samples tested. These compounds only ignited when the edge of the material was exposed to the test flame when the sample, after extended exposure, reached the melting temperature of the polymer and sagged, exposing the top edge of the samples. Very good bonding of loose EG strings is observed with EDAP and DABAP binary use with EDAP binary systems showing the most cohesive thermal barrier formation thus yielding excellent fire retardation as a result. All flame retarded samples prevented polymer flow.

The profiles displayed indicate the temperature variation from the bottom of the samples to the top of the samples from left to right. These results indicate an even sharper peak for the non-flame retarded sample. The 27 wt.% DABAP samples showed a further increase in surface temperature towards the top point of the exposed samples. This was caused by increased radiant heat absorption in the DABAP sample of the heat which rose across the sample surface from the point of flame exposure. Addition of EG prevented this heat absorption due to the increased thermal barrier delivered by the binary samples. A more peaked temperature curve was measured for the horizontal samples while the vertical samples maintained a bell curve shape. This phenomenon may be attributed to the formation of thicker thermal barrier around the point of exposure. This barrier lowers the spread of heat to the immediate surrounding area, causing temperature increases above the point of exposure in the non-foamed region of the sample alone.

One may note that the single flame retardant systems and the neat polyethylene sample each deliver a sharper temperature curve around the point of flame exposure. All the binary flame retarded systems lowered the local increase at the point of flame exposure due to continuous intumescence and formation of an effective thermal barrier at this point. This spread the heat towards the perimeter of the test specimen, lowering the chance of burn through at similar exposure times.

The profiles for the non-flame retarded sheet quickly develop a sharp temperature peak that results in ignition within a short period of time (15.4 s for this sample). A hole opened up in the sheet less than three seconds later. The strange shape of the temperature profile obtained at 19.3 s is an artifact of the hole that burned into the sheet. By comparison the temperature profiles for the flame retarded sample are flatter at similar times. The polymer is heated over a larger area owing to the shielding effect of the intumescent layer that forms. The temperature even reached values that exceed the melting point of material causing a softening that resulted in sagging. Only then did ignition occur.

A-8 – Open flame fire testing samples

Figure A-8-1: Vertically mounted sample

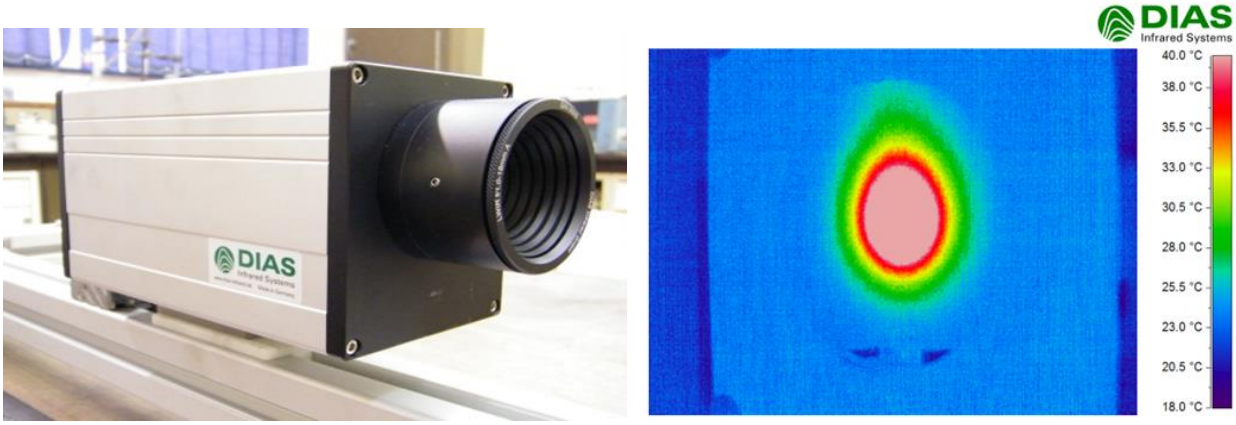

Figure A-8-2: IR apparatus and example of the IR video recorded in triplicate for each test specimen

Figure A-8-4: Engel Injection moulder used to make open flame fire testing samples

Figure A-8-5: 10% EG 20% DABA sample post exposure to open flame fire testing in the vertical configuration from below

Figure A-8-6: 10% EG 20% DABA sample post exposure to open flame fire testing in the vertical configuration from the side

One may note in Figure A-8-4 A and Figure A-8-5 A that in both configurations the sample performed extremely well and created a thick cohesive thermal barrier that prevented burn through of the sample

A-9 – Laser pyrolysis fire testing samples

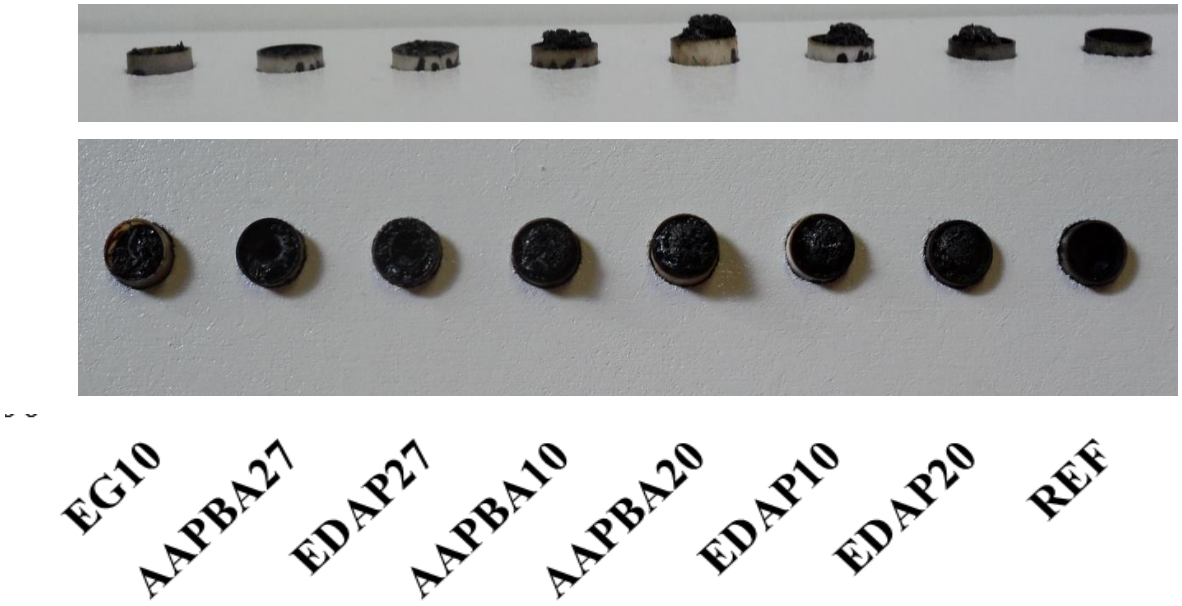

Figure A-9-1: Side and top view of laser pyrolysis samples clearly indicating the thermal barriers achieved for the samples tested

*Sample AAPBA refers to DABAP

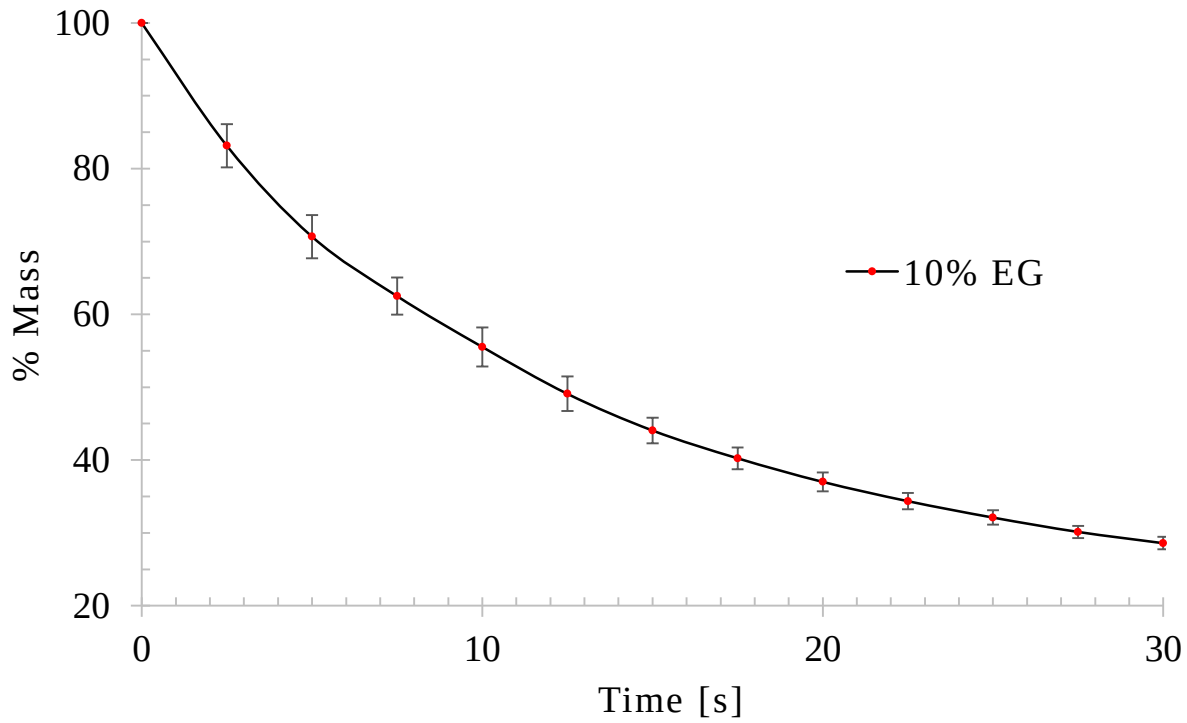

Figure A-9-2: A laser pyrolysis sample which displays the low variance achieved during testing of multiple samples.

A-10 – Cone calorimetry setup

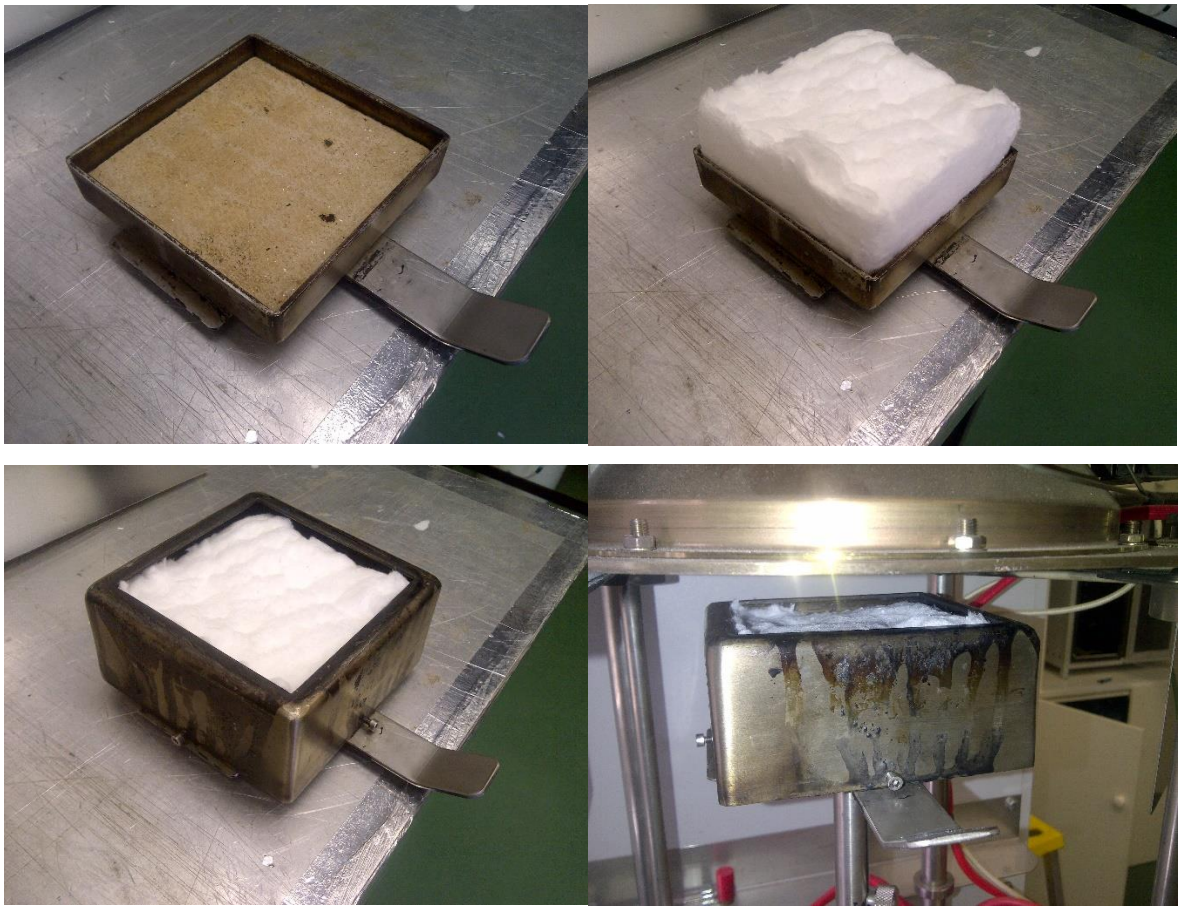

Figure A-10-1: Cone calorimetry apparatus used to mount the samples tested

Table A-10-1: Comparison of cone calorimeter and UL 94 fire testing indicating the large amount of variables measurable using cone calorimetry which has set it as the new standard in fire testing

Method	Cone Calorimetry	UL 94
Flame retardant performance indicators measured	heat release rate	time required for flame to self-extinguish
	total heat release	time required to ignite
	time to ignition	spread of flame after ignition
	time to flame out	monitors whether plastic drips
	time to peak heat release	
	mass loss over time	
	smoke production rate	
	specific smoke produced	
	specific extinction area	

Figure A-8-3: Hot plate press used to prepare the samples used for cone calorimetric testing

A-11 – Miscellaneous

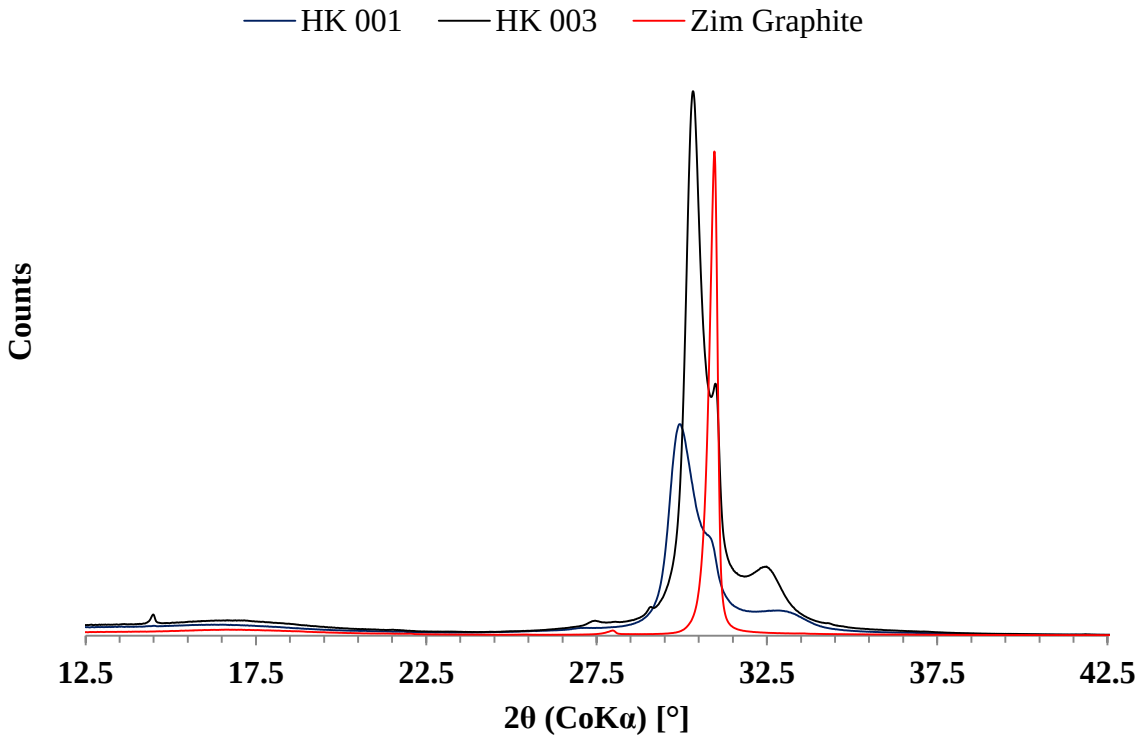

Figure A-11-1: XRD patterns for neat ES250, ES170 and Zimbabwe graphite

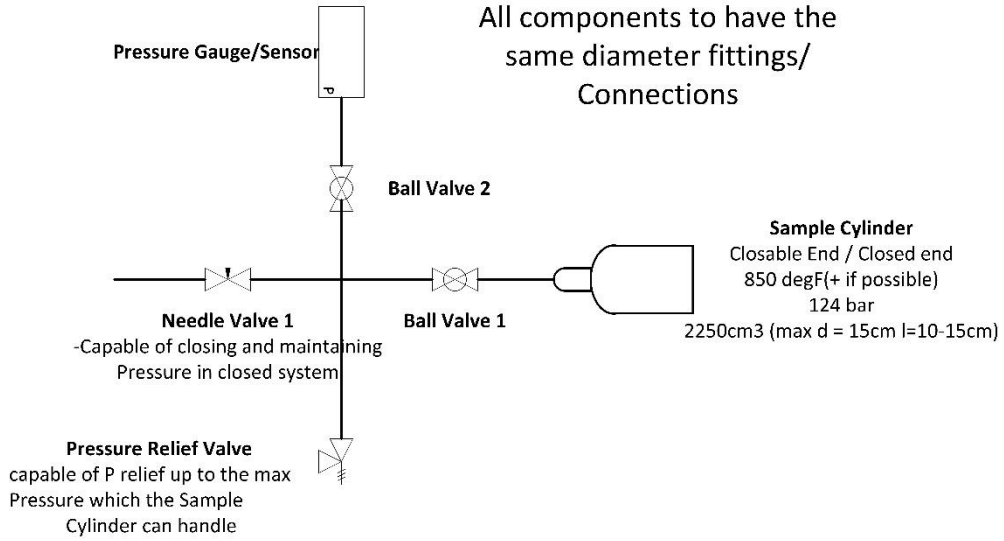

Figure A-11-1: Gas canister setup for EG gas release assessment